

**GROWTH AND DEATH  
OF ANIMAL CELLS  
IN BIOREACTORS**

**Dirk Egbert Martens**

920845

**Promotor** : dr. ir. J. Tramper  
hoogleraar in de bioprocestechnologie

**Co-promotoren** : dr. ir. C.D. de Gooijer  
universitair hoofddocent bij de sectie proceskunde  
dr. E.C. Beuvery  
hoofd laboratorium voor procesontwikkeling RIVM

UNO8201, 2158

**Derk Egbert Martens**

**GROWTH AND DEATH  
OF ANIMAL CELLS  
IN BIOREACTORS**

Proefschrift

ter verkrijging van de graad van doctor  
op gezag van de rector magnificus  
van de Landbouwniversiteit Wageningen,  
dr. C.M. Karssen,  
in het openbaar te verdedigen  
op woensdag 23 oktober 1996  
des namiddags te vier uur in de aula.

ISBN: 929845

ISBN 90-5485-593-2

WETTER  
LANDBOUWEN  
WA

Cover: Apoptosis

## Stellingen

- 1 De relatie van antilichaamproductiviteit met de integraal van de levende-celdichtheid, als gevonden door Renard et al., sluit het vrijkomen van antilichaam uit dode cellen als verklaring voor de toename van de antilichaamconcentratie in de afstervingsfase van batchkweken niet uit.  
 Renard J.M., Spagnoli, R., Mazier, C., Salles, M.F., Mandine, E. 1988. Evidence that monoclonal antibody production kinetics is related to the integral of the viable cells curve in batch systems. *Biotechnol. Lett.*, **12**:91-96.
- 2 Het wiskundige model van Suzuki et al. komt niet overeen met het door hen geschetste beeld van de celcyclus maar beschrijft een situatie waarin cellen met gelijke snelheid vanuit alle fasen de celcyclus verlaten, waarna ze niet meer terugkeren naar de celcyclus. Naast de correctie van hun wiskundige model als gedaan door Cazzador en Mariani, is ook deze aanpassing van het model een goede optie.  
 Suzuki, E., Ollis, D.F. 1989. Cell cycle model for antibody production. *Biotechnol. Bioeng.*, **34**:1398-1402. Cazzador, L. Mariani, L. 1993. Growth and production modelling in hybridoma continuous cultures. *Biotechnol. Bioeng.*, **37**:1322-1330. Hoofdstukken 2, 7 en 8 van dit proefschrift.
- 3 Gezien het geringe bereik van bestudeerde verdunningssnelheden sluiten de data van Lee et al. niet uit dat de afsterving van hybridomacellen gerelateerd is aan de celcyclus.  
 Lee, Y.-K., Yap, P.-K., Teoh, A.-P. 1995. Correlation between steady-state cell concentration and cell death of hybridoma cultures in chemostat. *Biotechnol. Bioeng.* **45**:18-26.
- 4 De slogan 'het is pas fijn als er bubbels zijn' waarmee Spa in de jaren 80 haar bronwater verkocht, gaat niet op voor dierlijke cellen in suspensie.  
 Dit proefschrift.
- 5 Het cliché 'hardlopers zijn doodlopers' is slechts ten dele van toepassing op hybridomacellen.  
 Hoofdstukken 7 en 8 van dit proefschrift.
- 6 Mensen die opruimen en ordenen tot een doel op zich hebben gemaakt, dienen zich te realiseren dat dit nooit leidt tot een afname van de chaos.  
 Tweede hoofdwet van de thermodynamica.
- 7 Een chaotisch niet opgeruimd bureau dwingt de geest geordend te blijven.  
 Concentrations of microcontaminants and response of organisms in laboratory experiments and rhine delta field surveys. A.J. Hendriks, stelling 13.
- 8 Doe nooit met bloeddruk wat je met oliedruk kunt doen.  
 Roel Martens (betreffende zware lichamelijke arbeid).

- 9 De journalistiek zou gebaat zijn bij een cursus inleiding statistiek.  
Volkskrant, Nieuwsblad van het Noorden, diverse actualiteitenprogramma's.
- 10 Een cliché is een cliché omdat men het niet werkelijk tot zich wil of kan nemen, hetgeen zeker ook geldt voor deze stelling.
- 11 Met betrekking tot natuurbeheer is het wenselijk dat de begrippen 'oorspronkelijke staat' en 'oer' gedefinieerd en gekwantificeerd worden.
- 12 Bij het vergelijken van het risico van vliegen en deelnemen aan het dagelijkse verkeer dient men te rekenen per uitgevoerde reis.  
Koffiepauze Proceskunde.
- 13 Bij het plaatsen van nestbeschermers dient rekening te worden gehouden met de nieuwsgierigheid van de koe.  
Weitsje en warje yn it gea. Nazorg in Friesland. Uitgave bond van Friese vogelbeschermingswachten.
- 14 De energie die aanstaande vaders steken in de verbouw van de kinderkamer gedurende de zwangerschap komt wellicht niet zozeer voort uit de oerdrang een nest te bouwen danwel uit het feit dat zij in die periode verder niet veel kunnen bijdragen.  
Eigen waarneming.
- 15 Aangezien wetenschappelijke wereldjes over het algemeen niet erg groot zijn en sommige auteurs ruimschoots naar zichzelf refereren, is het invoeren van een dubbelblind-principe bij de beoordeling van ter publicatie aangeboden artikelen praktisch niet zinvol. Het invoeren van een dubbelopen-principe daarentegen zal de kwaliteit van de beoordeling ten goede komen.  
Cascades of bioreactors. C.D. de Gooijer, stelling 25.
- 16 De benaming IBM-klonen voor veel goedkope PC's geeft aan dat informatietechnologen weinig kaas van biotechnologie hebben gegeten.
- 17 De afstand tussen de boven- en onderkant van de samenleving is kleiner dan velen zich realiseren.

Stellingen behorende bij het proefschrift 'Growth and Death of Animal Cells in Bioreactors'.

D.E. Martens

Wageningen, 18 september 1996.

*De redenaar kan als onwetende de onwetenden  
beter overtuigen dan de kenner.*

Plato (427-347 v.Chr.)

**aan mijn ouders  
voor Christel**

## VOORWOORD

Met het oog op het feit dat de mens zichzelf beschouwt als een intelligent wezen is het opvallend hoeveel wij nog leren door ervaring. Naast de wetenschappelijke kant is het verkrijgen van deze kennis een belangrijk onderdeel van het schrijven van een proefschrift. Dit proefschrift is het resultaat van vier jaar onderzoek bij het laboratorium voor procesontwikkeling (LPO), voorheen het laboratorium voor geïnactiveerde virusvaccins (LGV), van het Rijksinstituut voor Volksgezondheid en Milieuhygiëne (RIVM).

Allereerst wil ik mijn promotor Hans Tramper en mijn co-promotoren, Kees de Gooijer en Coen Beuvery bedanken. Hans, jij wist mij altijd weer te motiveren op momenten dat ik er zelf niet meer zo in geloofde. Jouw proceskundig zintuig bleek het maar al te vaak bij het juiste eind te hebben. Ook jouw stille diplomatie in de trein van Parijs naar Nice mag niet onderschat worden. Kees, ondanks het bouwen van een huis, het schrijven van een eigen proefschrift en het vaderschap wist je toch nog tijd te vinden al die concepten van commentaar te voorzien. Uiteindelijk is het geen 1 juni en ook geen 13 september geworden, maar zonder jouw gerichte adviezen was het proefschrift waarschijnlijk nog niet afgerond geweest. Coen, jouw wil ik bedanken voor de enthousiaste wijze waarop je het onderzoek gesteund hebt en de deuren die je voor mij geopend hebt om optimaal gebruik te maken van de mogelijkheden binnen het RIVM.

Mijn eerste contact met dierlijke cellen vond plaats gedurende mijn afstudeervak proceskunde bij TNO. Ilse Jöbses wil ik bedanken voor haar enthousiaste begeleiding gedurende dit afstudeervak, waarvan de resultaten in hoofdstuk 3 te vinden zijn.

Het praktische werk is uitgevoerd op het RIVM-terrein in gebouw H. Gedurende het onderzoek is er aan dit gebouw het nodige verspijkerd. Dat het ondanks de hiermee gepaard gaande stroomonderbrekingen en de aanwezigheid van niets ontziende timmerlieden toch nog mogelijk was de noodzakelijke continuculturen in 'steady state' te houden, mag een klein wonder heten. Dit is mede te danken aan de medewerkers van LPO, het vroegere LGV, een club waarin ik altijd met veel plezier gewerkt heb en die ik hierbij allen wil bedanken. Tiny, voor de mogelijkheden die je mij bood om gebruik te maken van de apparatuur in gebouw H en jouw inbreng in hoofdstuk 6 van dit proefschrift. Jan en Henk, jullie hebben mij veel geleerd op praktisch gebied onder andere het werken met de stoomlocomotief onder de bioreactoren, de Novo Paljas. Als ik denk aan het steriliseren van deze apparaten krijg ik het nog warm. Hans de Vries, jij hebt in het begin van het onderzoek een groot aantal analyses voor mij uitgevoerd. Joop Boon bedank ik voor het bereiden van media. Luc, jij hebt de aminozuurbepaling op de



HPLC van de grond gekregen en een groot aantal van deze analyses voor mij gedaan. Richard van der Meer, Jos, Ben, Stef, en Gerhan van jullie heb ik veel ondersteuning gehad met betrekking tot apparatuur en software. Giny voorzorg gebouw H van allerlei schone en steriele materialen. Ans en Gerda hadden 's morgens om 7 uur altijd de koffie klaar en mopperden nooit als ik ze in de weg liep bij het schoonmaken.

José, van jouw heb ik geleerd met de FACS te werken. Verder heeft jouw knoflooksoep met Spaanse worst een onuitwisbare indruk achtergelaten op mijn smaakpapillen evenals op de reukorganen van iedereen die in gebouw G10 werkte. Wim, van jouw heb ik geleerd dat biotechnologen eigenlijk prutsers zijn. Het kweken van cellen op en in microcarriers leerde ik van Margot, die tevens een belangrijke bijdrage heeft geleverd aan hoofdstuk 6. Richard Dorrestein, we zijn ongeveer tegelijk als AIOer begonnen. Samen hebben we in gebouw H heel wat cellen gekweekt, waarbij we aanvankelijk de regelapparatuur op nogal onconventionele wijze aan de praat hielden. Dick Smit, jouw bijdrage aan dit proefschrift ligt eigenlijk al voor mijn RIVM-periode toen jij bij de vakgroep Proceskunde van de landbouwuniversiteit als afstudeervakker werkte aan de afsterving van insectencellen in bellenkolommen. Verder wil ik Jakob bedanken voor het feit dat hij mij enige keren heeft geselecteerd voor het zaalvoetbalteam.

Een aantal studenten heeft een bijdrage geleverd aan dit proefschrift. Hans Risseeuw, jij was mijn eerste student en presteerde het om op een van je eerste werkdagen een prullenbak in brand te steken. Jouw onderzoek heeft de basis gelegd voor hoofdstuk 5. Chris Lammers, jouw eerste inleidend praatje heeft een enorme indruk achtergelaten op proceskunde. In het vervolg van je onderzoek heb je laten zien dat je tot beter in staat was. Joke van Adrichem, toen het kweken van de cellen in een air-lift reactor lastiger bleek dan we aanvankelijk dachten, vond jij al vrij snel op zelfstandige wijze je eigen weg binnen het onderzoek. Marijn Sipkema, jouw komst op de motor naar het RIVM heeft aldaar enige indruk gemaakt. De resultaten van jouw systematische aanpak voor het modeleren van de groei van dierlijke cellen zijn terug te vinden in het metabole deel van hoofdstuk 7. Tot slot, Ellen Nollen, van jouw heb ik het een en ander geleerd over het reilen en zeilen van een studentenvereniging. Jouw werk aan 'gladde' en poreuze microcarriers is terug te vinden in hoofdstuk 6.

Natuurlijk mag het secretariaat niet ontbreken. Hedy, Marijke, Joyce, Maria en Karin bedankt voor al de ondersteunende activiteiten. Voor materialen was ik regelmatig afhankelijk van de glasblazers, die ik hierbij wil bedanken voor de goede en snelle wijze waarop ze voor mij vele reactoren gemaakt hebben.

Gedurende het schrijven van een groot deel van dit proefschrift ben ik werkzaam geweest als Post-doc op de vakgroep Proceskunde. Graag wil ik de medewerkers van de vakgroep

bedanken voor de prettige werksfeer en het niet al te vaak stellen van de vraag wanneer het proefschrift nu eindelijk eens af zou zijn. Speciaal wil ik Klaas van 't Riet en Marcel Zwietering bedanken voor de ruimte die ze mij gegeven hebben om het proefschrift af te ronden. Het geeft geen goed gevoel om als Post-doc niet gepromoveerd te zijn. Verder wil ik Taco, Rob, Leonie, Imke en Marian bedanken voor de vele discussies die we gevoerd hebben over het schrijven van een proefschrift. We zaten samen op wat ook wel de wachtkamer voor promotie genoemd werd.

Het is een cliché, maar ook deze is maar al te waar, 'promoveren doe je niet alleen'. Mijn ouders wil ik bedanken voor de mogelijkheid die zij mij geboden hebben om te studeren. Onze eerste reis naar Wageningen had iets weg van een wereldreis. In de loop van de jaren is de afstand van Westervelde naar Wageningen steeds minder lang geworden en is ze nu bijna even kort als de weg van Wageningen naar Westervelde. Mijn broer wil ik bedanken voor zijn nuchtere kijk op het studentenwereldje, daarbij niet gehinderd door het feit dat hij ook zelf student was. Mijn opa wil ik bedanken voor het bijhouden van mijn 'vakliteratuur' in het Nieuwsblad van het Noorden en diverse agrarische vakbladen. Mijn oma wil ik bedanken voor de bloemen en planten waarmee ze het dagelijkse leven van Christel en mij opfleurde. Tot onze grote spijt kwamen deze promotie en ons trouwen voor haar een aantal maanden te laat.

Mijn schoonouders wil ik bedanken voor hun hulp bij vele praktische dingen van het dagelijks leven. De afronding van het proefschrift heeft iets langer geduurd dan verwacht en ik verbaas mij over het niet aflatend begrip dat mijn ouders en schoonouders hiervoor hebben gehad. In de toekomst zal ik bij bezoekjes mijn laptop proberen thuis te laten.

Dat je promoveren niet alleen doet geldt zeker voor Christel. Met mij is ook zij een beetje gepromoveerd. Gedurende een jaar had onze Haarweg slaapkamer met twee bureaus, twee PC's en de talloze concepthoofdstukken van een proefschrift en een afstudeerverslag veel weg van een kantoor. Belangrijker nog is dat het schrijven van een proefschrift veel beslag legt op de vrije tijd die je met zijn tweeën en samen met vrienden en familie doorbrengt. In de toekomst hoop ik iets minder van deze tijd te verliezen.

## CONTENTS

1	Introduction .....	1
2	Segregated models in animal-cell cultivation .....	11
3	Lethal events during gas sparging in animal-cell culture .....	51
4	Effect of serum concentration on hybridoma viable-cell density and production of monoclonal antibodies in CSTRs and on shear sensitivity in air-lift loop reactors ...	69
5	Effect of dilution rate on growth, productivity, cell cycle and size, and shear sensitivity of a hybridoma cell in a continuous culture .....	83
6	Death rate in a small air-lift loop reactor of Vero cells grown on solid microcarriers and in macroporous microcarriers .....	103
7	A combined cell-cycle and metabolic model for the growth of hybridoma cells in steady-state continuous culture .....	125
8	Use of a combined cell-cycle and metabolic model for the study of hybridoma cells in steady-state continuous culture .....	163
9	General discussion .....	191
	Summary .....	209
	Samenvatting .....	213
	Bibliography .....	217
	Curriculum vitae .....	221

## CHAPTER 1

## INTRODUCTION

Animal-cell cultivation is becoming increasingly important especially for the area of human-health products. The products range from vaccines (measles, polio and hepatitis A) to therapeutic proteins (EPO, TPA,  $\gamma$ -interferon, monoclonal antibodies) and the cells themselves (skin and bone-marrow transplantations). Of these products monoclonal antibodies (MAbs) form an important class. Monoclonal antibodies have the capacity to bind very specifically to a particular molecular structure (epitope), a quality that makes them suitable for application in *in vivo* and *in vitro* diagnostics, separation technology and for the *in vivo* targeting of drugs. For example, MAbs show promise with respect to the treatment of drug toxicity, organ transplantation, auto-immune disease and the *in vivo* imaging and treatment of malignancies<sup>8</sup>. As a result, large quantities of monoclonal antibodies as well as other animal-cell products are

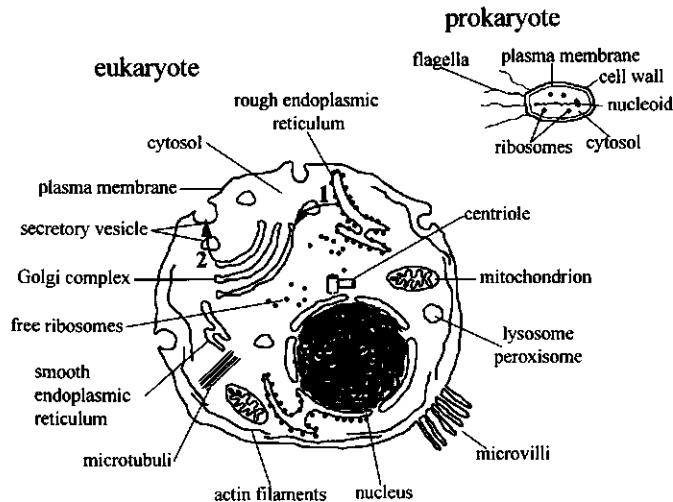


**Figure 1.** Schematic diagram of an eukaryotic animal cell and a prokaryotic cell. The secretion route for a secretory protein is denoted by the numbered arrows. 1) transport of the newly synthesized protein from the rough endoplasmic reticulum to the Golgi complex. 2) transport of the processed protein by secretory vesicles from the Golgi complex to the plasma membrane for secretion.

needed or are expected to be needed in the near future. The therapeutic application of these products puts high demands upon their quality, with respect to purity and primary, secondary, tertiary and quaternary structure. A correct folding and glycosylation is of importance for the activity of the protein, its *in vivo* clearance rate or half life and its possible immunogenicity. In most cases the correct folding and glycosylation can only be accomplished by production in animal cells. However, unlike bacterial and yeast cells, animal cells stem from a multicellular organism and as a consequence have properties that are quite different from those of bacterial and yeast cells. The most important differences are listed in Table I and shown in Figure 1<sup>1</sup>.

Due to their shear sensitivity, complex physiology and the related intricate medium demands, the culturing of animal cells in large-scale bioreactors is relatively difficult and poses specific demands regarding reactor and process design. Because of these specific problems, animal-cell technology has become an important field of research.

**Table I.** Properties of different cell types.

	prokaryote	yeast	animal cell
Size	1-5 $\mu\text{m}$	5-10 $\mu\text{m}$	3-30 $\mu\text{m}$
Plasma membrane	+	+	+
Cell wall	+	+	-
Nuclear envelope	-	+	+
Nucleolus	-	+	+
Endoplasmic reticulum	-	+	+
Ribosomes	+	+	+
Golgi complex	-	+	+
Glycosylation	-	$\pm$	+
Lysosomes	-	+	+
Peroxisomes	-	+	+
Mitochondria	-	+	+
Cytoskeleton	-	+	+
Shear sensitive	-	-	+

## PRODUCTIVITY

The overall productivity ( $\text{kg.y}^{-1}$ ) of an animal-cell culture depends on the product concentration ( $\text{kg.m}^{-3}$ ) in the harvest stream, the time-average harvest rate ( $\text{m}^3.\text{y}^{-1}$ ), and the efficiency of down-stream processing ( $\text{kg.kg}^{-1}$ ). In turn, the product concentration in the harvest stream depends on the specific productivity of the cells, the cell density, and the residence time in the reactor. Some of the main obstacles in animal-cell cultivation to reach high product concentrations and production levels include low productivities, low viable-cell densities, short culture spans, and the occurrence of cell death. Strategies to overcome these obstacles are the

genetic manipulation of cells and process optimisation. These strategies are generally aimed at increasing the specific productivity and the cell density and decreasing the amount of cell death. Examples of genetic manipulation are, for instance, gene amplification to increase the expression level of the desired product, introduction of genes that inhibit cell death and thus increase both, the viable-cell density and the culture span<sup>13</sup>, and the alleviation of metabolic bottlenecks<sup>4</sup>. Examples of process optimisation are, for instance, the reduction of the build-up of toxic products through medium design<sup>7,20</sup>, and the reduction of shear-related cell death through the design of new reactor types as well as the careful design of existing reactors<sup>18</sup>. The occurrence of cell death in bioreactors due to high levels of shear and adverse medium conditions is a main problem in animal-cell cultivation and is the subject of study in this thesis.

## **CELL DEATH**

Cell death may prevent the attainment of high viable-cell densities often required in order to reach high volumetric productivities. In addition, cell death leads to the formation of cell debris and the release of intracellular compounds like proteases, DNA, and under-processed MAbs in the culture fluid. Cell debris interferes with the process itself, for instance, through the fouling of filters and probes. Furthermore, the presence of cell debris and especially DNA puts special demands to down-stream processing in order to attain the required purity of the product. Last, the release of proteases may lead to degradation of the product, which together with the release of under-processed product may seriously affect the quality of the product.

### **Apoptosis and necrosis**

Cell death may follow two different pathways<sup>19</sup> with very distinct physiological and morphological features being apoptosis, or programmed cell death, and necrosis (Fig. 2). Necrosis is essentially a passive process generally caused by high levels of environmental stress where there is no time for the cells to respond to this stress<sup>10</sup>. High levels of stress may for instance be a result of vigorous agitation and air sparging required to supply sufficient oxygen. Necrosis is characterised by the marginal clumping of loosely textured nuclear chromatin, swelling of the cell and its organelles followed by loss of membrane integrity and the destruction of the cell and its organelles<sup>19</sup>. Apoptosis is an active, genetically controlled process occurring at mild stress conditions, where the cells have time to respond to the stress<sup>10</sup>. Mild stress conditions may for instance be nutrient starvation, build-up of toxic products, and mild shear. Apoptosis is characterized by membrane blebbing, cell shrinkage, condensation of nuclear

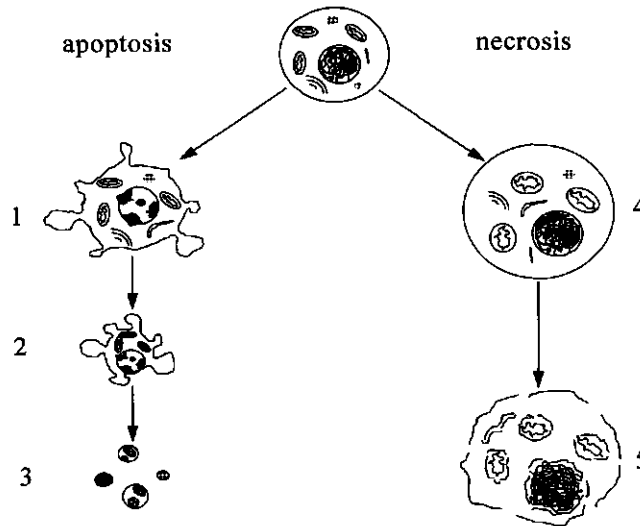


**Figure 2.** Schematic figure showing the main morphological changes during apoptosis and necrosis. Apoptosis: 1, 2) intensive blebbing of the cell; clumping and margination of the chromatin; condensation of the cytoplasm and reduction of the cell volume; 3) fragmentation of the cell into apoptotic bodies. Necrosis: 4) swelling of the cell and of the matrix of mitochondria; 5) disruption of the nuclear, organelle and plasma membranes.

chromatin, nuclear fragmentation, convolution of membranes, and the formation of apoptotic bodies inside which the contents of the dead cell remain<sup>19</sup>. In tissues such apoptotic bodies are phagocytosed and digested by resident cells. In this way the contents of the dying cells are recycled before they are released in the surrounding tissue, where they may damage neighbouring cells and cause inflammation. In bioreactors, however, the apoptotic bodies eventually lose their membrane integrity and their contents are released in the medium. In multicellular living systems harsh environmental conditions do not normally occur and cell death mainly follows apoptosis<sup>19</sup>. Apoptosis plays a role in for example healthy tissues to maintain homeostasis, with the rate of apoptosis balancing that of mitosis, in embryogenesis and metamorphosis, and in the immune system. Furthermore, apoptosis is induced by radiation, cancer chemotherapeutic agents, and nutrient deprivation inside tumours. In bioreactors harsh conditions like sparging as well as mild stresses like the slow occurrence of substrate limitation may occur and, consequently, cells may die through necrosis as well as apoptosis.

### **Cell death through shear**

To obtain the production levels of kilograms or even tonnes on a yearly basis, increase of the harvest rate through scale-up will be necessary. One of the main problems of scale-up in animal-cell cultivation is the supply of sufficient oxygen to the cultures, which requires sparging and intense agitation to disperse the bubbles. Hydrodynamic forces associated with agitation and the bursting of air bubbles are, however, detrimental to animal cells, which has led to the design of bubble-free aeration systems<sup>12</sup>. Although these reactors have been operated successfully<sup>12</sup>, they have a rather complex design and their application scale is limited. At larger scales the use of bubble-column and air-lift reactors may become feasible. These reactors have a relatively simple construction, proven performance and reliability and, even at larger scales, good oxygen- and mass-transfer characteristics. In addition, the mass transfer and hydrodynamic behaviour of these reactors are well documented in literature<sup>9</sup>. Finally, homogeneous conditions can be maintained, which makes it possible to take representative samples and to closely monitor and control the behaviour of the cell culture. Shear forces caused by bursting bubbles are very sudden and quite high, which makes necrosis the most probable mode of cell death. However, apoptotic cell death may occur in these reactors due to lower shear forces caused by liquid flow or for cells further away from the harsh environment of bursting bubbles<sup>3</sup>. The detrimental effects of bursting air bubbles in bubble-column and air-lift reactors may be minimized through a careful reactor design. In addition, shear-protective additives like Pluronic F68 may be added.

### **Cell death caused by adverse medium conditions**

Due to the slow growth and metabolism of animal cells, adverse medium conditions like the depletion of substrates and the build-up of toxic products usually evolve slowly in time. As a consequence, the main mode of cell death in such situations is likely to be apoptosis, at least, if apoptosis may occur in the cell line under study. Thus, the depletion of glutamine, glucose, and oxygen as well as the build-up of lactate and ammonia cause apoptosis in a number of cell types. Nevertheless, also the level of necrosis is increased under these conditions<sup>16</sup>. In general, animal cells consume glucose and glutamine as their main source of energy and building blocks. Part of the energy is generated from the anaerobic conversion of glucose to lactate. In addition, energy may also be generated by the complete oxidation to carbon dioxide and water. Last, energy may be generated from glutamine by glutaminolysis. However, glutamine is not crucial for energy provision but its essential role is to be found in protein and nucleotide synthesis. The consumption of glutamine generally leads to the formation of ammonia. The extent to which the different processes contribute to the energy generation depends on the medium conditions. Since



both lactate and ammonia are toxic for the cells, the anaerobic conversion of glucose as well as the consumption of glutamine should be minimized. This may be reached by a careful medium and process design, which in general means keeping the concentrations of glucose and glutamine at a low, non-limiting level<sup>20</sup> and supplying sufficient oxygen to the culture.

### **Intrinsic cell death**

Even under seemingly optimal conditions always a small amount of cell death occurs, for which there are no clear causes.

### **HYBRIDOMAS**

Hybridoma technology was introduced by Köhler and Milstein<sup>14</sup> in 1975 and embodies the fusion between an antibody-producing cell and its non-producing malignant counterpart. As a result a cloned hybridoma cell line may be grown in suspension culture and is immortal, which makes it suitable for growth in a continuous culture for an unlimited period of time. In addition, a hybridoma cell produces a single monoclonal antibody of predefined specificity, affinity, and isotype, of which in theory unlimited quantities may be obtained. The biosynthesis and secretion of antibody follows the same general pathways as that of other secretory and membrane glycoproteins and is shown in Figure 1. In short, monoclonal antibody light and heavy chains are formed on polyribosomes bound to the cytoplasmic site of the rough endoplasmic reticulum (RER). The secretory forms of the H chains pass the membrane of the RER into the lumen, where assembly of the L and H chains and initial glycosylation takes place. Next, the immunoglobulins are transported to the Golgi apparatus by vesicular transport. In the Golgi apparatus additional processing of the immunoglobulins takes place. Finally, the antibody molecules are transported by vesicles for secretion. Secretion of immunoglobulins is constitutive, however, for an individual cell it may depend on the cell-cycle phase<sup>15</sup>. The composition of the secreted proteins and especially that of the carbohydrate moieties may be affected by the culture conditions. Antibody is secreted in a period between 0.5 to 3 hours<sup>5</sup> after it is synthesized in the RER. Consequently, a substantial amount of not fully processed antibody may be present in the RER, Golgi, and vesicles inside the cell, which may be released in the medium upon cell death<sup>2</sup>. Hybridoma cells in general may die through apoptosis under adverse environmental conditions, which is not surprising if it is realized that both fusion partners stem from the immune system where apoptosis is a fundamental process. A clear disadvantage of hybridoma cells is that they are genetically not very stable, which may for instance lead to the occurrence of a non-producing subpopulation in continuous culture<sup>11,17</sup>.

## THESIS CONTENTS

In Figure 3 a schematic representation of the reactor types used in this thesis is given. In steady-state continuous cultures cells reach a state of balanced growth. In such a situation the average physiological state and the average behaviour of the cells is constant, which greatly facilitates the construction of segregated models. The use of segregated models and related aspects form the subject of Chapter 2, in which also a major class of segregated models, which are based on cell age, is reviewed. From the continuous cultures cells are obtained, which, as stated, have a constant average physiological condition. These cells are used in shear experiments in bubble-column and air-lift reactors at varying conditions.

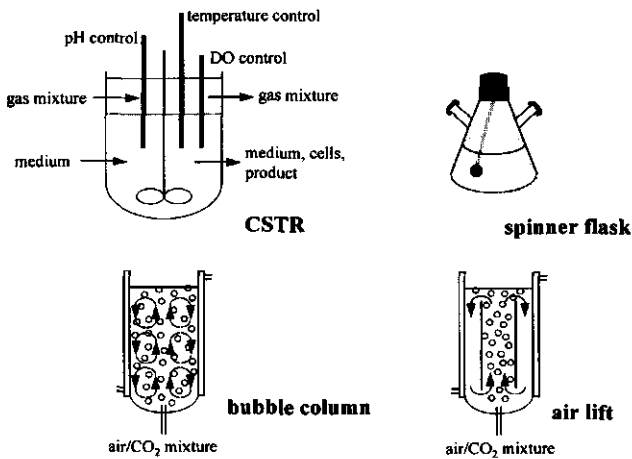


**Figure 3.** Schematic representation of the different reactors used in this thesis. CSTR: Continuous Stirred-Tank Reactor; DO: Dissolved Oxygen.

In Chapter 3 the death of the murine hybridoma cell line, Db2, is studied in small bubble columns at varying heights, diameters, gas flow rates and number of nozzles. In addition, the effect of the shear-protective additive Pluronic F68 is studied. In Chapter 4 the death rate of another murine hybridoma cell line, Mn12, is studied in a small air-lift reactor with an internal loop as a function of the gas flow and the reactor height. Furthermore, the effect of serum on the death rate is examined by changing the serum concentration in the steady-state continuous culture (physiological adaptation) or by adding serum shortly before a shear experiment (only a physical effect). In Chapter 5 a small air-lift reactor is used to determine the shear sensitivity of cells obtained from steady-state continuous cultures operated at different dilution rates. Thus, the shear

sensitivity of the cells is studied as a function of the growth rate of the cells. Besides the shear sensitivity, also the specific death rate, the macroscopic consumption and production rates, the cell-cycle distribution, and the forward scatter of the cells in the continuous culture is determined for the different steady states. In Chapter 6 the death rate of Vero cells on microcarriers is studied as a function of the gas flow rate. In addition, the protection offered by macroporous microcarriers is studied. In microcarrier cultures the amount of available surface for the cells becomes limiting towards the end of the culture. Since new surface cannot be made available to the cells in a continuous manner in a reactor, the use of steady-state continuous cultures is not possible. Thus, the cells are obtained from spinner-flask cultures. To assure that the cells in the different shear experiments have a more or less constant average physiological condition, the cells were harvested from the spinner flasks at a fixed point in the culture period.

As described in Chapter 2, a situation of balanced growth as obtained in steady-state continuous cultures greatly facilitates the construction of segregated models. In Chapter 7 such a segregated model is developed combining a cell-cycle model based on cell age with a metabolic model. Amongst other variables, the model describes the rate of apoptosis, the growth and death rate, the cell-cycle distribution, the consumption and production rates of glutamine, glucose, ammonia, lactate and monoclonal antibody. In Chapter 7 the model is partly validated using literature data. In Chapter 8 the cell-cycle part of the model is evaluated using the data obtained in Chapter 6. In addition, the model is extended with two types of production kinetics. The first is based on the passive release of monoclonal antibody by dead cells, while the second is based on an increased productivity by apoptotic cells as compared with proliferating cells. Finally, in the general discussion in Chapter 9 the hypothetical-killing-volume theory and some aspects of apoptosis are discussed with respect to the results obtained in this thesis. Also implications for reactor and process design are treated.

## REFERENCES

1. Alberts, B., Bray, D., Lewis, J., Raff, M., Roberts, K., Watson, J.D. 1983. *Molecular biology of the cell*. Garland, New York.
2. Al-Rubeai, M., Mills, D., Emery, A.N. 1990. Electron microscopy of hybridoma cells with special regard to monoclonal antibody production. *Cytotechnol.* 4: 13-28.
3. Al-Rubeai, M., Singh, R.P., Goldman, M.H., Emery, A.N. 1994. Death mechanisms of animal cells in conditions of intensive agitation. *Biotechnol. Bioeng.* 45: 463-472.
4. Bell, S.L., Bebbington, C., Scott, F., Wardell, J.N., Spier, R.E., Bushell, M.E., Sanders, P.G. 1995. Genetic engineering of hybridoma glutamine metabolism. *Enzyme Microbiol. Technol.* 17: 98-106.

## Chapter I

5. Bibila, T.A., Flickinger, M.C. 1991. A model of intraorganelle monoclonal antibody transport and secretion in mouse hybridoma cells. *Biotechnol. Bioeng.* **38**: 767-780.
6. Borys, M.C., Linzer, D.I.H., Papoutsakis, E.T. 1994. Ammonia affects the glycosylation patterns of recombinant mouse placental lactogen-I by chinese hamster ovary cells in a pH-dependent manner. *Biotechnol. Bioeng.* **43**: 505-514.
7. Chang, Y.-H., Grodzinsky, A.J., Wang, D.I.C. 1995. Nutrient enrichment and in-situ waste removal through electrical means for hybridoma cultures. *Biotechnol. Bioeng.* **47**: 319-326.
8. Chester, K.A., Hawkins, R.E. 1995. Clinical issues in antibody design. *TibTech.* **13**: 294-300.
9. Chisti, M. Y. 1989. *Airlift bioreactors*. Elsevier Science Publishers LTD, New York.
10. Cotter, T.G., Al-Rubeai, M. 1995. Cell death (apoptosis) in cell culture systems. *TibTech.* **13**: 150-155.
11. Couture, M.L., Heath, C.A. 1995. Relationship between loss of heavy chains and the appearance of nonproducing hybridomas. *Biotechnol. Bioeng.* **47**: 270-275.
12. Henzler, H.-J., Kauling, D. J. 1993. Oxygenation of cell cultures. *Bioproc. Eng.* **9**: 61-75.
13. Itoh, Y., Ueda, H., Suzuki, E. 1995. Overexpression of bcl-2, apoptosis suppressing gene: prolonged viable culture period and enhanced antibody production. *Biotechnol. Bioeng.* **48**: 118-122.
14. Köhler, G., Milstein, C. 1975. Continuous cultured of fused cells secreting antibody of predefined specificity. *Nature* **256**: 495-497.
15. Kromenaker, S.J., Srien, F. 1994. Cell cycle kinetics of the accumulation of heavy and light chain immunoglobulin proteins in a mouse hybridoma cell line. *Cytotechnol.* **14**: 205-218.
16. Mercille, S., Massie, B. 1994. Induction of apoptosis in nutrient-deprived cultures of hybridoma and myeloma cells. *Biotechnol. Bioeng.* **44**: 1140-1154.
17. Merrit, S.E., Palsson, B.O. 1993. Loss of antibody productivity is highly reproducible in multiple hybridoma subclones. *Biotechnol. Bioeng.* **42**: 247-250.
18. Tramper, J., Smit, D., Straatman, J., Vlask, J.M. 1988. Bubble column design for growth of fragile insect cells. *Bioproc. Eng.* **3**: 37-41.
19. Wyllie, A.H., Kerr, J.F.R., Currie, A.R. 1980. Cell death: The significance of apoptosis. *Int. Rev. Cytol.* **68**: 251-305.
20. Xie, L., Wang, D.I.C. 1993. Stoichiometric analysis of animal cell growth and its application in medium design. *Biotechnol. Bioeng.* **43**: 1164-1174.

## CHAPTER 2

### SEGREGATED MODELS IN ANIMAL-CELL CULTIVATION

#### ABSTRACT

The average behaviour of a cell population is the combined result of the random behaviour of individual cells in the population. Description of this average behaviour requires the construction of segregated models and the quantitative specification of the physiological state of individual cells. The application of a general framework for the construction of segregated models, as presented by Frederickson for prokaryotic cells, is discussed with respect to animal cells. The quantitative specification of a physiological state must be a simplified one, because only for a small number of compounds the amount inside individual cells can be measured. For animal cells the simplifications are even more severe due to the higher degree of structural and spatial organisation as compared to prokaryotic cells. Descriptions of physiological state often contain only one or two variables. However, with the progress in flow cytometry an increasing number of compounds can be measured inside individual cells and more detailed physiological-state descriptions are possible.

Based on specific physiological properties, cell populations can often be divided into subpopulations, which facilitates the description of the behaviour of the population as a whole. The subdivision of an animal-cell population into several subpopulations with defined physiological properties is given and incorporated in the framework.

The simplifications that have to be made for describing the physiological state may render the behaviour of a cell population explicitly dependent on time. To eliminate this time dependency the study of cell populations is done in situations of repetitive and balanced growth. The possibility and restraints to attain such a situation for animal-cell populations are addressed in the paper.

In the second part of the paper a number of segregated models using different physiological-state descriptions are presented. Since many segregated models in animal-cell biotechnology are based on cell age, a number of these age-structured models are reviewed. All

these models can describe the average behaviour of a cell population in steady-state continuous culture quite well. However, the presence of non-proliferative cells, as assumed in most age-structured models, is never experimentally verified, while only for one model the segregated nature of the model is evaluated.

## INTRODUCTION

The number of biologicals produced by animal cells as well as their absolute amount ( $\text{kg}\cdot\text{y}^{-1}$ ) has increased markedly during the last decade and is expected to keep increasing in the near future. Products from animal-cell cultivation include vaccines (measles, polio and hepatitis A), therapeutic proteins (EPO, TPA,  $\gamma$ -interferon, monoclonal antibodies) and the cells themselves (skin and bone-marrow transplantations). A distinct group of products is formed by monoclonal antibodies, which because of their specific binding characteristics are used for various purposes such as: purification, diagnostics (*in vivo* and *in vitro*), and immuno therapy (drug targeting)<sup>9</sup>. The amounts required for the therapeutic use of monoclonal antibodies are expected to be as high as 100 mg per dose, which means that required production levels can reach kilograms or even tonnes on a yearly basis. In addition, the therapeutic application of a protein puts high demands to its quality with respect to purity and primary, secondary, and tertiary structure. A correct folding and glycosylation, which is of importance for the activity of the protein, its *in vivo* clearance rate or half life, and its possible immunogenicity, can in most cases only be obtained by production in animal cells.

For optimizing the production process concerning product quality and profitability, one would like to be able to make predictions regarding quality and economic aspects as a function of different process variables, which implicitly means the use of models. In addition, models for predicting animal-cell behaviour are a useful tool in understanding the physiology of the cells and in the design of experiments. Finally, an integrated model of the whole production process may be used for process optimization and control. This paper focuses on the use of segregated mathematical models for describing the behaviour of animal-cell populations. Models in general may be classified according to Figure 1<sup>30</sup>. Two broad groups of models can be discerned being segregated or corpuscular models, and non-segregated or continuum models. In corpuscular models the system behaviour is caused by the concerted action of individual objects. The system is inhomogeneous if length scales of the size of the object are considered. In continuum models this corpuscular nature of reality is ignored and the system is considered to be continuous in space<sup>14,32</sup>. With respect to microbial- and animal-cell culture, segregated models take into account the fact that the biomass is segregated into individual cells, which are different with respect to

some distinguishable traits<sup>30</sup>. The non-segregated models assume that the biomass is uniformly distributed in space and that the cellular nature of biomass is irrelevant.

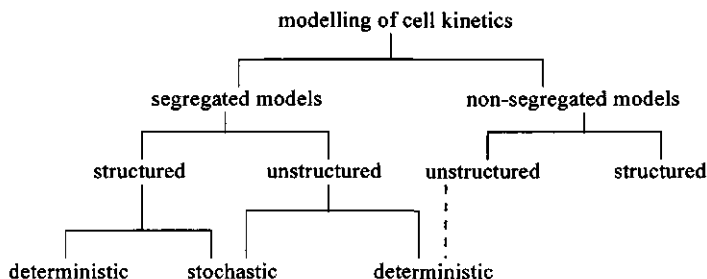


Figure 1. Classification of models after Ramkrishna<sup>30</sup>.

A further subdivision is that between structured and unstructured models. In the unstructured variant of non-segregated models the state of the biomass is assumed to be sufficiently specified by the total number of cells or the total dry weight. In a structured model the biomass is described in greater detail and is divided into two or more 'compartments', which may encompass a single compound or a group of compounds lumped together. In the structured variant of segregated models the structure of the cell is determined by one or more cellular quantities, whereas in the unstructured segregated models the identity of the cell is established merely by its existence<sup>30</sup>. The last point is in contradiction with the fact that in segregated models the cells are different with respect to some distinguishable traits. It therefore seems better to stick to the same way of defining unstructured segregated models as was done for non-segregated models. Thus, in unstructured segregated models the state of the individual cells is assumed to be sufficiently specified by their dry weight or volume. A further important distinction is that between deterministic and stochastic models. In deterministic models the future behaviour can be exactly predicted on the basis of the known physiological state of each cell. With stochastic models it is only possible to specify a probability that the physiological state will be within a certain range of possible physiological states. Stochastic models reflect a lack of knowledge and observability concerning the physiological state and the behaviour of the cells.

The behaviour of a cell population is the combined result of the behaviour of the individual cells in the population. Since the behaviour of individual cells is random and dependent on the composition of the cell, the description of small cell populations requires the development of a model that should be stochastic, segregated and structured. For large populations the random behaviour is averaged out and deterministic models can be used. Fluctuations around the expected value,  $n$ , of the absolute number of cells in a given range of

physiological states and in a given physical volume,  $\Delta V$ , are of the order of  $\sqrt{n}$ . Thus, a total number of  $10^4$  cells gives rise to a fluctuation of about 1%<sup>30</sup>. In culture processes cell numbers are usually much larger than  $10^5$  and the use of deterministic models is allowed. However, in some situations as, for instance, the emergence of a subpopulation of cells, or in continuous cultures operated very near to washout conditions, the number of cells within a specific range of physiological states may become so low that stochastic models have to be used.

In animal-cell populations a distribution of cells exists with respect to their physiological state. Cells with a different physiological state may be expected to contribute to the overall behaviour of the population in different ways and to a different extent. For example, cells in different phases of the cell cycle have been shown to possess quite different characteristics. For instance, the synthesis as well as the secretion of monoclonal antibody has been shown to occur at different rates in different phases of the cell cycle<sup>17,18</sup>. Also the onset of apoptosis has been shown to depend on the cell-cycle phase<sup>11</sup>. Furthermore, the size, morphology, and mechanical properties of a cell change as it progresses through the different cell-cycle phases<sup>26</sup>. Last, from the field of cancer therapy it is known that cells in different phases of the cell-cycle respond differently to drug treatment. From this it is clear that models which take into account the distribution of physiological states are likely to give a better description of the behaviour of a cell population and to be more reliable in scale-up and other extrapolations than their non-segregated counterparts<sup>4</sup>.

Frederickson et al.<sup>12</sup> have presented a general framework for the construction of deterministic segregated models for the behaviour of prokaryotic-cell populations. Animal cells, however, originate from a multicellular organism and are quite different from prokaryotic cells. For instance, animal cells have a more complex physiology, contain several compartments, are larger and are more sensitive to environmental conditions. These differences put special demands, such as the inclusion of growth arrest and cell death, to the construction of segregated models, which will be discussed here. A more general overview concerning all types of models used to describe animal-cell culture processes is given by Tziampazis and Sambanis<sup>41</sup>. In order to construct structured segregated models, first the physiological state of a cell and the state of the environment must be defined. It is assumed here that the environment is spatially homogeneous, which means that the state of the environment,  $c$ , can be described by the concentrations of the various compounds present ( $\text{mol.m}^{-3}$ ) and variables like the temperature ( $^{\circ}\text{K}$ ) and the level of shear ( $\text{N.m}^{-2}$ ).

In this paper, first the description of the physiological state will be discussed together with the consequences of the simplifications made in this description for predicting the behaviour



of a cell population. Next, the way the physiological-state distribution in a cell population changes in time is discussed and special growth situations, where the cell behaviour becomes time independent, are treated. Last, a number of segregated models using different physiological-state descriptions are presented and compared. In the intermezzos the mathematical description of the segregated models is given together with a simple example.

## PHYSIOLOGICAL STATE

The physiological state of a cell is completely defined by the quantities of all compounds making up the cell and the way they are structurally and spatially organised<sup>12</sup>. This will be called the true physiological state of the cell as opposed to the simplified descriptions of physiological state described further on. Clearly, a description of the true physiological state is far too complex from a mathematical and experimental point of view and, consequently, simplifications have to be made.

In a first simplification, the corpuscular nature of the compounds inside the cell is neglected and the cell is considered to be homogeneous at length scales of the compounds present. These length scales range from about  $3 \cdot 10^{-10}$  m ( $O_2$ ) to  $3 \cdot 10^{-8}$  m (ribosomes). This is allowed for molecules present in large amounts where the concentration variations due to Brownian motion can be averaged in time. However, for a number of compounds there may only be a small number of molecules present inside a cell or cell organelle. Consequently, the spatial distribution of these compounds inside the cell will vary with time and the cell cannot be considered homogeneous with respect to these compounds. In this case, neglect of the corpuscular nature will make the behaviour of the cell appear random. This random behaviour will be averaged out if sufficiently large cell numbers are considered.

In a second simplification, Frederickson et al.<sup>12</sup> define the physiological state of a cell by the amounts of the various compounds in the cell and, thus, neglect the structural and spatial organisation of the cell. The cell is assumed to be homogeneous at length scales of the organelles, which range from  $10^{-7}$  m (vesicles) to  $10^{-6}$  m (mitochondria). This is probably allowed for prokaryotic cells, which are relatively small and where the amount of structural organisation is low. However, animal cells contain several compartments such as mitochondria, endoplasmic reticulum, Golgi complex, lysosomes, peroxisomes, and the cell nucleus, which are spatially organized in the cell by the cytoskeleton. Furthermore, animal cells with different functions can show a quite different spatial organisation of organelles<sup>1</sup> and, consequently, it may be expected that the spatial structure is of importance for the behaviour of the cell. The presence of the different compartments may be included in the physiological-state description by describing the

physiological state of each single organelle, leading to a matrix description of the physiological state<sup>12</sup>, or by regarding compounds with the same chemical structure but in different compartments as being different. For example, a protein inside the endoplasmic reticulum may be regarded as being different from the same protein inside the Golgi.

---

### Mathematical

---

The simplified physiological state of a cell, which is obtained through the neglect of the corpuscular nature of the cell compounds and the neglect of the structural and spatial organisation of the cell, may be mathematically represented by a vector  $Z(t)$ :

$$Z(t) = \begin{bmatrix} Z_1(t) \\ Z_2(t) \\ \vdots \\ Z_N(t) \end{bmatrix} \quad (1)$$

with  $Z_i(t)^*$  (mol.cell<sup>-1</sup>) representing the amount of the  $i$ 'th chemical entity in a single cell selected at random from a population of cells at time  $t$ .  $N$  is the number of compounds associated with the cell. Since not all compounds of the cell are known, this definition of the physiological-state vector is still a hypothetical one. The set of all possible physiological-state vectors forms the physiological-state space denoted  $\Upsilon$ . The number density function,  $f_Z(z, t)$  (-), represents the fraction of cells at time  $t$  in an infinitesimal region of state space at physiological state  $z$ , i.e. with a physiological state between  $z$  and  $z+dv$  with  $dv=(dz_1, dz_2, \dots, dz_n)$ . Integrating this number density function over the whole physiological-state space must give unity. A conditional density function,  $f_{Z|z_1}(z, z_1, t)$  (-), may now be defined as the fraction of cells with a physiological state  $Z(t)$  in a large group of cells at a given condition  $z_1$ , which may be a fixed value of a single state variable or of a set of state variables.

#### Example

As an example, it is assumed that the true physiological state can be described by only two state variables  $Z_1$  and  $Z_2$  (mol.m<sup>-3</sup>).  $Z_1$  and  $Z_2$  could for instance be the total protein content and the amount of DNA<sup>17</sup>. In Figure 2 the number density function  $f_Z(z, t)$  is shown for the two physiological-state variables. The conditional density function  $f_{Z|z_1}(z_2, z_1, t)$  now represents the

---

\* After Frederickson<sup>12</sup> a capital letter denotes a random variable, while specific values will be denoted by the corresponding lowercase letter.

fraction of cells with a physiological state  $(z_1, z_2)$  in a large group of cells with a given value  $z_1$ , or more specifically the fraction of cells with a certain total protein content in a large group of cells with a given DNA content. This conditional density function is represented by the line on the surface at  $z_1$ , normalized for the total number of cells with a physiological state  $z_1$

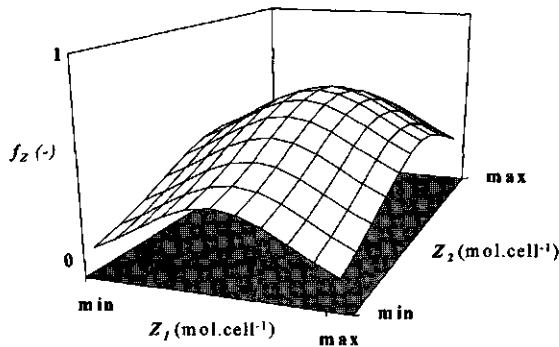


Figure 2. Number density function representing the fraction of cells with a physiological state between  $(Z_1=z_1, Z_2=z_2)$  and  $(Z_1=z_1+dz_1, Z_2=z_2+dz_2)$ .

---

end mathematical

---

## CELL BEHAVIOUR

The behaviour of a cell is defined as the way it qualitatively and quantitatively changes its own physiological state and the state of the environment. The behaviour of a cell can be specified by: intracellular reactions concerning cellular constituents as for example the synthesis of proteins and DNA from precursors; intracellular reactions concerning environmental compounds as for instance substrate uptake, secretion of products, and the passive release of intracellular compounds from dead cells; whether or not cell division takes place; the distribution of cell material over the two daughter cells in the case of cell division.

The behaviour of a cell will be entirely determined by its true physiological state and the state of the environment. In case a simplified description of physiological state is used, a large group of cells at a certain simplified physiological state will consist of cells with a range of different true physiological states and, consequently, contain cells that show a range of different behaviours. The average behaviour of the group of cells will now depend on the relative number of cells within the group at each true physiological state and the cell behaviour associated with this true physiological state.

The corpuscular nature of the cell at length scales of the size of molecules and enzymes may be described by Brownian motion. Because Brownian motion is random, neglect of the corpuscular nature at the mentioned length scales only, will result in the distribution of true physiological states for a large group of cells at a given simplified physiological state and a given environmental state to be constant. Consequently, the average behaviour of a large group of cells will be determined totally by the simplified physiological-state vector and the environmental conditions and will not explicitly depend on time.

In case also the structural organisation of a cell is neglected and the cell is assumed to be homogeneous at length scales of the organelles, the distribution of true physiological states within a large group of cells at a given simplified physiological state may well depend explicitly on time. For instance, in cells with an identical composition the compounds may be distributed differently over the organelles and also the spatial distribution of the organelles may be different. Since the spatial distribution of components over the cell is well organised and not random, it may well structurally change in time at otherwise identical conditions, i.e. at the same simplified physiological state and at the same environmental state. Consequently, the average behaviour of a group of cells at a given simplified physiological state and a given environmental state may change in time and the current behaviour of a cell population as a function of the simplified physiological-state vector and of the environmental state becomes dependent on the history of the cell population. The occurrence of a lag time in batch cultures and the transient behaviour of cells in continuous cultures are examples of this. Of course, the behaviour of a cell does depend implicitly on time due to changes in time of the environmental state and of the simplified physiological-state distribution.

Frederickson et al.<sup>12</sup> now assume that for the simplified state vector as given by Equation (1), where the structural organisation of the cell is neglected, the average behaviour of a cell is totally determined by its simplified physiological state and, thus, does not explicitly depend on time, which is also known as the fundamental simplifying hypothesis (fsh). For prokaryotic cells, where the amount of structure and compartmentalisation is minimal, this assumption is probably valid. However, as stated earlier, animal cells contain different organelles, which are spatially organized in the cell, and the fundamental simplifying hypothesis does not hold.

---

**Mathematical**


---

The different functions specifying cell behaviour may now be defined. For instance, the growth-rate vector is defined by:

$$\dot{Z}(t) = \begin{bmatrix} \dot{Z}_1(t) \\ \dot{Z}_2(t) \\ \vdots \\ \dot{Z}_n(t) \end{bmatrix} \quad (2)$$

with  $\dot{Z}_i(t)$  (mol.cell<sup>-1</sup>.s<sup>-1</sup>) representing the rate with which the amount of the *i*'th chemical compound changes inside a single cell selected at random. If the corpuscular nature of the cell at the length scales of molecules and enzymes is neglected, the behaviour of a cell and, thus, also the rate vector will be random. A conditional density function  $f_{\dot{Z}}|Z(\dot{z}, z, c)$  (-) is now defined representing the fraction of cells with a rate in between  $\dot{z}$  and  $\dot{z} + d\dot{v}$  in a large group of cells with a simplified physiological state  $z$  at environmental conditions  $c$ .  $d\dot{v} = (d\dot{z}_1, d\dot{z}_2, \dots, d\dot{z}_n)$  is a small region in the space of possible rate vectors ( $\dot{\mathbf{T}}$ ). The average rate vector,  $\bar{\dot{Z}}(z, c)$  (mol.cell<sup>-1</sup>.s<sup>-1</sup>), of a group of cells of physiological state  $Z(t)$  will now be given by:

$$\bar{\dot{Z}}(z, c) = \int_{\dot{\mathbf{T}}} \dot{z} f_{\dot{Z}}|Z(\dot{z}, z, c) d\dot{v} \quad (3)$$

Equation (3) represents the integration over the set of all possible rate vectors  $\dot{z}$  multiplied by the fraction of cells with a rate  $\dot{z}$  and physiological state  $z$  at environmental conditions  $c$ . For animal cells the neglect of the structural and spatial organisation of the cell may cause the distribution of true physiological states and the associated distribution of rates,  $f_{\dot{Z}}|Z(\dot{z}, z, c)$ , at a given simplified physiological state and a given environmental state to change with time. Thus,  $f_{\dot{Z}}|Z(\dot{z}, z, c)$  and, consequently, also  $\bar{\dot{Z}}(z, c)$  become explicitly dependent on time and should be replaced by  $f_{\dot{Z}}|Z(\dot{z}, z, c, t)$  (-) and  $\bar{\dot{Z}}(z, c, t)$  (mol.cell<sup>-1</sup>.s<sup>-1</sup>), respectively. Likewise, a division probability function  $\sigma(z, c, t)$  (s<sup>-1</sup>), a partitioning function  $\rho(z, z', c, t)$  (-), and a loss function  $\lambda(z, c, t)$  (s<sup>-1</sup>) are defined where,  $\sigma(z, c, t)dt$  represents the probability that during a time interval  $dt$  a cell with a physiological state  $z$ , at environmental conditions  $c$  will divide,  $\rho(z, z', c, t)$  represents the probability that the division of a mother cell of state  $z'$  in an environment of state  $c$  results in a daughter cell of state  $z$  at time  $t$ , and  $\lambda(z, c, t)dt$  represents the probability that in a time interval  $dt$  a cell of physiological state  $z$  at environmental state  $c$  will be lost from the cell population by means other than division. The time dependence of these functions has the same origin as that of the rate function  $\bar{\dot{Z}}(z, c, t)$  as discussed.

*Example (continued)*

The behaviour and thus the rate vector of a cell is totally determined by the values of  $Z_1$  and  $Z_2$  and the environmental conditions or  $\dot{z}(t) = g[z_1(t), z_2(t), c(t)]$  (mol.cell<sup>-1</sup>.s<sup>-1</sup>), where  $g$  is some unknown function. Thus, assuming a given constant environmental state, the rate vector of a cell at a physiological state  $(z_1, z_2)$  depends totally upon the values  $z_1$  and  $z_2$ . Next, the physiological-state description is simplified by neglecting  $Z_2$  and the simplified physiological-state vector thus only contains  $Z_1$ . A group of cells at a certain simplified physiological state (i.e. value of  $Z_1$ ) will consist out of cells with a range of true physiological states (i.e. values for  $Z_2$ ) and consequently with a range of different rate vectors. The average rate vector of a group of cells at a given simplified physiological state,  $z_1$ , will be determined by the rate vector of the cells at the different possible values for  $Z_2$  and the fraction of cells in the group at the different possible values for  $Z_2$ . Thus, Equation (3) for the simplified physiological-state vector becomes equal to:

$$\bar{\dot{Z}}(z_1, c, t) = \int_{Z_{2,\min}}^{Z_{2,\max}} g(z_1, z_2, c) f_{Z_2|Z_1}(z_2, z_1, t) dz_2 \quad (4)$$

The left term of Equation (4) is the average rate vector of a group of cells at a given simplified physiological state and a given environmental state, which is determined by the rate at different values of  $Z_2$  between its minimum,  $Z_{2,\min}$ , and maximum,  $Z_{2,\max}$ , value and the distribution of cells within this group with respect to  $Z_2$ . In case of the simplified physiological-state vector, the state variable  $Z_2$  and consequently the right terms of Equation (4) are not known and only the left part of the equation can be observed. As discussed, in general the fraction of cells with a true physiological state  $(Z_1, Z_2)$  will change with time in a growing population of cells, meaning the shape of the surface in Figure 2 changes in time. This also means that at a specific value of  $Z_1$ , the distribution of cells with respect to  $Z_2$  changes in time, meaning that the shape of a line on the surface in Figure 2 will change with time. This in turn signifies that the average rate vector of a group of cells as a function of the simplified state vector  $Z_1$  becomes explicitly dependent on time as also seen in Equation (4). The same reasoning can be applied to other functions determining the behaviour of a cell, like the division probability and the distribution of cell contents between the two daughter cells at division.

---

**end mathematical**

---

## OBSERVABILITY

Considering the large amount of different compounds constituting a cell, it is clear that it is not possible to describe nor measure the state of the cell on the basis of all compounds present. In practice, the physiological state is often described by only a few variables. Ideally, these variables should be able to explain the behaviour of the cells within specified limits. For instance, to predict the growth rate of a single cell in terms of increase in mass it may be sufficient to use only the current mass of the cell to describe its physiological state. However, to predict the productivity of a cell it may be necessary to know besides the mass of a cell also the amount of messenger RNA<sup>38</sup> for the pertinent protein or the position of the cell in the cell cycle<sup>18</sup>. The necessity to include certain variables in the physiological-state description in order to explain the cell behaviour is restrained by the demand that the variable should be observable in order to experimentally verify the model. The restraint of observability has been a major drawback for the use of segregated models. In order to determine the distribution of physiological states over a cell population, the value of one or more physiological-state variable(s) must be determined for a large number of individual cells. Whereas population average values for a number of parameters could be obtained experimentally, allowing for the construction of structured non-segregated models, the determination on a cell by cell basis has been difficult. However, with the present progress in flow cytometry an increasing amount of cellular quantities can be measured on a cell by cell basis<sup>4,16,19</sup>. With flow cytometry the amount of a specific compound inside as much as 10,000 individual cells can be measured within minutes. In addition, using the forward-scatter measurements it is possible to measure at the same time the size of the cells and thus calculate the concentration of a compound inside individual cells, which is of great value for use in reaction kinetics<sup>27</sup>. However, with respect to this it is important to realize that for a large number of compounds only a few molecules are present in the cell. In addition, some compounds are confined to specific compartments of the cell. Consequently, the use of macroscopic concentrations and reaction kinetics is questionable. Variables that may be used for the description of the physiological state may be individual compounds like cytoplasmic or membrane-bound antibody or a specific mRNA. Furthermore, a group of related compounds may be lumped into a single pool, which can be used as a state variable. Examples of these last variables are total protein, total DNA, total RNA, total lipids, dry weight, and cell size. An abstract variable to describe the state of a cell is the maturity of a cell. The cell is assumed to pass through a set of defined physiological states between two divisions. The maturity of a cell is its relative progression in this set of defined states. Finally, a major set of segregated models is based on the age of the cell, which is defined as the time that has past since a cell was born.

## SUBPOPULATIONS

Within a cell population subpopulations with certain distinct physiological features can be discerned. From a mathematical point of view it is convenient to divide the total-cell population into different subpopulations with distinct physiological features. Examples of this are the presence of spores and vegetative cells in bacterial-cell populations and of budding mother cells and unbudded daughter cells in yeast cultures. A population of animal cells may be divided into distinct subpopulations as pictured in Figure 3.

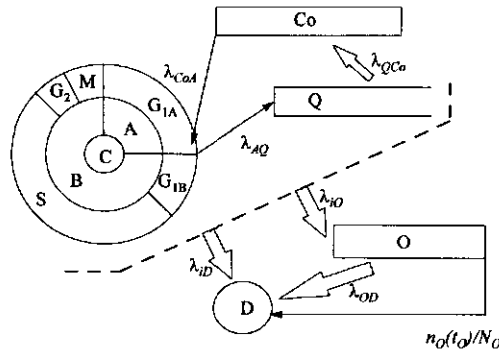


**Figure 3.** Division of an animal-cell population into subpopulations.  $G_{1A}$ ,  $G_{1B}$ ,  $S$ ,  $G_2$ ,  $M$ ,  $A$ ,  $B$ ,  $C$ ,  $Co$ ,  $Q$ ,  $O$ ,  $D$  represent the different subpopulations or phases that may be present in an animal-cell population as described in the text. Thin arrows represent transitions that occur at a defined age, while open arrows indicate transitions occurring at all ages in a subpopulation.  $\lambda_{ij}$  represents the rate constant for the transition from population  $i$  to  $j$  ( $s^{-1}$ ).  $n_O(t_O)/N_O$  ( $s^{-1}$ ) is the number of apoptotic cells of age  $t_O$  ( $s$ ),  $n_O(t_O)$  (cells. $s^{-1}$ ), divided by the total number of apoptotic cells,  $N_O$  (cells). This is equal to the rate constant with which cells leave the apoptotic phase after a fixed residence time  $t_O$ .

## Cell cycle

Between two subsequent divisions a cell passes through a well defined sequence of events called the cell cycle. The cell cycle is divided into four phases on the basis of the DNA content of the cell<sup>1</sup>. In the  $S$  phase of the cycle DNA is synthesized and the DNA content of the cell is doubled. In the  $M$  phase cell division takes place resulting in two new cells each having half the DNA content of the parent cell. Between the  $M$  and  $S$  phase there is a gap phase called the  $G_1$  phase, where cells have a single DNA content. Likewise, between the  $S$  and  $M$  phase a  $G_2$  phase can be found, where cells have a double DNA content. In another approach<sup>35</sup> the cell cycle is divided into an indeterminate phase  $A$ , consisting of part of the  $G_1$  phase ( $G_{1A}$ ) and a determinate phase  $B$ , consisting of a small part of  $G_1$  ( $G_{1B}$ ) and the  $S$ ,  $G_2$  and  $M$  phase. The transition from phase  $A$  to phase  $B$  is a random event and the mean duration a cell spends in phase  $A$  is



determined by a transition probability. While the duration of phase A is variable, the duration of phase B is more or less constant. The intrinsic growth rate of a cell population is determined by the percentage of cycling cells and the duration of the cell cycle.

### **Quiescence and competence**

Besides in one of the mentioned four phases, a state referred to as proliferating or cycling (C), a cell can also be arrested in a quiescent Q phase, a state referred to as non-proliferating or non-cycling<sup>29</sup>. Somewhere in the G<sub>1</sub> phase there exists a point called the restriction (R) point, where a cell decides to either go into the S phase and complete another cycle, or to enter the quiescent Q phase. Arrest of cells in the Q phase may be induced by a number of factors among which medium exhaustion, build-up of inhibitory compounds, presence or absence of specific growth factors, and contact inhibition. Given the right growth factors arrested cells may become competent cells (C<sub>0</sub>), which, if the growth conditions are favourable, return to the cell cycle in the G<sub>1</sub> phase shortly before the start of DNA synthesis. Cells in the Q phase have the same DNA content as G<sub>1</sub>-phase cells, but are usually smaller and have a lower RNA content and protein synthesis rate. In cancer cells, the switching mechanism between proliferation and quiescence at the R point is defective<sup>29</sup>.

### **Cell death by apoptosis and necrosis**

The net or apparent growth rate is the sum of the intrinsic growth rate and the death rate of the cells. Cell death may have a number of causes which may be divided into three categories, being: 1) substrate limitation or the presence of toxic products; 2) hydrodynamic forces; 3) intrinsic cell death, representing the fact that even at seemingly optimal conditions a small amount of cell death always occurs. Cell death may follow two distinct routes with very different features being necrosis and apoptosis<sup>10</sup>. Necrosis is a fast and instantaneous process generally caused by extreme stress conditions such as high hydrodynamic forces or the sudden addition of high levels of a toxic compound, where there is no time for the cell to respond to the stress. Necrosis may occur in all subpopulations described before. Apoptosis is a regulated process generally caused by mild levels of stress such as low shear levels, depletion of nutrients or the slow build-up of toxic wastes, where the cell has time to respond to the stress. The apoptotic process requires time and finally leads to cell death (D) through secondary necrosis<sup>10</sup>. Because apoptotic cells have very distinct physiological characteristics, they form a separate subpopulation (O). Cells may enter the apoptotic phase from all the previous described phases.

However, under certain conditions and depending on the cell line under study, cells may become apoptotic preferentially in a particular phase<sup>11</sup>.

Because the membrane of dead cells is leaky, they may release all kinds of compounds into the medium, like proteases and the product itself. The overall quality of the product may be affected by the proteases as well as by the premature release of not completely processed product. It thus may be necessary to describe the release rate of these compounds from the dead cells and also to model the distribution of physiological states for the dead-cell population.

### **EQUATIONS OF CHANGE**

Frederickson et al.<sup>12</sup> derive the so-called master equations of change describing the change of the distribution of physiological states and the state of the environment as a function of time. The master equations of change can in principle describe all kinds of growth situations as long as the number of cells in a given region of state space is sufficiently high for stochastic variations to be averaged out. In order to use the equations of change, first the physiological-state vector must be specified in such a way that it contains sufficient variables to adequately describe the behaviour of the cell population. However, all state variables must be observable in order to be able to experimentally verify the model. Second, the functions describing the average behaviour of the cells as a function of the physiological and environmental state must be specified. In addition, the initial conditions, i.e. the initial distribution of physiological states and the initial environmental conditions must be specified.

Due to the restraint of observability, the physiological-state description is in most cases reduced to only a few or even only one state variable. Because of the complex physiology of animal cells, it is highly unlikely that the complete behaviour of animal cells can be explained on the basis of only a few state variables. Thus, simplification of the physiological state to a few or only one state variable will certainly make the functions describing the average behaviour of the cells dependent on time. This in turn makes it very difficult to specify these functions. Therefore, the study of animal cells should be conducted under special growth conditions, where simplification of the physiological-state description does not lead to an explicit dependence of the cell behaviour on time. Repetitive growth is such a situation.

---

**Mathematical**


---

The equation of change for the distribution of states is derived by a number balance over an infinitesimal region,  $dv$ , of physiological-state space. The original equation of Frederickson<sup>12</sup> is slightly changed to include the possible existence of subpopulations. The equation of change for subpopulation  $i$  then becomes:

$$\frac{\partial}{\partial t} n_i(t) f_{z_i}(z, t) + \nabla_z [\bar{Z}(z, c) n_i(t) f_{z_i}(z, t)] = \sum_k 2 \int_{\Upsilon_k} \sigma_k(z', c) \rho_k(z, z', c) n_k(t) f_{z_k}(z', t) dv' - \left( \frac{1}{\theta} + \sigma_i(z, c) \right) n_i(t) f_{z_i}(z, t) \quad i, k = 1..N \quad (5)$$

$$- \sum_j \lambda_{ij}(z, c) n_j(t) f_{z_j}(z, t) + \sum_j \int_{\Upsilon_j} \kappa(z, z', c) \lambda_{ji}(z', c) n_j(t) f_{z_j}(z', t) dv' \quad j = 1..N, j \neq i$$

where the subscripts  $i$ ,  $j$ , and  $k$  denote the  $N$  different subpopulations.

The first term on the left side represents the accumulation of cells with a physiological state between  $z$  and  $z+dv$ , where  $n(t)$  is the cell concentration at time  $t$  (cells.m<sup>-3</sup>), which is assumed to be a non-random function of time.

The second term on the left side represents the net increase of the number of cells with a physiological state between  $z$  and  $z+dv$  as a consequence of a change in formation rate of the different biochemical compounds in the cell.  $\bar{Z}(z, c)$  (mol.cell<sup>-1</sup>.s<sup>-1</sup>) contains the mean or expected formation rates of the different biochemical compounds of a cell, which is a function only of the physiological state of the cell and the state of the environment.

The first term on the right side represents the entrance of cells in  $dv$  due to cell division, where  $z'$  denotes the physiological state of the mother cell. For reasons of generality, the first term of the right side contains a summation over all subpopulations, signifying that cells may enter a subpopulation by division from all other subpopulations. In practice, however, cells will always divide in the M phase (phase B) and newborn cells will always enter the G<sub>1</sub> phase (phase A).

The second term on the right side represents the exit of cells out of  $dv$  due to dilution and cell division, with  $\theta$  (s) being the residence time.

Terms are now added for the transition of a cell to and from other subpopulations. Cells leave the subpopulation by transition to another subpopulation as represented by the third term on the right side with  $\lambda_{ij}(z, c) dt$  (-) being the probability for a transition during a time interval  $dt$  of a cell with a physiological state  $z$  in population  $i$  to population  $j$  at environmental conditions  $c$ . Likewise, cells may enter a subpopulation by transition from another subpopulation as represented by the last term on the right side with  $\lambda_{ji}(z', c) dt$  (-) being again the probability that a cell in population  $j$  at physiological state  $z'$  enters population  $i$  in a time interval  $dt$  at

environmental conditions  $c$  and  $\kappa(z, z', c)$  (-) represents the probability that a cell of population  $j$  of state  $z'$ , which moves to population  $i$  enters population  $i$  at a physiological state  $z$  at environmental conditions  $c$ . Although the loss as well as the gain of cells by division theoretically may also be represented by a rate constant  $\lambda$  in the summation terms, it is always treated separately because of the special character of this event.

The formation rate of biochemical compounds inside the cell will depend on the reactions taking place inside the cell and thus, as is done by Frederickson et al.<sup>12</sup>, an expected reaction-rate vector,  $\bar{R}(z, c)$  (mol.cell<sup>-1</sup>.s<sup>-1</sup>), is defined containing the rates of all intracellular reactions of a cell of state  $z$  at environmental conditions  $c$ :

$$\bar{Z} = \beta \cdot \bar{R}(z, c) \quad (6)$$

where  $\beta$  (mol.mol<sup>-1</sup>) is a stoichiometry matrix for the conversion of intracellular substances. To make the description complete, the equation describing the change of the environmental-state vector is given by<sup>12</sup>:

$$\frac{dc}{dt} = \frac{1}{\theta} (c_f - c) + \gamma \int_{\Gamma} \bar{R}(z, c) n(t) f_z(z, t) dV \quad (7)$$

where  $c_f$  is the vector containing the concentrations in the medium feed (mol.m<sup>-3</sup>) and  $\gamma$  (mol extracellular.mol intracellular<sup>-1</sup>) is a stoichiometry matrix for conversion of compounds in the environment.

The functions  $\bar{R}(z, c)$ ,  $\sigma(z, c)$ ,  $\rho(z, z', c)$ ,  $\kappa(z, z', c)$ ,  $\lambda_{ij}(z, c)$  and the matrices  $\beta$  and  $\gamma$  together represent the behaviour of the cell and, according to the fundamental simplifying hypothesis, are only a function of the current physiological and environmental state. The functions  $\bar{R}(z, c)$ ,  $\sigma(z, c)$ ,  $\rho(z, z', c)$ ,  $\kappa(z, z', c)$ ,  $\lambda_{ij}(z, c)$  are random functions due to the neglect of molecular chaos as is the case for  $\bar{Z}(z, c)$ . In addition, these functions may become explicitly dependent on time if the physiological-state vector is further simplified, for example through the neglect of spatial structure.

---

end mathematical

---

## REPETITIVE GROWTH

Repetitive growth is the situation where *the same sequence of cellular events (the 'life cycle' of the cell) repeats itself over and over again, and at the same rate, in all cells of the population*<sup>12</sup>. In case of the presence of different subpopulations this definition of repetitive growth still holds in the sense that in each subpopulation the same sequence of cellular events occurs over and over again at the same rate. However, one can no longer speak of a cycle in all

subpopulations. Thus, in a situation of repetitive growth the cells pass per definition through a defined set of true physiological states and the behaviour of the cells at each of these true physiological states is also per definition independent of time. Since the behaviour of a group of cells at a given true physiological state only depends on the environmental conditions, this means that either the behaviour of the cells is independent of the environmental state or that the environmental conditions are constant. The first is often assumed to occur during the exponential phase of batch culture, while the latter occurs in steady-state continuous culture. In a situation of an asynchronous cell population in repetitive growth, the number density function for the true physiological states is independent of time<sup>12</sup>. Consequently, also the number-density functions for simplified state vectors as well as all other conditional density functions become time independent.

---

**Mathematical**

---

*Example (continued)*

In Figure 2, assuming that the true physiological state can be completely described by  $Z_1$  and  $Z_2$ , this means that the surface does not change in time in case of an asynchronous cell population in repetitive growth. It can then immediately be seen that also the conditional density function  $f_{Z_2|Z_1}(Z_2, z_1, t)$ , as represented by a line on the surface, becomes constant in time, which means the behaviour of the cells at a given simplified physiological state becomes independent of time. Likewise, the number density function  $f_{Z_1}(z_1, t)$  becomes constant in time.

---

**end mathematical**

---

An example of repetitive growth is formed by balanced growth. Growth is balanced over a certain time interval if during that interval every extensive property of the growing system increases by the same factor<sup>7</sup>. For balanced growth to be reached the specific rates of increase of all cell components as well as the specific multiplication rate must be equal and constant in time. This is certain to be true if the number-density function is independent of time and either the environmental conditions are constant or the behaviour of the cells is not dependent on these conditions. For bacterial cells a situation of balanced growth may be attained in continuous culture and it may be approached during exponential growth in batch and fed-batch culture. The attainment of balanced growth for animal cells is more difficult than for bacterial cells for a number of reasons.

First, as already discussed, the physiological-state vector of the animal cells is much more complex than that of bacterial cells. Consequently, it may be expected that a constant distribution of true physiological states will be more difficult to attain.

Second, animal cells have in general lower specific growth rates than prokaryotes, which means that, for instance in continuous culture, it takes longer to reach a situation of balanced growth. This puts higher demands to the operation of these cultures and is a drawback for the number of experiments that can be done within a certain period.

Third, animal cells are about a thousand times larger than bacterial cells and often a minimal inoculation density of about  $10^3$  cells.cm<sup>-3</sup> is required, which has consequences for the attainment of balanced growth in batch cultures. In batch cultures of bacterial cells, assuming an inoculation density of 100 cells.cm<sup>-3</sup>, the cells may grow exponentially for a period of about 15 doublings ( $=3 \cdot 10^6$  cells.cm<sup>-3</sup>), after which they start to change their environment resulting in a reduction of the specific growth rate. Animal cells in batch culture grow exponentially only for about 2-3 doublings after which they start changing their environment, which results in a rapid decrease of the specific growth rate. Consequently, the attainment of balanced growth is very difficult.

Fourth, transformed animal cells are genetically not very stable and consequently the average behaviour and the number-density function for the true physiological state may gradually change in time. This problem is especially important for continuous culture where fast growing cells are selected. Clear examples of this are the occurrence of non-producing cells in continuous culture.

Fifth, at low specific growth rates, a substantial amount of cell death occurs, which makes it difficult to attain a steady state and a situation of balanced growth at these low specific growth rates in batch as well as continuous cultures.

For animal cells balanced growth may be attained in continuous cultures. Furthermore, it may be approached in fed batch and in repeated batch cultures, where cells are transferred to fresh medium before the end of the exponential growth phase, keeping the environmental conditions as constant as possible. For simplified physiological-state vectors balanced growth may be easier to approach in the sense that only the specific growth rate of the population and the distribution of cells for the simplified physiological-state vector are constant. For example, Kromenaker and Srienc<sup>17</sup> show that the distribution functions of total protein becomes independent of time over a short period during batch culture. In the next part some of these simplified physiological-state vectors will be discussed in combination with some models in which they are actually used.

## SINGLE STATE VARIABLES

Until now segregated models based on intracellular compounds have only found a limited number of applications. This is a consequence of the earlier mentioned difficulty in measuring the value of particular physiological-state variables in individual cells. In addition, the physiology of a cell is very complex and there is a lack of knowledge concerning the cellular compounds and the mechanisms that determine the cell behaviour. Therefore, state variables that can be easily measured for individual cells, like cell volume, cell age (DNA content), and total protein content are used for the construction of segregated models.

---

### Mathematical

---

The equation of change for a single cellular state variable,  $S$ , as for instance volume, dry weight, or DNA content is given by:

$$\frac{\partial}{\partial t} n_i(t) f_{S_i}(s, t) + \frac{\partial}{\partial s} [\bar{S}_i(s, c, t) n_i(t) f_{S_i}(s, t)] = \sum_k 2 \int_0^\infty \sigma_k(s', c, t) \rho_k(s, s', c, t) n_k(t) f_{S_k}(s', t) ds' - \left( \frac{1}{\theta} + \sigma_i(s, c, t) \right) n_i(t) f_{S_i}(s, t) - \sum_j \lambda_j(s, c, t) n_j(t) f_{S_j}(s, t) + \sum_j \lambda_j(s, c, t) n_j(t) f_{S_j}(s, t) \quad (8)$$

$i, k = 1..N \quad j = 1..N; j \neq i$

The different terms and symbols in this equation have exactly the same origin as in Equation (5), where  $S$  instead of  $Z$  is the physiological-state descriptor and  $\bar{S}_i(s, c, t)$  (units. cell<sup>-1</sup>. s<sup>-1</sup>) is the average formation rate for the single cellular state variable  $S$ . Due to the simplification, the behaviour of the cells, as expressed by  $\bar{S}_i(s, c, t)$ ,  $\sigma(s, c, t)$ ,  $\rho(s, s', c, t)$ , and  $\lambda(s, c, t)$ , has become explicitly dependent on time. Consequently, although the above equation is valid for any growth situation, it is only useful in a situation of repetitive growth. Furthermore, it is assumed that in the last term of Equation (8) the quantity 's' is conserved upon transition of the cells between two subpopulations.

---

end mathematical

---

### Cell volume

Bell and Anderson<sup>6</sup> describe the behaviour of a cell in terms of the specific growth rate, division probability, and specific death rate, on the basis of cell age and cell volume. Age and volume are chosen as variables to describe the physiological state of the cell, because some reactions as, for instance, DNA replication and the synthesis of certain enzymes proceed sequentially during the life cycle of the cell and the state of these reactions may be characterized by cell age. Other reactions, such as the formation of ATP and the build up of structural

materials, take place throughout most of the cell life cycle and are assumed to depend more on cell volume through factors as diffusion times, surface to volume ratio, and number of ribosomes. Cell volume and cell age are assumed to completely determine the behaviour of the cell, which is thus not explicitly dependent on time. Cell age as a state variable will be discussed further on. A general model is constructed describing the development of a cell population on the basis of cell volume and cell age. The equations constituting the model may be derived from Equation (5) using appropriate boundary conditions. Although cell death is included, only the dynamics of the viable cells are described and Equation (5) is thus used for only one subpopulation with a single  $\lambda$  term describing the death of cells. In the next step, they simplify the physiological-state vector to contain only cell volume by integrating the general equations over all cell ages. As described, simplification leads to a time dependence of the cell behaviour and thus to eliminate this time dependence they only look at the special situation of balanced growth. By assuming cell division is restricted to a certain range of cell volumes and no cell death occurs, they are able to interpret experimentally measured volume spectra of animal-cell populations with the simplified model based on cell volume only.

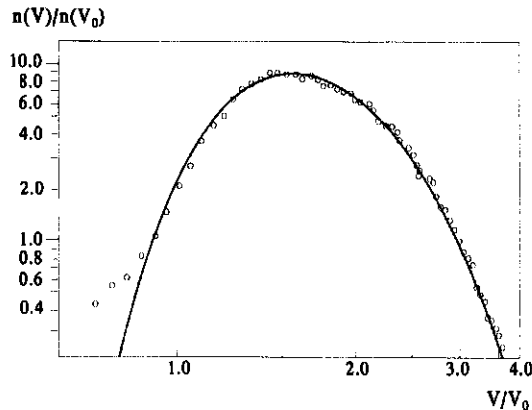


Figure 4. Comparison of a volume spectrum generated by a computer model with an experimental volume spectrum for murine fibroblasts (L cells). Taken from Bell and Anderson<sup>6</sup>.

A good agreement was obtained between an experimental volume spectrum of murine fibroblast (L cells) and the spectrum calculated by the model as shown in Figure 4. The good agreement was obtained for a volume growth rate proportional to the volume of the cells or in other words the volume of a cell increases exponentially. In addition, quite acceptable division probabilities as a function of cell volume were obtained. Only at low volumes the volume spectra show a less sharp edge as predicted, which presumably was due to the assumption of equal



division into daughter cells. Allowing for unequal division into daughter cells resulted in a better agreement of model outcomes with the data according to Bell and Anderson. As suggested in the paper, cell volume may not be a good descriptor of physiological state due to different degrees of hydration. Total protein content or dry weight are proposed to be more closely linked to basic synthesis rates and are thus better state variables.

### **Total protein and intracellular IgG**

Kromenaker and Srien<sup>17,18</sup> measured the distribution function for total protein, intact IgG, and heavy and light chains in a producing and non-producing variant of a hybridoma-cell culture during the exponential growth phase in batch cultures. During the measurement period the specific growth rate and the number-density function for total protein content were shown to be time independent and it was assumed that the culture was in a situation of balanced growth. Next, they calculate the rate of accumulation of total protein, intact IgG, and heavy and light chains as a function of their intracellular concentration inside  $G_1$ , S, and  $G_2/M$  phase cells by means of equations that may be derived from Equation (8). A high rate of protein accumulation was found for  $G_1$ -phase cells with a low total protein content as compared to  $G_1$ -phase cells with a higher total protein content and as compared to S-phase cells. For S-phase cells with a high total protein content the accumulation rate was more or less constant and independent of the pertinent protein content, while for the  $G_2/M$ -phase cells negative accumulation rates were found. Thus, only for a fraction of the  $G_1$ -phase and the S-phase cells an exponential increase in total protein content was observed, which is in contradiction with the exponential increase in volume found by Bell and Anderson<sup>6</sup>. This is probably due to the fact that hybridoma cells are secretory cells while the fibroblasts studied by Bell and Anderson are not. Since a substantial fraction (15%) of the total protein present in the cell consists of IgG, the total protein content of the cell is no longer a good descriptor of the physiological-state of the cell with respect to the increase of total protein and IgG content. In another paper, Kromenaker and Srien<sup>18</sup> show that the accumulation-rate patterns for intact IgG and the heavy and light IgG chains were similar to those of total protein.

### **Antibody-encoded messenger RNA**

Suzuki and Ollis<sup>38</sup> explained the increase in productivity at low dilution rates from the estimated number of monoclonal-antibody-coded messenger RNA per cell in combination with a cell-cycle theory. In the cell-cycle theory it was assumed that all cells are in one of the four phases,  $G_1$ , S,  $G_2$ , or M and are not arrested. Two cases were studied. In the first case, the

transcription and translation rates of mRNA coding for monoclonal antibody are assumed constant throughout the cell cycle. In the second case, the transcription and translation rates are assumed zero during only the M phase or during the M and the G<sub>2</sub> phase. In the other phases the transcription and translation rates are again assumed to be constant. Further, the degradation of mRNA was assumed to be first order in the mRNA concentration. Negative-growth-rate-associated production kinetics is now obtained because at lower specific growth rates the cycle time increases, while the transcription and translation rates stay constant. Consequently, the population average of the number of mRNA molecules per cell increases leading to an increase in productivity. For both cases the model was found to be consistent with the increase in productivity observed when the specific growth rate is decreased by growth inhibitors that do not directly interfere with antibody synthesis. However, quantitatively, deviations occur at low specific growth rates, which is probably due to the fact that the transcription, translation, and degradation rates change with the specific growth rate instead of being constant as assumed in the model. The cell-cycle part of the theory is based on the assumption that the cell population is in balanced growth. Since, the experiments were conducted in batch cultures to which different growth inhibitors were added, the attainment of true balanced growth is questionable, especially when the growth inhibitors are used.

### **Antibody production**

Lee et al.<sup>20</sup> present a population-balance model to describe the loss of antibody productivity due to the appearance and growth of a non-producing cell population. Thus, two subpopulations exist which are discriminated on the basis of their ability to produce antibody. Within each cell population the cells are assumed identical and the degree of segregation of the model is thus minimal. The growth of each subpopulation is assumed to be exponential with different specific growth rates for the producers [ $\mu_p$  (s<sup>-1</sup>)] and non-producers [ $\mu_n$  (s<sup>-1</sup>)], while cell death is neglected. Cells of the producer population are assumed to lose their productivity with a probability,  $p_n$  (-), due to mutation or loss of genetic material, which is realized following division. They show that a stable population of producers and non-producers can be obtained if  $p_n/\ln(2) + \mu_n/\mu_p < 1$ . In all other situations the non-producers take over. The time before the non-producers start appearing in a culture is shown to be highly dependent on the probability of loss of productivity. As described, in the case of the occurrence of a subpopulation of cells it is not allowed to use a deterministic model with a uniform specific growth rate as is done here. Thus, the presented deterministic approach may lead to a wrong calculation of the probability of loss of productivity. The conclusions with respect to the formation of a stable population balance or

the take over by non-producers will, however, not change, because these conclusions are concerned only with time-average values in which case the probabilistic nature will eventually be averaged out.

### Maturity

Cells of a subpopulation pass through a defined sequence of physiological states between the physiological boundaries of the subpopulation as given in Figure 3. Usually these boundaries are given by the moment cells enter the subpopulation to the moment they are destined to exit the subpopulation. For S-phase cells the sequence of physiological states starts with the moment DNA synthesis is initiated and ends with the completion of DNA synthesis, while for the apoptotic phase the sequence starts with the first apoptotic event and ends with the membrane of these cells becoming permeable to trypan blue. The maturity,  $\Omega$  (-), is now an unspecified measure of the relative progression of the cell in this sequence of physiological states. An important difference with the other physiological-state descriptions using only a single state-variable is that the boundaries are sharply defined. Thus, cells per definition divide at a maturity of one and newborn cells per definition have a maturity of zero. Likewise, for a number of transitions cells leave a sub-population at a maturity of one and enter a subpopulation at a maturity of zero. Notably, a cell may exit a subpopulation before it has passed through the complete sequence of physiological states. For instance, S-phase cells may become apoptotic or die through necrosis before DNA synthesis has been completed. However, if DNA synthesis is completed the cells enter per definition the  $G_2$  phase at zero maturity. Likewise, a cell may enter a subpopulation at a non-zero maturity. For instance, a competent cell may reenter the  $G_1$ -phase shortly before the onset of DNA synthesis. The maturity of cells in different subpopulations may be measured in different ways. Thus, the maturity of S-phase cells may be determined by their relative DNA content. Likewise, the maturity of a quiescent and competent cell may be based on its total protein or RNA content. In specifying the maturity of a cell in a certain subpopulation the physiological-state description and the equations of change become, apart from the boundary conditions, more or less equal to those using other single state-variables.

---

### Mathematical

---

The equation of change for the state variable maturity is now given by:

$$\frac{\partial}{\partial t} n_i(t) f_{\Omega_i}(\omega, t) + \frac{\partial}{\partial \omega} [\bar{\Omega}_i(\omega, c, t) n_i(t) f_{\Omega_i}(\omega, t)] = -\frac{1}{\theta} n_i(t) f_{\Omega_i}(\omega, t) - \sum_j \lambda_{ij}(\omega, c, t) n_j(t) f_{\Omega_i}(\omega, t) + \sum_j \int_0^1 \lambda_{ji}(\omega', c, t) \kappa_{ji}(\omega, \omega', c, t) n_j(t) f_{\Omega_j}(\omega', t) d\omega' \quad i, j = 1 \dots N; i \neq j \quad (9)$$

The terms are again mainly the same as in Equation (5) and (8). The first term on the left side represents the accumulation of cells with a maturity between  $\omega$  and  $\omega+d\omega$  (-), where  $f_{\Omega_i}(\omega, t)(-)$  represents the fraction of cells with a maturity between  $\omega$  and  $\omega+d\omega$ . The second term represents the increase in cells with a maturity between  $\omega$  and  $\omega+d\omega$  as a consequence of a change in the average maturation rate  $\bar{\bar{\Omega}}(\omega, c, t)$  ( $s^{-1}$ ). The first term on the right side represents the exit of cells due to dilution out of the system. The second term on the right side represents the transition of cells with a maturity between  $\omega$  and  $\omega+d\omega$  to another subpopulation with  $\lambda_{ij}(\omega, c, t)dt$  (-) representing the probability for a transition from population  $i$  to  $j$  in a time interval  $dt$  for a cell of maturity  $\omega$  at environmental conditions  $c$ . The last term on the right side represents the increase in cells with a maturity between  $\omega$  and  $\omega+d\omega$  due to transition from another population. Cells that leave a certain population with a maturity  $\omega'$  will not necessarily enter the other population with the same maturity. Thus, a function  $\kappa(\omega, \omega', c, t)$  is introduced which represents the probability that a cell leaving population  $j$  with a maturity  $\omega'$  enters population  $i$  with a maturity  $\omega$  at environmental conditions  $c$ .

The behaviour of the cells as expressed by the functions  $\bar{\bar{\Omega}}(\omega, c, t)$ ,  $\kappa(\omega, \omega', c, t)$  and  $\lambda_{ij}(\omega, c, t)$  again is dependent on time, which restricts the usefulness of Equation (9) to situations of repetitive growth.

The important difference with Equation (8) is that cells per definition divide at a given maturity and newborn cells enter a population also per definition at a given maturity. Consequently, the terms that describe the loss and gain of cells due to cell division have disappeared from Equation (8) and are present in the boundary conditions. Likewise, also transitions between cell populations that occur at defined maturities appear in the boundary conditions. Boundary conditions for the subpopulations described in Figure 3, with the cell cycle divided into phase A and B and the maturity normalized between 0 and 1, are given in Table I.

**Table I.** Boundary conditions for the maturity models. The subscripts A, B, Co, Q and O denote the different subpopulations.

$n_A(t)\bar{\bar{\Omega}}_A(0, c, t)f_{\Omega_A}(0, t) = 2n_B(t)\bar{\bar{\Omega}}_B(1, c, t)f_{\Omega_B}(1, t)$	<b>B1</b>
$n_B(t)\bar{\bar{\Omega}}_B(0, c, t)f_{\Omega_B}(0, t) = p_B(c, t)n_A(t)\bar{\bar{\Omega}}_A(1, c, t)f_{\Omega_A}(1, t) + n_{Co}(t)\bar{\bar{\Omega}}_{Co}(1, c, t)f_{\Omega_{Co}}(1, t)$	<b>B2</b>
$n_Q(t)\bar{\bar{\Omega}}_Q(0, c, t)f_{\Omega_Q}(0, t) = (1 - p_B(c, t))n_A(t)\bar{\bar{\Omega}}_A(1, c, t)f_{\Omega_A}(1, t)$	<b>B3</b>
$n_O(t)\bar{\bar{\Omega}}_O(0, c, t)f_{\Omega_O}(0, t) = \sum_j \int_0^1 \lambda_{jO}(\omega, c, t)n_j(t)f_{\Omega_j}(\omega, t)d\omega \quad j=A, B, Q, Co$	<b>B4</b>

Boundary condition B1 expresses the fact that the rate with which cells enter phase A is twice the rate with which cells leave phase B through division. Boundary condition B2 states that the rate with which cells enter phase B at a zero maturity is equal to the sum of rates with which cells leave phase A at a maturity of one multiplied with the probability,  $p_B(c,t)$  (-), that a cell leaving phase A enters phase B and the rate with which competent cells leave phase Co at a maturity of one and enter phase B. Boundary condition B3 states that the rate with which cells enter the quiescent phase at a maturity of zero is equal to the rate with which cells leave phase A at a maturity one multiplied with the probability  $(1-p_B(c,t))$  that a cell leaving phase A enters phase Q. The last boundary condition, B4, states that the rate with which cells enter the apoptotic phase at a maturity of zero is equal to the rate with which they leave all of the other phases at all maturities to become apoptotic. The transition of the quiescent phase to the competent phase is not included in the boundary conditions due to a lack of knowledge concerning this event. Table I may be extended with boundary conditions for the dead-cell subpopulation and the  $G_{1A}$ ,  $G_{1B}$ , S,  $G_2$  and M phase if desired.

---

**end mathematical**

---

### Cell age

A great deal of segregated models found in literature are based on cell age, which is assumed to represent the physiological state of the cell. The age of a cell in a certain subpopulation is defined as the time elapsed since it entered the subpopulation<sup>8</sup>. Consequently, the rate with which a cell becomes older as a function of time is per definition equal to unity. A major problem of using cell age as a description of state is that a particular cell age may represent different physiological states for different situations of balanced growth. First, imagine a situation where cells may only be in a cycling phase C as pictured in Figure 3 and cells pass through a defined set of physiological states between birth and the next division. Each physiological state may now be given a certain maturity. In a situation of balanced growth with a certain specific growth rate a cell will pass through this set of physiological states or maturities with a maturation rate that only depends on the current maturity of the cell and is independent of time. In such a situation the duration of the cycle is constant and the age of the cell represents a certain maturity or physiological state. At another situation of balanced growth at a defined, but lower, specific growth rate the maturation rate will be slower and the duration of the cycle will become longer. A certain maturity will now still correspond to the same physiological state. However, due to the elongation of the cell cycle and the lower maturation rate the age of the cell will now represent a different physiological state as compared to the higher specific growth rate.

Second, cells that return from the competent state to the  $G_1$  phase shortly before the start of DNA synthesis have a zero age. On the other hand cells that have just divided and have entered the cell cycle at the start of  $G_1$  also have a zero age. Thus, cells at different positions in the cycle and with a different physiological state both have an age of zero. This problem may be solved by regarding cells before and after the re-entry point in the cell cycle as belonging to different cell populations. Thus, cells that return to the cycle from the competent phase are assumed to re-enter at the start of phase B and thus have the same age as cells that enter phase B from phase A

A clear advantage of the maturity as a variable over cell age is thus that a subpopulation of cells of a given maturity always represents the same set of physiological states. In contrast, cells of a given age may under different conditions represent different sets of physiological state. In addition, the maturity concept allows cells to enter a subpopulation at each maturity, while in the age models cells enter a population per definition at age zero. Last, in the maturity models a cell may move to a less mature state, whereas in the age models a cell always becomes older. Therefore, the maturity concept is probably better for the construction of dynamic models. However, since the aging rate is always one and cells always enter a subpopulation at an age of zero, the equations for age as a physiological-state variable are less complex than the equations for the maturity. Consequently, models based on age are easier to solve.

---

### Mathematical

---

For age as a variable Equation (5) now becomes:

$$\frac{\partial}{\partial t} n_i(t) f_{A_i}(a, t) + \frac{\partial}{\partial a} n_i(t) f_{A_i}(a, t) = -(\Gamma_i(a, c, t) + \frac{1}{\theta}) n_i(t) f_{A_i}(a, t) - \sum_j \lambda_{ij}(a, c, t) n_i(t) f_{A_i}(a, t) \quad (10)$$

The first term again represents the accumulation of cells with an age between  $a$  and  $a+da$  (s). The second term is the net accumulation due to aging. Since the aging rate is equal to unity, it is no longer present in Equation (10). The first term on the right side represents the loss through division with  $\Gamma(a, c, t) dt$  (-) being the probability that a cell of age  $a$  will divide at environmental conditions  $c$  during a time interval  $dt$  at time  $t$ , which is comparable to the  $\sigma$  term in the previous equations. The second term on the right side represents loss by dilution and the third term represents loss by transition to another subpopulation with  $\lambda_{ij}(a, c, t) dt$  (s<sup>-1</sup>) being the probability of transition from population  $i$  to  $j$  for a cell of age  $a$  in a time interval  $dt$  at environmental conditions  $c$ . Since cells enter a subpopulation per definition at an age of zero, the terms for entrance of cells through division and transition from another subpopulation appear in the boundary conditions. Likewise, if cells leave a subpopulation at a defined age the terms will

also appear in the boundary conditions. Boundary conditions for the subpopulations as shown in Figure 3 are given in Table II, where the cell cycle is divided in phase A and B. For these boundary conditions it is assumed that cell division and the transitions from phase A to phase B and Q, from phase Co to phase B, and from all phases to phase O occur at a range of different ages.

**Table II.** Boundary conditions for the age models. The subscripts A, B, Q, Co and O denote the different subpopulations.

$n_A(t)f_{AA}(0,t) = 2 \int_0^\infty n_B(t)\Gamma(a,c,t)f_{AB}(a,t)da$	<b>B5</b>
$n_B(t)f_{AB}(0,t) = \int_0^\infty n_A(t)\lambda_{AB}(a,c,t)f_{AA}(a,t)da + \int_0^\infty n_{Co}(t)\lambda_{CoB}(a,c,t)f_{ACo}(a,t)da$	<b>B6</b>
$n_Q(t)f_{AQ}(0,t) = \int_0^\infty n_A(t)\lambda_{AQ}(a,c,t)f_{AA}(a,t)da$	<b>B7</b>
$n_O(t)f_{AO}(0,t) = \sum_j \int_0^\infty \lambda_{jO}(a,c,t)n_j(t)f_{Aj}(a,t)da \quad j=A,B,Q,Co$	<b>B8</b>

Boundary condition B5 describes that the number of cells that divide in phase B at different ages equals the number of cells that enter phase A at an age of zero. Boundary condition B6 states that the number of cells entering phase B at age of zero equals the sum of the number of cells going from phase A to phase B and the number of cells leaving the competent phase Co at different ages. Boundary condition B7 gives the number of cells entering the quiescent phase at age zero from phase A. Last boundary condition B8 states that the number of cells entering the apoptotic phase at an age of zero is equal to the sum of the number of cells that become apoptotic in all other phases at different ages.

**end mathematical**

Age-structured population theory for cell populations has been extensively described in theory and analytical solutions of Equation (10) are given for a number of special situations<sup>33,39,40,42</sup>. It is not within the scope of this paper to review this work. Moreover an extensive monograph has appeared covering the mathematical theory of continuous nonlinear models of populations with age structure<sup>43</sup>. Here the use of age-structured models in animal-cell biotechnology will be addressed.

With respect to animal-cell biotechnology only a limited number of segregated models based on cell age have been presented until now. These models are mainly focussed at predicting

the often reported increase in average productivity and specific death rate of hybridoma cells at decreasing dilution rates in steady-state continuous culture. It is assumed that a population of hybridoma cells can be divided into a subpopulation of proliferative or cycling cells and a subpopulation of non-proliferative or arrested cells. The non-proliferative cells are next assumed to have a higher productivity and specific death rate. Consequently, an increase of the fraction of this subpopulation at decreasing dilution rates leads to an increase in the productivity and specific death rate as observed. In the next section the models presented by Suzuki and Ollis<sup>37</sup>, Linardos et al.<sup>21</sup>, Cazzador and Mariani<sup>8</sup>, and Martens et al.<sup>22,23</sup> will be discussed and compared. All authors used the continuous-culture data presented by Miller et al.<sup>24</sup> for model evaluation, which makes it easy to compare the different models.

### *Suzuki and Ollis*

In the cell-cycle model of Suzuki and Ollis<sup>37</sup> cells may be found in a cycling (C) or arrested phase (Q) as depicted in Figure 3, while the apoptotic, competent and dead-cell phase are not considered. In the model, cells may get arrested in phase Q at the end of the G<sub>1</sub> phase. Cells in all subpopulations are characterized by the same specific death rate. The fraction of arrested cells and the cycle time are next related to the dilution rate and viability by the next relation:

$$\mu = \frac{D}{v} = (1 - f_Q) \frac{\ln(2)}{t_C} \quad (11)$$

Where  $\mu$  (s<sup>-1</sup>) is the specific growth rate,  $v$  (s<sup>-1</sup>) is the viability,  $f_Q$  (-) is the fraction of arrested cells and  $t_C$  (s) is the cycle time. The productivity,  $q$  (g.cell<sup>-1</sup>.s<sup>-1</sup>), is next given by:

$$q = (1 - f_Q)k_C + f_Qk_Q \quad (12)$$

where  $k_C$  and  $k_Q$  (g.cell<sup>-1</sup>.s<sup>-1</sup>) are the productivities of the cycling and arrested cells, respectively. Three different cases are studied. In case 1 the fraction of arrested cells is assumed to be zero at all dilution rates and the cycle time changes with the specific growth rate as given by Equation (11). The increase in average productivity at lower dilution rates is obtained by assuming a higher productivity of the G<sub>1</sub> cells, the fraction of which increases at lower dilution rates. In case 2 the cycle time is assumed constant and the fraction of arrested cells changes with the specific growth rate. The increase in average productivity at lower dilution rates is obtained by assuming a higher productivity of the arrested cells, the fraction of which increases at lower dilution rates. The most interesting case is case 3 where the model is fitted to the productivity data of Miller



et al.<sup>24</sup>. The productivity of the arrested cells,  $k_D$ , is obtained by extrapolating to a situation where all cells are arrested while the productivity of the cycling cells,  $k_C$ , is obtained by extrapolating to the situation where all cells are in the cycling phase. Assuming these productivities are constant, the model is fitted to the productivity data, which gives the fraction of arrested cells [Eq. (12)] and the cycle time at each dilution rate [Eq. (11)]. For high dilution rates the fraction of arrested cells has an almost constant value of 2 %, while the cycle time increases at decreasing dilution rates. At low dilution rates the cycle time becomes constant and the fraction of arrested cells increases at decreasing dilution rates.

Notably, the mathematical model of Suzuki and Ollis<sup>37</sup> does not correspond to their verbal model. Their mathematical model corresponds to a situation where cells enter the arrested phase from every position in the cell cycle with an equal first-order rate constant and the cells do not return from the arrested phase to phases A and B. This has been observed by Cazzador and Mariani<sup>8</sup>, who give the correct mathematical formulation for the verbal model of Suzuki and Ollis.

#### *Linardos et al.*

The model of Linardos et al.<sup>21</sup> includes phase A, B and Q as depicted in Figure 3. Newborn cells enter in phase A at age zero and move randomly from this phase to phase B with a rate  $\lambda$  ( $s^{-1}$ ) that is independent of the age of the cell. In addition, cells may leave phase A through cell death and dilution out of the reactor. Cells in phase A with an age equal to a certain critical age,  $T_C$  (s), shift to the arrested phase Q. Cells in the arrested phase are characterized by a higher specific death rate and monoclonal-antibody production rate. In addition, the arrested cells are assumed to move randomly to phase B with the same rate  $\lambda$  as the phase-A cells. As the dilution rate decreases the duration of phase B stays constant while that of phase A increases. Consequently, as the duration of phase A increases, the fraction of arrested cells increases, which results in an increase in the population average productivity and specific death rate. The model is used to describe steady-state data of Miller et al.<sup>24</sup> and their own data. The productivities of the arrested and cycling cells are first estimated from experimental data. Next the fraction of arrested cells is calculated according to previously described case 3 [Eq. (12)] of the model of Suzuki and Ollis<sup>37</sup>. Using the fraction of arrested cells, the death-rate constants of the arrested cells and phase-A and phase-B cells were estimated from the experimental measured specific death rates by least-square regression. Finally, the value of the critical age was estimated by fitting the model-calculated fraction of arrested cells to the fraction calculated from the productivities. The model could be fitted well to the data with respect to the specific death rate

and the productivity, which are shown together with the model-calculated fraction of arrested cells in Figure 5.

As reviewed by Cazzador and Mariani<sup>8</sup>, the time a cell spends in phase A is not correctly calculated because the generation time is not in general equal to the duplication time. This will lead to a somewhat smaller, value for the critical-age parameter.

#### *Cazzador and Mariani*

In the model presented by Cazzador and Mariani<sup>8</sup> the inconsistencies of the models of Suzuki and Ollis<sup>37</sup> and Linardos et al.<sup>21</sup> are overcome. The model is based on the hypothesis that there is a critical compound or factor, dependent on growth conditions, that controls the cell arrest. Cells at the point of entering phase B become arrested if they do not contain a certain minimal amount of the critical factor. Arrested cells may next return to the cycle if they increase this factor to the required level. For the probability of cell arrest,  $p_Q$  (-), the next sigmoidal function is derived:

$$p_Q = \frac{K^n}{\mu^n + K^n} \quad (13)$$

Where  $\mu$  ( $s^{-1}$ ) is the specific growth rate of the cycling cells and  $K$  ( $s^{-1}$ ) is the median point, being the value of  $\mu$  where  $p_Q=0.5$ . The probability of a cell to return to the cell cycle,  $\xi_Q$  (-), is next given by:

$$\xi_Q = \frac{D + b_Q}{D + c_Q} \quad (14)$$

where  $D$  ( $s^{-1}$ ) is the dilution rate, and  $b_Q$  and  $c_Q$  ( $s^{-1}$ ) are constants with  $b_Q/c_Q$  representing the minimum recovering fraction for  $D=0$   $s^{-1}$ . Two different model situations are considered. In the first situation, the restriction case, cell arrest is assumed to occur at the end of phase A with a probability  $p_Q$ . In the second situation, the competence case, cell arrest is assumed to occur at the beginning of a new cycle, before entering phase A, with a probability  $p_Q$ . For each of the two model situations two cases are studied with respect to the transition from phase A to phase B and Q. In one case cells are assumed to exit phase A at a fixed age,  $T_A$  (s), while in the other case cells are assumed to leave phase A at a constant rate,  $\lambda_A$  ( $s^{-1}$ ). Both  $T_A$  and  $\lambda_A$  depend on the growth conditions. Furthermore, in all cases arrested cells are characterized by a higher specific death rate and monoclonal-antibody production rate. The model is evaluated with respect to the data of Miller et al.<sup>24</sup> and the 9 model parameters are estimated from these data. The model

outcomes (Fig. 5) showed that there is an optimal dilution rate at which the specific production rate is maximal, which is not seen in the data of Miller et al.<sup>24</sup>. However, this optimal dilution rate is lower than the lowest dilution rate measured by Miller et al.<sup>24</sup>. Moreover, like with the models of Suzuki and Ollis<sup>37</sup> and of Linardos et al.<sup>21</sup>, model outcomes are only compared regarding the production-, death- and growth-rate data and not with respect to age distributions or the fractions of cells in each subpopulation. Thus, at the moment there is no real experimental support for the segregated part of these models.

*Martens et al.*

In the model of Martens et al.<sup>22</sup> it is assumed that hybridoma cells cannot be arrested in a quiescent phase Q due to a defective control mechanism in G<sub>1</sub>. Consequently, the quiescent and competent phase are not present in the description shown in Figure 3. Instead, it is assumed that cells become apoptotic if the growth conditions get unfavourable and the specific growth rate drops below a critical value. Cells enter the apoptotic phase from phase A and B with a rate independent of their age. Thus, for specific growth rates below the critical value the duration of phase A is assumed constant, while the rate with which cells become apoptotic increases as the specific growth rate decreases. Above the critical specific growth rate, the duration of phase A decreases at increasing specific growth rates and no cells enter the apoptotic phase. It is assumed that apoptotic cells die at a fixed age, decrease in volume with increasing age, and consume no glucose and glutamine. Consequently, below the critical value of the dilution rate, a decrease in dilution rate leads to an increase in the rate with which cells become apoptotic, an increase in the population-average specific death rate, and a decrease of the average cell volume. The model could predict the steady-state data of Miller et al.<sup>24</sup> with respect to cell numbers, glucose, glutamine, lactate and ammonia concentrations and the specific growth and death rate. In a second paper, the segregated aspect of the model, i.e. the distribution of the cells over the different subpopulations, is evaluated by comparing model calculations for the fraction of cells in the G<sub>1</sub>, S, G<sub>2</sub>, and M phase to experimental data<sup>23</sup>. The S-phase fraction could be predicted quite well. However, the G<sub>1</sub> and G<sub>2</sub>/M fraction were not predicted very well, which may have been due to cells entering the apoptotic state preferentially from one phase. In addition, the cell-cycle fractions could be well predicted if it was assumed that the duration of the G<sub>2</sub>/M phase was not constant, but increased from 1.8 to 3.8 hours as the specific growth rate decreased from the maximum to the critical value. Furthermore, it is shown that the model-predicted cell volume, which is calculated from the fraction of apoptotic cells, was proportional to the forward scatter as measured by flow cytometry. The increase in productivity at decreasing dilution rates could

be explained by passive release of antibody from dead cells as well as by an increased productivity of apoptotic cells. Last, on the basis of literature<sup>25,36</sup> the sharp transition from a situation of no apoptosis above the critical specific growth rate to a situation of constant cell-cycle duration below the critical specific growth rate seems to be unlikely and is replaced by a more gradual transition. The model results for the specific death rate, productivity and fraction of arrested cells are shown in Figure 5 for the sharp-transition case.

### Comparison of the age models

With respect to the specific death rate and the productivity, the models of Linardos et al., Cazzador and Mariani, and Martens et al. all give a good prediction of the data and only show minor differences for the range of dilution rates studied by Miller et al.<sup>24</sup>. At lower dilution rates the model of Cazzador and Mariani predicts a maximum value not predicted by the other models. In addition, the values predicted by the model of Martens et al. are higher than those given by the other models at low dilution rates.

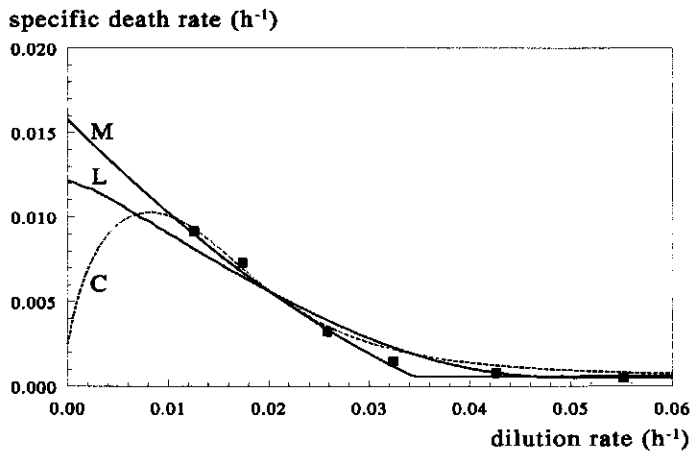


**Figure 5A.** Specific death rate as a function of the dilution rate. Measured specific death rates by Miller et al. (■), and computed specific death rates by: Linardos (L, —), Cazzador (C, ..... ) and Martens (M, —). For the model of Cazzador and Mariani the model predictions for the different cases only differ slightly for the specific death rate and only the results for the restriction case with the cells leaving phase A after a constant time period (case R(a)) are shown. For the model of Martens et al. the sharp-transition case is shown.

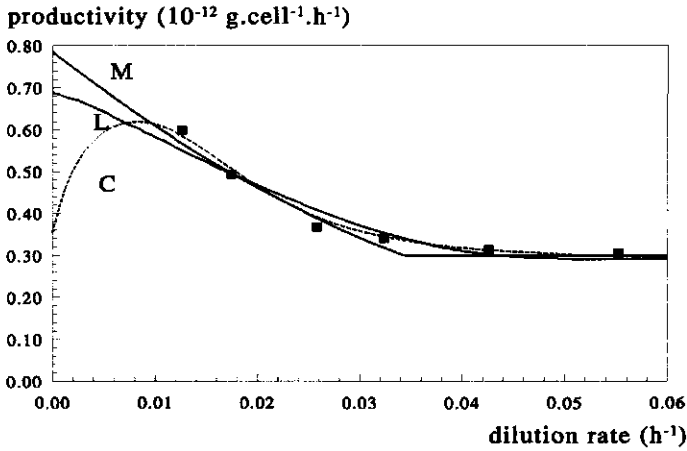


**Figure 5B.** Productivity as a function of the dilution rate. Measured productivities by Miller et al. (■), and computed productivities by: Linardos (L, —), Cazzador (C, ..... ) and Martens (M, —). For the model of Cazzador and Mariani the model predictions for the different cases only differ slightly for the productivity and only the results for the restriction case with the cells leaving phase A after a constant time period (case R(a)) are shown. The model predictions of Martens et al. are for the case of passive release of antibody from dead cells and a sharp transition.

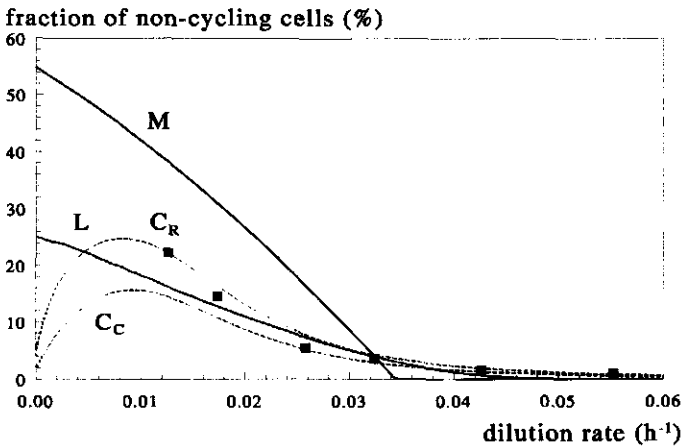


**Figure 5C.** Model predictions for the fraction of arrested cells as a function of the dilution rate. Suzuki et al. (■), Linardos (L, —), Cazzador case R ( $C_R$ , .....), Cazzador case C ( $C_C$ , ..... ) and Martens (M, —). For the model of Cazzador and Mariani the model predictions of the restriction and competence case with the cells leaving phase A after a constant time period (case R(a) and C(a)) are shown. For the case where the cells leave phase A at a constant rate similar results are obtained. For the model of Martens et al. the sharp-transition case is shown.

With respect to the fraction of arrested cells the model outcomes cannot be compared to experimental data, because the existence of arrested cells is not shown by Miller et al.<sup>24</sup> nor by Linardos et al.<sup>21</sup>. Martens et al.<sup>23</sup> do show the presence of apoptotic cells but were not able to quantify this fraction. Thus, the data shown in Figure 5C are all model predictions, including those of Suzuki and Ollis (squares). Again a maximum is observed for the model of Cazzador and Mariani, which is not seen for the other models. Furthermore, the fraction of non-proliferating cells is much higher in case of the model of Martens et al. as compared to the other models. This is because the model of Martens et al. calculates the fraction of non-proliferating cells directly from the growth conditions, while the other models calculate the fraction of arrested cells from the productivity data [Eq. (12)]. This means, that in these other models the fraction of non-proliferating cells is highly correlated to the value used for the productivity of the non-proliferating cells,  $k_D$ . This value is obtained by extrapolation and as a consequence is not very reliable. If the value of this parameter is chosen lower, the fraction of arrested cells will be higher for these models.

The segregated nature of the models is only experimentally tested by Martens et al.<sup>23</sup>. Last, the critical specific growth rate of Martens et al.<sup>22</sup> is equivalent to the critical duration of phase A presented by Linardos et al.<sup>21</sup> and is related to the specific growth rate at which the transition probability is 0.5 in the approach of Cazzador and Mariani<sup>8</sup>. Also in the model results of Suzuki and Ollis<sup>37</sup> such a critical point can be observed.

## FUTURE DEVELOPMENTS

At present large effort is directed towards the elucidation of the control of the cell cycle and apoptosis and an increasing variety of proteins and mechanisms is discovered playing a role in these processes. Thus, it may become possible to define the physiological state of a cell on the basis of the proteins involved in the regulation of the cell cycle and apoptosis. The cell behaviour may next be related to this physiological-state vector through knowledge concerning the mechanism in which these proteins are involved. In addition, other variables, like, for instance, the quality of the product may be related to this physiological-state description. For instance, with respect to cell-cycle control a special class of proteins, cyclins, plays an important role and Hatzimanikatis et al.<sup>15</sup> have used the cyclic accumulation of cyclin E to model the  $G_1$ -S transition. Another example is the model of Novak and Tyson<sup>28</sup>, which is based on the biochemistry of M-phase-promoting factor (MPF) in *Xenopus* oocyte extracts. Furthermore, an increasing amount of compounds can be measured inside individual cells by flow cytometry and the measurement of intracellular compounds by flow cytometry seems to be only limited by the

availability of proper labelling techniques. Thus, segregated, structured models may become experimental verifiable.

A large number of biologicals is produced in batch or fed-batch culture. As discussed, these cultures may not be in a situation of balanced growth, which implies that the behaviour of the cells cannot be explained from the currently incomplete physiological-state description and becomes time dependent. Consequently, dynamic models are required to predict cell behaviour. One of the main problems for dynamic models is that the dynamic behaviour of a cell population depends on unknown physiological-state variables. For example, in the situation of Figure 2 at a certain given simplified physiological state  $z$ , the distribution of true physiological states may have an infinite number of different shapes in a dynamic situation, with each different shape corresponding to a different dynamic behaviour. Notably, this is also the reason why data obtained in continuous culture cannot be translated to batch cultures. Insight in the dynamic behaviour of cells may be obtained by step experiments in continuous cultures in steady state. A promising system for the study of dynamic responses of animal cells is formed by two continuous stirred-tank reactors in series<sup>5</sup>. Cells going from the first to the second reactor experience a sudden change of environment to which they have to adapt. Consequently, the growth of these cells in the second vessel is not balanced. Nevertheless, a steady state occurs in the second vessel, and the distribution functions of the cells for the true as well as for simplified physiological-state vectors are constant. Adjusting the conditions in the second vessel allows for the study of dynamic responses as for instance the onset of apoptosis, of cells under different constant external conditions. In addition, this can be done for different conditions in the first vessel giving information on the dynamic behaviour of cells with different physiological states. An additional advantage of this system is that in the second vessel steady states at very low specific growth rates may be obtained, which are difficult to attain in a single vessel.

## CONCLUSIONS

Incorporating the segregated nature of cell populations in models may greatly improve the predictive capability of these models under different environmental conditions. Studying cell behaviour in a situation of balanced growth greatly facilitates the development of these segregated models. Until now the practical application of segregated models is limited to simplified state vectors and to repetitive growth situations. However, at the moment a fast increasing amount of knowledge concerning the physiology of cell growth and death, productivity and cell-cycle control becomes available. In addition, the progress in flow-cytometric techniques makes it possible to measure an increasing amount of different compounds

## Chapter 2

inside individual cells. Thus, the physiological state of individual cells and processes changing this state can be more accurately measured and can be incorporated in segregated models. Furthermore, with the increase in calculation power of computers the mathematical equations may be solved numerically and it becomes possible to extend the use of segregated structured models to non-repetitive, dynamic, growth situations.

### SYMBOLS

$A, a$	Cell age	(s)
$b_Q, c_Q$	Constants in the function describing the return of cells from the arrested phase in the model of Cazzador and Mariani <sup>8</sup> .	(s <sup>-1</sup> )
$c$	Environmental state vector.	
$D$	Dilution rate.	(s <sup>-1</sup> )
$f_X(x, t)$	Number density function representing the fraction of cells at time $t$ , and a physiological state $x$ , where $x$ may represent the physiological-state vector $z$ , a single physiological-state variable, $s$ , the maturity, $\omega$ , or the age, $a$ .	(-)
$f_{z z_i}(z, z_i, t)$	Conditional density function representing the fraction of cells at time $t$ with a physiological state $z$ at a given condition $z_i$ , where $z_i$ represents a fixed value for one or more state variables.	(-)
$f_{\dot{z} z}(\dot{z}, z, c)$	Fraction of cells with a rate $\dot{z}$ at a given physiological state $z$ .	(-)
$f_Q$	Fraction of arrested cells in the model of Suzuki and Ollis <sup>37</sup> .	(-)
$g[z(t), c(t)]$	Unknown function giving the rate with which the physiological state changes at time $t$ as a function of the physiological ( $z(t)$ ) and environmental state ( $c(t)$ ).	
$K$	Median point for the function describing cell arrest in the model of Cazzador and Mariani <sup>8</sup> .	(s <sup>-1</sup> )
$k_C, k_Q$	Productivity of the cycling and arrested cells, respectively, in the model of Suzuki and Ollis <sup>37</sup> .	(g.cell <sup>-1</sup> .s <sup>-1</sup> )
$n(t)$	Concentration of cells.	(cells.m <sup>-3</sup> )
$p_B(c, t)$	Probability for a cell of phase A of entering phase B in case of a transition at environmental conditions $c$ and time $t$ .	(-)
$p_n$	Probability of loss of productivity in the model of Lee et al. <sup>20</sup>	(-)
$p_Q$	Probability of cell arrest in the model of Cazzador and Mariani <sup>8</sup> .	(-)
$\bar{R}(z, c)$	Average reaction rate for the $i$ 'th reaction taking place inside a cell at physiological state $z$ and environmental state $c$ .	(mol.cell <sup>-1</sup> .s <sup>-1</sup> )
$S(t)$	Single physiological-state variable of a single cell at time $t$ .	(units of S)
$\bar{S}(s, c, t)$	Average rate of change of a single physiological state variable as a function of the value of this variable $s$ , the environmental conditions $c$ , and the time $t$ .	(units S.cell <sup>-1</sup> .s <sup>-1</sup> )
$t_C$	Cycle time.	(s)
$T_A$	Duration of phase A in the model of Cazzador and Mariani <sup>8</sup> .	(s)



## Chapter 2

$T_{c_r}$	Critical age of phase-A cells in the model of Linardos et al. <sup>21</sup> .	(s)
$Z_1, Z_2$	Specified, single physiological-state variables.	(mol.cell <sup>-1</sup> )
$Z(t)$	Physiological-state vector containing the amounts of the different chemical compounds in a single cell at time $t$ .	(mol.cell <sup>-1</sup> )
$\dot{Z}(t)$	Vector containing the rates with which the amounts of the different chemical compounds changes in a single cell at time $t$ .	(mol.cell <sup>-1</sup> .s <sup>-1</sup> )
$\bar{Z}(z, c)$	Vector containing the average rates with which the amounts of the different chemical compound inside a single cell change as a function of the physiological state $z$ and environmental state $c$ .	(mol.cell <sup>-1</sup> .s <sup>-1</sup> )
$v$	Viability.	(-)
$q$	Productivity	(g.cell <sup>-1</sup> .s <sup>-1</sup> )
$\beta$	Stoichiometry matrix for the intracellular reactions concerning intracellular compounds.	(mol.mol <sup>-1</sup> )
$\gamma$	Stoichiometry matrix for the intracellular reactions concerning extracellular compounds.	(mol.mol <sup>-1</sup> )
$\Gamma(a, c, t)$	$\Gamma(a, c, t)dt$ is the probability that in a time interval $dt$ a cell of age $a$ divides at environmental conditions $c$ and time $t$ .	(s <sup>-1</sup> )
$\theta$	Residence time in the reactor	(s)
$\kappa_{ij}(z, z', c)$	$\kappa_{ij}(z, z', c)$ represents the probability that a cell of physiological state $z'$ in population $i$ will enter population $j$ at physiological state $z$ upon transition at environmental conditions $c$ . This function may become explicitly dependent on time.	(-)
$\kappa_{ij}(\omega, \omega', c, t)$	$\kappa_{ij}(\omega, \omega', c, t)$ represents the probability that a cell of maturity $\omega'$ in population $i$ will enter population $j$ at a maturity $\omega$ upon transition at environmental conditions $c$ and time $t$ .	(-)
$\lambda_A$	Specific rate with which cells leave phase A in the model of Cazzador and Mariani <sup>8</sup> .	(s <sup>-1</sup> )
$\lambda_{ij}(z, c)$	$\lambda_{ij}(z, c)dt$ represents the probability that in a time interval $dt$ a cell at physiological state $z$ will transit from population $i$ to population $j$ at environmental conditions $c$ . This function may become explicitly dependent on time.	(s <sup>-1</sup> )
$\lambda_{ij}(x, c, t)$	$\lambda_{ij}(x, c, t)dt$ represents the probability that in a time interval $dt$ a cell at a simplified physiological state $x$ will transit from population $i$ to population $j$ at environmental conditions $c$ at time $t$ , where $x$ is a single physiological state variable, $s$ , the maturity, $\omega$ , or the age, $a$ .	(s <sup>-1</sup> )
$\mu$	Specific growth-rate constant.	(s <sup>-1</sup> )
$\mu_p, \mu_n$	Specific growth-rate constants of producers and non producers, respectively, in the model of Lee et al. <sup>20</sup> .	(s <sup>-1</sup> )

## Chapter 2

$\rho(z, z', c)$	$\rho(z, z', c)$ represents the probability that division of a mother cell of physiological state $z'$ will result in a daughter cell of physiological state $z$ at environmental conditions $c$ . This function may become explicitly dependent on time.	(-)
$\rho(x, x', c, t)$	$\rho(x, x', c, t)$ represents the probability that division of a mother cell of simplified physiological state $x'$ will result in a daughter cell of simplified physiological state $x$ at environmental conditions $c$ at time $t$ , where $x$ may be a single physiological state variable, $s$ , or the maturity, $\omega$ .	(-)
$\sigma(z, c)$	$\sigma(z, c)dt$ represents the probability that in a time interval $dt$ a cell of physiological state $z$ at environmental conditions $c$ will divide. This function may become explicitly dependent on time.	(s <sup>-1</sup> )
$\sigma(x, c, t)$	$\sigma(x, c, t)dt$ represents the probability that in a time interval $dt$ a cell of physiological state $x$ at environmental conditions $c$ will divide, where $x$ is a single physiological state variable, $s$ , or the maturity, $\omega$ .	(s <sup>-1</sup> )
$\Upsilon$	Physiological-state space.	
$\dot{\Upsilon}$	Space containing all possible rate vectors.	
$dv$	Small region in physiological-state space.	
$d\dot{v}$	Small region in the rate space.	
$\bar{\Omega}(t), \omega(t)$	Maturity of a single cell at time $t$ .	(-)
$\bar{\bar{\Omega}}(\omega, c, t)$	Average maturation rate of a cell at maturity $\omega$ , environmental conditions $c$ , and time $t$ .	(s <sup>-1</sup> )

## REFERENCES

1. Alberts, B., Bray, D., Lewis, J., Raff, M., Roberts, K., Watson, J. D. 1983. *Molecular biology of the cell*. Garland, New York.
2. Al-Rubeai, M., Emery, A.N. 1993. Flow cytometry in animal cell culture. *Biotechnol.* **11**: 572-579.
3. Al-Rubeai, M., Singh, R.P., Emery, A.N., Zhang, Z. 1995. Cell cycle and cell size dependence of susceptibility to hydrodynamic forces. *Biotechnol. Bioeng.* **46**: 88-92.
4. Bailey, J.E., Fazel-Madjlessi J., McQuitty, D.N., Lee, L.Y., Oro, J.A. 1978. Measurement of structured microbial population dynamics by flow micro fluorometry. *AIChE J.* **24**: 570-577.
5. Bakker, W.A.M., Schäfer, T., Beefink, H.H., Tramper, J., De Gooijer, C.D. 1995. Hybridomas in a bioreactor cascade: modelling and determination of growth and death kinetics. Submitted for publication.
6. Bell, G.I., Anderson, E.C. 1967. Cell growth and division. I. A mathematical model with applications to cell volume distributions in mammalian suspension cultures. *Biophys. J.* **7**: 329-351.
7. Campbell, A. 1957. Synchronization of cell division. *Bacteriol. Rev.* **21**: 263-272.
8. Cazzador, L., Mariani, L. 1993. Growth and production modelling in hybridoma continuous cultures. *Biotechnol. Bioeng.* **42**: 1322-1330.
9. Chester, K.A., Hawkins, R.E. 1995. Clinical issues in antibody design. *TibTech* **13**: 294-300.
10. Cotter, T.G., Al-Rubeai, M. 1995. Cell death (apoptosis) in cell culture systems. *TibTech* **13**: 150-155.

## Chapter 2

11. Darzynkiewicz, Z., Bruno, S., Del Bino, G., Gorczyca, W., Hotz, M.A., Lassota, P., Traganos, F. 1992. Features of apoptotic cells measured by flow cytometry. *Cytometry* **13**: 795-808.
12. Frederickson, A.G., Ramkrishna, D., Tsuchiya, H.M. 1967. Statistics and dynamics of prokaryotic cell populations. *Math. Biosci.* **1**: 327-374.
13. Goebel, N.K., Huehn, R., Flickinger, M.C. 1990. Methods for determination of growth-rate dependent changes in hybridoma volume, shape and surface structure during continuous recycle. *Cytotechnol.* **4**: 45-57.
14. Harder, A., Roels, J.A. 1982. Application of simple structured models in bioengineering. *Adv. Biochem. Eng.* **21**: 55-107.
15. Hatzimanikatis, V., Lee, K.H., Renner, W.A., Bailey, J.E. 1995. A mathematical model for the G<sub>1</sub>/S transition of the mammalian cell cycle. *Biotechnol. Lett.* **17**: 669-674.
16. Horan, P.K., Wheelless, Jr., L.L. 1977. Quantitative single cell analysis and sorting. *Science* **198**: 149-157.
17. Kromenaker, S.J., Srienc, F. 1991. Cell-cycle-dependent protein accumulation by producer and nonproducer murine hybridoma cell lines: A population analysis. *Biotechnol. Bioeng.* **38**: 665-677.
18. Kromenaker, S.J., Srienc, F. 1994. Effect of lactic acid on the kinetics of growth and antibody production in a murine hybridoma: secretion patterns during cell cycle. *J. Biotechnol.* **34**: 13-34.
19. Kruth, H.S. 1982. Flow cytometry: Rapid biochemical analysis of single cells. *Anal. Biochem.* **125**: 225-242.
20. Lee, G. M., Varma, A., Palsson, O. 1991. Application of population balance model to the loss of hybridoma antibody productivity. *Biotechnol. Prog.* **7**: 72-75.
21. Linardos, T.J., Kalogerakis, N., Behie, L.A. 1992. Cell cycle model for specific growth rate and death rate in continuous suspension hybridoma cultures. *Biotechnol. Bioeng.* **40**: 359-368.
22. Martens, D.E., Sipkema, E.M., Gooijer, C.D. de, Beuvery, E.C., Tramper, J. 1995. A combined cell-cycle and metabolic model for the growth of hybridoma cells in steady-state continuous culture. *Biotechnol. Bioeng.* **48**: 49-65.
23. Martens, D.E., Gooijer, C.D. de, Beuvery, E.C., Tramper, J. 1996. Use of a combined cell-cycle and metabolic model for the study of hybridoma cells in steady-state continuous culture. Submitted for publication.
24. Miller, W.M., Blanch, H.W., Wilke, C.R. 1988. A kinetic analysis of hybridoma growth and metabolism in batch and continuous suspension culture: Effect of nutrient concentration, dilution rate, and pH. *Biotechnol. Bioeng.* **32**: 947-965.
25. Moore, A., Donahue, C.J., Hooley, J., Stocks, D.L., Bauer, K.D., Mather, J.P. 1995. Apoptosis in CHO cell batch cultures: examination by flow cytometry. *Cytotechnol.* **17**: 1-11.
26. Needham, D., Ting-Beall, H.P., Tran-son-Tay, R. 1991. A physical characterization of GAP A3 hybridoma cells: morphology, geometry and mechanical properties. **38**: 838-852.
27. Nielsen, J., Villadsen, J. 1992. Modelling of microbial kinetics. *Chem. Eng. Sci.* **47**: 4225-4270.
28. Novak, B., Tyson, J.J. 1993. Numerical analysis of a comprehensive model on M-phase control in *Xenopus* oocyte extracts and intact embryos. *J. Cell Sci.* **106**: 1153-1168.
29. Pardee, A.B., 1989. G<sub>1</sub> events and regulation of cell proliferation. *Science* **246**: 603-608.
30. Ramkrishna, D. 1979. Statistical models of cell populations. *Advanc. Biochem. Eng.* **11**: 1-47.
31. Reed, S.I., Bailly, E., Dulic, V., Hengst, L., Resnitzky, D. and Slingerland, J. 1994. G<sub>1</sub> control in mammalian cells. *J. Cell Sci. Suppl.* **18**: 69-73.
32. Roels, J. A. 1983. *Energetics and kinetics in biotechnology.* Elsevier Biomedical Press, Amsterdam.

## Chapter 2

33. Rubinow, S.I. 1968. Age-structured equations in the theory of cell populations.
34. Sherr, C.J. 1993. Mammalian G<sub>1</sub> cyclins. *Cell* **73**: 1059-1065.
35. Smith, J.A., Martin, L. 1973. Do cells cycle? *Proc. Natl. Acad. Sci.* **70**: 1263-1267.
36. Soliz-Recendez, M.G., Perani, A., D'Habit, B., Stacey, G.N., Maugras, M. 1995. Hybridoma cell cultures continuously undergo apoptosis and reveal a novel 100 bp DNA fragment. *J. Biotechnol.* **38**: 117-127.
37. Suzuki, E., Ollis, D.F. 1989. Cell cycle model for antibody production. *Biotechnol. Bioeng.* **34**: 1398-1402.
38. Suzuki, E., Ollis, D.F. 1990. Enhanced antibody production at slowed specific growth rates: Experimental demonstration and a simple structured model. *Biotechnol. Prog.* **6**: 231-236.
39. Trucco, E. 1965. Mathematical models for cellular systems the Von Foerster equation. Part I. *Bull. Math. Biophys.* **27**: 285-304.
40. Trucco, E. 1965. Mathematical models for cellular systems the Von Foerster equation. Part II. *Bull. Math. Biophys.* **27**: 449-471.
41. Tziampazis, E., Sambanis, A. 1994. Modelling cell culture processes. *Cytotechnol.* **14**: 191-204.
42. Von Foerster, H. 1959. Some remarks on changing populations. Pp. 382-407. In: Stohlman, F. Jr. (Ed.) *The kinetics of cellular proliferation*. Grune and Stratton, New York.
43. Webb, G.F. 1985. *Theory of nonlinear age-dependent population dynamics*. Marcel Dekker, Inc. New York.

## CHAPTER 3

# LETHAL EVENTS DURING GAS SPARGING IN ANIMAL CELL CULTURE

### ABSTRACT

The lethal effects of gas sparging on hybridoma cells obtained from a chemostat culture were examined in a bubble column. Experiments were performed to identify and quantify the main hazardous event: bubble formation, bubble rising or bubble break-up. The results indicate that bubble break-up is the main cause of cell death. The protective activity of the surfactant Pluronic F68 against sparging seems to result from a direct interaction with the cells rather than influencing the bubble-liquid interface properties.

### INTRODUCTION

Oxygen consumption rates of animal cell cultures are low compared to cultures of microorganisms, due to the low growth rates and low cell densities. However, animal cells are more sensitive to vigorous mixing and gas sparging. Therefore, oxygen supply is still one of the main problems in large-scale and/or high-density mammalian-cell cultures. From a technological point of view, oxygen supply to cell cultures by means of direct sparging is most convenient. In bubble-column and air-lift reactors, sparging is also used for fluid mixing.

The nature of the physical forces caused by mixing or sparging which lead to impaired cell growth, cell damage and eventually cell death is not fully understood yet. Attempts have been made to quantify detrimental hydrodynamic forces in terms of shear stress, shear rate and turbulence intensity represented by the specific power input<sup>1-5,10,12,13</sup>. Hybridomas are reported<sup>1,12,13</sup> to be sensitive to shear stresses beyond 1-5 N.m<sup>-2</sup>. Turbulent fluid flows appear to be more hazardous to cells than laminar flows<sup>1</sup>. Furthermore, the growth stage and culture history with respect to agitation conditions appear to be important factors for the shear sensitivity of cells<sup>12</sup>. Both, mechanical agitation and sparging cause cell damage and it is not known if they affect cell integrity by the same mechanism. The effects of gas sparging can be divided into fluid

mixing phenomena and gas-liquid interface events. Bulk fluid mixing is mainly accomplished by the rising of gas bubbles. Besides fluid-mixing effects, gas-liquid interface formation and disruption occurs during bubble formation at the sparger site and bubble escape at the fluid surface, respectively. In addition, bubble escape can also lead to foam formation.

The question is: what events are the main cause of cell damage so appropriate technological measures can be taken to minimize their effects: bubble formation at the sparger site, rising of the gas bubbles, or bubble break-up at the culture surface. The work of Handa et al.<sup>6,7</sup> shows that bubble rising is not the main cause of growth inhibition in sparged hybridoma cultures. Presumably, bubble escape at the culture surface is the cell-damaging event as judged by video-film registration. The work of Tramper et al.<sup>14</sup> on insect cells agrees with the conclusion that bubble rising is not the major cell damaging event. In this article we try to distinguish experimentally between the effects of bubble formation, bubble rising and bubble break-up on the survival of hybridoma cells in a bubble column. Localization of the lethal events during gas sparging could provide a rational basis for reactor-design optimization.

## THEORY

Several attempts have been made in literature to identify the physical phenomena responsible for cell injury during mixing and sparging<sup>1-5,10,12,13</sup>. It appears that a correlation exists between cell damage and the following three quantities: shear rate, shear stress, and smallest eddy length.

The shear rate,  $\dot{\gamma}$  ( $s^{-1}$ ), and shear stress,  $\tau$  ( $N \cdot m^{-2}$ ), are defined and measurable quantities in laminar flow fields and are expressed by Equations (1) and (2), respectively:

$$\dot{\gamma} = \frac{dv_x}{dy} \quad (1)$$

$$\tau = \eta \frac{dv_x}{dy} \quad (2)$$

in which  $v_x$  is the fluid velocity in the x direction ( $m \cdot s^{-1}$ ),  $y$  is the coordinate in the direction perpendicular to  $x$  (m), and  $\eta$  is the fluid dynamic viscosity ( $N \cdot s \cdot m^{-2}$ ).

The smallest eddy length is a quantity defined in a model proposed by Kolmogorov and represents a measure for turbulence intensity and energy dissipation on micro-scale. Hydrodynamic energy is transferred from large energy-containing eddies to eddies gradually decreasing in size and energy content. The smallest eddy which still contains energy then

disappears and 'loses' its energy in the form of heat. The length,  $\lambda$  (m), of the smallest eddy is given by Equation (3):

$$\lambda = \left(\frac{v^3}{\epsilon}\right)^{1/4} \quad (3)$$

where  $v$  is the kinematic viscosity ( $\text{m}^2 \cdot \text{s}^{-1}$ ) and  $\epsilon$  is the power dissipation per unit mass ( $\text{W} \cdot \text{kg}^{-1}$ ). If the smallest energy-containing eddy is of the same size or smaller than the cells, cell injury can occur<sup>10</sup>. In the case of microcarrier cultures, eddies smaller than the microcarriers can affect the cells or break up cell attachment leading to cell death<sup>3</sup>.

All three quantities, shear rate, shear stress and smallest eddy length are linked to each other by the power input and it is difficult to discriminate experimentally between them. The only difference between these quantities is the role of fluid viscosity. Until now, only one systematic study on this subject has been published, which indicates that cell damage can be described consistently with the smallest-eddy-length model<sup>4</sup>.

The power input per unit mass ( $\epsilon$ ) performed by sparging in a bubble-column or air-lift reactor equals the work (compression) that is performed on the gas by the fluid column in the reactor:

$$\epsilon = \frac{RTF_m}{\rho V} \ln\left(\frac{P_0 + \rho g H}{P_0}\right) \quad (4)$$

in which  $R$  is the gas constant ( $8.31 \text{ J} \cdot \text{mol}^{-1} \cdot \text{K}^{-1}$ ),  $T$  is the temperature (K),  $F_m$  is the gas-mass flow ( $\text{Kg} \cdot \text{s}^{-1}$ ),  $V$  is the culture volume ( $\text{m}^3$ ),  $\rho$  is the specific mass ( $\text{Kg} \cdot \text{m}^{-3}$ ),  $P_0$  is the pressure at the orifice ( $\text{N} \cdot \text{m}^{-2}$ ),  $g$  is the gravity constant ( $9.81 \text{ m} \cdot \text{s}^{-2}$ ), and  $H$  is the fluid height (m).

Irrespective of the exact nature of the physical quantities which are responsible for cell damage, we tried to identify the events that occur during sparging which lead to cell damage. The cell death rate can be described by first-order kinetics in analogy to the cell growth rate. Provided that the cell growth rate is zero or negligible compared to the cell death rate, the decrease in viable cell concentration can be described by:

$$\frac{dC_{xv}}{dt} = -k_d C_{xv} \quad (5)$$

in which  $k_d$  is the specific death-rate constant ( $\text{h}^{-1}$ ) and  $C_{xv}$  is the viable-cell concentration ( $\text{cells} \cdot \text{m}^{-3}$ ).  $k_d$  can be estimated from the decline in viable-cell concentration after integration of Equation (5):

$$\ln\left(\frac{C_{xv}(t)}{C_{xv}(0)}\right) = -k_d t \quad (6)$$

where  $C_{xv}(0)$  is the viable-cell concentration at time zero ( $\text{cells.m}^{-3}$ ). Tramper et al.<sup>14</sup> proposed a model for cell damage caused by sparging, in which a hypothetical killing volume,  $V_k$  ( $\text{m}^3$ ), is associated with each air bubble during its life time. The death-rate constant in this model is proportional to the rate at which gas bubbles are sparged ( $6F/\pi d_b^3$ ) per unit reactor volume and their hypothetical killing volume:

$$k_d = \frac{6FV_k}{\pi d_b^3 V} \quad (7)$$

where  $F$  is the gas flow rate ( $\text{m}^3.\text{s}^{-1}$ ),  $d_b$  is the bubble diameter (m), and  $V$  is the culture volume ( $\text{m}^3$ ).

Three events can be distinguished during sparging: bubble formation at the sparger, bubble rising through the culture fluid, and bubble break-up at the culture surface. In order to discriminate experimentally between these events and address one as the main cause for cell injury, we specified Equation (7) for each event to yield verifiable correlations between the cell death rate and particular culture parameters.

### Bubble rising

In the case that cell death occurs due to bubble rising, the cell death rate should be proportional to the chance of collision between gas bubbles and cells, and the collision force. The chance of collision is proportional to the cell concentration and the bubble concentration and size. The cell size is assumed to be constant. The bubble concentration is given by the product of the number of gas bubbles sparged per unit time ( $6F/\pi d_b^3$ ) per unit culture volume and the bubble residence time ( $H/v_b$ ), where  $H$  is the culture height (m). The rising velocity,  $v_b$  ( $\text{m.s}^{-1}$ ), will also affect the collision force, but is assumed to be constant ( $0.25 \text{ m.s}^{-1}$ ) within our range of bubble sizes<sup>8</sup>. The bubble size is a parameter which plays a role in the chance of collision as well as in the collision force, but since it is not known what the exact correlation is (volume, cross-sectional area etc.) we refer to it as a function of the bubble diameter [ $f(d_b)$ ]. In summary, loss of viable cells is represented by:

$$\frac{dC_{xv}}{dt} = -k_1 \frac{F}{d_b^3 V} f(d_b) \frac{H}{v_b} C_{xv} \quad (8)$$



in which  $k_1$  is a proportionality constant which contains mathematical ( $\pi$ ) and numerical constants. At a constant bubble size all terms, including  $v_b$ , which contain the bubble diameter become constant. Insertion of  $\frac{1}{4}\pi HD_r^2$  for the volume,  $V$ , of a cylindrical vessel and rewriting Equation (8) leads to Equation (9):

$$\frac{dC_{Xv}}{dt} = -k_2 \frac{F}{D_r^2} C_{Xv} \quad (9)$$

$k_2$  is again a proportionality constant ( $m^{-1}$ ) and  $D_r$  is the reactor diameter (m). In conclusion, at a constant reactor cross-sectional area and a constant bubble size, the cell death-rate constant is only a function of the gas flow rate. If bubble rising is the cause of cell death, the specific death-rate constant will be independent of the culture height.

### Sparger site

If cell death occurs at the sparger site, we assume that it is an instantaneous process. The cell death rate is proportional to the chance of collision and collision force. As in the former case, the chance of collision depends on the cell concentration and the number of bubbles leaving the sparger per unit time per unit culture volume. Both, the chance of collision and the collision force are also a function of the bubble size [ $f(d_b)$ ]. Furthermore, the collision force will be proportional to the entrance velocity of the gas, i.e. proportional to  $4F/\pi d_o^2 n_o$  ( $\pi d_o^2/4$  is the cross-sectional area of the orifice of one nozzle,  $d_o$  (m) is the diameter of the orifice, and  $n_o$  is the number of nozzles). Combining all terms, the cell death rate caused by gas entrance at the sparger can be described by Equation (10):

$$\frac{dC_{Xv}}{dt} = -K_3 \frac{F}{d_o^2 n_o} \frac{F}{d_b^3 V} f(d_b) C_{Xv} \quad (10)$$

where  $k_3$  is a proportionality constant. In this case, the specific cell death rate will increase with decreasing numbers of nozzles, i.e. with increasing gas-entrance velocities, provided that the total gas flow rate, bubble size, orifice diameters and culture volume are constant.

### Bubble escape

If cell death occurs due to bubble escape at the fluid surface, this process will again be instantaneous as in the former case. The description of the chance of collision is therefore equal to the former case. However, the collision force during bubble escape is the result of the force with which the bubble penetrates the fluid surface and the force accompanied with bubble

break-up. We expect both forces to depend on bubble size and bubble rising velocity. The terminal bubble rising velocity is a function of bubble size and is independent of reactor height. The forces associated with fluid-surface penetration and bubble break-up will be influenced by the fluid viscosity and the surface tension, which are constants for a given system. So, the force of bubble break-up is only dependent on bubble size and is in this case contained in the term  $f(d_b)$ . Loss in viable cell concentration can now be described by Equation (11):

$$\frac{dC_{Xv}}{dt} = -k_d \frac{F}{d_b^3 V} f(d_b) C_{Xv} \quad (11)$$

Again  $k_d$  is a proportionality constant. Equation (11) predicts that cell disruption during bubble escape is proportional to the gas flow rate per unit volume only.

## MATERIALS AND METHODS

### Cell culture

The cell line used was a murine hybridoma designated Db 2 and was a kind gift from Dr. van der Meide, TNO-Research Institute Rijswijk. Cells were grown in a chemostat culture in a stirred fermenter (at 200 rpm) with a working volume of 0.8 dm<sup>3</sup> and a dilution rate of 0.024 h<sup>-1</sup>. The medium consisted of a 1:1 mixture of DMEM and Ham's F12 basal medium, supplemented with 1% newborn calf serum (Seromed) and 100 mg.dm<sup>-3</sup> antibiotics (kanamycin or a penicillin/streptomycin mixture). The conditions were: temperature 37°C, pH 7.2 controlled by automatic addition of 0.4 M NaOH, pO<sub>2</sub> 60% air saturation controlled by automatic sparging of pure oxygen, surface aeration with air containing 5% CO<sub>2</sub>. Under these conditions hardly any foaming occurred and addition of antifoam was not necessary.

### Sparging experiments

Experiments were performed on 40-200 cm<sup>3</sup> samples from the chemostat culture. Each sample was placed in a bubble column, thermostated at 37°C by a water jacket. Air containing 5% CO<sub>2</sub> (for maintaining pH at 7.2) was sparged through one to four nozzles (as stated) with 1 mm i.d. Flow rates were controlled with a Brooks rotameter; if more than one nozzle was used, flows were controlled separately per nozzle to ensure equal gas distribution and velocities.

The inner diameters of the bubble columns varied from 2.1 to 3.4 cm and the fluid heights were varied between 8 and 25 cm as stated. Gas flow rates were varied between 2 and 10 dm<sup>3</sup>.h<sup>-1</sup>. Antifoam Silicon B (BDH) was added up to 0.01% unless stated otherwise. Pluronic F68 was

a gift from BASF. Part of the chemostat-sample was placed in a static culture flask in a CO<sub>2</sub> incubator as a control.

### Stirring experiments

A 500 cm<sup>3</sup> graduated measuring cylinder equipped with a top stirrer was placed in a water bath at 37°C. A marine impeller with 45° angle blades and a total diameter of 2 cm was used. A 225 cm<sup>3</sup> sample of the chemostat culture was placed in the cylinder and covered with a plastic sheet through which an air + 5% CO<sub>2</sub> gas mixture was blown over the culture to keep pH at 7.2. A control sample of 25 cm<sup>3</sup> was incubated statically in a CO<sub>2</sub> incubator.

### Measurements

Duplicate samples (about 1 cm<sup>3</sup>) were drawn every half hour during the experiments. Trypan blue was added to the sample (final concentration 0.1%) for staining dead cells. After 5 minutes the viable-cell concentration was determined by counting a defined volume in a Burker-Turk hemacytometer using a light microscope (magnification 400x). Duplicate counts were performed on each sample.

## RESULTS

Experiments were performed on cells obtained from a steady-state chemostat culture, to ensure that their physiological state was equal at the onset of the experiments. The chemostat culture was run at a dilution rate of 0.024 h<sup>-1</sup>, using medium supplemented with 1% serum. The steady-state cell concentration was 1.6 (±0.2) 10<sup>9</sup> cells.dm<sup>-3</sup> with a viability of 80-90%. Sparging and stirring experiments were performed on 40-200 cm<sup>3</sup> chemostat samples, within a time span of 3 hours to avoid interference of nutritional limitations or cell growth and possible infections. Due to the presence of 1% serum in the medium, sparging caused excessive foam formation. Therefore, we added in all experiments Silicon-B antifoam at concentrations of 0.005-0.01% to the test and control sample. The control sample was incubated in a static flask in a CO<sub>2</sub>-incubator. The viable-cell counts of the control samples did not change within 3 hours and the antifoam had no effect on the viability.

In all experiments, viable-cell loss was accompanied with a high level of cell lysis. Reliable dead-cell counts were not possible as various sizes of cell fragments were observed. Therefore, cell damage was measured by the decrease in viable-cell count. The cell death rate was taken first order in cell concentration. The cell death-rate constant,  $k_d$ , was estimated by linear regression based on Equation (6). An example is shown in Figure 1.

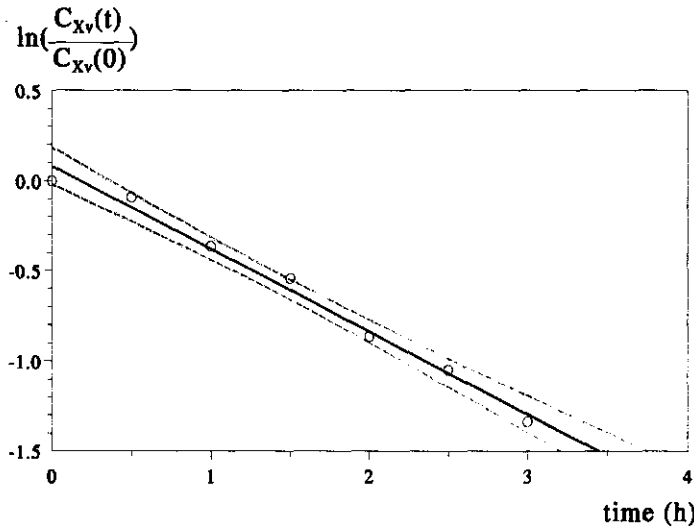


**Figure 1.** Estimation of the specific death-rate constant,  $k_d$ . The parameter  $k_d$  is estimated from the decline in viable-cell concentration according to Equation (6), by linear regression. Experimental conditions in this example are a gas flow rate of  $8 \text{ dm}^3 \cdot \text{h}^{-1}$  and a cell suspension volume of  $0.14 \text{ dm}^3$ . The parameter  $k_d$  is estimated as  $0.46 \pm 0.02 \text{ h}^{-1}$ : (o) experimental data; (solid line) relationship estimated by linear regression; (broken lines) 95% confidence region of the regression line.

### Sparging experiments

First, the hypothesis that cell death occurs during bubble rising as represented by Equation (8) was examined. In a series of experiments, the culture height was varied at a constant flow rate ( $8 \text{ dm}^3 \cdot \text{h}^{-1}$ ) and column diameter (3.2 cm). If Equation (8) holds, the cell death rate should increase with increasing bubble residence time, which is proportional to the reactor height. Since this effect is counteracted by the larger culture volume and hence the smaller chance of collision, the net result would be that the cell death rate is independent of culture height [Eq. (9)]. From the experimental results, summarized in Figure 2, it is clear that the specific cell death rate is not independent of culture height and, so, bubble rising as the main source of cell damage can be rejected.

Next, we tested the possibility that cell death occurs mainly at the sparger during bubble formation. In that case, we expect cell loss to depend on the force of bubble formation, i.e. the velocity of gas entrance out of the nozzle as described in Equation (10). Two sets of experiments were performed, in which the gas entrance velocity was varied by varying the number of nozzles between one and four at a constant total gas flow rate. The results are shown in Figure 3. It

appears that at both total gas flow rates ( $3.6$  and  $7.2 \text{ dm}^3 \cdot \text{h}^{-1}$ ) the number of nozzles had no significant effect on the cell death rate.

The results might be biased, however, by differences in bubble size as a consequence of the differences in formation velocities. At a low flow rate per nozzle, smaller bubbles can be formed leading to a higher bubble frequency and consequently to a higher cell death rate. At the same time however, surface area and volume per bubble decrease and might counteract this effect. Handa et al.<sup>6</sup> reported that smaller bubbles (below  $2 \text{ mm}$  in diameter) are more hazardous

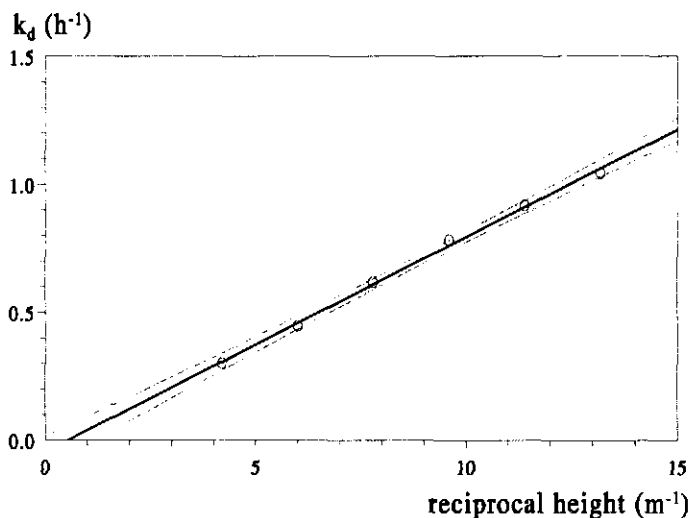


**Figure 2.** Correlation between the specific death-rate constant and culture height. Experimental conditions are: gas flow rate of  $8 \text{ dm}^3 \cdot \text{h}^{-1}$ ; one nozzle; fixed column diameter of  $3.1 \text{ cm}$ ; the culture volume was varied between  $60$  and  $90 \text{ cm}^3$ . (O) experimental data; (solid line) linear-regression line; (broken line) 95% confidence limit of the regression line.

to hybridoma cells than larger bubbles. However, according to Tramper et al.<sup>14</sup> for bubbles between  $2$  and  $6 \text{ mm}$  in diameter, there is no influence of bubble size on the specific death rate of insect cells.

In our experiments we obtained bubble diameters larger than  $4 \text{ mm}$ , as measured from photographs. The relationship between gas flow rate and bubble diameter is shown in Table I. Within one experiment in Figure 3, the bubble diameter does not vary largely: at  $3.6 \text{ dm}^3 \cdot \text{h}^{-1}$  the diameter increases from  $4.2$  to  $4.5 \text{ mm}$  going from four nozzles to one nozzle and at  $7.2 \text{ dm}^3 \cdot \text{h}^{-1}$  the diameter increases from  $4.3$  to  $4.8 \text{ mm}$  going from four nozzles to one nozzle. Since the

bubble diameters were fairly constant, the results show that there is no significant effect of bubble formation velocity on the specific cell death rate and, hence, it is not likely that cell death occurs at the sparger site under this set of conditions.

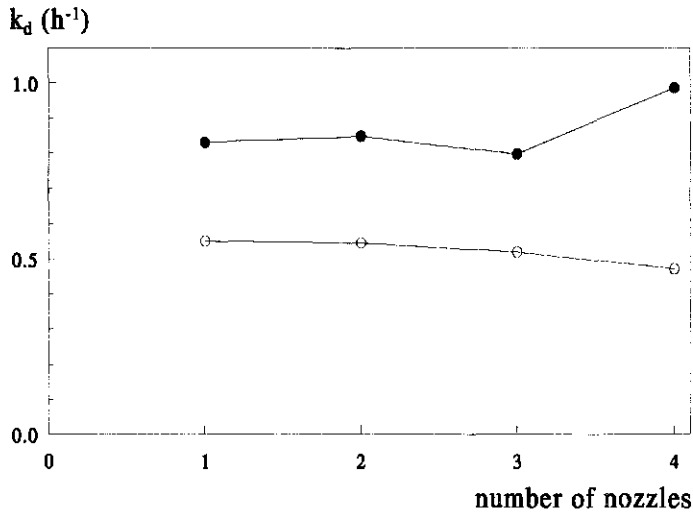


**Figure 3.** Effects of gas entrance velocity on the specific cell death-rate constant. The gas entrance velocity was varied by varying the number of nozzles between one and four, while the total gas flow rate was kept constant. Conditions were: column diameter of 2.9 cm; volume of 80 cm<sup>3</sup>; (O) total gas flow rate of 3.6 dm<sup>3</sup>.h<sup>-1</sup>, gas entrance velocities of 1.3-0.3 m.s<sup>-1</sup>; (●) total gas flow rate of 7.2 dm<sup>3</sup>.h<sup>-1</sup>, gas entrance velocities of 2.5-0.6 m.s<sup>-1</sup>.

**Table I.** Influence of gas flow rate on average bubble diameter. Bubble diameters were estimated from photographs. Gas was sparged through one nozzle. The average diameters are shown with their standard deviations.

Gas flow rate (dm <sup>3</sup> .h <sup>-1</sup> )	Bubble diameter (10 <sup>-3</sup> m)	Standard deviation (10 <sup>-3</sup> m)
2	4.3	0.4
4	4.5	0.2
6	4.5	0.4
8	5.0	0.4
10	5.8	0.9
12	6.8	0.8
14	7.2	1.2

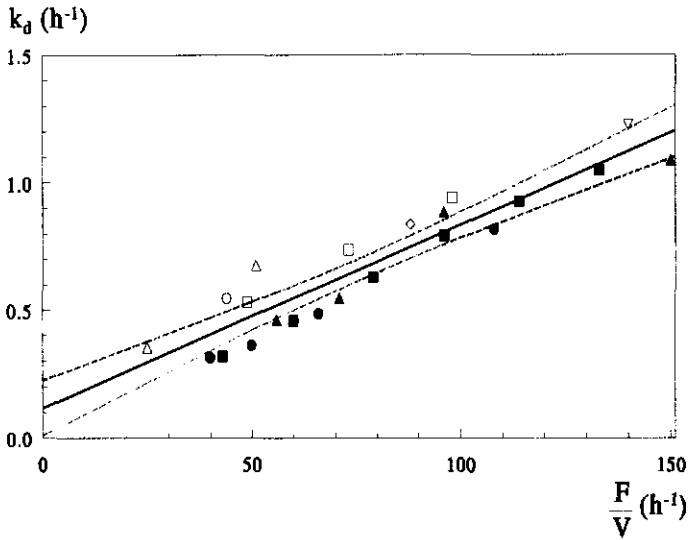


Figure 4. Plot of specific cell death-rate constants versus gas flows per unit culture volume. Different data signs represent independent experiments using the following gas flow rates and conditions :

Sign	Flow rate ( $\text{dm}^3 \cdot \text{h}^{-1}$ )	Volume ( $\text{cm}^3$ )	Height (cm)	Diameter (cm)
$\Delta$	2	80	12	2.9
	2	40	8	2.5
$\circ$	3.7 <sup>a</sup>	80	12	2.9
$\nabla$	5.5	40	8	2.5
$\diamond$	7.2 <sup>a</sup>	80	12	2.9
$\square$	4.0-8.0	80	12	2.9
$\blacksquare$	8	60-190	8-25	3.1
$\bullet$	8	73-195	21	2.1-3.4
$\blacktriangle$	9	60-160	8-21	3.1

<sup>a</sup> The average cell death rates of Figure 3, using one to four nozzles, are used. The solid line shows the correlation estimated by linear regression, while the broken line shows the 95% confidence region of the regression line.

This leaves bubble break-up at the surface as the main cell-killing event. According to Equation (11), the ratio between gas flow and culture volume (at constant bubble size) is linearly related to the cell death rate. The results of the experiments in which the culture heights were

varied are in agreement with this. Additionally, a large number of experiments were performed in which column diameter, culture volume, gas flow rate and number of nozzles were varied and the resulting death rate constants are plotted against the flow rate per culture volume in Figure 4. From this figure it appears, that within a flow range of 4 to 9 dm<sup>3</sup>.h<sup>-1</sup>, resulting in bubble diameters between 4.2 and 5.5 mm, the cell death rate is linearly proportional to the gas flow rate per unit volume. Equation (11) can therefore be simplified to Equation (12):

$$\frac{dC_{Xv}}{dt} = -k_5 \frac{F}{V} C_{Xv} \quad (12)$$

where  $k_5$  is a dimensionless constant.

### Protection

Since cell death probably occurs during bubble break-up at the culture surface, altering the surface tension should influence the specific cell death rate. In fact, it is well known<sup>5,9,11</sup> that the surfactant Pluronic F68, a block copolymer of polyethylene and polypropylene, protects cells against hydrodynamic forces.

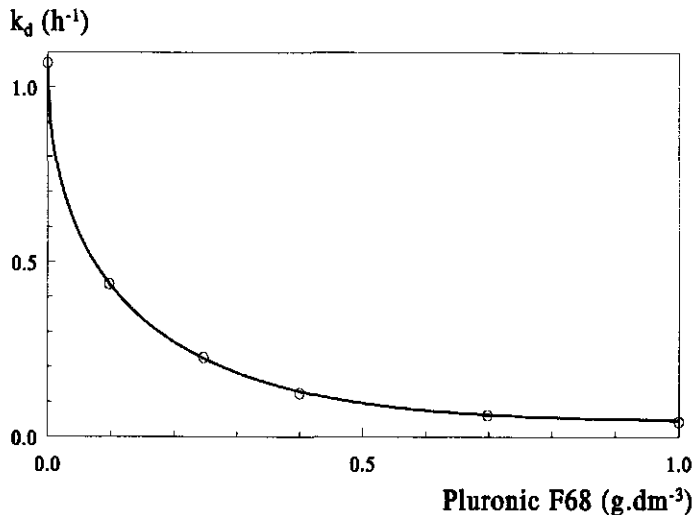


**Figure 5.** Protective activity of pluronic F68 against sparging. Several concentrations of Pluronic F68 were tested. Experimental conditions were gas flow rate of 10 dm<sup>3</sup>.h<sup>-1</sup>, one nozzle, column diameter of 2.9 cm, and culture volume of 80 cm<sup>3</sup>.



Various concentrations Pluronic F68 were tested for their effectiveness. The results are shown in Figure 5. It is clear that Pluronic F68 has a strong protective effect; at a concentration of  $0.1 \text{ g.dm}^{-3}$  the  $k_d$  is diminished from  $1.1$  to  $0.4 \text{ h}^{-1}$  and is decreased further to  $0.05 \text{ h}^{-1}$  at a concentration of  $1 \text{ g.dm}^{-3}$ . A possible effect of Pluronic F68 on the average bubble diameter, which could affect the cell death rate as discussed for the experiments described in Figure 3, was investigated. Table II shows that the presence of higher concentrations of Pluronic F68 result in a decrease in bubble size, which indicates that bubble coalescence might play a role at this gas flow rate ( $10 \text{ dm}^3.\text{h}^{-1}$ ). Since Pluronic F68 in concentrations up to at least  $0.1 \text{ g.dm}^{-3}$  has no effect on bubble size but still protect against sparging damage, it can be concluded that the protection offered by Pluronic F68 is not caused by a decrease in bubble size only. The question arises by what mechanism Pluronic exerts its protective action: by decreasing the surface tension and hence the force of bubble break-up, by formation of a stagnant film around the bubbles or by the action on cells themselves by forming a 'skin' or stagnant film around them.

**Table II.** Effects of Pluronics F68 on bubble diameter. Bubble diameters were estimated from photographs. Gas was sparged through one nozzle at a flow rate of  $10 \text{ dm}^3.\text{h}^{-1}$ . The average diameters are shown with their standard deviations.

Pluronic F68 concentration ( $\text{g.dm}^{-3}$ )	Bubble diameter ( $10^{-3} \text{ m}$ )	Standard deviation ( $10^{-3} \text{ m}$ )
-	5.8	0.9
0.1	5.9	0.7
0.4	5.5	0.7
0.7	4.9	0.4
1	4.9	0.3

These possibilities were investigated by testing the protective property of Pluronic F68 in a situation of hydrodynamic stress in the absence of gas bubbles. A culture sample of  $225 \text{ cm}^3$  was submitted to extensive mixing by a marine impeller at  $600 \text{ rpm}$  in a graduated measuring cylinder. In the presence of Pluronic F68 as well as in the control experiment, a deep vortex was created, but no air bubbles were entrained into the fluid. As shown in Table III, the same protective effect of Pluronic was observed as in the sparging experiment. This result indicates, that Pluronic F68 acts directly on the cells and not on the bubble-liquid interface.

**Table III.** Effect of Pluronic F68 on cell death rate caused by bubble-free hydrodynamic stress. The hydrodynamic stress was applied to culture volumes of 225 cm<sup>3</sup> by stirring at 600 rpm. Under these conditions bubble entrainment did not occur.

Pluronic F68 concentration (g.dm <sup>-3</sup> )	$k_d$ (h <sup>-1</sup> )	95% confidence interval (h <sup>-1</sup> )
0	2	1.2
1	0.03	0.08

## DISCUSSION

The cell death rate appears to be a simple linear function of the specific gas flow rate  $F/V$ , for bubble sizes between 4 and 5.5 mm. The sparging experiments in which the bubble residence time is varied clearly demonstrate that cell death in a bubble column is not caused by bubble rising. This result is in agreement with the work of Handa et al. on hybridomas<sup>7</sup> and the work of Tramper et al. on insect cells<sup>14</sup>. It implies that reactor performance can be optimized by increasing the reactor height: the bubble residence time then increases, enhancing the oxygen transfer rate while cell damage does not increase.

Variation of the gas entrance velocities, with only minor effects on bubble size, had no significant effect on the cell death rate. Therefore, it can be concluded that cell death is not invoked at the sparger site. One precaution should be made however: if the gas entrance velocity or bubble formation force was always above the killing limit under all the conditions examined, a gradation in cell death rates can not be expected at various gas entrance rates. Since the bubble formation velocity and the bubble size<sup>14</sup> within a diameter range of 2-6 mm do not affect the cell death rate, reactor performance can be optimized by designing a sparger that creates small bubbles. Small bubbles have a larger surface to volume ratio than large bubbles, which results in a higher oxygen transfer rate per unit gas volume. However, the lower limit for bubble diameter size seems to be 2 mm. Below this diameter, it appears that small bubbles are more detrimental to hybridoma cells<sup>6</sup> than large bubbles.

The result, that cell death does not occur during bubble rising but occurs at the surface during bubble escape (or more unlikely, during bubble formation at the sparger site), means that the physical forces during bubble rising are smaller. According to Equation (4), however, energy dissipation by gas sparging is only a function of the reactor height, i.e. the energy transfer from the bubbles to the fluid occurs during bubble rising. This contradiction might be explained in two ways. First, it is possible that the local instantaneous energy dissipation during bubble formation

or escape is much higher than during bubble rising, but does not account significantly to the total energy dissipation. Second, energy dissipation from a gas during sparging in a small culture vessel might not be described adequately by Equation (4), and energy dissipation terms for gas-liquid interface formation and disruption during bubble formation and bubble break-up should be included.

Handa et al.<sup>7</sup> conclude from high-speed video recordings of microscopic observations, that Pluronic exerts its protecting activity by lowering the force of bubble escape at the surface and by prohibiting the cells from encountering the gas-liquid interface. In our experiments on bubble-free fluid mixing, however, Pluronic F68 protected cells against physical damage to the same degree as in sparging experiments. These results indicate, that the shear protecting activity of Pluronic F68 is mainly the result of a direct action of Pluronic F68 on the cells, possibly by the formation of a stagnant fluid film around the cells. A concomitant lowering effect on the force of bubble break-up is quite expectable, since Pluronic F68 as a surfactant decreases the fluid surface tension. Additionally, at higher Pluronic concentrations, bubble diameters decreased. This could increase the cell death rate by the increase in bubble frequency but it could also, theoretically, decrease the cell death rate by the decrease in surface area and volume per bubble which would decrease the change of collision between a cell and a bubble and also the force of bubble break-up at the surface.

The decrease of bubble size upon addition of high concentrations of Pluronic could result from a faster separation of the bubbles at the orifice of the nozzle and/or from the inhibition of bubble coalescence. Occurrence of bubble coalescence at lower gas flow rates could be possible and, consequently, might cause cell damage. Since bubble coalescence (and break-up) is a continuous process which occurs during a longer time span as bubble residence time is increased and since the cell death rate is found not to be dependent on bubble residence time, we conclude that either bubble coalescence did not occur to a large extent or that it is not the main killing event in sparged cultures.

The effects of bubble size and bubble coalescence on the cell death rate require further investigations. The strong shear-protecting activity of Pluronic F68, during sparging as well as mixing, offers a valuable tool in cell culture scale-up. Further research concerning the protecting mechanism(s) and the possible influences of Pluronics or other detergents on product formation and downstream purification processes is necessary.

## SYMBOLS

$C_{xv}$	Cell concentration	(cells.m <sup>-3</sup> )
$D_r$	Reactor diameter	(m)
$d_b$	Bubble diameter	(m)
$d_o$	Orifice diameter	(m)
$F$	Volumetric gas flow	(m <sup>3</sup> .s <sup>-1</sup> )
$F_m$	Gas mass flow	(kg.s <sup>-1</sup> )
$f(d_b)$	A function of the bubble diameter	
$g$	Gravity constant	(9.81 m.s <sup>-2</sup> )
$H$	Fluid height	(m)
$k_d$	Specific cell death-rate constant	(s <sup>-1</sup> )
$k_i$	A constant	
$P_o$	Pressure at orifice	(N.m <sup>-2</sup> )
$R$	Gas constant	(8.31 J.mol <sup>-1</sup> .K <sup>-1</sup> )
$T$	Temperature	(K)
$t$	Time	(s)
$V$	Culture volume	(m <sup>3</sup> )
$v_b$	Bubble rising velocity	(m.s <sup>-1</sup> )
$V_k$	Hypothetical killing volume of bubble	(m <sup>3</sup> )
$v_x$	Fluid velocity in x-direction	(m.s <sup>-1</sup> )
$y$	Coordinate perpendicular to x-direction	(m)
$\dot{\gamma}$	Shear rate	(s <sup>-1</sup> )
$\epsilon$	Power dissipation per unit mass	(W.kg <sup>-1</sup> )
$\lambda$	Length of smallest eddy	(m)
$\eta$	Fluid dynamic viscosity	(N.m <sup>-2</sup> .s)
$\nu$	Kinematic viscosity	(m <sup>2</sup> .s <sup>-1</sup> )
$\rho$	Specific mass	(kg.m <sup>-3</sup> )
$\tau$	Shear stress	(N.m <sup>-2</sup> )

## REFERENCES

1. Abu-Reesh, I., Kargi, F. 1989. Biological responses of hybridoma cells to defined hydrodynamic shear stress. *J. Biotechnol.* 9: 167-178.
2. Cherry, R.S., Papoutsakis, E.T. 1986. Hydrodynamic effects on cells in agitated tissue culture reactors. *Bioproc. Eng.* 1: 29-41.
3. Croughan, M.S., Hamel, J.F., Wang, D.I.C. 1987. Hydrodynamic effects on animal cells grown in microcarrier cultures. *Biotechnol. Bioeng.* 24: 130-141.
4. Croughan, M.S., Sayre, E.S., Wang, D.I.C. 1989. Viscous reduction of turbulent damage in animal cell culture. *Biotechnol. Bioeng.* 33: 862-872.
5. Handa, A., Emery, A.N., Spier, R.E. 1987. On the evaluation of gas-liquid interfacial effects on hybridoma viability in bubble column bioreactors. *Develop. Biol. Stand.* 66: 241-253.

### Chapter 3

6. Handa, A., Emery, A.N., Spier, R.E. 1987. Proc. 4th Eur. Cong. Biotechnol. **3**: 601-604.
7. Handa-Corrigan, A., Emery, A.N., Spier, R.E. 1989. Effect of gas-liquid interfaces on the growth of suspended mammalian cells: mechanisms of cell damage by bubbles. *Enzyme Microb. Technol.* **11**: 230-235.
8. Heijnen, J.J., Riet, van 't K. 1984. Mass transfer, mixing and heat transfer phenomena in low viscosity bubble column reactors. *Chem. Eng. J.* **28**: B21-B41.
9. Kilburn, D.G, Webb, F.C. 1968. *Biotechnol. Bioeng.* **10**: 801-814.
10. McQueen, A., Meilhoc, E., Baily, J.E. 1987. Influence of serum level, cell line, flow type and viscosity on flow-induced lysis of suspended mammalian cells. *Biotechnol.Lett.* **9**: 831-836.
11. Mizrahi A. 1984. *Develop. Biol. Stand.* **55**: 93-102.
12. Petersen, J.F., McIntire, L.V., Papoutsakis, E.T. 1988. Shear sensitivity of cultured hybridoma cells (CRL-8018) depends on mode of growth, culture age and metabolite concentration. *J. Biotechnol.* **7**: 229-246.
13. Schurch, U., Kramer, H., Einsele, A., Widmer, F., Eppenberger, H. 1988. Experimental evaluation of laminar shear stress on the behaviour of hybridoma mass cell cultures, producing monoclonal antibodies against mitochondrial creatine kinase. *J. Biotechnol.* **7**: 179-184.
14. Tramper, J., Smit, D., Straatman, J., Vlak, J.M. 1987. Bubble column design for growth of fragile insect cells. *Bioproc. Eng.* **3**: 37-41.

## CHAPTER 4

# EFFECT OF SERUM CONCENTRATION ON HYBRIDOMA VIABLE-CELL DENSITY AND PRODUCTION OF MONOCLONAL ANTIBODIES IN CSTRs AND ON SHEAR SENSITIVITY IN AIR-LIFT LOOP REACTORS

### ABSTRACT

The death rate of hybridoma cells, grown in a continuous culture, has been studied in a small air-lift loop reactor as a function of reactor height and injected gas flow rate. The first-order death-rate constant was found to be proportional to the reciprocal height and to the gas flow rate, in accordance with the hypothetical-killing-volume model for insect cells in bubble columns. Furthermore, the effect of the serum concentration on viable-cell concentration and monoclonal-antibody production has been investigated in a continuous culture. A serum component became growth limiting when the serum concentration was decreased from 2% to 1%. No effect of the serum concentration on specific monoclonal-antibody productivity could be measured. Samples from this culture were also studied in the air-lift loop reactor to determine the effect of serum concentration on the shear sensitivity. The shear sensitivity of the cells increased with decreasing serum concentration. The protective effect of serum was found to be physical as well as physiological.

### INTRODUCTION

Many valuable biologicals require specific post-translational modifications, which can only be properly performed in animal cells. As a consequence, the use of animal cells for the *in vitro* production of many biologicals is becoming increasingly important. A prominent example of such an animal cell is the hybridoma cell, used for the *in vitro* production of monoclonal antibodies. Monoclonal antibodies find their way into a number of applications, including diagnostics, immuno-purification, tumour imaging and therapeutic treatments. It is expected that

they will be required in kilogram quantities in the future<sup>2</sup>. Since the productivities of the hybridomas reached *in vitro* are still low compared with those achieved *in vivo*, much research has been devoted to increasing the productivity and scale of hybridoma cultures. Scale-up is most easily done in conventional reactors, for example the continuous stirred-tank reactor (CSTR), the bubble-column reactor and the air-lift loop reactor. Compared with other reactor types, like hollow-fibre and ceramic-support reactors, these classical reactors have the advantage of a relatively simple construction, proven performance and reliability, and existing industrial capacity. Furthermore, it is easy to maintain homogeneous conditions and, therefore, possible to take representative samples and to closely monitor and control cell behaviour.

One of the main problems in the scale-up of these conventional reactors is to supply sufficient oxygen to the culture. Although oxygen consumption rates of animal cells are low compared with microbial cultures, oxygen limitation may still occur at larger scales. In small, stirred, animal-cell cultures sufficient oxygen can be supplied by head-space aeration. The oxygen transfer rate in these systems can be increased by sparging. A further increase can be accomplished by increasing the stirrer speed to disperse the air bubbles. The presence of air bubbles as well as agitation cause hydrodynamic forces. Animal cells, due to their size and the lack of a cell wall, are very sensitive to these forces. Vigorous mixing and gas sparging will thus inevitably lead to cell damage and should be kept to a minimum. Thus, a stirred-tank reactor will only be favourable on a small scale, when the oxygen can be supplied by head-space aeration. In air-lift loop reactors there is no mechanical agitation leading to a more simple construction and lower shear forces as compared with the CSTR. Furthermore, air-lift loop reactors have, even at larger scales, good oxygen- and mass-transfer characteristics. Altogether, the air-lift loop reactor seems to be a well-suited reactor for culturing fragile animal cells at large scale.

As stated before, the presence of air bubbles, either as a consequence of sparging or as a result of bubble entrainment, causes damage to the fragile animal cells<sup>1,4,5,6,10,13,17,18,20</sup>. The exact nature of the forces and mechanisms involved is still not fully understood. Tramper et al.<sup>20</sup> distinguish three regions in a bubble column where cell death might occur: (1) at the sparger where the bubbles are formed, (2) in the region where the bubbles rise, and (3) at the surface where bubble disengagement occurs. They find for insect cells in bubble columns that the most probable region of cell death is the surface where the bubbles break up. Jöbses et al.<sup>10</sup> come to the same conclusion for hybridomas in bubble columns, although they do not exclude the sparger region as a possible place for cell death. In agreement with these findings, Handa et al.<sup>6</sup> have shown by direct visualisation with a video-camera, that cell damage occurs at the surface and may be caused by two mechanisms: (1) damage as a result of rapid oscillations caused by

bursting bubbles and (2) damage caused by a physical shearing effect in the draining liquid films in unstable foams. Kunas and Papoutsakis<sup>13</sup> were able to culture hybridoma cells without growth retardation at agitation rates as high as 600 rpm in the presence of small air bubbles as long as these could not interact with a freely moving gas-liquid interface. In the presence of such an interface, cell damage occurred, which agrees with the findings of Handa et al.<sup>6</sup> and Tramper et al.<sup>20</sup> that cell death occurs at the surface. Furthermore, this makes clear that the presence of air bubbles interacting with the surface is far more damaging than agitation.

Murhammer et al.<sup>16</sup> compared the growth of insect cells in two air-lift bioreactors with a comparable geometry but different gas spargers. They concluded that cell death may also occur at the sparger site.

Irrespective of the exact nature of the physical forces which are responsible for cell damage, Tramper et al.<sup>20,21,22</sup> developed a model describing cell death in a bubble column. They assume that cell death can be described by first-order kinetics as described by Equation (1).

$$\ln\left(\frac{C_{Xv}(t)}{C_{Xv}(0)}\right) = -k_d t \quad (1)$$

where  $C_{Xv}(t)$  and  $C_{Xv}(0)$  are the number of viable cells (cells.m<sup>-3</sup>) at time  $t=t$  and  $t=0$  s respectively,  $k_d$  is the first-order death-rate constant (s<sup>-1</sup>) and  $t$  is the time (s). Furthermore, they associate with each air bubble a hypothetical killing volume  $V_k$  (m<sup>3</sup>) in which all viable cells are killed. After validating the model for the column height, column diameter, gas flow and the air-bubble diameter, they find that the first-order death-rate constant may be described by Equation (2).

$$k_d = \frac{4FV'_k}{\pi D_r^2 H} \quad (2)$$

where  $F$  is the gas flow (m<sup>3</sup>.s<sup>-1</sup>),  $D_r$  is the column diameter (m),  $H$  is the column height (m) and  $V'_k$  is the specific hypothetical killing volume (m<sup>3</sup>.m<sup>-3</sup>) being the hypothetical killing volume divided by the volume of the air bubble.

The model was validated for insect cells in a bubble column<sup>21</sup> and for hybridomas in a bubble column<sup>10,18</sup>. Jöbses et al.<sup>10</sup> further elaborated the model by specifying the three different zones of possible cell death as distinguished by Tramper et al.<sup>20</sup>.

The sensitivity of the animal cells for hydrodynamic forces is dependent upon the serum concentration<sup>11,12,18</sup>. Besides this protective effect, serum also has a growth-stimulating effect<sup>7</sup>. Nevertheless, serum-free cultivation of animal cells is preferred for a number of reasons. First



serum is expensive, a possible source of contamination, and its composition varies from batch to batch. Furthermore, it has to be removed in the product-recovery step. In the study we have tested the hypothetical-killing-volume model for hybridomas not in a bubble column but in an air-lift loop reactor. Besides this, the effects of serum concentration on the shear sensitivity, the productivity, and the viability of the cells are described in more detail.

## **MATERIAL AND METHODS**

### **Cell culture**

The mouse-mouse hybridoma Mn12 (RIVM Bilthoven, The Netherlands), producing IgG2a antibodies directed against the outer membrane protein P1.16 of *Neisseria Meningitides*, was grown in a continuous culture in a stirred fermenter (at 60 rpm) with a working volume of 2 dm<sup>3</sup> and a dilution rate of 0.021 h<sup>-1</sup>. The medium used was Iscove's modified Dulbecco's medium (Gibco laboratories, Paisley, Scotland) supplemented with 0.25% (w/v) Primatone RL (Sheffield products, Norwich, NY, USA), 5% (v/v) heat-inactivated fetal bovine serum (FBS) (Flow-laboratories, Woodstock Hill, UK) and antibiotics (35,000 U/l polymyxin B, 14,000 U/l neomycin and 75,000 U/l streptomycin). The culture conditions were controlled at pH 7.2, temperature 37°C, Po<sub>2</sub> 50% air saturation and a stirrer speed of 60 rpm. The pH and the PO<sub>2</sub> were controlled by blowing a mixture of air, N<sub>2</sub>, O<sub>2</sub> and CO<sub>2</sub> over the culture surface and by the addition of NaHCO<sub>3</sub>. At serum concentrations of 5% and 3% sparging was necessary in order to supply sufficient oxygen to the culture.

Two cultures were run under these conditions. In one culture the serum concentration was reduced stepwise from 5% to 3% and eventually to 2% (v/v). In the second culture the serum concentration was reduced from 2% to 1% and eventually to 0.5% (v/v). After a change of serum concentration the cultures were run at least five residence times (being 10 days), a time within which a hydraulic steady state is reached.

### **Sparging experiments**

Experiments were executed with 45-235 cm<sup>3</sup> samples taken from the continuous culture when it had reached a hydraulic steady state. After a sample was taken the culture was run fed batch. Because the maximum period a culture was operated fed batch was about 5.5 hours, it is not likely that the steady state was substantially disturbed. The samples were placed in an air-lift reactor with an internal loop. The air lift was thermostated at 37°C by a water jacket. Air containing 5% CO<sub>2</sub> was sparged into the inner tube through a nozzle with a diameter of about

$10^{-3}$  m. The flow rates were controlled by a Brooks rotameter and measured exactly after each experiment.

The inner diameter of the draught tube varied between 0.01 and 0.02 m and the fluid heights were varied from 0.06 to 0.33 m. The inner diameter of the outer tube was kept constant at 0.025 m. Gas flow rates ranged from 3 to  $16 \text{ dm}^3 \cdot \text{h}^{-1}$ . During the experiments  $0.1 \text{ cm}^3$  of a 0.01% (v/v) antifoam Silicone B (Baker, Deventer, the Netherlands) solution was added every time foaming occurred. The maximum amount of antifoam added during all the experiments was 0.03% (v/v), based upon original strength. Because lysis and complete destruction of the cells occurred, only the viable cells were counted. The decrease in viable-cell number was then used to calculate the first-order death-rate constant.

### **Cell counts**

Cells were counted using a Fuchs-Rosenthal haemocytometer, using the exclusion of trypan blue (1% w/v) as a measure for culture viability. The samples were diluted to such an extent that the error in the number of cells counted was about 10% or smaller.

### **Productivity**

The monoclonal-antibody concentration was determined by a mouse-IgG-specific ELISA as described by Jiskoot et al.<sup>9</sup>

## **RESULTS AND DISCUSSION**

### **Continuous culture**

Experiments were executed with cells obtained from a continuous culture, to ensure that the physiological state of the cells at the onset of a set of different experiments was as similar as possible. Two continuous cultures were run after each other at a dilution rate of  $0.021 \text{ h}^{-1}$  but at different serum concentrations. In the first culture, a decrease in the viable-cell number occurred (Fig. 1, Table I) when the serum concentration was reduced from 5% through 3% to a concentration of 2%. The decrease was very gradual over the whole culture period, and no difference could be seen when going from one concentration to the other. For this reason, it is not clear if the reduction of the viable-cell number is caused by the lowering of the serum concentration or by the fact that the serum concentration was changed before a physiological steady state had actually been reached. It is generally accepted, and also assumed in this study, that a hydrodynamic steady state is reached after 5 volume refreshments. However, this does not mean that a physiological steady state is also reached, which likely takes a much longer time.

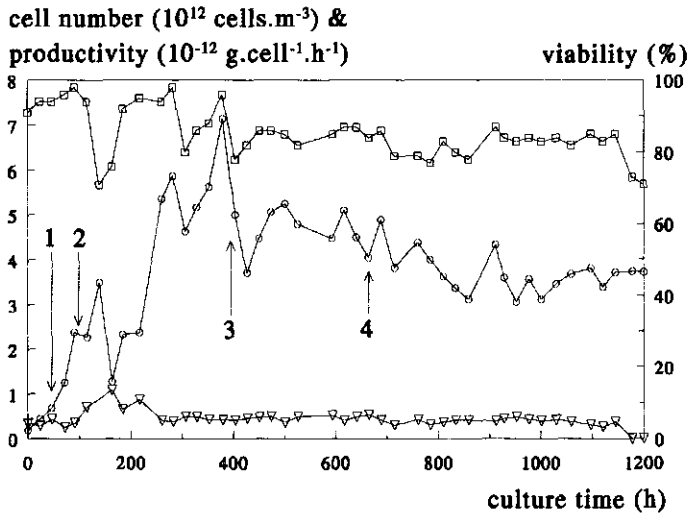


**Figure 1.** Number of viable cells (O), viability (□) and the specific productivity (∇) for culture I. The numbers in the figure correspond to changes in the culture. 1: Start of medium flow. 2: Start of sparging and 16 hours batch run due to pump failure. 3: Change from 5% FCS to 3% FCS. 4: Change from 3% FCS to 2% FCS.

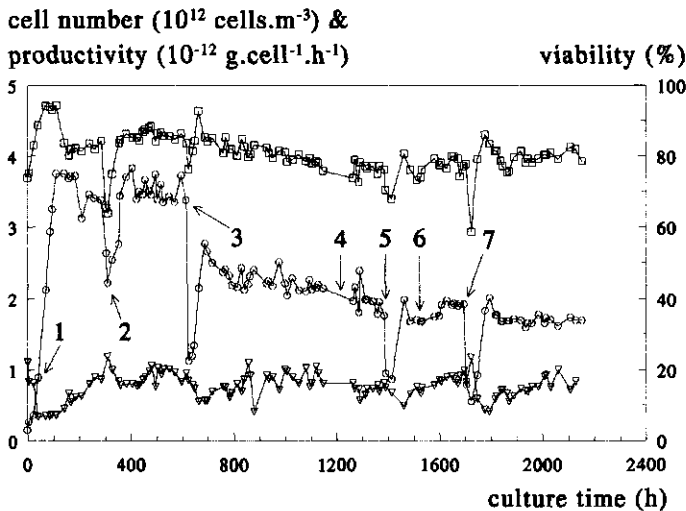


**Figure 2.** Number of viable cells (O), viability (□) and the specific productivity (∇) for culture II. The numbers in the figure correspond to changes in the culture. 1: Start medium flow. 2: Power failure 3: Change from 2% FCS to 1% FCS. 4: Increased glucose consumption and lactate production rate observed. 5: Change from 1% FCS to 0.5% FCS. 6: Change from 0.5% FCS to 1% FCS. 7: Change back to 0.5% FCS. The spikes in figure are caused by the replacement of part of the fermenter contents, including cells, by fresh medium.

Van der Pol et al.<sup>18</sup> also notice a slight decrease in viable-cell number at the serum concentrations used here. In this first run, the serum concentration was changed by simply replacing the feed flask, causing a very gradual change of the serum concentration. In order to reach the hydrodynamic steady state quicker, in the second culture, part of the fermenter contents including cells was removed and replaced by medium with the new serum concentration, causing a more sudden and quicker change of the serum concentration. Besides again observing a gradual decrease in the viable-cell number within a hydrodynamic steady state, a clear drop in the viable-cell number also occurred when going from 2% serum to 1% serum and subsequently to 0.5% serum (Table I, Fig. 2). This means that going from 2% serum to 1% serum an unknown serum component becomes growth-rate limiting. The viable-cell number in the two different cultures at 2% serum is comparable. In the second culture the hydrodynamic steady state was not reached in the period going from 1532 hours to 1704 hours, due to a mistake in medium formulation. Data obtained in this period were not used.

**Table I.** Viable-cell number and productivity for the different serum concentrations.

	Serum (%)	Period (h)	Number of datum points	Viable-cell number ( $10^{12}$ cells.m <sup>-3</sup> )	Productivity ( $10^{-13}$ g.cell <sup>-1</sup> .h <sup>-1</sup> )
I	5	261-404	7	5.5 ± 1.0	4.3 ± 0.9
	3	642-715	4	4.5 ± 1.1	4.5 ± 1.9
	2	952-1145	8	3.5 ± 0.8	3.9 ± 1.4
II	2	448-616	12	3.5 ± 0.3	9.5 ± 1.9
	1	854-1147	17	2.2 ± 0.2	8.4 ± 3.3
	0.5	1943-2152	10	1.7 ± 0.1	7.7 ± 2.4

Note: The ± values represent the 95% confidence levels. The number of datum points used for the calculation of the mean values is also given. The mean values and confidence levels were calculated over the indicated period. I: first continuous culture; II: second continuous culture.

Despite the changes in viable-cell number, the change in the specific productivity is not statistically significant (Figs. 1 and 2, Table I) within each culture. The cause for the difference in specific productivity between the two cultures is not known. Although the inocula used for the two different cultures were obtained from the same frozen batch, a real change in the specific productivity of the cells cannot be excluded. Since the determination of the specific productivity of the second culture was done later than that of the first culture, and the specific productivities measured in other cultures of Mn12 were all lying round  $4\text{-}5 \cdot 10^{-7}$  g.cell<sup>-1</sup>.h<sup>-1</sup>, it is more likely

that a mistake in the analysis of the antibody concentrations of the second culture is made. However, because the specific productivity of each culture was analysed at one time in one set of ELISAs, the specific productivities may be compared within one culture.

### Shear sensitivity

Shear experiments were done with cells taken from the two continuous cultures when in a hydraulic steady state. After a sample was taken the culture was run fed batch for a period of maximal 5.5 hours. It was assumed that this would not severely destabilize the steady state. In all the shear experiments executed, the assumption of first-order death-rate kinetics proved to be

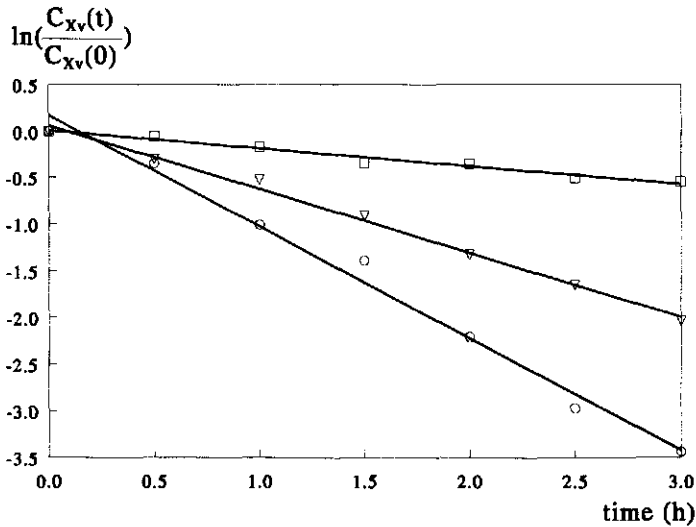


**Figure 3.** The logarithm of the number of viable cells at time  $t$  divided by the initial number of viable cells plotted against the time for three different heights of the air-lift reactor:  $H=0.06$  m (○);  $H=0.10$  m (▽);  $H=0.33$  m (□).

correct (Fig. 3). Furthermore, the  $k_d$  values were usually higher than  $0.1 \text{ h}^{-1}$ , except for a few experiments conducted at relatively large heights. The specific growth rate in the continuous culture was  $0.021 \text{ h}^{-1}$ . Because the concentration of the growth-rate-limiting component can only decrease, the specific growth rate in the air lift was probably lower than  $0.021 \text{ h}^{-1}$ . For this reason, the growth can be neglected during one shear experiment.

Varying the gas flow results in a linear correlation between  $k_d$  and the gas flow (Fig. 4), meaning that  $V_k'$  in Equation (2) is independent of the gas flow. A similar plot can be made for  $k_d$  versus the reciprocal of the air-lift height, resulting also in a linear correlation (Fig. 5). This

indicates that  $V_k'$  is also independent of the column height and that the rising of air bubbles is not detrimental for animal cells. This is consistent with the hypothetical-killing-volume model of Trampler et al. Based upon this, one may conclude that, in order to culture cells successfully in air-lift loop reactors a certain minimal height is necessary above which the death-rate constant becomes smaller than the growth-rate constant. This minimal required height will be dependent upon the gas flow necessary to supply sufficient oxygen to the culture and to ensure a proper functioning of the air lift. The effect of the diameter  $D$ , upon  $k_d$  remains to be investigated. Each set of experiments, in which one air-lift parameter was changed, was done with cells taken from the same hydraulic steady state at one particular serum concentration. Different sets of experiments at different serum concentrations were done. Each set contained one experiment done at a standard air-lift height and a standard gas flow. By comparing the standard experiments of different sets at different serum concentrations we can solely look at the effect of the steady-state serum concentration on the shear sensitivity.

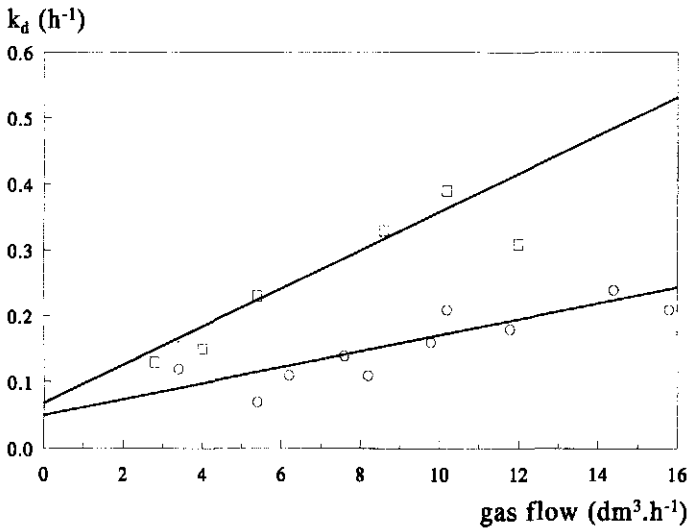


Figure 4. The first-order death-rate constant,  $k_d$ , as a function of the gas flow rate for two different serum concentrations of 3% (O) and 2% (□).

To compare the experiments done at different serum concentrations, the hypothetical killing volume  $V_k'$  was calculated according to Equation (2) from the slopes of the lines shown in Figures 4 and 5. The values are shown by the open and filled squares in Figure 6. When comparing these  $V_k'$  values to those calculated from the previous mentioned standard experiments, no differences could be seen. This means that it is allowed to compare  $V_k'$  values

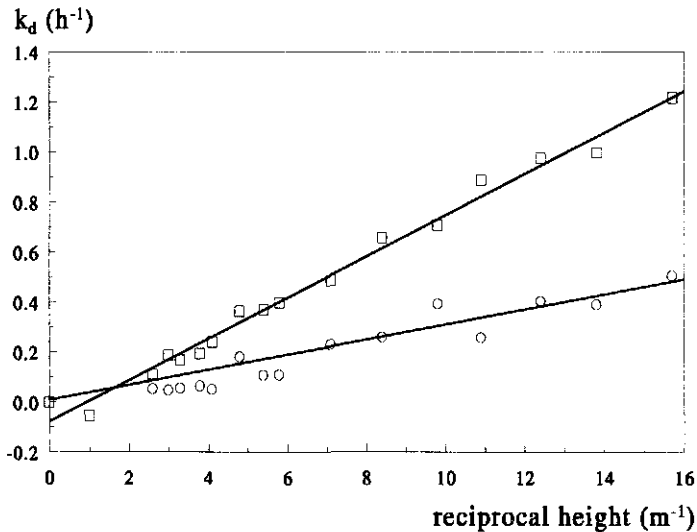
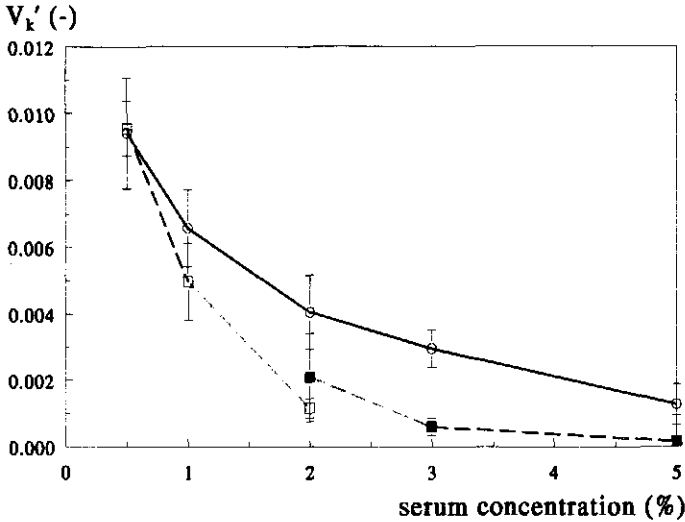


Figure 5. The first-order death-rate constant,  $k_d$ , as a function of the reciprocal air-lift height for two different serum concentrations of 1% (○) and 0.5% (□).

obtained from an experiment where the gas flow was varied with the  $V_k'$  values obtained from an experiment where the height was varied. It can be seen that the difference between the hypothetical killing volumes of the cells from the two different cultures at 2% FCS is not statistically significant. Furthermore, the hypothetical killing volume gets smaller as the steady-state serum concentration increases, meaning that the cells become less susceptible to hydrodynamic forces. This protective effect of serum against hydrodynamic forces is also reported by other authors<sup>11,12,14,18,19</sup>. The protection against hydrodynamic forces might have a physical or/and a physiological origin. We tried to discriminate experimentally between the physical and physiological part of the protection. The reduction in hypothetical killing volume, as presented by the squares in Figure 6, can be caused by both effects. It can be caused by a physical effect, because the serum is actually present, and it can be caused by a physiological effect, because cells are taken from a hydraulic steady state, meaning they have had time to adapt their physiology to the pertinent serum concentration.

In another set of experiments, cells were taken from a steady state at 0.5% serum. Serum was then added up to a concentration of 1%, 2%, 3% and 5%. Immediately after serum addition, the cells were subjected to shear stress in the small air-lift reactor. Because the cells had no time to adapt their physiology to the new serum concentration, any possible protective effect seen could only have a physical origin. The hypothetical killing volumes, calculated from the first-

order death-rate constants according to Equation (2), are presented by the open circles in Figure 6. It can be seen that serum also provides protection in this case, indicating that the mechanism offering this protection is at least in part physical. When these results are compared to the earlier results as is done in Figure 6, we see that in the case where cells had more time to adapt their physiology to the serum concentration, although an actual physiological steady state



**Figure 6.** The hypothetical killing volume,  $V_k$ , as a function of serum concentration.  $V_k'$  concerning cells taken from steady states of culture I (■) and culture II (□).  $V_k'$  concerning cells obtained from steady states containing 0.5% serum and subjected to shear immediately after serum addition to the shown concentration. (○). The error bars represent 95% confidence levels. The number of datum points used is, respectively: 5 (■, 5%), 10 (■, 3%), 18 (■, 2%), 14 (□, 2%), 30 (□, 1%), 21 (□, 0.5%), and 2 (○).

might not have been reached, an extra protection is provided as indicated by the even smaller hypothetical killing volumes. This clearly demonstrates that serum offers protection by two mechanisms: (1) a physical mechanism, working instantaneous after addition of the serum; and (2) a physiological mechanism, which needs time to become effective. Kunas et al.<sup>12</sup> state that the protective effect is at least in part physical. Van der Pol et al.<sup>18</sup>, who used a different experimental setup, find that protection by serum is largely physical, although there might be a small physiological effect. Michaels et al.<sup>15</sup> distinguish three kinds of protection: (1) physical, (2) fast-acting biological, and (3) metabolic biological protection. Our physiological mechanism could be compared to the metabolic biological mechanism of Michaels et al., while our physical mechanism is either comparable to the physical protection or to the fast-acting biological



protection or to both kinds of protection. Michaels et al. find that the protection offered by serum is physical and metabolic biological. Because we cannot differentiate between the physical protection and the fast-acting biological protection, as defined by Michaels, this does not disagree with the results presented here.

The nature of the two different mechanisms we distinguish is still unclear. The physical mechanism might be due to absorption of certain compounds on or into the plasma membrane rendering the cell less fragile. Ramirez et al.<sup>19</sup>, who found a correlation between the plasma-membrane fluidity and the shear sensitivity of hybridoma cells, propose that the protective action of serum is related to the modulation of the membrane fluidity due to a facilitated transfer of cholesterol or analogous compounds to the membrane, reducing the membrane fluidity and thus the shear sensitivity of the cells. Another possibility is that the cells are sheltered from the hydrodynamic forces, for instance, by formation of a stable foam which is not entered by the cells as proposed by Handa et al.<sup>6</sup>. A third possibility is that the hydrodynamic forces are reduced by addition of serum through an increase in viscosity<sup>3</sup>. Because the effect of serum on viscosity of the medium is small, increase of the viscosity may be ruled out as a possible cause of protection as also found by Kunas et al.<sup>12</sup>. The physiological mechanism might involve property changes of the cell cytoskeleton, plasma membrane, or other cell parts and organelles. Several authors have reported the protective effect of polymers on the growth of mammalian<sup>6,8,10</sup> and insect<sup>16</sup> cells under hydrodynamic stress, which is usually ascribed to a physical effect. On the basis of the findings reported here, one may doubt if this protection is as complete as the protection provided by the serum, which also has a physiological basis.

Furthermore, the minimal required height to culture animal cells in an air lift will, besides depending on the used gas flow, also depend on the serum concentration used. A lower serum concentration will lead to cells that are more shear sensitive and will thus result in a higher minimal required height of the air lift.

## CONCLUSIONS

At a specific growth rate of  $0.021 \text{ h}^{-1}$  an unknown serum component becomes growth-rate limiting when reducing the concentration from 2% to 1% serum, as can be seen by a drop in the viable-cell density in a continuous culture. Furthermore, going from 5% serum to 2% serum, and within the hydraulic steady states at 1% and 0.5% serum, a small but continuous decrease of the viable-cell number is observed. It is not clear if this is due to the decreasing serum concentration or to the fact that the cells need a much longer time to reach a physiological steady state. No

significant effect of serum reduction upon the specific productivity is seen, although, for unexplained reasons, the specific productivity in the second culture was about twice as high.

The cell death rate in an air-lift loop reactor increased proportionally with increasing gas flow and increasing reciprocal reactor height. Thus, the hypothetical-killing-volume model proved to be valid for hybridomas in an air-lift loop reactor with respect to the gas flow and the reactor height.

The protection offered by serum against hydrodynamic forces is based upon two mechanisms: (1) a physical mechanism working instantaneous after the addition of serum; (2) a physiological mechanism which requires a certain adaptation time of the cells to the new serum concentration in order to offer protection.

## REFERENCES

1. Al-Rubeai, M., Oh, S.K.W., Musaheb, R., Emery, A.N. 1990. Modified cellular metabolism in hybridomas subjected to hydrodynamic and other stresses. *Biotechnol. Lett.* **12**: 323-328.
2. Birch, J.R., Boraston, R., Wood, L. 1985. Bulk production of monoclonal antibodies in fermenters. *Trends Biotechnol.* **3**: 162-166.
3. Croughan, M.S., Sayre, E.S., Wang, D.I.C. 1989. Viscous reduction of turbulent damage in animal cell culture. *Biotechnol. Bioeng.* **33**: 862-872.
4. Gardner, A.R., Gainer, J.L., Kirwan, D.J. 1990. Effects of sparging on cultured hybridoma cells. *Biotechnol. Bioeng.* **35**: 940-947.
5. Handa, A., Emery, A.N., Spier, R.E. 1987. On the evaluation of gas-liquid interfacial effects on hybridoma viability in bubble-column bioreactors. *Develop. Biol. Standard.* **66**: 241-253.
6. Handa-Corrigan, A., Emery, A.N., Spier, R.E. 1989. Effect of gas-liquid interfaces on the growth of suspended mammalian cells: Mechanisms of cell damage by bubbles. *Enzym. Microbiol. Technol.* **11**: 230-235.
7. Heath, C., Dilwith, R., Belfort, G. 1990. Methods for increasing monoclonal-antibody production in suspension and entrapped cell cultures: Biochemical and flow cytometric analysis as a function of medium serum content. *J. Biotechnol.* **15**: 71-90.
8. Hülscher, M., Onken, U. 1988. Influence of bovine serum albumin on the growth of hybridoma cells in air-lift loop reactors using serum-free medium. *Biotechnol. Lett.* **10**: 689-694.
9. Jiskoot, W., Hertrooij, J.C.C., Van, Klein Gebbinck, J.W.T.M., Van der Velden-de Groot, T., Crommelin, D.J.A., Beuvery, E.C. 1989. Two-step purification of a murine monoclonal antibody intended for therapeutic application in man. Optimisation of purification conditions and scaling up. *J. Immunol. Methods.* **124**: 143-156.
10. Jöbses, I.M.L., Martens, D.E., Tramper, J. 1991. Lethal events during gas sparging in animal cell culture. *Biotechnol. Bioeng.* **37**: 484-490.
11. Kunas, K.T., Papoutsakis, E.T. 1989. Increasing serum concentrations decrease cell death and allow growth of hybridoma cells at higher agitation rates. *Biotechnol. Lett.* **11**: 525-530.
12. Kunas, K.T., Papoutsakis, E.T. 1990. The protective effect of serum against hydrodynamic damage of hybridoma cells in agitated and surface-aerated bioreactors. *J. Biotechnol.* **15**: 57-70.

## Chapter 4

13. Kunas, K.T., Papoutsakis, E.T. 1990. Damage mechanisms of suspended animal cells in agitated bioreactors with and without bubble entrainment. *Biotechnol. Bioeng.* **36**: 476-483.
14. McQueen, A., Bailey, J.E. 1989. Influence of serum level, cell line, flow type, and viscosity on flow-induced lysis of suspended mammalian cells. *Biotechnol. Lett.* **11**: 531-536.
15. Michaels J.D., Petersen J.F., McIntire L.V., Papoutsakis E.T. 1991. Protection mechanisms of freely suspended animal cells (CRL 8018) from fluid-mechanical injury. Viscometric and bioreactor studies using serum, Pluronic F68, and polyethylene glycol. *Biotechnol. Bioeng.* **38**: 169-180.
16. Murhammer, D.W., Goochee, C.F. 1990. Sparged animal cell bioreactors: Mechanism of cell damage and Pluronic F-68 protection. *Biotechnol. Prog.* **6**: 391-397.
17. Oh, S.K.W., Nienow, A.W., Al-Rubeai, M., Emery, A.N. 1989. The effects of agitation with and without continuous sparging on the growth and antibody production of hybridoma cells. *J. Biotechnol.* **12**: 45-62.
18. Pol, L. van der, Zijlstra, G., Thalen, M., Tramper, J. 1990. Effect of serum concentration on production of monoclonal antibodies and on shear sensitivity of a hybridoma. *Bioproc. Eng.* **5**: 241-245.
19. Ramirez, O.T., Mutharasan, R. 1990. The role of plasma membrane fluidity on the shear sensitivity of hybridomas grown under hydrodynamic stress. *Biotechnol. Bioeng.* **36**: 911-920.
20. Tramper, J., Williams, J.B., Joustra, D., Vlak, J.M. 1986. Shear sensitivity of insect cells in suspension. *Enzym. Microbiol. Technol.* **8**: 33-36.
21. Tramper, J., Smit, D., Straatman, J., Vlak, J.M. 1987. Bubble column design for growth of fragile insect cells. *Bioproc. Eng.* **2**: 37-41.
22. Tramper, J., Joustra, D., Vlak, J.M. 1987. Bioreactor design for growth of shear sensitive insect cells. p. 125-136 In: C. Webb, F. Ativuna (eds.), *Plant and animal cell cultures, process possibilities*, Ellis Horwood, Chichester, UK.

## CHAPTER 5

# EFFECT OF DILUTION RATE ON GROWTH, PRODUCTIVITY, CELL CYCLE AND SIZE, AND SHEAR SENSITIVITY OF A HYBRIDOMA CELL IN A CONTINUOUS CULTURE

### ABSTRACT

To study the effects of the specific growth rate of the hybridoma cell Mn12 on productivity, cell cycle, cell size, and shear sensitivity, six continuous cultures were run at dilution rates of 0.011, 0.021, 0.023, 0.030, 0.042, and 0.058 h<sup>-1</sup>. This particular hybridoma cell appeared to be unstable in continuous culture with respect to specific productivity, as a sudden drop occurred after about 30 generations in continuous culture, accompanied by the appearance of two populations with respect to the cytoplasmic IgG content. The specific productivity increased at decreasing specific growth rates. The first-order death-rate constant measured in continuous culture decreased with increasing specific growth rates. The shear sensitivity of the cells, as measured in a small air-lift loop reactor, increased with increasing specific growth rates. The mean relative cell size, as determined with a flow cytometer, increased with increasing specific growth rates. Furthermore, the fraction of cells in the S phase increased and the fraction of cells in the G<sub>1</sub>/G<sub>0</sub> phase decreased with increasing specific growth rates.

### INTRODUCTION

An important parameter with respect to the optimization of a hybridoma-cell culture is the specific growth rate. The growth of cells can be described as a cycle consisting of four distinct phases<sup>1,28,35</sup>: the gap-1 phase (G<sub>1</sub>), the DNA-synthesizing phase (S), the gap-2 phase (G<sub>2</sub>), and the mitotic phase (M). An additional phase can be identified as a resting phase (G<sub>0</sub>). Cells enter this phase at a point late in the G<sub>1</sub>, called the restriction point (R), when the conditions are unfavourable for growth<sup>1,28</sup>. Unfavourable conditions may be, for instance, a lack of nutrients or

specific growth factors, or the presence of a growth inhibitor. When the favourable conditions for growth are restored, the  $G_0$  cells can re-enter the cell cycle in  $G_1$ . Once the cells have passed the restriction point and entered the S phase, they are committed to another cell cycle. The switches in and out of  $G_0$  are the main determinants in post-embryonic cell-proliferation rate and are defectively controlled in cancer cells like hybridomas<sup>28</sup>. As a consequence, the time a cell spends in the  $G_1$  and  $G_0$  phase shows large variations with the specific growth rate. The time needed by the cells to progress through one of the other phases is relatively constant<sup>1</sup>.

Cells in different phases of the cell cycle have different properties with respect to their size, metabolic production and consumption rates, and shear sensitivity<sup>15,27,31,36</sup>. Consequently, the average values of these properties, measured in an asynchronous culture, will change with the specific growth rate.

The aim of this work is to study the effect of the specific growth rate of a continuous suspension culture on the mean number of viable and dead cells, the cell size, the shear sensitivity, the specific productivity, and the cell cycle of a hybridoma cell.

## THEORY

To culture hybridoma cells at different specific growth rates, a number of continuous cultures were run at different dilution rates. The balances of viable-, dead-, and total-cell numbers, and of the product concentration are given by:

$$\frac{dC_{Xv}}{dt} = (\mu - \mu_d - D)C_{Xv} \quad (1)$$

$$\frac{dC_{Xd}}{dt} = \mu_d C_{Xv} - DC_{Xd} - k_{lysis} C_{Xd} \quad (2)$$

$$\frac{dC_{Xt}}{dt} = \mu C_{Xv} - DC_{Xt} - k_{lysis} C_{Xd} \quad (3)$$

$$\frac{dC_p}{dt} = q_p C_{Xv} - DC_p \quad (4)$$

where  $C_{Xv}$ ,  $C_{Xd}$ , and  $C_{Xt}$  are the viable-, dead-, and total-cell number ( $\text{cells.m}^{-3}$ ),  $\mu$  is the specific growth-rate constant ( $\text{h}^{-1}$ ),  $\mu_d$  the first-order death-rate constant ( $\text{h}^{-1}$ ),  $k_{lysis}$  the first-order rate constant for lysis of dead cells ( $\text{h}^{-1}$ ),  $D$  the dilution rate ( $\text{h}^{-1}$ ),  $C_p$  the product concentration ( $\text{g.m}^{-3}$ ), and  $q_p$  the specific productivity ( $\text{g.cell}^{-1}.\text{h}^{-1}$ ). It is assumed that viable cells die before they lyse

and that the lysis of cells is not accompanied by a release of substantial amounts of intracellular antibody.

Knowing the dilution rate, the steady-state viability, and the fraction of  $G_0$ -phase cells of a continuous culture, the specific growth rate and cycle time can be calculated according to Equations (5) and (6).

$$\mu = \frac{D}{v} \quad (5)$$

$$t_c = \frac{(1-f_{G0})\ln(2)}{\mu} \quad (6)$$

where  $v$  is the viability (-),  $f_{G0}$  the fraction of cells in the  $G_0$  phase, and  $t_c$  the cycle time (h). The frequency of cells located at time  $t$  from the beginning of the  $G_1$  phase is proportional to<sup>35</sup>  $2^{t-t/c}$ . The fractions of cells in certain phases of the cell cycle are given by Equations (7), (8), (9), and (10)<sup>35</sup>.

$$f_{G1} = \frac{(1-f_{G0}) \int_0^{t_c} 2^{(1-t/t_c)} dt}{t_c \ln(2)} \quad (7)$$

$$f_S = \frac{(1-f_{G0}) \int_{t_{G1}}^{t_c} 2^{(1-t/t_c)} dt}{t_c \ln(2)} \quad (8)$$

$$f_{G2} = \frac{(1-f_{G0}) \int_{t_S}^{t_c} 2^{(1-t/t_c)} dt}{t_c \ln(2)} \quad (9)$$

$$f_M = \frac{(1-f_{G0}) \int_{t_{G2}}^{t_c} 2^{(1-t/t_c)} dt}{t_c \ln(2)} \quad (10)$$

where  $f_x$  represents the fraction of cells in a specific phase (-), and  $t_x$  (h) the time a cell remains in the specific phase x before entering the next phase in its cycle, with x being the  $G_0$ ,  $G_1$ , S,  $G_2$ , or M phase. The integral in the numerator is proportional to the number of cells in a specific phase, while the term in the denominator is equal to the total number of cells participating in the cell cycle. In order to get the fraction of cells in a specific phase with regard to the total number of cells present (including  $G_0$  cells) the fraction has to be multiplied with  $(1-f_{G0})$ .

## MATERIAL AND METHODS

### Cell culture

The mouse-mouse hybridoma Mn12 (RIVM Bilthoven, The Netherlands), producing IgG2a antibodies directed against the outer-membrane protein P1.16 of *Neisseria meningitides*, was grown in a series of six continuous cultures in a stirred fermenter (at 60 rpm) with a working volume of 2 dm<sup>3</sup> at dilution rates of 0.011 h<sup>-1</sup>, 0.021 h<sup>-1</sup>, 0.023 h<sup>-1</sup>, 0.030 h<sup>-1</sup>, 0.042 h<sup>-1</sup>, and 0.058 h<sup>-1</sup>. The medium used was Iscove's modified Dulbecco's medium (Gibco laboratories, Paisley, Scotland) supplemented with 0.25% (w/v) Primatone RL (Sheffield products, Norwich, NY, USA), 1% (v/v) heat-inactivated fetal-calf serum (FCS) (Flow-laboratories, Woodstock Hill, UK) and antibiotics (35,000 U.dm<sup>-3</sup> polymyxin B, 14,000 U.dm<sup>-3</sup> neomycin and 75,000 U.dm<sup>-3</sup> streptomycin). The culture conditions were controlled at pH 7.2, a temperature of 37°C, and a pO<sub>2</sub> at 50% air saturation. The pH and the pO<sub>2</sub> were controlled by head-space aeration with a mixture of air, N<sub>2</sub>, O<sub>2</sub> and CO<sub>2</sub> and by the addition of NaHCO<sub>3</sub>.

Two groups of continuous cultures were run. The cultures run at 0.030 h<sup>-1</sup> and 0.042 h<sup>-1</sup> were inoculated with cells taken from the culture run at 0.023 h<sup>-1</sup>, while the cultures run at 0.011 h<sup>-1</sup> and 0.058 h<sup>-1</sup> were inoculated with cells taken from the culture run at 0.021 h<sup>-1</sup>. The cultures that provided the inocula serve as a reference and a duplo run. Furthermore, these two reference cultures were inoculated with cells from the same working cell bank.

After a culture had run for at least five residence times, samples for analysis were taken. After five residence times 99% of the liquid volume in the reactor is replaced, which is enough to ensure hydraulic steady state. Hydraulic steady state is reached, when 95% of the original reactor contents is replaced, which is the case after three residence times.

### Flow cytometry

Samples were analysed with a flow cytometer (FACScan; Becton Dickinson BV, Etten-Leur, The Netherlands). An HP310 computer (Hewlett-Packard corporation, Pittsburgh, PA) with a Consort 30 program (Becton Dickinson) was used for data processing. On the basis of the

forward-angle and right-angle scattering of the cells we were able to discriminate between dead and viable cells. All flow-cytometer data stem from the viable-cell fraction.

The scatter properties, forward scatter (FSC) and side scatter (SSC), were measured on the flow cytometer without pretreatment of the samples.

For determination of the cell distribution over the  $G_1$ , S, and  $G_2/M$  phase of the cell cycle, cell suspensions, containing a total of  $2.5 \cdot 10^6$  cells, were incubated with 5-BromodesoxyUridine (BrdU) (Sigma, St.Louis, MO) at a final concentration of  $10 \mu\text{M}$  for 1 h at  $37^\circ\text{C}$ . BrdU is incorporated in the DNA of DNA-synthesizing cells (S phase). Next the cells were washed with phosphate-buffered saline (PBS), containing 0.2% bovine serum albumin (BSA) (PBS/0.2% BSA) and then incubated in 70% ethanol ( $1 \text{ cm}^3$ ) at  $0^\circ\text{C}$  for 1 h. After two washes with PBS/0.2% BSA the cells were incubated for 20 min with  $1 \text{ cm}^3$  1 M hydrochloric acid at  $0^\circ\text{C}$ . The cells were then washed again with PBS/0.2% BSA and incubated with anti-BrdU monoclonal antibodies ( $20 \cdot 10^{-3} \text{ cm}^3$ ; Becton Dickinson) for 30 min at  $0^\circ\text{C}$ . Subsequently, the cells were washed with PBS/0.2% BSA and incubated with fluorescein isothiocyanate (FITC)-labelled goat anti-mouse IgG1 antibodies ( $20 \cdot 10^{-3} \text{ cm}^3$ ; Southern Biotechnology Association, Birmingham, AL) for 30 min at  $0^\circ\text{C}$ . After the final washes and resuspension in  $0.5 \text{ cm}^3$  PBS/0.2% BSA, the cells were incubated for 10 min with propidium iodide ( $2.6 \cdot 10^{-3} \text{ cm}^3$ ;  $1.9 \text{ mg}\cdot\text{cm}^{-3}$ ; Sigma, St. Louis, Mo)<sup>7</sup>. Propidium iodide intercalates in double stranded DNA. Next, the sample is analysed on the FACS. S-phase cells may be discriminated by their green fluorescence.  $G_2$ -phase cells can be discriminated from  $G_1/G_0$ -phase cells by the fact that they contain twice as much DNA and thus show a two times higher red fluorescence. Because it was not possible to make a discrimination between  $G_1$ -phase cells and  $G_0$ -phase cells and between  $G_2$ -phase cells and M-phase cells, they are treated as one population ( $G_0/G_1$  and  $G_2/M$ ).

### Shear sensitivity

The shear sensitivity of the cells was determined in a small air-lift reactor with an internal loop. Experiments were executed with  $60 \text{ cm}^3$  samples taken from a continuous culture that had reached a hydraulic steady state. After a sample was taken, the culture was run fed batch. Because the maximum period a culture was operated fed batch was about three hours, and the volume reduction was only 3%, it is not likely that the steady state was substantially disturbed. The air lift was thermostated at  $37^\circ\text{C}$  by a water jacket. Air containing 5%  $\text{CO}_2$  was sparged into the inner tube through a nozzle with a diameter of  $10^{-3} \text{ m}$ . The flow rates were controlled by a Brooks rotameter and measured exactly after each experiment.



The conditions were kept constant for all the sparging experiments. The inner diameter of the draught tube was 0.017 m, the fluid height 0.08 m, the inner diameter of the outer tube was 0.025 m, and the gas flow rate was 7.5 dm<sup>3</sup>.h<sup>-1</sup>. During the experiments 0.1 cm<sup>3</sup> of a 0.01% (v/v) antifoam Silicone B (Baker, Deventer, NL) solution was added every time foaming occurred. The maximum amount of antifoam added during all the experiments was 0.03% (v/v), based upon original strength. Because lysis and complete destruction of the cells occurred, only the viable cells were counted. Samples were sheared for a period of 3 hours and the viable cells were counted every half hour. Assuming first-order death-rate kinetics<sup>23,37</sup>, the first-order death-rate constant was calculated using the decrease in viable-cell number according to Equation (11):

$$\ln \frac{C_{Xv}(t)}{C_{Xv}(0)} = -k_d t \quad (11)$$

where  $C_{Xv}(t)$  and  $C_{Xv}(0)$  are the number of viable cells (cells.m<sup>-3</sup>) at time  $t=t$  (h) and  $t=0$  (h), respectively;  $k_d$  is the first-order death-rate constant (h<sup>-1</sup>).

### Cell counts

Cells were counted using a Fuchs-Rosenthal haemocytometer, using the exclusion of trypan blue (1% w/v) as a measure for culture viability. The samples were diluted to such an extent that a minimal number of 200 cells were counted.

### Productivity

The monoclonal-antibody concentration was determined by a mouse-IgG-specific ELISA as described by Jiskoot et al.<sup>19</sup>.

## RESULTS AND DISCUSSION

### Continuous cultures

Figure 1 shows the typical behaviour of Mn12 cells in a continuous culture. This particular culture was run at a dilution rate of 0.021 h<sup>-1</sup>. All the other cultures gave rise to similar plots, although different steady-state values were reached. The medium flow was started after 50 hours. At about 300 hours, corresponding to five volume replacements, hydraulic steady state is certainly reached. In Figure 1, one can see that already after 200 hours steady cell numbers were reached. However, the fraction of cells in a certain phase as well as the  $k_d$  and the forward scatter reach steady levels only after 400 hours. Differences between the two groups of continuous

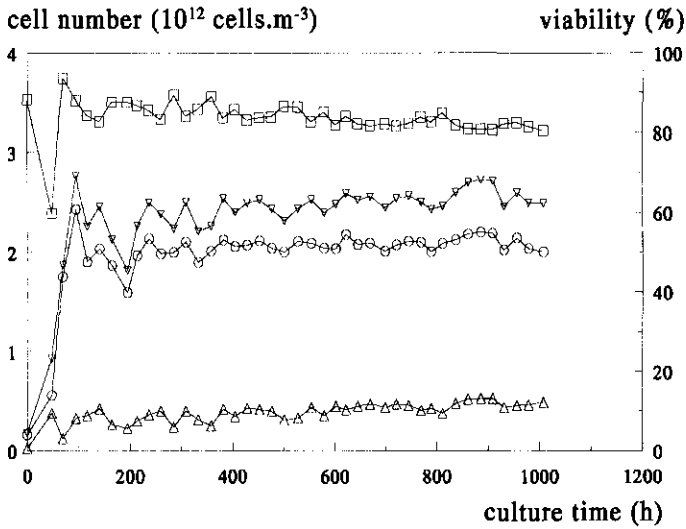


Figure 1A. Concentration of viable cells (○), dead cells (△) and total cells (▽) and the viability (□) as a function of culture time in a continuous culture run at a dilution rate of 0.021 h<sup>-1</sup>.

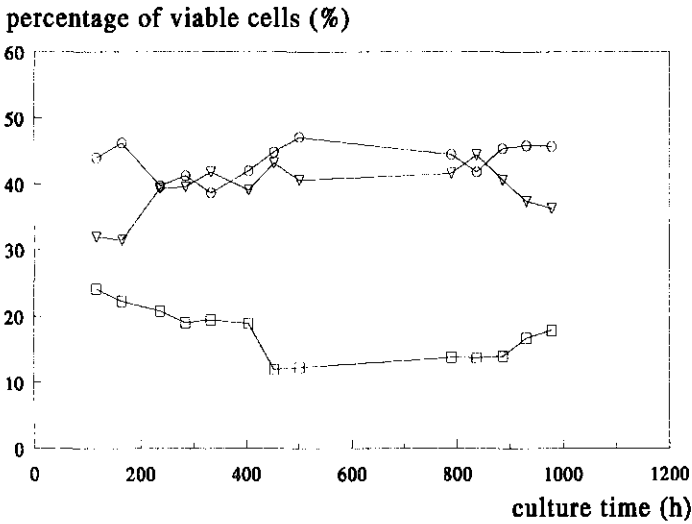
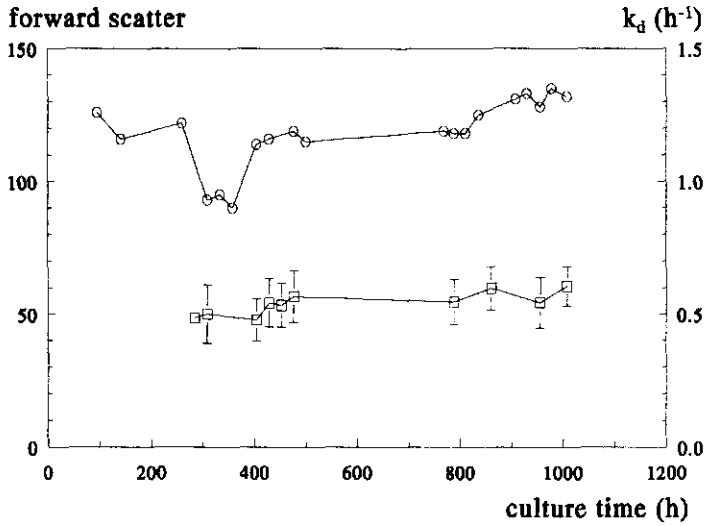
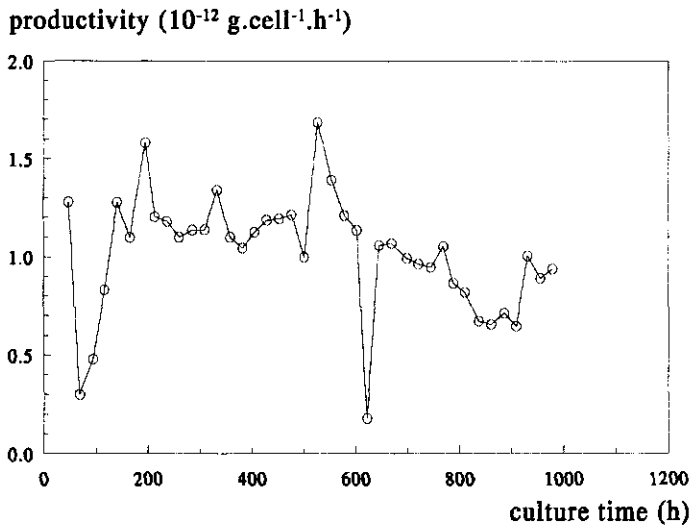


Figure 1B. Percentage of viable cells in the G<sub>1</sub> phase (○), S phase (▽) and G<sub>2</sub>/M phase (□) as a function of culture time in a continuous culture run at a dilution rate of 0.021 h<sup>-1</sup>.



**Figure 1C.** Forward scatter (○) and first-order death-rate constant measured in a small air-lift loop reactor (□) as a function of culture time in a continuous culture run at a dilution rate of  $0.021 h^{-1}$ .



**Figure 1D.** Productivity (○) as a function of culture time in a continuous culture run at a dilution rate of  $0.021 h^{-1}$ .

cultures as a consequence of differences in inocula are minimized by inoculating the two reference cultures from the same working cell bank.

In two continuous cultures, run at dilution rates of  $0.021 \text{ h}^{-1}$  (Fig. 1) and  $0.058 \text{ h}^{-1}$  (data not shown), respectively, a drop in the specific productivity occurred, accompanied by the appearance of two populations with respect to the cytoplasmic IgG content (data not shown). The culture shown in Figure 1 also showed a slight increase in the forward scatter. The culture run at  $D=0.058 \text{ h}^{-1}$  was inoculated with cells from the culture run at  $D=0.021 \text{ h}^{-1}$ , which served as a reference culture. The only parameter that changed during a specific culture was the culture age or the number of generations a culture had undergone. For both cultures the drop in specific productivity and the appearance of the two populations occurred after about 30 generations, counted from the inoculation of the reference culture with cells from the working cell bank. The occurrence of two populations concerning the cytoplasmic IgG content has also been observed by other authors<sup>11,17</sup>. In previous cultures of the hybridoma cell Mn12, this instability also occurred after a comparable number of generations of about  $34^8$ . The population with a lower cytoplasmic IgG content might represent a non-producing population, thus explaining the lower specific productivity.

In the reference culture the specific productivity, the forward scatter, and the fraction of S-phase cells exhibit a change in value. This means that, except for these parameters, the culture run at  $D=0.058 \text{ h}^{-1}$  still may be compared to the cultures run at the other dilution rates. In these other four continuous cultures the total number of generations, measured from the start of the culture, was smaller, ranging from 16 to 25, and no instabilities occurred.

### Cell numbers

The viable-cell number is more or less constant at a level of  $2 \cdot 10^6 \text{ cells.cm}^{-3}$  for the different dilution rates (Fig. 2), although a slight decrease can be detected at the highest dilution rate. This small decrease in the viable-cell number indicates that the maximum specific growth rate of the cells is nearly reached. As the dilution rate is decreased an exponential increase in the dead- and total-cell number can be seen. This trend is also reported by other authors<sup>12,18,22,24,33</sup>. To see whether the specific death rate of the cells also increased at lower dilution rates, the first-order death-rate constant,  $\mu_d$ , was calculated according to Equation (2). In Figure 3,  $\mu_d$  is plotted against the dilution rate, showing an exponential increase at decreasing dilution rates as was also found by Glacken<sup>14</sup>. Because the total biomass produced is dependent upon the total-cell number and the biomass per cell, the increase in total-cell number from about  $2 \cdot 10^6$  to  $4 \cdot 10^6 \text{ cells.cm}^{-3}$  does not necessarily mean that the biomass also increases with a factor 2. As will be shown, the

volume of the cells decreases as the dilution rate decreases. Frame and Hu<sup>10</sup> showed that a decrease in the cell volume corresponds to a decrease in the biomass per cell.

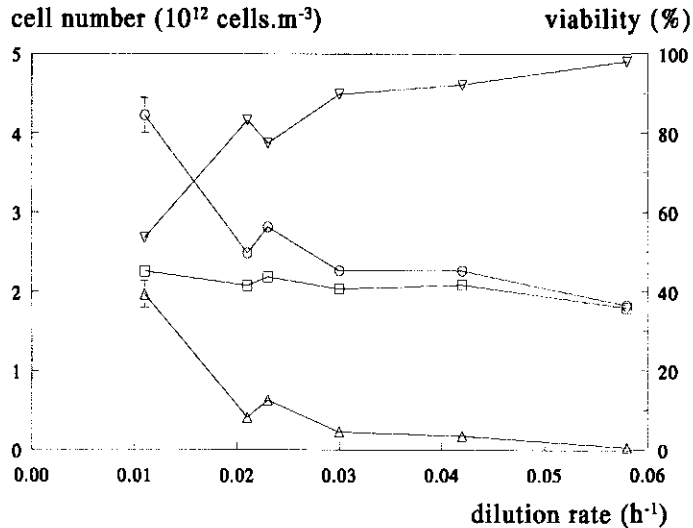


**Figure 2.** Concentration of viable cells (□), dead cells (Δ) and total cells (O), and the viability (∇) as a function of the dilution rate.

Knowing the viability, the specific growth rate can be calculated according to Equation (5). The result is also shown in Figure 3. At high dilution rates the viability approaches 100% and the specific growth rate thus approximates the dilution rate. As the dilution rate decreases, the viability decreases with it and, as a consequence, the specific growth rate is higher than the dilution rate. In Figure 3, the points at low  $D$  deviate from the  $\mu = D$  line. This would be in accordance with the work of Glacken<sup>14</sup> reporting on a minimal specific growth rate.

We have not accounted for, nor measured, the lysis of cells. If lysis occurs, the viability should be calculated including the lysed cells. Consequently, the viability would become smaller and the specific growth rate would increase. Because the shear in the continuous culture is very low, lysis is most probable a consequence of disintegration of dead cells, meaning that more lysis is likely to occur if more dead cells are present. This would result in higher specific growth rates at the lower dilution rates and thus in a higher minimal specific growth rate.

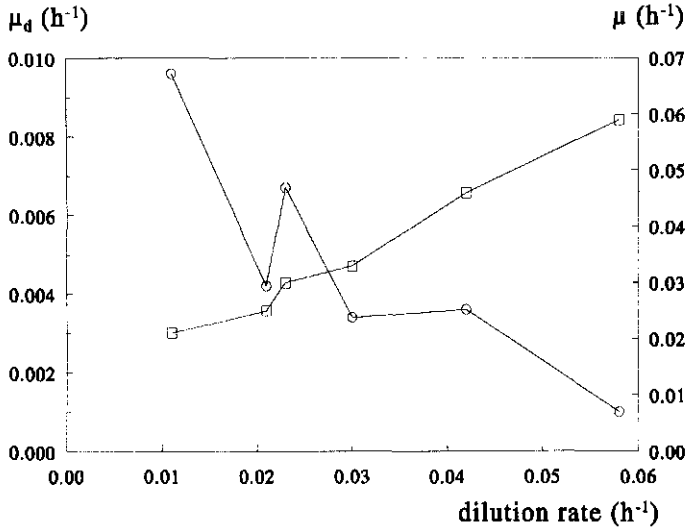
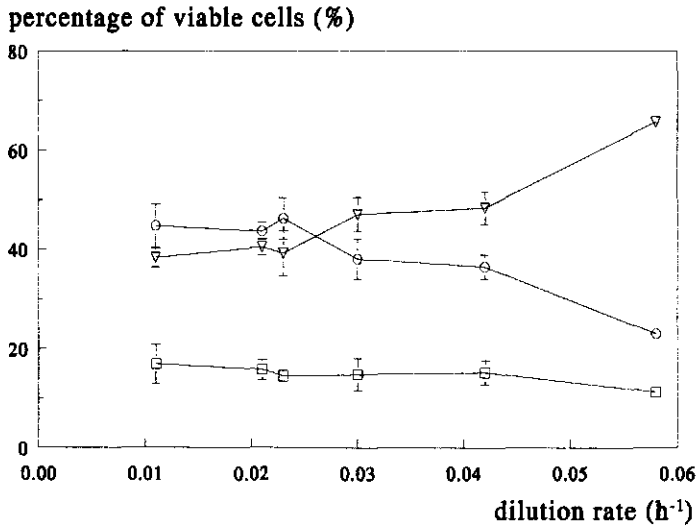


Figure 3. The specific growth-rate constant ( $\square$ ) and the first-order death-rate constant measured in a continuous culture ( $\circ$ ) as a function of the dilution rate.

### Cell cycle

The percentages of viable cells in the  $G_1/G_0$ , S, and  $G_2/M$  phase are shown in Figure 4 as a function of the dilution rate. As expected, an increase in the percentage of S-phase cells and a decrease in the percentage of  $G_1/G_0$ -phase cells occurs with increasing specific growth rate. The percentage of cells in the  $G_2/M$  phase is more or less constant. Using these percentages, the time a cell remains in a specific phase is numerically calculated using Equations (7), (8), (9) and (10). Because we were not able to discriminate  $G_0$ -phase cells, we have to either assume a value for the  $G_0$  fraction, leading to varying cycle times, or choose a constant cycle time, leading to varying  $G_0$  fractions.

In principle, it should be possible to discriminate between  $G_1$  and  $G_0$  cells on the basis of the fact that the  $G_0$  cells are smaller than  $G_1$  cells<sup>13</sup>. Because two subpopulations in the  $G_1/G_0$  area could not be detected, we first assumed the  $G_0$  fraction to be zero for the calculation. It is known for cancer cells that, in contrast with normal cells, they continue to cycle and do not enter a  $G_0$  phase under unfavourable growth conditions<sup>28</sup>. The results of the calculation (Fig. 5) show a decrease in time interval with increasing specific growth rate for all the phases. However, the decrease for the  $G_1$ -phase time interval is the most prominent. Literature data for non-tumorigenic cells also show large variations in the  $G_1$ -phase time interval, but the time intervals



**Figure 4.** Percentage of viable cells in respectively the G<sub>1</sub> phase (O), S phase (∇), and G<sub>2</sub>/M phase (□) as a function of the dilution rate.

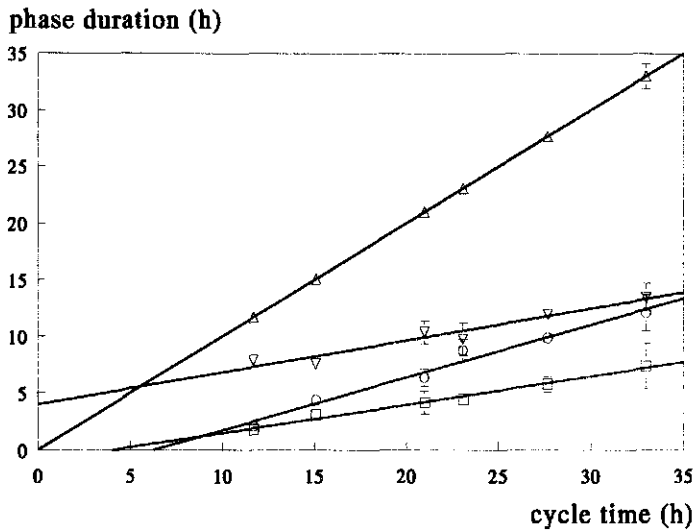


**Figure 5.** The time a cell spends in respectively the G<sub>1</sub> phase (O), S phase (∇), and G<sub>2</sub>/M phase (□) as a function of the cycle time. For comparison the cycle time itself is also plotted (Δ).

found for S-phase and  $G_2/M$ -phase cells are relatively constant, being 8 and 2 hours, respectively. This corresponds to the time intervals found for the culture run at the highest dilution rate, where the assumption of a zero  $G_0$  fraction is most plausible.

It is also possible to do the calculation keeping the cycle time constant and calculating a  $G_0$  fraction using Equation (6), followed by the numeric calculation of the phase times. Keeping the cycle time constant at 12 hours, which is close to the minimal cycle time of 11.5 hours, leads to calculated  $G_1/G_0$  fractions which are larger than the measured ones. Theoretically, we can solve this problem by assuming lysis of cells. This would lead to a lower viability and a higher specific growth rate [Eq. (5)], and thus to smaller  $G_0$  fractions. In this way, the calculated  $G_1$ -, S- and  $G_2$ -phase durations are far more constant and lay within 0.5 to 1.5, 7 to 8, and 2 to 3 hours, respectively. Although this is very hypothetical, it is better in accordance with literature.

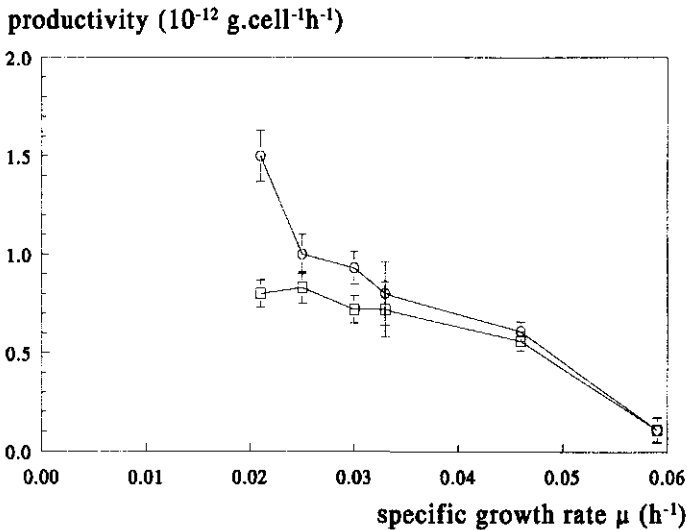


**Figure 6.** The specific production rate given per viable cell ( $\square$ ) and per total cell ( $\circ$ ) as a function of the specific growth rate.

### Productivity

The specific productivity shows a sharp increase at the lowest specific growth rate (Fig. 6). In the literature, many cases are reported of increased productivity at slower specific growth rates<sup>2,24,31,32,35,36</sup>, although this is not a universal finding. For example, Boraston et al.<sup>4</sup> found that dilution rate had no effect on specific productivity and Low et al.<sup>22</sup> reported a similar



finding which they described as a saturated profile. Phillips et al.<sup>30</sup> have analysed the secondary data obtained from batch and continuous cultures of hybridomas in more detail and concluded that more caution should be used when interpreting such data. There are three possible explanations for the increase in specific productivity as shown in Figure 6.

First, since the dead- and total-cell numbers increase when the specific growth rate decreases, this increase in specific productivity might be a consequence of the passive release of antibodies by dead cells. Mohan and Lydiatt<sup>25</sup> have shown that the passive release of monoclonal antibodies can indeed be substantial. If we calculate the specific productivity on the basis of the total-cell instead of the viable-cell number, as is also shown in Figure 6, the specific productivity is more or less constant for the low specific growth rates. At the two faster specific growth rates a decrease in specific productivity occurs.

A second reason for the increased specific productivity could be a true increase in the production rate of the viable cells. This, in turn, could be the consequence of an elevated synthesis and/or secretion of monoclonal antibodies in the  $G_1/G_0$  phase compared with the other phases<sup>31,32,35,36</sup>.

A third possible reason could arise from the ELISA method used, which cannot discriminate between intact and fragmented monoclonal antibodies. If fragmented antibodies would be secreted at the lower specific growth rates, this would result in a higher productivity as measured by the ELISA method. However, fragmentation has never been detected in previous experiments with Mn12. Most likely the passive release of antibodies by dead cells is the cause of the increased specific productivity.

### Cell size and shear sensitivity

Cell size is extensively used as a marker for the growth state of the culture<sup>9,15,31</sup>. The size of a cell increases as it progresses from the  $G_1$ -phase through the cell cycle. Cells in the quiescent  $G_0$  phase are even smaller than the  $G_1$ -phase cells<sup>1,13</sup>. Because the fraction of S- and  $G_2/M$ -phase cells increases and the fraction of  $G_1/G_0$ -phase cells decreases with the specific growth rate, the mean cell size of a cell culture will increase with the specific growth rate<sup>9,27,31</sup>.

The size of the cells is measured by means of the forward (or small-angle) scatter (FSC) on a flow cytometer. A higher FSC is associated with a larger volume. Mullaney et al.<sup>26</sup> theoretically calculated and experimentally found a linear relationship between the cell volume and the forward scatter<sup>26,34</sup>. The FSC is shown as a function of the specific growth rate in Figure 7. As can be seen the size (FSC) of the cells increases with the specific growth rate as expected.

In Figure 7 it can be seen that the  $k_d$ , as determined in a small air-lift loop reactor, increases with the specific growth rate. This seems contradictory to the results shown in Figure 3, where the first-order death-rate constant  $\mu_d$ , measured in the continuous cultures, decreases with the specific growth rate. However, the mechanisms responsible for cell death are quite different. In the continuous culture the shear is very low due to mild agitation conditions and the absence of air bubbles. Consequently, cell death is not caused by shear but more likely by the lack of nutrients or the presence of a toxic substance. At lower dilution rates, this lack of nutrients or build-up of toxic components will be more substantial, thus resulting in higher  $\mu_d$  values. In the air lift, however, the cells are rapidly killed<sup>23</sup>. Comparing the values of  $\mu_d$  with the values of  $k_d$ , it can be seen that  $\mu_d$  is maximally 4% of the value of  $k_d$ , thus indicating that the death caused by nutrient limitation or build-up of a toxic component can be neglected in the air-lift experiments. Furthermore, the specific growth rate  $\mu$  in the continuous culture is maximally 8% of the  $k_d$  value. Because the specific growth rate will not increase and very probably declines when a sample is put in the air lift, it is also neglected with respect to the death rate in the air lift.

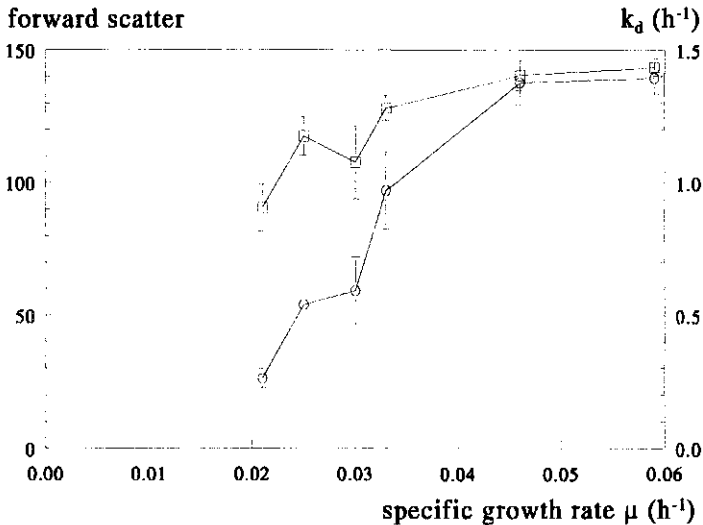


**Figure 7.** The forward scatter ( $\square$ ) and the first-order death-rate constant measured in a small air-lift loop reactor ( $\circ$ ) as a function of the specific growth rate.

Petersen and McIntire<sup>29</sup> have found that cells in the lag and stationary phase are more shear sensitive than exponentially growing cells. Furthermore, they found that as long as cells were actively (exponentially) growing, their shear sensitivity did not depend on the specific growth rate or metabolic state of the cells as expressed by metabolic yields. This does not

coincide with the results presented here and might be explained by the different method used to measure the shear sensitivity. Petersen looked at laminar shear stresses in a viscosimeter, while in this study the shear stresses causing cell death are associated with the presence of air bubbles. Additionally, the steady-state data shown in Figure 7 do not agree with the transient data shown in Figure 1C. In the continuous culture, after hydrodynamic steady state has been reached, an increase in FSC from about 110 to 130 leads to an increase in  $k_d$  from 0.55 to only 0.59, while, looking at steady-state data, such an increase in FSC leads to an increase in  $k_d$  from 0.54 to 0.97. This particular culture is the only one where such an increase in FSC occurred after hydrodynamic steady state had been reached. We have no explanation for this difference in transient and steady-state data.

To get a better insight into the possible explanations for the increase in  $k_d$  at increasing specific growth rates, a good understanding of the mechanisms causing cell death in an air-lift loop reactor is necessary. Tramper et al.<sup>37</sup> have derived an equation for the first-order death-rate constant  $k_d$  as given by Equation (11). In addition to first-order death-rate kinetics, they assumed a hypothetical killing volume,  $V_k$  (m<sup>3</sup>), within which every cell is killed. On the basis of the number of air bubbles formed per unit reactor volume, they derived the following equation for  $k_d$ :

$$k_d = \frac{24FV_k}{\pi^2 d_b^3 D_r^2 H} \quad (12)$$

where  $F$  is the air flow (m<sup>3</sup>.h<sup>-1</sup>),  $V_k$  the hypothetical killing volume (m<sup>3</sup>),  $d_b$  the bubble diameter (m),  $D_r$  the reactor diameter (m), and  $H$  the reactor height (m).

The place of cell death is most probably at the surface, where the bubbles break up<sup>16,20,21,23,37</sup>. To obtain a better understanding of the mechanisms causing cell death at the surface, a number of authors have studied the effect of bubble break-up on the death of animal cells<sup>5,6,16</sup>. In short, Cherry and Hulle<sup>6</sup> stated that cell death occurs in the expanding rim that occurs when a bubble breaks up. Chalmers and Bavarian<sup>5</sup> also suggested that the cells are killed by the rapid accelerations in the rim when the bubble film breaks up. They also proposed that cells are killed by the high levels of shear stress occurring in the boundary layer flow into the bubble cavity. They suggested that the hypothetical killing volume, as defined by Tramper et al.<sup>37</sup>, consists of the medium and cells that make up the bubble film and the thin shell surrounding the bubble cavity, although in their volume not all of the cells are killed as is assumed in the hypothetical-killing-volume model.

The increase in mean shear sensitivity of the cells, as indicated by the increase in the hypothetical killing volume at higher specific growth rates, can have two reasons.

First, the hypothetical killing volume will increase when the shear sensitivity of the cells increases. The increase in shear sensitivity can be the consequence of the fact that cells in the S phase are more shear sensitive than cells in the  $G_1/G_0$  phase, as discussed by Needham et al.<sup>27</sup>. It also can be solely caused by the increase in cell size, with larger cells being more shear sensitive (Fig. 8).

Second, it is reported that cells attach to air-bubbles<sup>3,5</sup>. This would lead to an increase in the cell concentration near the surface of an air bubble, and thus to an increase in the cell concentration in the hypothetical killing volume. Equation (12) is based on a uniform cell concentration everywhere in the reactor. When this is not the case, the hypothetical killing volume should contain a factor accounting for the enrichment of cells in the volume. Increased attachment of cells to air bubbles would then lead to an increase in the hypothetical killing volume. This increased attachment might be related to medium components, or the change in the distribution of the cells over the different phases of the cell cycle, with cells in a particular phase having a higher affinity to air bubbles. It also can be directly related to the cell size, with larger cells having a larger surface area for attachment. Furthermore, larger cells give rise to a larger volume fraction of cells and thus to an increased probability of an encounter between a cell and an air bubble.

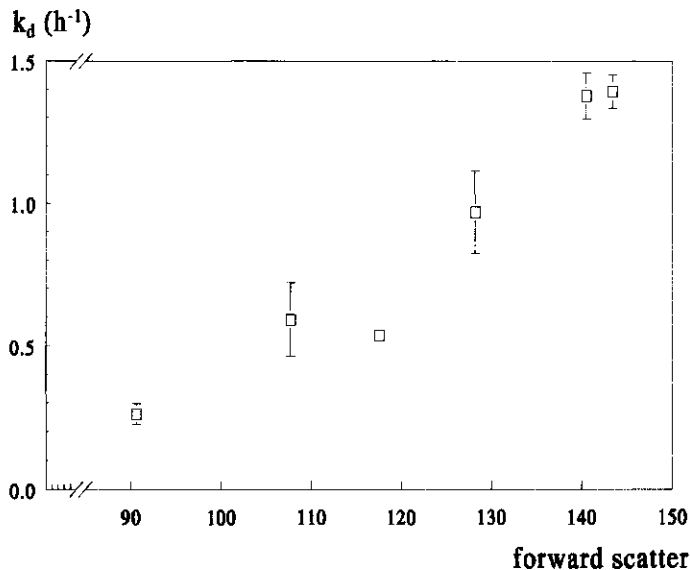


Figure 8. The first-order death-rate constant measured in a small air-lift loop reactor ( $\square$ ) as a function of the forward scatter.

## CONCLUSIONS

The first-order death-rate constant of hybridoma cells cultured in continuous suspension culture increases with decreasing specific growth rates. Consequently, a certain minimal specific growth rate is required to get overall growth. When the specific growth rate increases, the percentage of cells in the S phase increases and the percentage of cells in the  $G_1/G_0$  phase decreases. The specific productivity increases with decreasing specific growth rates. This can be caused by an increase in the synthesis and/or secretion rate of antibody per viable cell or, most likely, by the passive release of intact or fragmented intracellular antibody from dead cells.

The mean relative cell size, as measured by flow cytometry, and the first-order death-rate constant, as determined in a small air-lift loop reactor, both increase with the specific growth rate.

## REFERENCES

1. Alberts, B., Bray, D., Lewis, J., Raff, M., Roberts, K., Watson, J.D. 1983. *Molecular Biology of the Cell*. Garland Publishing, New York.
2. Al-Rubeai, M., Emery, A.N. 1990. Mechanisms and kinetics of monoclonal antibody synthesis and secretion in synchronous and asynchronous hybridoma cell culture. *J. Biotechnol.* **16**: 67-86.
3. Bavarian, F., Fan, L.S., Chalmers, J.J. 1991. Microscopic visualization of insect cell-bubble interactions. I: Rising bubbles, air-medium interface, and the foam layer. *Biotechnol. Prog.* **7**: 140-150.
4. Boraston, R., Thjompson, P.W., Garland, S. Birch, J.R. 1984. Growth and oxygen requirements of antibody producing mouse hybridoma cells in suspension culture. *Develop. Biol. Standard.* **55**: 103-111.
5. Chalmers, J.J., Bavarian, F. 1991. Microscopic visualization of insect cell-bubble interactions. II: The bubble film and bubble rupture. *Biotechnol. Prog.* **7**: 151-158.
6. Cherry, R.S., Hulle, C.T. 1992. Cell death in the thin films of bursting bubbles. *Biotechnol. Prog.* **8**: 11-18.
7. Coco-Martin, J.M., Oberink, J.W., van der Velden-de Groot, C.A.M., Beuvery, E.C. 1993. The potential of flowcytometric analysis for the characterization of hybridoma cells in suspension cultures. Accepted for publication in *Cytotechnol.*
8. Coco-Martin, J.M., Martens, D.E., van der Velden-de Groot, C.A.M., Beuvery, E.C. 1993. Cultivation of the hybridoma cell line MN12 in a homogeneous continuous culture system: effects of culture age. *Cytotechnol.* **13**: 213-220.
9. Dalili, M., Ollis, D.F. 1990. A Flow-cytometric analysis of hybridoma growth and monoclonal antibody production. *Biotechnol. Bioeng.* **36**: 64-737.
10. Frame, K.K., Hu, W-S. 1990. Cell volume measurement as an estimation of mammalian cell biomass. *Biotechnol. Bioeng.* **36**: 191-197.
11. Frame, K.K., Hu, W-S. 1991. Comparison of growth kinetics of producing and nonproducing hybridoma cells in batch culture. *Enzym. Microbiol. Technol.* **13**: 690-696.
12. Frame, K.K., Hu, W-S. 1991. Kinetic study of hybridoma cell growth in Continuous culture: II. Behaviour of producers and comparison to nonproducers. *Biotechnol. Bioeng.* **38**: 1020-1028.

13. Giaretti, W., Nuesse, M., Bruno, S., Di Vinci, A., Geido, E. 1989. A new method to discriminate G<sub>1</sub>, S, G<sub>2</sub>, M, and G<sub>1</sub> postmitotic cells. *Exp. Cell Res.* **182**: 290-295.
14. Glacken, M.W., Huang, C., Sinskey, A.J. 1989. Mathematical descriptions of hybridoma culture kinetics. III. Simulation of fed-batch bioreactors. *J. Biotechnol.* **10**: 39-66.
15. Goebel, N.K., Kuehn, R., Flickinger, M.C. 1990. Methods for determination of growth-rate-dependent changes in hybridoma volume, shape and surface structure during continuous culture. *Cytotechnol.* **4**: 45-57.
16. Handa-Corrigan, A., Emery, A.N., Spier, R.E. 1989. Effect of gas-liquid interfaces on the growth of suspended mammalian cells: Mechanisms of cell damage by bubbles. *Enzym. Microbiol. Technol.* **11**: 230-235.
17. Heath, C., Dilwith, R., Belfort, G. 1990. Methods for increasing monoclonal antibody production in suspension and entrapped cell cultures: Biochemical and flow cytometric analysis as a function of medium serum content. *J. Biotechnol.* **15**: 71-90.
18. Hiller, G.W., Aeschlimann, A.D., Clark, D.S., Blanch, H.W. 1991. A Kinetic analysis of hybridoma growth and metabolism in continuous suspension culture on serum-free medium. *Biotechnol. Bioeng.* **38**: 733-741.
19. Jiskoot, W., Hertrooij, J.C.C. van, Klein Gebbinck, J.W.T.M., van der Velden-de Groot, T., Crommelin, D.J.A., Beuvery, E.C. 1989. Two-step purification of a murine monoclonal antibody intended for therapeutic application in man. Optimisation of purification conditions and scaling up. *J. Immunol. Methods.* **124**: 143-156.
20. Jöbses, I., Martens, D., Tramper, J. 1991. Lethal events during gas sparging in animal cell culture. *Biotechnol. Bioeng.* **37**: 484-490.
21. Kunas, K.T., Papoutsakis, E.T. 1990. Damage mechanisms of suspended animal cells in agitated bioreactors with and without bubble entrainment. *Biotechnol. Bioeng.* **36**: 476-483.
22. Low, K.S., Harbour, C., Barford, J.P. 1987. A study of hybridoma cell growth and antibody production kinetics in continuous culture. *Biotech. Techniques* **1**: 239-244.
23. Martens, D.E., Gooijer, C.D. de, Beuvery, E.C., Tramper, J. 1992. Effect of serum concentration on hybridoma viable cell density and production of monoclonal antibodies in CSTRs and on shear sensitivity in air-lift loop reactors. *Biotechnol. Bioeng.* **39**: 891-897.
24. Miller, W.M., Blanch, H.W., Wilke, C.R. 1987. A kinetic analysis of hybridoma growth and metabolism in batch and continuous suspension culture: Effect of nutrient concentration, dilution rate, and pH. *Biotechnol. Bioeng.* **32**: 947-965.
25. Mohan, S.B., Lydiatt, A. 1991. Passive release of monoclonal antibodies from hybridoma cells. *Cytotechnol.* **5**: 201-209.
26. Mullaney, P.F., Dilla, M.A. van, Coulter, J.R., Dean, P.N. 1969. Cell sizing: A light scattering photometer for rapid volume determination. *Rev. Sci. Instr.* **40**: 1029-1032.
27. Needham, D., Ting-Beall, H.P., Tran-Son-Tay, R. 1991. A physical characterization of GAP A3 hybridoma cells: Morphology, Geometry, and Mechanical properties. *Biotechnol. Bioeng.* **38**: 838-852.
28. Pardee, A.B. 1989. G<sub>1</sub> events and regulation of cell proliferation. *Science* **241**: 603-608.
29. Petersen, J.F., McIntire, L.V. 1990. Shear sensitivity of hybridoma cells in batch, fed-batch, and continuous cultures. *Biotechnol. Prog.* **6**: 114-120.
30. Phillips, P.J., Marquis, C.P., Barford, J.P., Harbour, C. 1991. An analysis of some batch and continuous kinetic data of specific monoclonal antibody production from hybridomas. *Cytotechnol.* **6**: 189-195.

## Chapter 5

31. Ramirez, O.T., Mutharasan, R. 1990. Cell cycle- and growth phase-dependent variations in size distributions, antibody productivity, and oxygen demand in hybridoma cultures. *Biotechnol. Bioeng.* **36**: 839-848.
32. Richieri, R.A., Williams, L.S., Chau, P.C. 1991. Cell cycle dependency of monoclonal antibody production in asynchronous serum-free hybridoma cultures. *Cytotechnol.* **5**: 243-254.
33. Robinson, D.K., Memmert, K.W. 1991. Kinetics of recombinant immunoglobulin production by mammalian cells in continuous culture. *Biotechn. Bioeng.* **38**: 972-976 .
34. Sen, S., Srien, F., Hu, W-S. 1989. Distinct volume distributions of viable and non-viable hybridoma cells: A flow cytometric study. *Cytotechnol.* **2**: 85-94 .
35. Suzuki, E., Ollis, D.F. 1989. Cell cycle model for antibody production kinetics. *Biotechnol. Bioeng.* **34**: 1398-1402.
36. Suzuki, E., Ollis, D.F. 1990. Enhanced antibody production at slowed growth rates: Experimental demonstration and a simple structured model. *Biotechnol. Prog.* **6**, 231-236.
37. Tramper, J., Joustra, D., Vlak, J.M. 1987. Bioreactor design for the growth of shear sensitive insect cells. p. 125-136 In. Webb, C., Ativuna (Ed.), *Plant and animal cell cultures. Process possibilities*: Chichester, Ellis Horwood.

## CHAPTER 6

# DEATH RATE IN A SMALL AIR-LIFT LOOP REACTOR OF VERO CELLS GROWN ON SOLID MICROCARRIERS AND IN MACROPOROUS MICROCARRIERS

### ABSTRACT

The death rate of Vero cells grown on Cytodex-3 microcarriers was studied as a function of the gas flow rate in a small air-lift loop reactor. The death rate may be described by first-order death-rate kinetics. The first-order death-rate constant as calculated from the decrease in viable cells, the increase in dead cells and the increase in LDH activity is linear proportional to the gas flow rate, with a specific hypothetical killing volume in which all cells are killed of about  $2 \cdot 10^{-3}$  m<sup>3</sup> liquid per m<sup>3</sup> of air bubbles.

In addition, an experiment was conducted in the same air-lift reactor with Vero cells grown inside porous Asahi microcarriers. The specific hypothetical killing volume calculated from this experiment had a value of  $3 \cdot 10^{-4}$  m<sup>3</sup> liquid per m<sup>3</sup> of air bubbles, which shows that the porous microcarriers were at least in part able to protect the cells against the detrimental hydrodynamic forces generated by the bubbles.

### INTRODUCTION

In small-scale microcarrier cultures of animal cells gentle agitation is required to keep the microcarriers from settling and to provide a homogeneous environment. At larger scales more vigorous agitation is needed in order to enhance the mass transfer rate of nutrients and toxic metabolites. In addition to more vigorous agitation, sparging may be required to increase the oxygen transfer rate. However, hydrodynamic forces associated with agitation and sparging are detrimental to animal cells, which has led to the design of bubble-free-aeration reactors<sup>14</sup>. Although these reactors have been operated successfully, they are also limited in their application scale and usually have a more complex design than the standard reactors, like the stirred-tank,



bubble-column and air-lift loop reactor<sup>14</sup>. At larger scales the use of bubble-column and air-lift loop reactors may become feasible. These reactors have, even at larger scales, good oxygen- and mass-transfer characteristics, a relative simple design through the absence of mechanical agitation and the hydrodynamic behaviour and mass-transfer characteristics are well documented in literature<sup>8</sup>. However, as stated, the presence of air bubbles causes cell damage and death.

The effect of hydrodynamic forces generated by air bubbles on suspension cells has been extensively studied<sup>1,5,7,13,15-17,22,23,32,36-38</sup> as well as the effect of agitation on microcarrier cultures<sup>6,9,10,18</sup> and has been reviewed by Papoutsakis<sup>30</sup>. Nonetheless, not much is known about the detrimental effects of air bubbles on microcarrier cultures. This is mainly because the upward moving air bubbles cause aggregation of the microcarriers and accumulation of the microcarriers at the air-medium interface making the application of microcarriers in bubble-column and air-lift reactors impractical<sup>30</sup>.

The problems of microcarrier aggregation and accumulation at the air-medium interface could be overcome in this study by reducing the foam formation through the careful addition of antifoam, which made it possible to study the effect of sparging on microcarrier cultures. A careful study of the death rate in air-lift and bubble-column reactors as a function of process and reactor parameters, like the gas flow rate and the height and diameter of the reactor, might lead to a minimization of cell death in these reactors and to an optimal reactor design. Cell damage might also be reduced through the addition of shear-protective agents like Pluronics. In this paper the death rate of Vero cells grown on Cytodex-3 microcarriers in a small air-lift loop reactor is studied at varying gas flow rates. In addition, an experiment was conducted with Vero cells grown inside porous Asahi microcarriers, to study if these microcarriers can protect the cells from the detrimental hydrodynamic forces caused by sparging.

## **MATERIAL AND METHODS**

### **Cell culture**

For the shear experiments at varying gas flow rates Vero cells were cultured on Cytodex-3 microcarriers (Pharmacia, Uppsala, Sweden) at a concentration of 2.5 g.dm<sup>-3</sup>. Cultures were conducted in spinner flasks (Technic, Cambridge, UK) with a working volume of 0.25 dm<sup>3</sup> at a temperature of 37°C and an agitation rate of 25 rpm. The medium was Iscove's modified Dulbecco's medium (Gibco laboratories, Paisley, Scotland) supplemented with antibiotics (35000 U.dm<sup>-3</sup> polymyxin, 1400 U.dm<sup>-3</sup> neomycin and 7500 U.dm<sup>-3</sup> streptomycin) and 5% (v/v) heat-inactivated (30 minutes 56°C) fetal-calf serum (FCS) (Sanbio, Uden, the Netherlands). A mixture of air/5% CO<sub>2</sub> was blown over the surface of the cultures twice daily to maintain the pH

above 7.0 and the dissolved oxygen concentration above zero. If the microcarriers were fully grown with cells, which was always the case after about 95 hours, they were used for the shear experiments.

For the experiments with the porous microcarriers Vero cells were grown in the same medium inside Asahi microcarriers (Asahi Chemical Industry, Osaka, Japan) at a concentration of  $1 \text{ g.dm}^{-3}$ . In parallel to these cultures reference cultures were conducted with Vero cells on Cytodex-3 microcarriers. In order to have the same available surface for growth, the concentration of Cytodex-3 microcarriers was  $5 \text{ g.dm}^{-3}$  in these reference cultures. Samples for shear experiments were taken after 50 and 95 hours of culture.

### Shear sensitivity

The shear sensitivity of the cells was determined in a small air-lift reactor with an internal loop. For the experiments  $65 \text{ cm}^3$  samples were taken from spinner-flask cultures of which  $45 \text{ cm}^3$  was put directly in the air lift. The other  $20 \text{ cm}^3$  was centrifuged and the cell-free supernatant was used during the shear experiment as will be described. The air lift was thermostated at  $37^\circ\text{C}$  by a water jacket. Air containing 5%  $\text{CO}_2$  was sparged into the inner tube through a nozzle with a diameter of 0.001 m. The flow rates were controlled by a Brooks rotameter and measured exactly after each experiment.

The inner diameter of the draught tube was 0.012 m, the fluid height 0.07 m and the inner diameter of the outer tube was 0.03 m. Experiments were carried out in duplo at gas flow rates of  $0.7 \cdot 10^{-6}$ ,  $1.1 \cdot 10^{-6}$ ,  $2.2 \cdot 10^{-6}$ ,  $5 \cdot 10^{-6}$ , and  $8.4 \cdot 10^{-6} \text{ m}^3 \cdot \text{s}^{-1}$ . During the experiments 1% (v/v) antifoam Silicone B (Baker, Deventer, NI) solution in phosphate buffered saline (PBS) was added every time foaming occurred. The total amount of antifoam added was smaller than 0.1% (v/v) for the experiments at the three lower gas flows. For the experiments conducted at a gas flow rate of  $5 \cdot 10^{-6}$  and  $8.4 \cdot 10^{-6} \text{ m}^3 \cdot \text{s}^{-1}$  this was 0.2% (v/v) and 0.3% (v/v), respectively. Samples were sheared for a period of 3 hours and every half hour an amount of 3 or  $4 \text{ cm}^3$  was withdrawn for measurement of the viable-cell concentration, dead-cell concentration and LDH activity. If the liquid volume of the air lift dropped below  $45 \text{ cm}^3$  due to sampling, 3 or  $4 \text{ cm}^3$  of the previously obtained cell-free medium was added depending on the sample volume. If, due to the addition of antifoam, the volume was higher than  $45 \text{ cm}^3$  after sampling, no medium was added. As a consequence of the addition of antifoam and medium, the contents of the air lift were diluted resulting in lower cell concentrations. Furthermore, in the case of medium addition also small amounts of LDH activity and serum, which were originally present in the spinner culture, were added. Using the amount of added antifoam and medium and the volume of the sample, the

measured concentrations were calculated back to theoretical concentrations that would have been actual if no additions or withdrawals had taken place.

### Cell Counts

Cells were counted using a Fuchs-Rosenthal haemocytometer. Cells in suspension were counted using the exclusion of trypan blue (1% w/v) to discriminate between viable and dead cells. The concentration of attached cells was determined by incubating the carriers with a solution of crystal violet (1 g.dm<sup>-3</sup>) in citric acid (0.1 M). The error in the cell count was about 10%.

### Lactate-dehydrogenase (LDH) activity

Lactate-dehydrogenase activity was determined by an enzymatic assay (Baker, Deventer, NI).

### Photography

Photographs were taken of cells on microcarriers stained with haematoxylin (1 g.dm<sup>-3</sup>) at different stages during a shear experiment using an Minolta MPS camera with a Ektachrome (Kodak) film placed on a Leitz Wetzlar microscope.

### Determination methods death-rate constant

Three methods, based on the viable-cell, dead-cell, and LDH concentrations, respectively, were used to determine the first-order death-rate constant. The first method uses the decrease in the viable-cell concentration and the associated first-order death-rate constant may be calculated according to:

$$-\ln\left(\frac{C_{X_v}(t)}{C_{X_v}(0)}\right) = k_{dv}t \quad (1)$$

where  $C_{X_v}(t)$  and  $C_{X_v}(0)$  are the viable-cell concentrations (cells.m<sup>-3</sup>) at time  $t=t$  (s) and  $t=0$  (s), respectively, and  $k_{dv}$  is the viable-cell-based first-order death-rate constant (s<sup>-1</sup>).

The second method uses the increase in the dead-cell concentration and assumes that no lysis of cells occurs. This first-order death-rate constant may be calculated according to:

$$-\ln\left(\frac{C_{X_v}(0) - C_{X_d}(t) + C_{X_d}(0)}{C_{X_v}(0)}\right) = k_{dd}t \quad (2)$$

where  $C_{Xd}(t)$  and  $C_{Xd}(0)$  are the dead-cell concentrations ( $\text{cells.m}^{-3}$ ) at time  $t=t$  (s) and  $t=0$  (s), respectively, and  $k_{d,d}$  is the dead-cell-based first-order death-rate constant ( $\text{s}^{-1}$ ).

The third method uses the increase in the LDH activity and assumes that a constant amount of LDH activity is released per dead cell formed. The pertinent first-order death-rate constant is calculated according to:

$$-Ln\left(\frac{C_{LDH}(\infty) - C_{LDH}(t)}{C_{LDH}(\infty) - C_{LDH}(0)}\right) = k_{d,l}t \quad (3)$$

where  $C_{LDH}(\infty)$  is the maximum attainable LDH activity if all cells are killed ( $\text{U.m}^{-3}$ ),  $C_{LDH}(t)$  and  $C_{LDH}(0)$  are the LDH activities ( $\text{U.m}^{-3}$ ) at time  $t=t$  (s) and  $t=0$  (s), respectively, and  $k_{d,l}$  is the LDH-based first-order death-rate constant ( $\text{s}^{-1}$ ). The maximum attainable amount of LDH activity is calculated from the LDH activity released per dead cell formed,  $Y_{LDH}$  ( $\text{U.cell}^{-1}$ ), and from the viable-cell concentration and LDH activity at the start of the experiment according to:

$$C_{LDH}(\infty) = Y_{LDH}C_{X_v}(0) + C_{LDH}(0) \quad (4)$$

Since small variations in the amount of LDH activity per cell exist between the experiments, the value of  $Y_{LDH}$  used is not the average value of all experiments, but is calculated for each individual shear experiment.

As will be shown, large variations occur in the total- and viable-cell concentration due to difficulties in taking a representative sample of microcarriers. As can be seen in Equation (1), (2), (3), and (4) an error in the concentration of viable cells at time zero [ $C_{X_v}(0)$ ] enlarges the error in each datum point and, consequently, causes an increase in the error in the calculated first-order death-rate constant. Taking more samples per datum point would result in a too large withdrawal of medium with microcarriers. Therefore, a more reliable value for the concentration of viable cells at the start of the experiment is obtained by calculating it from the average total-cell concentration at all datum points and the dead-cell concentration at the start of the experiment according to:

$$C_{X_v}(0) = \left\{ \frac{1}{7} \sum_{n=1}^7 C_{X_t}(t_n) \right\} - C_{X_d}(0) \quad (5)$$

where  $C_{X_t}(t_n)$  is the total-cell concentration ( $\text{cells.m}^{-3}$ ) at time  $t=t_n$ .

For the measurements of the LDH activity and the dead-cell concentration the problem of taking a representative sample does not exist and thus the measured values are more reliable. However, for the calculation of the LDH- and dead-cell-based death-rate constant an extra subtraction has to be executed as compared to the calculation of the viable-cell-based death-rate

constant. Especially at high gas flow rates, when the LDH activities and dead-cell concentrations become large and the result of the subtraction is small, this leads to large confidence intervals for the first-order death-rate constants. A clear advantage of using the LDH activity is that it requires only very small (200  $\mu\text{l}$ ) sample volumes. This makes it possible to take more samples during the experiment without diluting the air-lift contents. In addition, this method also accounts for cell lysis. If cell lysis occurs, the value of  $Y_{LDH}$  may be obtained by lysing all cells at the end of a shear experiment. Thus, the three calculation methods are related through a cell and LDH balance and provided that no lysis of cells occurs and that a constant amount of LDH is released upon cell death they should give the same values for the death-rate constant. The difference between the three methods lies in the accuracy with which these values can be determined.

## RESULTS AND DISCUSSION

### Growth curves

Figure 1 shows three typical growth curves for Vero cells on Cytodex-3 microcarriers ( $2.5 \text{ g.dm}^{-3}$ ). By plotting the logarithm of the viable-cell concentration against time, the specific growth rate may be determined from the slope of the least-square regression line through the datum points measured during the exponential growth phase. The thus obtained average specific growth rate in the exponential phase was  $0.025 \text{ h}^{-1}$  and the final cell densities were about

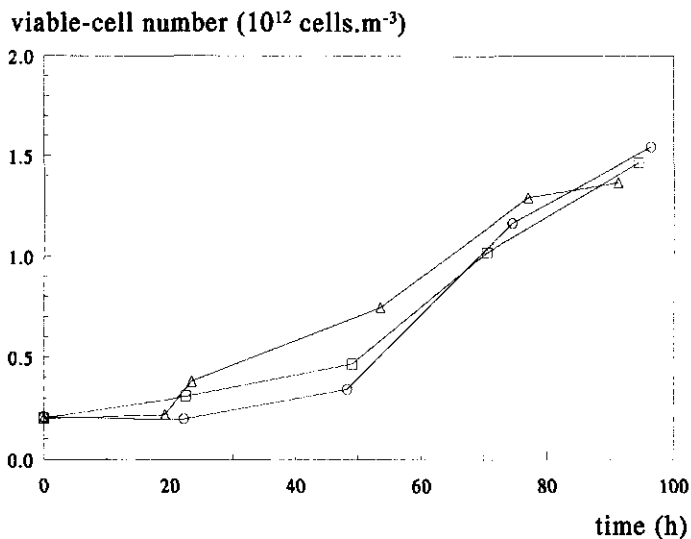


**Figure 1.** Growth curves of Vero cells grown on Cytodex-3 microcarriers ( $2.5 \text{ g.dm}^{-3}$ ). Different symbols denote separate batch cultures conducted at identical conditions .

$1.5 \times 10^6 \text{ cells.cm}^{-3}$ . Differences between samples in terms of physiological state of the cells, medium composition and number of cells per carrier, are minimized by conducting all batch cultures in the same way and by taking the samples for the shear experiments always after 95 hours of culture, when the microcarriers were totally covered with cells. Furthermore, duplo or even triplo shear experiments were conducted with cells taken from different batch cultures as is shown in Table I.

**Table I.** First-order death-rate constants with 95% confidence intervals for the three determination methods at varying gas flow rates. The number between parentheses in the first column indicates the batch culture from which the sample was taken.

Experiment	F ( $10^{-6} \text{ m}^3 \cdot \text{s}^{-1}$ )	V ( $10^{-6} \text{ m}^3$ )	$k_{d,\text{viable}}$ ( $10^{-5} \text{ s}^{-1}$ )	$k_{d,\text{dead}}$ ( $10^{-5} \text{ s}^{-1}$ )	$k_{d,\text{LDH}}$ ( $10^{-5} \text{ s}^{-1}$ )
Flow 1A (2)	0.68	56.6	4.2±4.0	6.4±2.6	6.7±1.1
Flow 1B (8)	0.70	46.0	2.5±2.9	5.0±2.1	3.4±1.4
Flow 1C (5)	0.65	50.6	3.5±4.1	5.5±3.2	5.0±1.6
Flow 2A (1)	1.17	50.1	8.4±5.0	7.7±2.3	5.7±1.6
Flow 2B (5)	1.15	42.5	6.8±4.6	11.9±6.3	9.7±3.5
Flow 3A (2)	2.22	50.8	12.1±4.2	10.8±1.4	9.9±1.8
Flow 3B (7)	2.30	43.9	11.4±2.7	11.1±7.3	12.9±1.7
Flow 3C (6)	2.25	47.2	12.5±4.5	10.3±5.8	10.8±2.6
Flow 4A (3)	5.09	48.3	22.6±9.1	21.0±9.1	22.3±10.1
Flow 4B (8)	5.10	49.9	22.2±5.7	22.0±15.5	25.5±7.8
Flow 5A (4)	8.35	52.3	32.6±18.8	32.4±39.2	38.3±20.6
Flow 5B (8)	8.51	51.6	33.2±7.1	45.2±52.1	50.9±26.7
Antifoam (9)	0.68	45.6	5.9±2.7	9.4±2.3	10.6±10.1

### LDH and cell concentrations during a shear experiment

Figure 2 shows the LDH activities and the viable-, dead- and total-cell concentrations as a function of exposure time in the small air-lift reactor at the lowest (2A,  $0.7 \times 10^{-6} \text{ m}^3 \cdot \text{s}^{-1}$ ), an intermediate (2B,  $5.0 \times 10^{-6} \text{ m}^3 \cdot \text{s}^{-1}$ ), and the highest (2C,  $8.4 \times 10^{-6} \text{ m}^3 \cdot \text{s}^{-1}$ ) gas flow rate. For the other three gas flow rates comparable figures are obtained. The confidence limits represent the

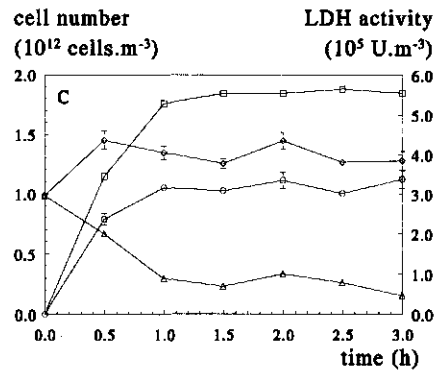
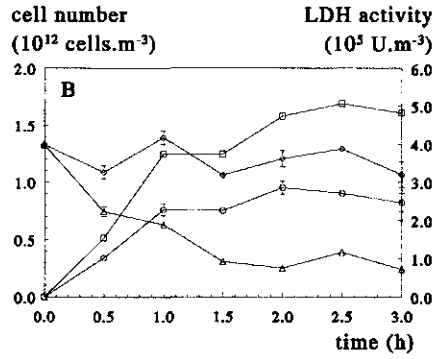
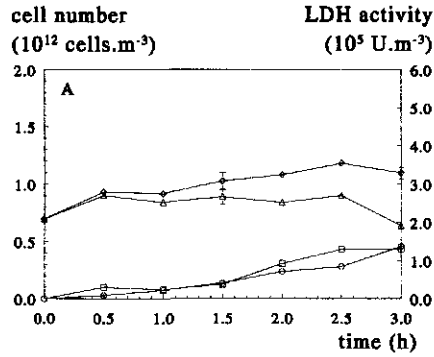


**Figure 2.** Viable-, dead-, and total-cell numbers and LDH activities for shear experiments conducted at gas flow rates of  $0.7 \times 10^{-6} \text{ m}^3 \cdot \text{s}^{-1}$  (A),  $5.0 \times 10^{-6} \text{ m}^3 \cdot \text{s}^{-1}$  (B) and  $8.4 \times 10^{-6} \text{ m}^3 \cdot \text{s}^{-1}$  (C). ( $\circ$ ) total cells, ( $\Delta$ ) viable cells, ( $\square$ ) dead cells, ( $\square$ ) LDH activity.

variation of the cell counts and LDH activities within a sample and not between the samples. At the lowest gas flow rate of  $0.7 \cdot 10^{-6} \text{ m}^3 \cdot \text{s}^{-1}$  a small amount of growth seems to occur when looking at the total-cell concentration. At higher gas flow rates no significant increase or decrease in the total-cell concentration occurs. For the experiment at the highest gas flow rate (Fig. 2C) a large increase in the total-cell density occurs at the second sample ( $t=0.5 \text{ h}$ ). Because the total-cell density remains constant thereafter, this is probably due to an error in the sampling at  $t=0 \text{ h}$ , resulting in a too low total-cell concentration at this point. The on average constant total-cell concentration at gas flow rates higher than  $0.7 \cdot 10^{-6} \text{ m}^3 \cdot \text{s}^{-1}$  may be the result of the growth rate being equal to the rate of cell lysis due to shear forces. However, if cell lysis occurs it may be expected to increase at higher gas flow rates. Because the specific growth rate is likely to have more or less the same value in all shear experiments and will always be smaller than  $0.025 \text{ h}^{-1}$ , this would lead to a decrease in the total-cell concentration at high gas flow rates, which is not seen. Thus, cell growth and the amount of cell lysis may assumed to be negligible.

#### LDH activity per dead cell formed

In Figure 3 the LDH activity is plotted as a function of the concentration of dead cells in suspension for all shear experiments. In addition, the least-square regression line and the 95% prediction intervals are shown. All cells in suspension were dead, while the amount of dead cells

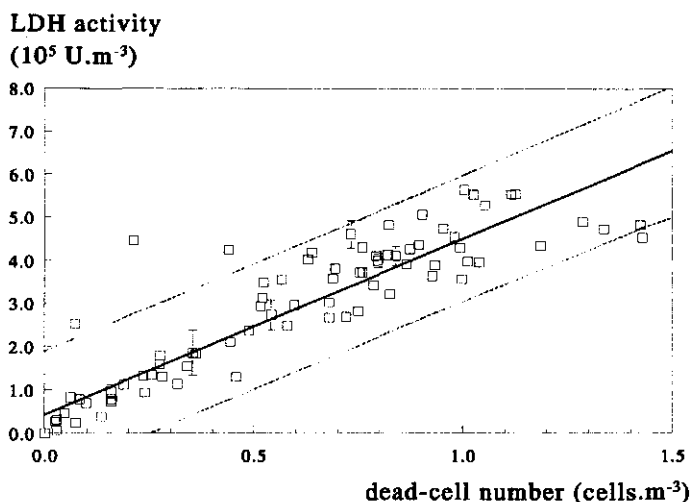


Figure 3. LDH activities ( $\square$ ), least-square regression line (solid line) and 95% prediction intervals (dashed lines) as a function of the dead-cell concentration for all shear experiments.



still attached to microcarriers was negligible. As can be seen the LDH activity is linear proportional to the dead-cell concentration. With the amount of cell lysis being negligible, the amount of LDH activity released per dead cell formed,  $Y_{LDH}$  ( $\text{U}\cdot\text{cell}^{-1}$ ), is equal to the slope of the least-square regression line through the datum points, which has a value of  $4.1 \pm 0.4 \cdot 10^{-7} \text{ U}\cdot\text{cell}^{-1}$ . This is of the same order of magnitude as the values found by Legrand et al.<sup>19</sup> of  $4\text{--}5.5 \cdot 10^{-7} \text{ U}\cdot\text{cell}^{-1}$  and by Gardner et al.<sup>11</sup> of  $2.85 \cdot 10^{-7} \text{ U}\cdot\text{cell}^{-1}$ . Geauguey et al.<sup>12</sup> showed that the LDH activity depended on the physiological state of the cell with regard to the oxygen tension. They found a value of  $2.7 \cdot 10^{-7} \text{ U}\cdot\text{cell}^{-1}$  at a dissolved-oxygen tension of 30% and a value of  $6.2 \cdot 10^{-7} \text{ U}\cdot\text{cell}^{-1}$  for a dissolved-oxygen tension of 1%. Here, all cell cultures were conducted in the same way and thus probably have on average the same dissolved-oxygen tension. In Figure 3, no large differences in the intracellular LDH content exist between the cell cultures indicating that the physiological state of the cells is more or less equal with respect to the LDH content.

### First-order death-rate constant as a function of the gas flow rate

#### Shear experiments

In Figure 4 the logarithm of the relative decrease in the viable-cell concentration [Eq. (1)] is plotted as a function of time for a single series of shear experiments. For the duplo series of

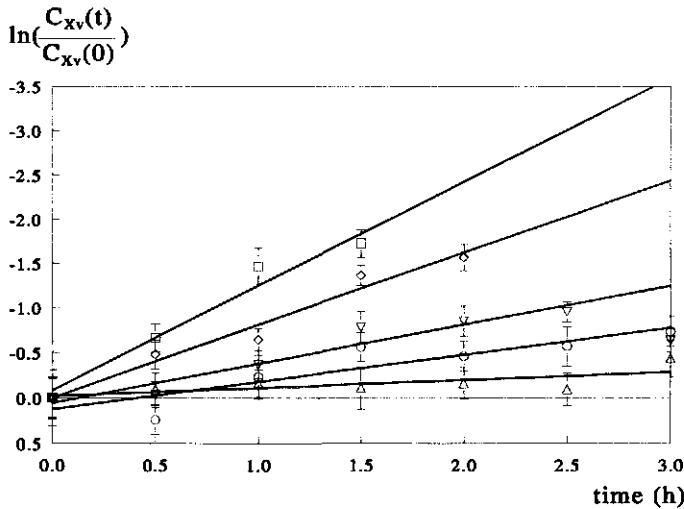


**Figure 4.** Logarithmic plot for the determination of the first-order death-rate constant according to the decrease in viable-cell concentration [Eq. (1)]. ( $\Delta$ )  $0.7 \cdot 10^{-6} \text{ m}^3\cdot\text{s}^{-1}$ , ( $\circ$ )  $1.17 \cdot 10^{-6} \text{ m}^3\cdot\text{s}^{-1}$ , ( $\nabla$ )  $2.22 \cdot 10^{-6} \text{ m}^3\cdot\text{s}^{-1}$ , ( $\diamond$ )  $5.0 \cdot 10^{-6} \text{ m}^3\cdot\text{s}^{-1}$ , ( $\square$ )  $8.4 \cdot 10^{-6} \text{ m}^3\cdot\text{s}^{-1}$ .

experiments comparable figures are obtained. Also for the dead-cell [Eq. (2)] and LDH [Eq. (3)] data comparable plots are obtained, where only the confidence intervals for the datum points are larger. The gas flow rates, average volume during the experiment, and the calculated death-rate constants for the three different determination methods are given in Table I for all experiments. In general, the cell death can be described by first-order death-rate kinetics. Only for the dead-cell-based data [Eq. (2)] of the experiments at the two lowest gas flow rates (1A, 1B, 1C, 2A, and 2B) and the LDH-based data [Eq. (3)] of experiment 1C and 2B a small increase is seen in the death rate during the experiment (data not shown). Because this is only seen at the two lowest gas flow rates, it may be due to the occurrence of a small amount of cell growth during the experiment. For the experiments at the two highest gas flow rates almost all cells were killed after 1.5 to 2 hours and the experiments were stopped then.

Because cell lysis is negligible and the amount of LDH activity released per dead cell formed is more or less constant (Fig. 3), the three different methods should give the same values for the first-order death-rate constant, which is indeed the case (Table I). In addition, there are no significant differences between duplo and triplo measurements, indicating that with respect to shear sensitivity the physiological state of the cells in the different experiments was the same. In the experiments conducted at the highest gas flow rate (Flow 5B), the dead-cell-based and

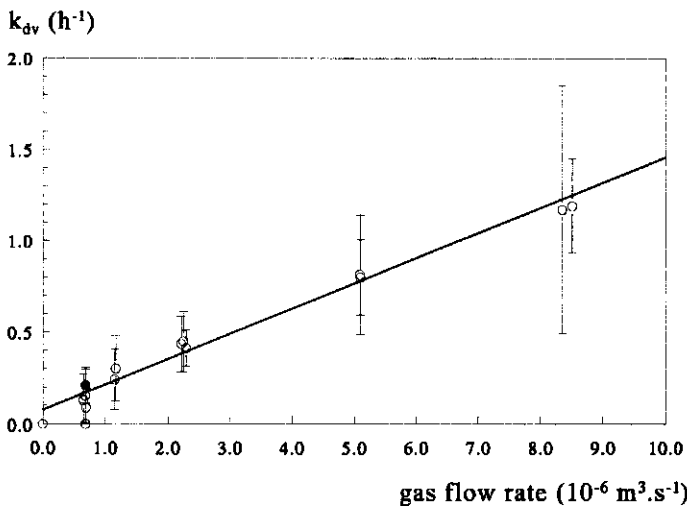


**Figure 5.** First-order death-rate constant as a function of the gas flow rate calculated on the basis of the decrease in the viable-cell concentration. The filled symbol represents an experiment executed at  $0.7 \cdot 10^{-6} \text{ m}^3 \cdot \text{s}^{-1}$  with the same amount of antifoam added as in the experiment conducted at  $8.4 \cdot 10^{-6} \text{ m}^3 \cdot \text{s}^{-1}$ .

LDH-based death-rate constant deviate quite much from the viable-cell-based value and from their values in the duplo experiment (Flow 5A). However, as expected, the dead-cell-, and LDH-based death-rate constants become quite unreliable at higher gas flow rates and the deviations are not significant. When looking at the full range of studied gas flow rates, the viable-cell-based method has about the same reliability as the other methods at lower gas flow rates and is more reliable at the higher gas flow rates. As shown for the viable-cell-based method in Figure 5, the first-order death-rate constant is linearly proportional to the gas flow rate.

### *Influence of antifoam*

During the sparging experiments small amounts of antifoam were added whenever foam formation occurred. At low gas flow rates (below  $5.0 \cdot 10^{-6} \text{ m}^3 \cdot \text{s}^{-1}$ ) less than 0.1% antifoam was added. According to van der Pol et al.<sup>33</sup> this would still increase the death rate by a factor two. However, they added all the antifoam at the start of the experiment, while here it was added only if foaming started to occur. Additionally, in parallel to the air-lift experiment conducted at a gas flow rate of  $2.2 \cdot 10^{-6} \text{ m}^3 \cdot \text{s}^{-1}$  a spinner flask experiment was conducted. For this experiment, microcarriers totally covered with cells and from the same origin as the ones used in the air-lift experiment, were put in a small spinner flask agitated at 100 rpm. During a period of three hours

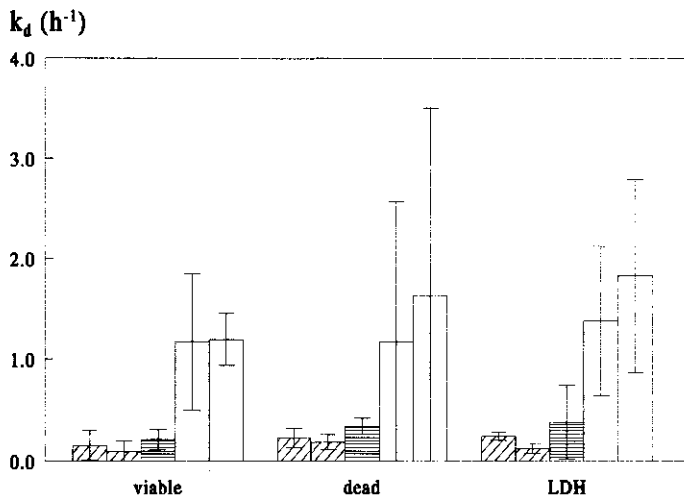


**Figure 6.** First-order death-rate constants for the antifoam control experiment. Inclined dashed :  $F=0.69 \cdot 10^{-6} \text{ m}^3 \cdot \text{s}^{-1}$ , [AF]=0.05%, horizontally dashed : Antifoam control experiment  $F=0.69 \cdot 10^{-6} \text{ m}^3 \cdot \text{s}^{-1}$ , [AF]=0.3 %, blank :  $F=8.4 \cdot 10^{-6} \text{ m}^3 \cdot \text{s}^{-1}$ , [AF]=0.3%.

every time antifoam was added to the air lift, an equal amount was added to the spinner flask. No cell death occurred in the spinner flask showing that antifoam in itself was not responsible for cell death. To test if antifoam would render the cells more sensitive to sparging, an air-lift experiment was conducted at a gas flow rate of  $0.7 \cdot 10^{-6} \text{ m}^3 \cdot \text{s}^{-1}$  to which the same amounts of antifoam were added as in the experiment conducted at a gas flow rate of  $8.4 \cdot 10^{-6} \text{ m}^3 \cdot \text{s}^{-1}$ . The final concentration was 0.3% as compared to a final concentration of 0.05% normal for experiments at this gas flow rate. The results in Figure 6 and Table I show a small and insignificant increase in the death-rate constant as compared to the experiment conducted at  $0.7 \cdot 10^{-6} \text{ m}^3 \cdot \text{s}^{-1}$  with a final antifoam concentration of about 0.05%. This increase is negligible compared to the increase in the death-rate constant caused by the increase in gas flow rate to  $8.4 \cdot 10^{-6} \text{ m}^3 \cdot \text{s}^{-1}$ . Thus, effects of antifoam on the death-rate constant may be neglected. For comparison the death-rate constant of the antifoam experiment is also shown in Figure 5 (filled symbol).

#### *Specific hypothetical killing volume*

To describe the death rate of suspension cells in bubble-column and air-lift reactors the hypothetical-killing-volume model of Tramper et al.<sup>34,36,37</sup> may be used. The model assumes first-order death-rate kinetics and a hypothetical killing volume associated with each air bubble during its life time, in which all cells are killed. This results in the following equation for the first-order death-rate constant,  $k_d$  ( $\text{s}^{-1}$ ):

$$k_d = \frac{24FV_K}{\pi^2 d_b^3 D_r^2 H} \quad (6)$$

where  $F$  is the gas flow rate ( $\text{m}^3 \cdot \text{s}^{-1}$ ),  $d_b$  is the bubble diameter (m),  $D_r$  is the reactor diameter (m),  $H$  is the reactor height (m), and  $V_K$  is the hypothetical killing volume ( $\text{m}^3$ ). Tramper et al.<sup>37</sup> showed that the hypothetical killing volume is proportional to the bubble volume for bubble diameters in the range of  $2\text{-}6 \cdot 10^{-3}$  m and thus Equation (6) can be simplified to:

$$k_d = \frac{4FV_K'}{\pi D_r^2 H} \quad (7)$$

where  $V_K'$  is the specific hypothetical killing volume (-) being the hypothetical killing volume divided by the volume of the air bubble. Trinh et al.<sup>38</sup> and Jordan et al.<sup>16</sup> relate the hypothetical killing volume to a real volume associated with an air bubble.

The hypothetical killing volume model is used here to describe the death rate of Vero cells immobilized on Cytodex-3 microcarriers in a small air-lift loop reactor as a function of the

gas flow rate. By plotting the first-order death-rate constant as a function of the gas flow rate, the specific hypothetical killing volume may be calculated according to Equation (7) from the slope of the least-square regression line for all three methods. The line is shown in Figure 5 for the viable-cell-based data. The volume of the samples in the different shear experiments varies between about 43 and 52 cm<sup>3</sup> and an average value obtained from all experiments of 48 cm<sup>3</sup> is used in Equation (7). Because no differences existed between the death-rate constants of the three methods, no significant differences in specific hypothetical killing volume are found between the three different determination methods. The average value of the specific hypothetical killing volume is  $2.0 \pm 0.2 \cdot 10^{-3}$  (-).

Literature values for the specific hypothetical killing volume show a large variation. This is caused by the fact that the specific hypothetical killing volume will depend on the cell line and type, serum concentration<sup>22,32</sup> and specific growth rate<sup>23</sup>, which are distinct in the experiments presented by the different authors. For insect cells in bubble columns Tramper et al.<sup>37</sup> found a value of  $4 \cdot 10^{-3}$  at a serum concentration of 10%. For hybridoma cells in bubble columns Jöbbses et al.<sup>15</sup> reported a value of  $7 \cdot 10^{-3}$  (1% serum) and van der Pol et al.<sup>32</sup> a value of  $9 \cdot 10^{-3}$  (5% serum). For hybridoma cells in an air-lift reactor a value of  $2 \cdot 10^{-4}$  (5% serum) is found<sup>22</sup>. Because of the variations in experimental conditions, it is difficult to compare the results, although the value of the specific killing volume for Vero cells on Cytodex-3 microcarriers is of the same order of magnitude as the values found for suspension cells.

Summarizing it may be concluded that the death of Vero cells on Cytodex-3 microcarriers in a small air-lift reactor can be described by first-order kinetics and is linear proportional to the gas flow rate.

### Photography

Figure 7 shows a series of representative photographs of Vero cells on Cytodex-3 microcarriers after 0, 1, 2, and 3 hours of shearing at a gas flow rate of  $0.7 \cdot 10^{-6} \text{ m}^3 \cdot \text{s}^{-1}$ . In all experiments clear regions could be discerned, where whole groups of cells were removed. Furthermore, in all experiments at higher gas flow rates clusters of two or three microcarriers were seen towards the end of an experiment (data not shown). The clusters were held together by cells, which seemed to pile up in the contact regions and were marked as dead by trypan-blue staining.

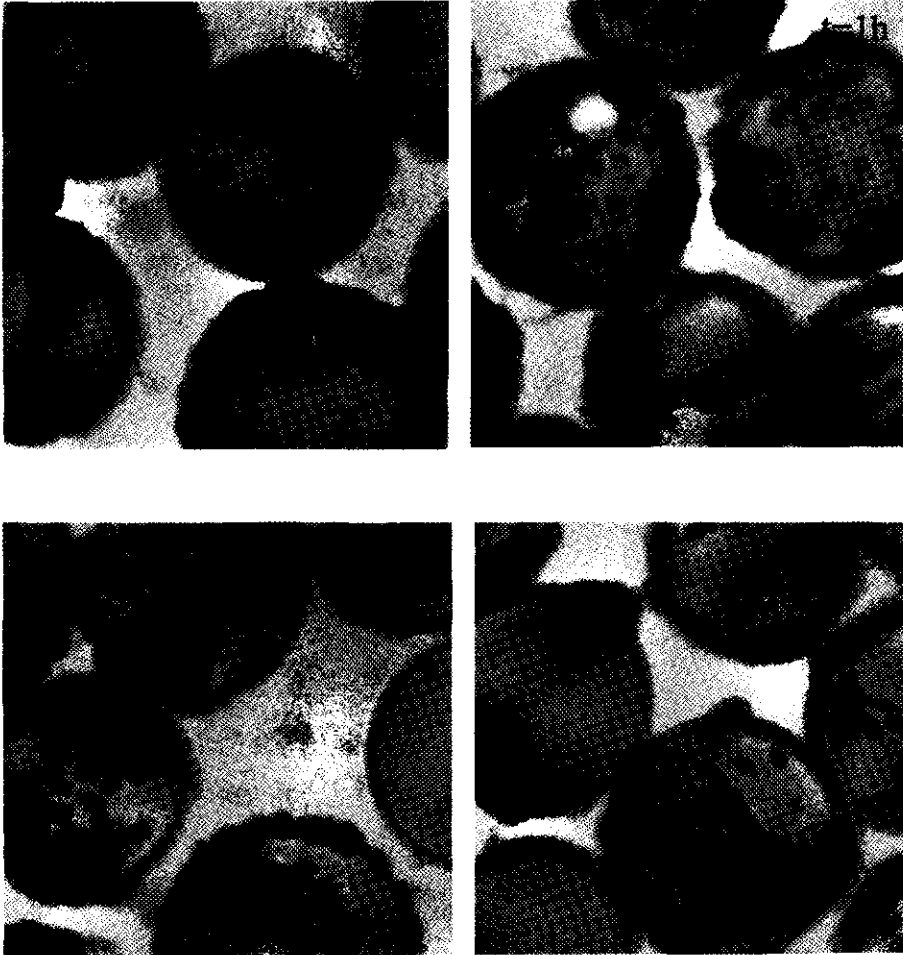


**Figure 7.** Photographs of Vero cells on Cytodex-3 microcarriers after 0 (upper left), 1 (upper right), 2 (under left) and 3 (under right) hours of shearing in the air-lift reactor at a gas flow rate of  $0.7 \cdot 10^{-6} \text{ m}^3 \cdot \text{s}^{-1}$ .

#### **Death rate of Vero cells immobilized inside porous Asahi carriers.**

One of the advantages of using porous microcarriers rather than solid microcarriers is that the matrix of the porous microcarrier might protect the cells against hydrodynamic forces. Bugarski et al.<sup>3</sup> successfully cultured hybridomas inside alginate beads and microcapsules in an air-lift reactor with an external loop. Shiragami et al.<sup>35</sup> showed that porous Cultisphere microcarriers could protect CHO cells against the detrimental effect of air bubbles. Additionally, porous microcarriers have a larger available surface for growth and thus support higher cell concentrations at the same microcarrier loading. However, growth inside the porous microcarrier may be limited by the diffusion rate of nutrients into the microcarrier and toxic metabolites out

of the microcarrier<sup>4</sup>. Furthermore, it may be difficult to count the amount of viable cells due to difficulties in extracting the cells from the inside of the microcarrier without killing them<sup>4</sup>. An experiment was executed to see if a porous microcarrier could indeed protect cells from hydrodynamic forces generated by air bubbles. For this the death rate in the small air-lift reactor was compared for Vero cells immobilized inside porous Asahi microcarriers and Vero cells immobilized on Cytodex-3 microcarriers. The protective effect is quantified by calculating the specific hypothetical killing volume.

Cells for the shear experiments were grown on Cytodex-3 and inside Asahi microcarriers in spinner flasks. To obtain an equal available surface for growth in both systems, the microcarrier concentration was  $5 \text{ g.dm}^{-3}$  for Cytodex-3 and  $1 \text{ g.dm}^{-3}$  for the Asahi microcarriers. The specific growth rate was determined as described and had a value of  $0.022 \text{ h}^{-1}$  for cells grown on Cytodex-3 microcarriers and  $0.018 \text{ h}^{-1}$  for cells grown inside Asahi microcarriers. Two samples at 50 and 95 hours of culture, respectively were taken for shear experiments. The gas flow rate during the shear measurements in the air lift was  $5.0 \cdot 10^{-6} \text{ m}^3 \cdot \text{s}^{-1}$ . Experiments for cells

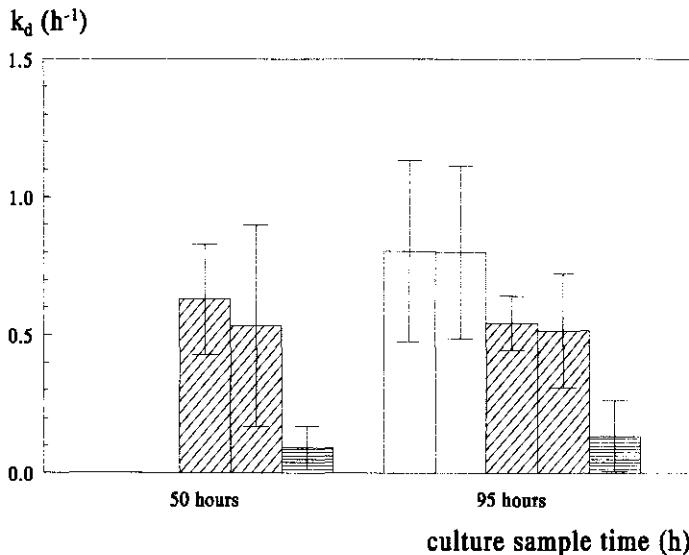


**Figure 8.** First-order death-rate constants for Vero cells grown on Cytodex-3 microcarriers at  $2.5 \text{ g.dm}^{-3}$  (blank) and  $5 \text{ g.dm}^{-3}$  (inclined dashed) and Vero cells grown in Asahi microcarriers at  $1 \text{ g.dm}^{-3}$  (horizontally dashed). Experiments with Cytodex-3 microcarriers were all done in duplicate. Experiments for Cytodex-3 microcarriers ( $5 \text{ g.dm}^{-3}$ ) and Asahi microcarriers were conducted with samples taken from batch cultures at 50 and 95 hours of culture.

grown on Cytodex-3 microcarriers were done in duplo. The death-rate constants with cells obtained at 50 and 95 hours of culture are shown in Figure 8 and Table II. For comparison, the death-rate constants for Vero cells on Cytodex-3 microcarriers at a concentration of  $2.5 \text{ g.dm}^{-3}$  and the same gas flow rate are also given.

**Table II.** First-order death-rate constants and 95% confidence intervals determined from the decrease in viable cells for cells grown on Cytodex-3 and in Asahi microcarriers. For Asahi and Cytodex-3 ( $5 \text{ g.dm}^{-3}$ ) microcarriers the death-rate constant was determined after cells were cultured in spinner flasks for 50 hours and 95 hours. For cells grown on Cytodex-3 microcarriers ( $2.5 \text{ g.dm}^{-3}$ ) the death-rate constant was determined after 95 hours of culture only (These are the same data as presented in Table I).

Experiment	F ( $10^{-6} \text{ m}^3 \cdot \text{s}^{-1}$ )	V ( $10^{-6} \text{ m}^3$ )	$k_{dv}$ (50 h) ( $10^{-5} \text{ s}^{-1}$ )	$k_{dv}$ (95 h) ( $10^{-5} \text{ s}^{-1}$ )
Cytodex ( $5 \text{ g.dm}^{-3}$ )	5.0	47.7	$17.5 \pm 5.6$	$15.1 \pm 2.7$
Cytodex ( $5 \text{ g.dm}^{-3}$ )	5.8	47.8	$14.8 \pm 10.0$	$14.4 \pm 5.7$
Asahi ( $1 \text{ g.dm}^{-3}$ )	5.0	47.9	$2.5 \pm 2.2$	$3.7 \pm 3.6$
Cytodex Flow 4A ( $2.5 \text{ g.dm}^{-3}$ )	5.1	48.3	(-)	$22.3 \pm 9.1$
Cytodex flow 4B ( $2.5 \text{ g.dm}^{-3}$ )	5.1	49.9	(-)	$22.2 \pm 8.7$

As can be seen there is no significant difference between the death-rate constants of cells after 50 and 95 hours of culture. The death-rate constant is significantly smaller for cells inside Asahi microcarriers as compared to cells on Cytodex-3 microcarriers ( $5 \text{ g.dm}^{-3}$ ) for both sampling times. Because samples are taken at different growth stages of the culture, the reduction in the death rate cannot be explained by a difference in growth state of the cells. Furthermore, the specific hypothetical killing volume calculated from the first-order death-rate constants for Vero cells inside Asahi microcarriers is  $3 \cdot 10^{-4} \text{ m}^3$  liquid per  $\text{m}^3$  of air bubbles, which is substantial smaller than the value of  $2 \cdot 10^{-3}$  found for Vero cells on Cytodex-3 microcarriers ( $2.5 \text{ g.dm}^{-3}$ ). These results form a clear indication that the porous Asahi microcarriers protect the cells against hydrodynamic forces. Because the death rate of Vero cells inside Asahi microcarriers still exceeds zero, the protection is only partial. Probably cells growing on the periphery of the microcarrier still may be killed by the air bubbles. Shiragami et al.<sup>35</sup> also found that the protection of CHO cells in porous Cultisphere microcarriers was only partial, with cells on the periphery of the microcarrier being especially susceptible to mechanical damage. Nikolai and Hu<sup>27</sup> found that no growth of Vero cells on Cultisphere microcarriers occurred at agitation rates just high enough to keep the microcarriers from settling. All the cells died and were found in the



exterior region of the microcarrier. In a stationary situation cells grew inside the microcarrier cavities. However, they do not report if these cells inside the microcarrier may be protected from hydrodynamic damage. In addition, differences in microcarrier properties other than the porosity, like for instance the strength with which the cells are adhered to the microcarriers as well as an influence of the microcarrier type on the strength of the cells themselves, may also affect the first-order death-rate constant.

### **Damage mechanisms**

Cells on microcarriers in the air lift may be killed directly by hydrodynamic forces or through the collision of microcarriers<sup>6</sup>. At the microcarrier hold up of 0.005 used here, cell death as a consequence of the collision of microcarriers may be neglected<sup>2</sup>. For the shear-related death of cells on microcarriers that, like Vero cells, cannot survive in suspension, the strength of the cell itself as well as the strength with which the cell is attached to the microcarrier is of importance. The tightness of the binding of the cells will depend on the cell line, the microcarrier characteristics, the growth phase of the culture, the medium composition<sup>18</sup>, and the amount of cells per microcarrier. Cell cell contacts may cause the cell to be more tightly bound to the microcarrier and thus to be less shear sensitive<sup>18</sup>. Thus, removal of a cell may render the neighbouring cells more shear sensitive. In addition, hydrodynamic forces affecting a cell may also affect the neighbouring cells either directly or through the cell cell contacts. This may explain the observation of the clear spots in Figure 7, where whole groups of cells have been removed from the carrier.

Like for suspension cells<sup>34</sup>, death of cells on microcarriers due to hydrodynamic forces may occur at three positions in the air lift: (1) in the sparger region due to the formation of the bubbles; (2) in the riser and downcomer section due to hydrodynamic forces caused by the rising of the bubbles and the liquid flow; (3) at the surface due to the bursting of the bubbles.

In the sparger region suspension cells are killed if they come in contact with newly formed bubbles, which are not yet covered with surfactants<sup>16</sup>. It seems reasonable to assume that also cells on microcarriers are killed if they come in contact with these bubbles. Because microcarriers totally covered with cells are used, probably a group of cells at a certain spot of the microcarrier will adsorb to the bubble instead of only one cell. This again may explain the observation from the photographs (Fig. 7) that it appears that cells are removed in groups from the microcarriers. Apart from this, Murhammer and Goochee<sup>26</sup> also state that cell death in air-lift reactors may occur in the sparger region and is related to the pressure drop over the orifice.

In case the bubbles are partially saturated with surfactants, the cell-bubble contact is not lethal and the cells adsorb to the bubble<sup>16</sup>. Adsorption of cells to bubbles has also been shown by Bavarian et al.<sup>1</sup>. Microcarriers that have adsorbed to the bubbles may rise with the bubbles to the surface. Although Jordan et al.<sup>16</sup> showed that adsorbed cells could not easily be detached from the bubbles, this may be different for microcarriers, which experience a higher drag force due to their larger size. On the other hand, the contact area between the bubble and the microcarrier may be larger leading to a more tight binding to the bubble. In the case of suspension cells it is shown that the death rate is proportional to the reciprocal reactor height indicating that no cell death occurs in the riser and downcomer section due to the rising of air bubbles or due to the liquid flow<sup>22</sup>. However, due to the relatively large size of a microcarrier (200  $\mu\text{m}$ ) as compared with a suspension cell (20  $\mu\text{m}$ ), the liquid velocity a cell on a microcarrier experiences in a laminar flow field will be substantially higher than the liquid velocity a suspension cell experiences in the same flow field. For the case of turbulent flow, occurring in stirred-tank and bubble-column reactors, the size of the eddies that cause cell death is substantially larger for cells on microcarriers than for suspension cells<sup>9,18,29,17</sup>. Thus, cells on microcarriers may be damaged at much lower energy dissipation rates than suspension cells and death of cells on microcarriers in the riser and downcomer section cannot be excluded. Shear experiments in air-lift reactors at varying heights may reveal if events associated with the liquid flow and the rising of air bubbles are detrimental to cells on microcarriers.

At the bubble disengagement zone suspension cells present in the bubble film and near the cavity wall are killed as the bubble ruptures<sup>5,7,38</sup>. Trinh et al.<sup>38</sup> calculated that a specific killing volume of  $2 \cdot 10^{-3}$  would correspond to a film thickness around the air-bubble of about 1 to 2  $\mu\text{m}$ . Cherry and Hulle<sup>7</sup> did the same calculation for a specific killing volume of  $4 \cdot 10^{-3}$  and found a value of 5  $\mu\text{m}$ . According to Trinh et al.<sup>38</sup> the thickness of 1 to 2  $\mu\text{m}$  would imply that only cells attached to the bubble are killed. For microcarriers, which are substantially larger than 1 to 2  $\mu\text{m}$ , this would mean that only the cells, which are adsorbed to the air bubble or are very near to it are killed. This also may explain the observation from the photographs (Fig. 7) that it appears that cells are removed in groups from the microcarriers.

In conclusion, since forces associated with bubble rupture are high enough to kill suspension cells, it is very likely that they also cause the death of cells immobilized on microcarriers in case these microcarriers are near the bursting bubble. Evidence that larger particles may be near the bursting bubbles is given by Lu et al.<sup>20</sup>, who showed that nylon microcapsules varying in size from 20 to 300  $\mu\text{m}$  were ejected in the upward jet formed at bubble

break-up. In addition to cell death due to bubble break-up, damage in other parts of the reactor cannot be excluded.

## CONCLUSIONS

The death rate of Vero cells on Cytodex-3 microcarriers can be described by first-order kinetics. The first-order death-rate constant as calculated from the decrease in viable cells, increase in dead cells and increase in LDH activity, is linear proportional to the gas flow rate, which is in accordance with the hypothetical-killing-volume theory. The specific hypothetical killing volume has a value of  $2 \cdot 10^{-3} \text{ m}^3 \text{ liquid per m}^3 \text{ of air bubbles}$ .

Macroporous Asahi microcarriers were able to partly protect the cells against hydrodynamic shear caused by air bubbles. For cells in these microcarriers the hypothetical killing volume was found to be  $3 \cdot 10^{-4} \text{ m}^3 \text{ liquid per m}^3 \text{ of air bubbles}$ .

## REFERENCES

1. Bavarian, F., Fan, L.S., Chalmers, J. 1991. Microscopic visualization of insect cell bubble interactions. I: Rising bubbles, air-medium interface, and the foam layer. *Biotechnol. Prog.* **7**: 140-150.
2. Beverloo, W.A., Tramper, J. 1994. Intensity of microcarrier collisions in turbulent flow. *Bioproc. Eng.* **11**: 177-184.
3. Bugarski, B., King, G. A., Daugulis, A.J., Goosen, M.F.A. 1989. Performance of an external air-lift bioreactor for the production of monoclonal antibodies by immobilized hybridoma cells. *Applied Microbiol. Biotechnol.* **30**: 264-269.
4. Cahn, F. 1990. Biomaterials aspects of porous microcarriers for animal cell culture. *Tibtech* **8**: 131-136.
5. Chalmers, J.J., Bavarian, F. 1991. Microscopic visualization of insect cell-bubble interactions. II: The bubble film and bubble rupture. *Biotechnol. Prog.* **70**: 151-158.
6. Cherry, R.S., Papoutsakis, E.T. 1986. Hydrodynamic effects on cells in agitated tissue culture reactors. *Bioproc. Eng.* **1**: 29-41.
7. Cherry, R.S., Hulle, C.T. 1992. Cell death in the thin films of bursting bubbles. *Biotechnol. Prog.* **8**: 11-18.
8. Chisti, M.Y. 1989. *Airlift bioreactors*. Elsevier Science Publishers LTD, New York.
9. Croughan, M.S., Sayre, E.S., Wang, D.I.C. 1989. Viscous reduction of turbulent damage in animal cell culture. *Biotechnol. Bioeng.* **33**: 862-872.
10. Croughan, M.S., Wang, D.I.C. 1990. Reversible removal and hydrodynamic phenomena in CHO microcarrier cultures. *Biotechnol. Bioeng.* **38**: 316-319.
11. Gardner, A.R., Gainer, J.L., Kirwan, D.J. 1990. Effects of stirring and sparging on cultured hybridoma cells. *Biotechnol. Bioeng.* **35**: 940-947.
12. Geaugey, V., Pascal, F., Engasser, J.M., Marc, A. 1990. Influence of the culture oxygenation on the release of LDH by hybridoma cells. *Biotechnol. Techn.* **4**: 257-262.
13. Handa-Corrigan A., Emery, A.N., Spier, R.E. 1989. Effect of gas-liquid interfaces on the growth of suspended mammalian cells: Mechanisms of cell damage by bubbles. *Enzyme Microb. Technol.* **11**: 230-235.

14. Henzler, H.-J., Kauling, D.J. 1993. Oxygenation of cell cultures. *Bioproc. Eng.* **9**: 61-75.
15. Jöbses, I., Martens, D., Tramper, J. 1991. Lethal events during gas sparging in animal cell culture. *Biotechnol. Bioeng.* **37**: 484-490.
16. Jordan, M., Sucker, H., Einsele, F., Eppenberger, H.M. 1994. Interactions between animal cells and gas bubbles: The influence of serum and pluronic F68 on the physical properties of the bubble surface. *Biotechnol. Bioeng.* **43**: 446-454.
17. Kunas, K.T., Papoutsakis, E.T. 1990. Damage mechanisms of suspended animal cells in agitated bioreactors with and without bubble entrainment. *Biotechnol. Bioeng.* **36**: 476-483.
18. Lakhotia, S., Papoutsakis, E.T. 1992. Agitation induced cell injury in microcarrier cultures. Protective effect of viscosity is agitation intensity dependent: Experiments and modelling. *Biotechnol. Bioeng.* **39**: 95-107.
19. Legrand, C., Bour, J.M., Capiamont, J., Martial, A., Marc, A., Wudtke, M., Kretzmer, G., Demangel, C., Duval, D., Hache, J. 1992. Lactate dehydrogenase (LDH) activity of the number of dead cells in the medium of cultured eukaryotic cells as marker. *J. Biotechnol.* **25**: 231-243.
20. Lu, G.Z., Thompson, B.G., Gray, M.R. 1992. Physical modelling of animal cell damage by hydrodynamic forces in suspension cultures. *Biotechnol. Bioeng.* **40**: 1277-1281.
21. Ludwig, A., Kretzmer, G., Schütgerl, K. 1992. Determination of a 'critical shear stress level' applied to adherent mammalian cells. *Enzyme Microb. Technol.* **14**: 209-213.
22. Martens, D.E., Gooijer, C.D. de, Beuvery, E.C., Tramper, J. 1992. Effect of serum concentration on hybridoma viable cell density and production of monoclonal antibodies in CSTRs and on shear sensitivity in air-lift loop reactors. *Biotechnol. Bioeng.* **39**: 891-897.
23. Martens, D.E., Gooijer, C.D. de, Velden-de Groot, C.A.M. van der, Beuvery, E.C., Tramper, J. 1993. Effect of dilution rate on growth, productivity, cell cycle and size, and shear sensitivity of a hybridoma cell in a continuous culture. *Biotechnol. Bioeng.* **41**: 429-439.
24. Michaels, J.D., Petersen, J.F., McIntire, L.V., Papoutsakis, E.T. 1991. Protection mechanism of freely suspended animal cells (CRL 8018) from fluid-mechanical injury. Viscometric and bioreactor studies using serum, pluronic F68 and polyethylene glycol. *Biotechnol. Bioeng.* **38**: 169-180.
25. Mukhopadhyay, A., Mukhopadhyay, S.N., Talwar, G.P. 1993. Cellular affinity is the only deciding factor for microcarrier selection for the cultivation of anchorage dependent cells. *Biotechnol. Techn.* **7**: 173-176.
26. Murhammer, D.W., Goochee, C.F. 1990. Sparged animal cell bioreactors: Mechanism of cell damage and pluronic F-68 protection. *Biotechnol. Prog.* **6**: 391-397.
27. Nikolai, T., Hu, W.-S. 1992. Cultivation of mammalian cells on macroporous microcarriers. *Enzyme Microb. Technol.* **14**: 203-213.
28. Nollert, M.U., Diamond, S.L., McIntire, L.V. 1991. Hydrodynamic shear stress and mass transport modulation of endothelial cell metabolism. *Biotechnol. Bioeng.* **38**: 588-602.
29. O'Connor, K.C., Papoutsakis, E.T. 1992. Agitation effects on microcarrier and suspension CHO cells. *Biotechnol. Techn.* **6**: 323-328.
30. Papoutsakis, E.T. 1991. Fluid-mechanical damage of animal cells in bioreactors. *TibTech* **9**: 427-437.
31. Petersen, J.F., McIntire, L.V., Papoutsakis, E.T. 1988. Shear sensitivity of cultured hybridoma cells (CRL-81018) depends on mode of growth, culture age and metabolic concentrations. *J. Biotechnol.* **7**: 229-246.

## Chapter 6

32. Pol, L. van der, Zijlstra, G., Thalen, M., Tramper J. 1990. Effect of serum concentration on production of monoclonal antibodies and on shear sensitivity of a hybridoma. *Bioproc. Eng.* 5: 241-245.
33. Pol, L. van der, Bonarius, D., Wouw, G. van de, Tramper, J. 1993. Effect of silicone antifoam on shear sensitivity of hybridoma cells in sparged cultures. *Biotechnol. Prog.* 9: 504-509.
34. Riet, K. van't, Tramper, J. 1991. *Basic bioreactor design.* Marcel Dekker Inc, New York.
35. Shiragami, N., Honda, H., Unno, H. 1993 Anchorage dependent animal cell culture using a porous microcarrier. *Bioproc. Eng.* 8: 295-299.
36. Tramper, J., Williams, J.B., Joustra, D. 1986. Shear sensitivity of insect cells in suspension. *Enzyme Microbiol. Technol.* 8: 33-36.
37. Tramper, J., Smit, D., Straatman, J., Vlak, J.M. 1988. Bubble column design for growth of fragile insect cells. *Bioproc. Eng.* 3: 37-41.
38. Trinh, K., Garcia-Briones, M., Chalmers, J.J. 1994. Quantification of damage to suspended insect cells as a result of bubble rupture. *Biotechnol. Bioeng.* 43: 37-45.

## CHAPTER 7

# A COMBINED CELL-CYCLE AND METABOLIC MODEL FOR THE GROWTH OF HYBRIDOMA CELLS IN STEADY-STATE CONTINUOUS CULTURE

### ABSTRACT

The model presented in this work demonstrates the combination of a cell-cycle model with a model describing the growth and conversion kinetics of hybridoma cells in a steady-state continuous culture. The cell-cycle model is based upon a population-balance model as described by Cazzador and Mariani and assumes the existence of a cycling and apoptotic cell population, which together form the viable-cell population. In this part the fraction of apoptotic cells, the age distribution of the cycling and apoptotic cell population, the mean volume and biomass content per cell of the cycling, apoptotic and viable cells, and the specific growth and death rates of the cells are calculated.

The metabolic part consists of a Monod-type growth equation, four elemental balances, an equation assuming a constant yield of ammonia on glutamine, an equation for product formation, and the relation of Glacken for energy production. Furthermore, a maintenance-energy model for the consumption of glucose and glutamine is introduced, which combines the approaches of Herbert and Pirt into one model in a way similar to Beeftink et al. For energy consumption a Pirt model is assumed.

The model is capable of predicting trends in steady-state values of a large number of variables of interest like specific growth rate, specific death rate, viability, cell numbers, mean viable-cell volume and concentrations and conversion rates of product, glucose, glutamine, lactate, and ammonia. Also the concentrations and conversion rates of oxygen and carbon dioxide are qualitatively predicted. The values of the model predictions are generally close to experimental data obtained from literature.

## INTRODUCTION

Animal cells are still necessary for the production of many biological-active proteins. These include therapeutic and diagnostic antibodies, vaccines, and hormones. Although scientific research has improved the cost-efficient production of these proteins during the last years, some of the main problems associated with animal-cell cultivation still remain. These include low specific productivities, low cell densities in conventional reactor systems like the stirred-tank and air-lift loop reactor, relatively high costs of medium components, and the shear sensitivity of the cells. A better understanding of cell physiology, medium development, and optimization of process control are possible strategies to overcome these problems. For optimizing process control, the use of a mathematical model describing the relations between the relevant parameters of an animal-cell culture is an essential tool. Furthermore, depending upon its amount of physiological detail and structure, a model can also be of great value in getting a better insight into the physiology of animal cells.

In literature a number of unstructured and more or less structured models are described for animal-cell culture. The unstructured models<sup>8,14,17,46,47</sup> make no assumptions with respect to cellular processes. In most cases a Monod-type growth equation is used in combination with Pirt's linear equation for substrate consumption. The courses of the concentrations in time are calculated using a set of first-order differential equations. Besides these unstructured models, also a number of more or less structured models have been described. Structured models have been reported based on the cell cycle<sup>10,22,23,44</sup> and on assumptions concerning metabolic processes<sup>4,5</sup>. Furthermore, models exist, describing only the metabolic pathway of antibody production<sup>7,45</sup>.

The integrated description of cell-cycle and metabolic processes has in many cases been restricted to antibody production<sup>10,23,44,45</sup>. In this work a partly structured model for the growth of hybridoma cells is described, demonstrating the combination of a cell-cycle model with a model describing metabolic processes. The metabolic part includes a Monod-type growth equation, an equation for product formation, a constant yield of ammonium on glutamine and four elemental balances for, respectively, carbon, hydrogen, oxygen, and nitrogen. For the consumption of glucose and glutamine a maintenance-energy model analogous to the one presented by Beeftink et al.<sup>6</sup> is included, which combines the approaches of Herbert and Pirt. Further structure is incorporated in the model by introducing the relation of Glacken for ATP production<sup>16</sup>. For the consumption of ATP a Pirt relation is used<sup>43</sup>, assuming ATP is produced with the same rate as it is consumed. More structure is added to the model by introducing a cell-cycle model based upon steady-state age distributions of a cycling subpopulation and an apoptotic, non-cycling subpopulation of cells. The presented model provides a means to relate

operating conditions to the rate of apoptosis and may be used for any suspension cell with properties comparable to hybridoma cells.

## THEORY

### Cell-cycle model

#### *System description*

With respect to the cell cycle, animal cells may be found in one of five different phases. Immediately after cell division the newborn cells enter the indeterminate phase A. Different models exist with respect to the transition of cells from this phase to the determinate phase B and to the quiescent phase Q<sup>10,23</sup>, respectively. Cells that have entered phase B double their DNA content and are determined to undergo cell division. Cells that do not enter phase B become quiescent by entering phase Q in which they stay until they are provided with the right growth factors and become competent cells. If sufficient nutrients are present, the competent cells re-enter the division cycle (phase A + phase B) at the start of phase B or shortly before this point in phase A<sup>32</sup>. Besides these four phases, a fifth phase (O) can be discerned called the apoptotic phase<sup>18,27,33,34,48</sup>. Somewhere in this phase there is an irreversible step after which cells are destined to die and cannot return to the cycle<sup>18</sup>. It is not known where in the apoptotic process this irreversible step is situated and for the moment it is assumed that apoptotic cells do not return to phases A and B. Apoptosis is a regulated process generally requiring protein synthesis and energy and is accompanied by DNA fragmentation, condensation of the cytoplasm, disappearance of actin filaments, and a decrease in size<sup>18,27,33,34,40,41,48</sup>. Besides through apoptosis, cells also die and enter the dead cell population D through necrosis<sup>18,27,40,41</sup>.

If the growth conditions are unfavourable, for instance towards the end of a batch culture or in continuous cultures at low dilution rates, the death rate of hybridoma cells increases rapidly<sup>2,3,9,15,21,23,25,28,31,35</sup>. This indicates that in standard laboratory cultures these cells cannot be maintained in a non-proliferative or quiescent phase for long times<sup>2</sup>. If cell arrest occurs somewhere in phase A, all arrested cells will have a single DNA content, because DNA synthesis takes place in phase B. Thus, as the specific growth rate approaches zero and cells become arrested, the fraction of cells with a single DNA content should become one and, consequently, the fraction with an intermediate or double DNA content should become zero. Nevertheless, DNA distributions show that, even at very low or zero specific growth rates, still a considerable amount of cells have an intermediate or double DNA content<sup>2,25,31</sup>. This indicates that cells stop cycling everywhere in the cycle instead of becoming arrested at a specific point in this cycle. This is supported by the results of Al-Rubeai et al.<sup>2,3</sup> showing that the DNA distribution of dead



cells at the end of batch cultures is equal to that of the viable cells. Apparently, hybridoma cells experiencing unfavourable conditions for growth, die everywhere in phases A and B instead of becoming arrested in a quiescent phase. This is in agreement with the fact that in cancer cells, like hybridoma cells, the switching mechanism between quiescence and proliferation is defective<sup>32</sup>. In conclusion, the quiescent and consequently the competent phase are assumed not to be present in hybridoma cells. At unfavourable conditions for growth, cells die either through necrosis or through apoptosis. Since apoptosis is demonstrated in a number of B-cell hybridomas<sup>27,33,40,41,48</sup> and since these cells originate from cells out of the immune system, where apoptosis is an elementary process<sup>18</sup>, we assume that the increased death rate at unfavourable growth conditions is caused by apoptosis. Part of the apoptotic cells are classified as viable using dye-exclusion methods<sup>27,33,34,41</sup>, meaning their membrane is more or less intact. Since these apoptotic cells are marked as viable but are non-proliferative and have a relative low metabolic activity, they must be taken into account as a separate sub-population<sup>27</sup>.

#### *Steady-state age distributions*

The resulting cell-cycle model is shown in Figure 1. Phases A, B, and O are the indeterminate, determinate and apoptotic phase, respectively. The age distribution of the cell populations in these phases may be described by the age/time equation of M'Kendrick, which was rediscovered for its use in cell-cycle kinetics by von Foerster<sup>49</sup>:

$$\frac{\partial n_i(a,t)}{\partial t} + \frac{\partial n_i(a,t)}{\partial a} = -\lambda_i(a,t)n_i(a,t) \quad i=A,B,O \quad (1)$$

where  $n_i(a,t)$  is the age density function (cells.m<sup>-3</sup>.s<sup>-1</sup>) of cells of age  $a$  (s) at time  $t$  (s) and  $\lambda_i(a,t)$  is the loss term (s<sup>-1</sup>). The loss term consists of loss terms for cell death,  $\lambda_{di}(a,t)$  (s<sup>-1</sup>), for migration to another population  $j$ , also called the intrinsic loss,  $\lambda_{mij}(a,t)$  (s<sup>-1</sup>), and loss by transport out of the system,  $D_i(a,t)$  (s<sup>-1</sup>):

$$\lambda_i(a,t) = \lambda_{di}(a,t) + \sum_{j=A,B,O \text{ if } i \neq j} \lambda_{mij}(a,t) + D_i(a,t) \quad i=A,B,O \quad / \quad \lambda_{mOA} = \lambda_{mOB} = 0 \quad (2)$$

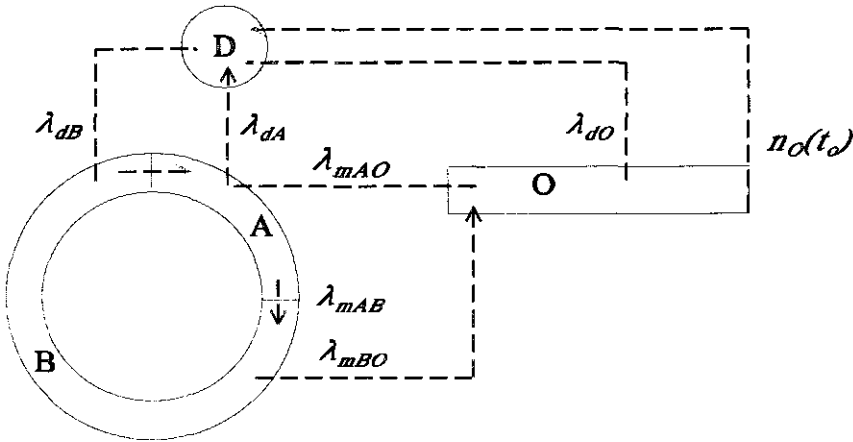


**Figure 1.** Schematic representation of the cell cycle: A, indeterminate phase; B, determinate phase; O, apoptotic phase; D, dead cell population. The arrows indicate the phase transitions that occur. For each transition the rate constant  $\lambda_{ij}$  ( $s^{-1}$ ) is given.

In order to solve Equation (1) for the three different phases additional assumptions have to be made:

1. The continuous culture is in steady state. Equation (1) is thus independent of the time,  $n_i(a,t) = n_i(a)$ ,  $\lambda_i(a,t) = \lambda_i(a)$  and may be solved with respect to age.

2. The transition from phase B to phase A occurs at a constant age  $t_B$  (s) of the phase-B cells. Thus, the rate of transition from phase B to phase A,  $\lambda_{mBA}$ , can be replaced by the boundary condition  $n_A(0) = 2n_B(t_B)$ .

3. The transition from phase A to phase B occurs at age  $t_A$  (s) of the phase-A cells. Thus, the rate of transition from phase A to phase B,  $\lambda_{mAB}$ , can be replaced by the boundary condition  $n_A(t_A) = n_B(0)$ .

4. Loss of cells due to dilution out of the system is independent of the age of the cell and the phase it is in,  $D_A(a) = D_B(a) = D_O(a) = D$ .

5. Cells enter phase O from phase A and phase B at an equal rate independent of their age,  $\lambda_{mAO} = \lambda_{mBO}$ . Al-Rubeai et al.<sup>2,3</sup> showed that cells die everywhere in the cycle. In addition, Singh et al.<sup>41</sup> could identify at high agitation rates a population of small cells, which showed some but not all characteristics of apoptosis and had a full cell-cycle distribution. This supports the assumption that cells enter apoptosis from every stage of the cell-cycle. Whether this happens with a rate independent of their age remains to be investigated.

6. Cells in phase O die after a fixed residence time  $t_o$  (s). From the work of Perreault and Lemieux<sup>33</sup> this residence time is estimated to be about 24 hours. In addition, cells may also die during the process of apoptosis as stated in assumption 7. This death will be difficult to distinguish from the death occurring at the end of the apoptotic process.

7. Cell loss due to necrosis is equal for cells in phases A, B, and O and is assumed to be independent of age,  $\lambda_{dA} = \lambda_{dB} = \lambda_{dO}$ .

**Table I.** Balance equations, steady-state solutions  $n_i(a)$ , total number of cells  $N_i$  and boundary conditions for phase C and phase O.

Steady-state balance equation:

$$\frac{\partial n_i(a)}{\partial a} = -\lambda_i n_i(a) \quad i=C, O \quad \text{T1}$$

Steady-state solution phase C:

$$n_C(a) = n_C(0) e^{-(D+\lambda_{mCO}+\lambda_{dC})a} \quad 0 \leq a \leq t_C \quad \text{T2}$$

$$N_C = \frac{n_C(0)}{D+\lambda_{mCO}+\lambda_{dC}} (1 - e^{-(D+\lambda_{mCO}+\lambda_{dC})t_C}) \quad \text{T3}$$

Steady-state solution phase O:

$$n_O(a) = n_O(0) e^{-(D+\lambda_{dO})a} \quad 0 \leq a \leq t_O \quad \text{T4}$$

$$N_O = \frac{n_O(0)}{D+\lambda_{dO}} (1 - e^{-(D+\lambda_{dO})t_O}) \quad \text{T5}$$

Boundary condition phase-C cells:

$$n_C(0) = 2n_C(t_C) \quad \text{T6}$$

Boundary condition phase-O cells:

$$n_O(0) = \lambda_{mCO} N_C \quad \text{T7}$$

Based upon these assumptions, phases A and B can be mathematically combined into one phase called the cycling phase C with a duration  $t_C (=t_A+t_B)$  (s), a loss term for cell death,  $\lambda_{dC}$  ( $=\lambda_{dA}=\lambda_{dB}$ ) ( $s^{-1}$ ), and a loss term for transition to phase O,  $\lambda_{mCO}$  ( $=\lambda_{mA0}=\lambda_{mBO}$ ) ( $s^{-1}$ ). With these assumptions Equation (1) may be solved for the cycling phase C and the apoptotic phase O. Solutions for the age distributions  $n_C(a)$  and  $n_O(a)$  (cells. $m^{-3}.s^{-1}$ ) are given in Table I together with the boundary conditions. In addition, the total amount of cells  $N_C$  and  $N_O$  (cells. $m^{-3}$ ) are given,

which are obtained by integration of the age distributions from age 0 to age  $t_C$  for phase C and from age 0 to age  $t_O$  for phase O.

Applying the boundary condition for the cycling cells [Table I, Eq. (T6)] to the steady-state age distribution of these cells [Table I, Eq. (T2)] leads to the following relation, which must be satisfied in case of a steady state:

$$(\lambda_{dC} + \lambda_{mCO} + D) = \frac{\ln(2)}{t_C} \quad (3)$$

From a cell balance over the cycling (C) cells the next relation is obtained for the specific growth-rate constant  $\mu$  ( $s^{-1}$ ):

$$\mu = (D + \lambda_{dC} + \lambda_{mCO})(1 - F_O) \quad (4)$$

where  $F_O$  is the fraction of cells in phase O. The fraction of phase-O cells is computed from  $N_O/(N_O + N_C)$  by using the equations presented in Table I giving:

$$F_O = \frac{\lambda_{mCO}}{\lambda_{mCO} + \frac{D + \lambda_{dO}}{1 - e^{-(D + \lambda_{dO})t_O}}} \quad (5)$$

Equations (3), (4) and (5) form a set of three independent relations. Since  $\lambda_{dC}$ ,  $\lambda_{dO}$ ,  $t_B$ , and  $t_O$  are fixed parameters obtained either from the experimental data or from literature, there are four unknown variables left, being  $\mu$ ,  $\lambda_{mCO}$ ,  $F_O$ , and  $t_A$ . Thus, in order to solve the set of equations one of these unknown variables has to be fixed.

Looking at literature data<sup>15,21,28,35</sup> concerning hybridoma cells, including our own data<sup>25</sup>, it can be seen that if the specific growth rate decreases below a critical specific growth rate, the specific death rate starts increasing rapidly. This indicates that at specific growth rates above this critical specific growth rate, cells hardly enter the apoptotic phase and the specific growth rate is regulated by variation of the duration of phase A,  $t_A$ , and thus of the cycle time  $t_C$ . At specific growth rates below the critical specific growth rate cells start entering phase O and  $t_A$  and  $t_C$  stay more or less constant. For specific growth rates below the critical specific growth rate  $t_A$  is set to a constant critical value,  $t_{cr}$  (s), and thus  $\lambda_{mCO}$  increases with further decreasing specific growth rates. For specific growth rates above the critical specific growth rate,  $\lambda_{mCO}$  is set to zero and thus  $t_A$  decreases with increasing specific growth rates. Combining this with Equation (3) results in:

$$t_C = t_A + t_B = \frac{\ln(2)}{\lambda_{dC} + D}, \quad \lambda_{mCO} = 0 \quad \mu \geq \mu_{cr} \quad (6)$$

$$\lambda_{mCO} = \frac{\ln(2)}{t_{cr} + t_B} - \lambda_{dC} - D, \quad t_A = t_{cr} \quad \mu < \mu_{cr}$$

where  $\mu_{cr}$  is the critical specific growth rate ( $s^{-1}$ ), which may be determined from a plot of the specific death rate or viability as a function of the specific growth rate. From literature data this critical specific growth rate appears to be about half the maximum specific growth rate,  $\mu_m$  ( $s^{-1}$ ), meaning that cells start shifting to phase O as soon as the substrate concentration drops below the Monod constant. Perreault and Lemieux<sup>33</sup> have found that apoptosis is rapidly triggered in B-cell hybridomas when protein synthesis is reduced by 50% from the maximum value.

The duration of phase B,  $t_B$ , is calculated from the maximum specific growth rate ( $t_B = \ln(2)/\mu_m$ ), when the duration of phase A is zero. The critical duration of phase A,  $t_{cr}$ , may now be obtained from the critical specific growth rate ( $t_{cr} = (\ln(2)/\mu_{cr}) - t_B$ ). The specific death rate of the cycling cells,  $\lambda_{dc}$ , is equal to the specific death rate of the viable cells at specific growth rates substantially larger than the critical specific growth rate, when no apoptotic cells are present. The specific death rate constant during apoptosis,  $\lambda_{do}$ , is assumed to be equal to  $\lambda_{dc}$ . Now,  $\lambda_{mCO}$  and  $t_A$  may be obtained from Equation (6). Next  $F_O$  can be calculated from Equation (5) and  $\mu$  from Equation (4). Subsequently, the age distributions of the cells in phase C and phase O can be calculated [Table I, Eqs. (T2) and (T4)]. From the age distributions, other cell-population characteristics can be calculated as shown below.

#### Death-rate constant

The overall death-rate constant,  $\mu_d$  ( $s^{-1}$ ), is derived in appendix A and may be calculated according to:

$$\mu_d = (1 - F_O)\lambda_{dC} + \left(\lambda_{dO} + \frac{D + \lambda_{dO}}{e^{(D + \lambda_{dO})t_O} - 1}\right)F_O \quad (7)$$

#### Volume and biomass content of phase-C cells

Additional assumptions have to be made for the change of cell volume and biomass content with age of the cells in phase C and phase O. Cells in phase C are assumed to exponentially double their volume and biomass in a period starting immediately after cell division at age  $a=0$  until they enter mitosis at age  $a=t_C - t_m$ , where  $t_m$  (s) is the duration of the mitosis, being about 1-2

hours. Other functions for the increase in average cell volume with cell-cycle age may be incorporated here. The average volume of the cycling cells,  $V_C$  ( $\text{m}^3$ ), thus becomes:

$$V_C = \frac{\int_0^{t_c - t_m} V_A e^{\frac{\ln(2)}{t_c - t_m} a} n_C(0) e^{-(D + \lambda_{mco} + \lambda_{dc})a} da + \int_{t_c - t_m}^{t_c} 2V_A n_C(0) e^{-(D + \lambda_{mco} + \lambda_{dc})a} da}{\int_0^{t_c} n_C(0) e^{-(D + \lambda_{mco} + \lambda_{dc})a} da} \quad (8)$$

where  $V_A$  is the volume of the cells just after mitosis ( $\text{m}^3$ ),  $n_C(0)$  is the number of cells of age zero ( $\text{cells} \cdot \text{m}^{-3} \cdot \text{s}^{-1}$ ). Integrating Equation (8) and substituting Equation (3) results in:

$$V_C = 2V_A \frac{t_c}{t_m} (e^{\frac{t_m \ln(2)}{t_c}} - 1) \quad (9)$$

With a constant density of the cells<sup>12</sup> in phase C,  $\rho_{cell}$  ( $\text{g} \cdot \text{m}^{-3}$ ), the average biomass content of phase-C cells,  $CM_C$  ( $\text{C} \cdot \text{mol} \cdot \text{cell}^{-1}$ ), becomes:

$$CM_C = \frac{\rho_{cell} V_C}{M_{cell}} \quad (10)$$

where  $M_{cell}$  is the C-molar mass ( $\text{g} \cdot \text{C} \cdot \text{mol}^{-1}$ ). The C-molar mass may be calculated from the ash fraction,  $ash_x$ , and the hydrogen,  $a_x$ , oxygen,  $b_x$ , and nitrogen,  $c_x$ , content per C-mol of biomass according to:

$$M_{cell} = \frac{1}{1 - ash_x} (12 + a_x + 16b_x + 14c_x) \quad (11)$$

#### Volume and biomass content of phase-O cells

As stated, apoptosis is accompanied by a decrease in cell size. This decrease is caused by the extrusion of water and cross-linkage of proteins, which turns the apoptotic cell into a rigid and relatively stable structure<sup>27,34</sup>. Not much is known about the magnitude of the volume decrease in phase O. Here the average volume of the cells leaving phase O at age  $t_o$ ,  $V_{Oe}$  ( $\text{m}^3$ ), is assumed equal to the volume of the dead cells<sup>12,38</sup>. The average volume of the cells entering phase O is equal to that of the cycling cells being  $V_C$ . It is assumed now that in a period  $t_o$  the average volume of phase-O cells decreases exponentially from  $V_C$  to  $V_{Oe}$  with a rate constant  $k_{vo}$  ( $\text{s}^{-1}$ ) ( $= [1/t_o] \ln[V_C/V_{Oe}]$ ). The average volume of the cells in phase O,  $V_O$  ( $\text{m}^3$ ), is next given by:

$$V_o = \frac{\int_0^{t_o} V_C n_o(0) e^{-(k_{vo} + D + \lambda_{do})a} da}{\int_0^{t_o} n_o(0) e^{-(D + \lambda_{do})a} da} \quad (12)$$

Integrating this equation results in:

$$V_o = \frac{V_C (D + \lambda_{do}) (1 - e^{-(k_{vo} + D + \lambda_{do})t_o})}{(k_{vo} + D + \lambda_{do}) (1 - e^{-(D + \lambda_{do})t_o})} \quad (13)$$

For the cycling cells a constant density was assumed in order to calculate the average amount of biomass per cycling cell,  $CM_C$  [Eq. (10)]. However, the density of the apoptotic cells is probably not constant and, consequently, the average amount of biomass per apoptotic cell,  $CM_o$  (C-mol.cell<sup>-1</sup>), cannot be calculated from the average cell volume of the apoptotic cells. Therefore, the average amount of biomass per apoptotic cell is calculated from the average amount of biomass per cycling cell. As will be discussed in the metabolic part further on, it is assumed that apoptotic cells derive the energy required for the apoptotic process entirely from biomass decay. The energy requirements during apoptosis are not known and are here assumed to be equal to the energy requirements of the cycling cells for maintenance. Furthermore, the yield of energy on biomass is approximated to be the inverse of the biomass yield on energy. Thus, the rate of biomass decay is equal to the required energy divided by the energy yield from biomass, leading to the following equation for the first-order decay constant  $k_{xo}$  (s<sup>-1</sup>):

$$k_{xo} = m_e Y_{xe} \quad (14)$$

where  $m_e$  is the maintenance coefficient for ATP (mol ATP.C-mol<sup>-1</sup>.s<sup>-1</sup>) and  $Y_{xe}$  is the biomass yield on ATP (C-mol.mol ATP<sup>-1</sup>). Now the average biomass content of the phase-O cells,  $CM_o$ , may be calculated by replacing  $V_o$  by  $CM_o$ ,  $V_C$  by  $CM_C$  and  $k_{vo}$  by  $k_{xo}$  in Equation (13) leading to:

$$CM_o = \frac{CM_C (D + \lambda_{do}) (1 - e^{-(k_{xo} + D + \lambda_{do})t_o})}{(k_{xo} + D + \lambda_{do}) (1 - e^{-(D + \lambda_{do})t_o})} \quad (15)$$

In addition, the average amount of C-moles per cell dying at the end of phase O,  $CM_{Oe}$  (C-mol.cell<sup>-1</sup>), may be calculated according to:

$$CM_{Oe} = CM_C e^{-k_{xo}t_o} \quad (16)$$

*Cell volume and biomass content of the viable cells*

The average volume,  $V_v$  (m<sup>3</sup>), and biomass content,  $CM_v$  (C-mol.cell<sup>-1</sup>), of the whole viable cell population becomes:

$$V_v = (1 - F_o)V_c + F_oV_o \quad (17)$$

$$CM_v = (1 - F_o)CM_c + F_oCM_o \quad (18)$$

**Metabolic model***Introduction*

Correct treatment of reality would demand the construction of corpuscular models. However, the object under study, in this case the growth, consumption and production rates by hybridoma cells, is not associated with the behaviour of individual particles or cells, but with the overall behaviour of a large collection (population) of such objects. In such a case the macroscopic treatment may be employed<sup>36</sup>. The macroscopic description treats systems in macroscopic properties of which there are two types: intensive, non-additive properties (e.g. temperature, concentration, pressure) and extensive, additive properties (e.g. volume, mass, energy). The basic tool of the macroscopic description is the balance equation, that can be formulated for each extensive property of the system.

$$\text{accumulation} = \text{transport} + \text{conversion} \quad (19)$$

In this case the system is defined as a given amount of dry biomass. It contains about 800 chemical compounds<sup>1</sup>, for each of which a macroscopic balance equation can be formulated. This means that, in order to completely define the system, the rate of transport and production for each compound has to be known. In a steady-state situation there is no accumulation and the transport term must equal the conversion term. The number of compounds that have to be considered can be drastically reduced by making two assumptions.

First, it is assumed that there is no accumulation or depletion of a specific intracellular compound. Such a situation, called a pseudo-steady state, may also be assumed if the variations around a mean value of the concentration of intracellular compounds are fast with respect to the specific growth rate<sup>36</sup>. In a pseudo-steady state the elemental composition of the biomass is constant.



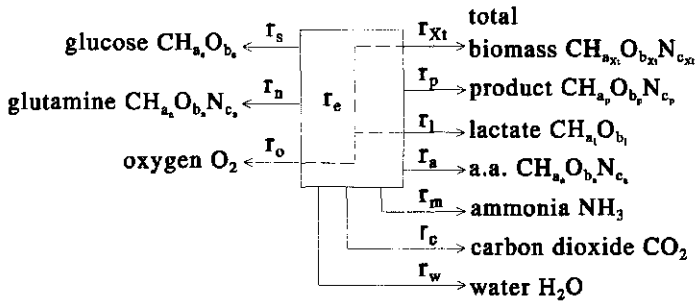


**Figure 2.** System definition for a hybridoma cell. The arrows indicate the production flows of the compounds. The dashed line represents the energy balance relating the oxygen consumption rate and lactate production rate to the formation and maintenance requirements of biomass.  $r_i$ , conversion rate of compound  $i$  which is positive in the case of production and negative in the case of consumption;  $a_i$ ,  $b_i$ ,  $c_i$ , hydrogen, oxygen, and nitrogen content of compound  $i$ . a.a., lumped amino acid.

The second assumption states that there is no transport of intracellular compounds across the system barrier (cell membrane). If these two assumptions are valid, all intracellular compounds do not have to be considered. Furthermore, of the extracellular compounds only those substances are taken into account that are consumed or produced in relatively large amounts. The resulting system definition is shown in Figure 2. All flows are regarded as production flows, which is why all arrows are directed outwards. Thus, production rates have a positive value and consumption rates have a negative value. Although all intracellular compounds can be omitted, the model does take into account one such compound, being ATP. Equations for the production and consumption of ATP are incorporated in the model and represent a simplification of the energy transformations in the cell. These equations link the consumption of oxygen and the production of lactate to the biomass formation as indicated by the dashed line in Figure 2 and thus provide an extra relation, which is needed to solve the set of equations as will become clear further on. Except for glutamine the production and consumption of amino acids is very variable for different cell lines and culture conditions<sup>11,19,21,24,29,30,31,37</sup>. Since it is very difficult to find a general applicable equation for the conversion kinetics of each of these amino acids, a lumped amino acid is introduced. This lumped amino acid serves as a lump parameter for the production and consumption of all amino acids except glutamine. For several literature data<sup>11,19,21,24,29,30,31,37</sup> the net rates of production of the elements nitrogen, carbon, hydrogen and oxygen in the form of amino acids were calculated using the presented production rates and the known elemental composition of these amino acids. The resulting values were averaged for the four mentioned

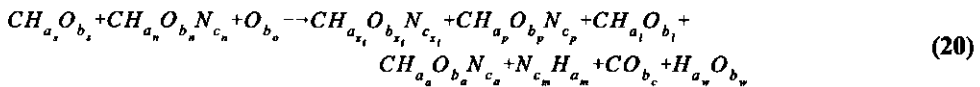
elements. The relative net rates of production of the four elements in the form of amino acids was next taken as the average composition of this lumped amino acid and can be found together with the elemental composition of the other compounds in Table II.

**Table II.** Hydrogen  $a_i$  (H), oxygen  $b_i$  (O) and nitrogen  $c_i$  (N) content and molecular mass  $M_i$  per C-mol for the compounds implemented in the model.

Compound	Symbol	$a_i$ (H)	$b_i$ (O)	$c_i$ (N)	$M_i$ (g.C-mol <sup>-1</sup> )
Glucose	s	2	1		30
Glutamine	n	2	0.6	0.4	29.2
Oxygen	o		2		16
Biomass	$x_i$	1.784	0.434	0.251	24.25
Product	p	1.5	0.25	0.25	21
Lactate	l	2	1		30
Ammonia	m	3		1	17
Carbon dioxide	c		2		44
Water	w	2	1		18
Lumped amino acid	a	2.1	0.51	0.28	26.2

### Reaction equation

The reaction equation for the growth of hybridoma cells and their production is:



The subscripts  $a_i$ ,  $b_i$  and  $c_i$  denote respectively the hydrogen, oxygen and nitrogen content of one C-mol of compound  $i$  as given in Table II, with  $i$  being glucose (s), glutamine (n), oxygen (o), total biomass ( $x_i$ ), product (p), lactate (l), lumped amino acid (a), ammonia (m), carbon dioxide (c) and water (w). The total biomass consists out of phase-C, phase-O and dead cells, which are assumed to have the same elemental composition.

### Growth and death rate

The rate of the reaction is determined by the growth rate, death rate and production rate. These in turn depend on the specific growth- and death-rate constants  $\mu$  and  $\mu_d$  as calculated in the cell-cycle part [Eqs. (4) and (7)] and on the productivity. At a certain viable-cell

concentration,  $C_{Xv}^{cell}$  (cells.m<sup>-3</sup>), the growth rate and the death rate may be calculated from:

$$r_{x_i}^{cell} = \mu C_{x_v}^{cell} \quad (21)$$

$$r_{x_d}^{cell} = \mu_d C_{x_v}^{cell} \quad (22)$$

$$r_{x_v}^{cell} = r_{x_i}^{cell} - r_{x_d}^{cell} \quad (23)$$

where  $r_{x_i}^{cell}$ ,  $r_{x_v}^{cell}$  and  $r_{x_d}^{cell}$  are the rates of total-, viable-, and dead-cell production (cells.m<sup>-3</sup>.s<sup>-1</sup>).

The superscript 'cell' denotes that the biomass is expressed in cell numbers.

In order to use the biomass formation rates [Eqs. (21)-(23)] in the next part of the metabolic model, they need to be expressed in C-moles. For this the amount of C-moles per cell has to be known, which is calculated in the cell-cycle part for cells in phase C and O [Eqs. (10), (15), (16) and (18)]. In a steady state the net rate of viable-biomass formation,  $r_{x_v}$  (C-mol.m<sup>-3</sup>.s<sup>-1</sup>), is equal to the rate with which it is diluted out of the culture and is given by:

$$r_{x_v} = D C M_v C_{x_v}^{cell} \quad (24)$$

The rate of dead-biomass formation,  $r_{x_d}$  (C-mol.m<sup>-3</sup>.s<sup>-1</sup>), is derived in appendix A and is given by:

$$r_{x_d} = \left[ (\lambda_{d0} C M_0 + \frac{D + \lambda_{d0}}{e^{(D + \lambda_{d0}) \tau_0} - 1} C M_{Oe}) F_0 + \lambda_{dc} C M_C (1 - F_0) \right] C_{x_v}^{cell} \quad (25)$$

The total biomass formation rate,  $r_{x_t}$  (C-mol.m<sup>-3</sup>.s<sup>-1</sup>), now becomes:

$$r_{x_t} = r_{x_v} + r_{x_d} \quad (26)$$

For cells in phase O part of the biomass formed in phase C is degraded when they progress through phase O. Thus, the observed total biomass formation rate [Eq. (26)] is the result of the true biomass formation rate minus the biomass decay rate in phase O. The true biomass formation rate,  $r_{x_{true}}$  (C-mol.m<sup>-3</sup>.s<sup>-1</sup>), is equal to the amount of biomass formed in the cycling phase, which under steady-state conditions is equal to:

$$r_{x_{true}} = (D + \lambda_{dc} + \lambda_{mCO}) (1 - F_0) C M_C C_{x_v}^{cell} \quad (27)$$

The biomass decay rate may now be obtained by subtracting the observed [Eq. (26)] from the true biomass formation rate [Eq. (27)].

*Maintenance-energy model*

According to the maintenance-energy models of Herbert and Pirt, substrate and energy is used for growth, production and maintenance<sup>6</sup>. Both models assume a constant requirement of energy per C-mol of viable biomass for maintenance. The model of Herbert assumes that this maintenance energy is coming entirely from biomass decay, while the Pirt model assumes it is provided by the degradation of an external substrate. Both models have their peculiarities. In the Pirt model substrate is still consumed even if its concentration is zero. In the Herbert model the substrate consumption is zero at a zero substrate concentration. However, in this model, even at high substrate concentrations and specific growth rates, the maintenance energy is still obtained through the decay of biomass. Both approaches, Herbert at high substrate concentrations and Pirt at low and zero substrate concentrations, seem to be incorrect. Beeftink et al.<sup>6</sup> have presented a model that combines the two approaches. Their model describes energy for maintenance purposes as being obtained simultaneously from biomass degradation as well as from substrate degradation in excess of growth requirements. The ratio between both catabolic processes is taken to be growth-rate dependent.

In animal cells like hybridoma cells there is a constant breakdown of macro-molecules which have to be resynthesized<sup>1,32</sup>. Energy required for this may be obtained from an external substrate if present (Pirt model). If no external substrate is present, cells enter the apoptotic phase, which is accompanied by a reduction of metabolic activity and a decrease in cell volume and biomass. The breakdown products of the decayed biomass may be used for the production of energy, in accordance with the model of Herbert. In the model presented here it is assumed that apoptotic cells derive their energy entirely from biomass decay. Since the fraction of phase-O cells is dependent on the specific growth rate, a maintenance model comparable to the one presented by Beeftink et al.<sup>6</sup> is obtained. At low or zero substrate levels and zero specific growth rate the fraction of phase-O cells approaches 1 and, subsequently, all energy is derived from biomass decay with the substrate consumption becoming zero. At high substrate levels and high specific growth rates the fraction of phase-O cells is 0 and substrate will be used for maintenance, while the biomass decay rate is zero. The ATP or energy requirement for the formation and maintenance of biomass is calculated on the basis of the model of Pirt for substrate consumption<sup>43</sup>. In a steady-state situation this ATP requirement must equal the ATP production rate, as will be described further on. The next equations are proposed for the consumption rate of glucose,  $r_s$  (C-mol.m<sup>-3</sup>.s<sup>-1</sup>), and glutamine,  $r_n$  (C-mol.m<sup>-3</sup>.s<sup>-1</sup>), and for the required ATP production rate,  $r_e$  (mol.m<sup>-3</sup>.s<sup>-1</sup>):

$$r_s = -\left(\frac{r_{x_{msc}}}{Y_{xs}} + (1-F_O)m_s CM_v C_{x_v}^{cell}\right) \quad (28)$$

$$r_n = -\left(\frac{r_{x_{msc}}}{Y_{xn}} + (1-F_O)m_n CM_v C_{x_v}^{cell}\right) \quad (29)$$

$$r_e = \frac{r_{x_{msc}}}{Y_{xe}} + m_e CM_v C_{x_v}^{cell} \quad (30)$$

where  $Y_{xi}$  is the yield of biomass on compound  $i$  (C-mol.(C)-mol<sup>-1</sup>) and  $m_i$  is the maintenance coefficient for compound  $i$  ((C)-mol.C-mol<sup>-1</sup>.s<sup>-1</sup>), with  $i$  being glucose (s), glutamine (n) and ATP (e), respectively.

#### *Ammonia and monoclonal-antibody production rates*

Knowing the consumption rate of glutamine, the production rate of ammonia,  $r_m$  (mol.m<sup>-3</sup>.s<sup>-1</sup>), may now be calculated by assuming a constant yield of ammonia on glutamine,  $Y_{mn}$  (mol.C-mol<sup>-1</sup>).

$$r_m = -Y_{mn}r_n \quad (31)$$

A general equation for the product formation rate,  $r_p$  (C-mol.m<sup>-3</sup>.s<sup>-1</sup>), is:

$$r_p = Y_{px}r_{xt} + q_p CM_v C_{x_v}^{cell} \quad (32)$$

where  $Y_{px}$  is the yield of product on biomass (C-mol.C-mol<sup>-1</sup>) and  $q_p$  is the non-growth-rate-associated production constant (C-mol.C-mol<sup>-1</sup>.s<sup>-1</sup>). The term non-growth-rate-associated production indicates that the production rate is not correlated with the specific growth rate.

#### *Elemental balances and energy production*

From the initial eleven unknown rates there are still five left, being the production rates of lactate, oxygen, carbon dioxide, water, and the lumped amino acid. Thus, five extra equations are needed to solve the model. Four extra equations may be obtained from the elemental balances for carbon, hydrogen, oxygen and nitrogen. Since the elements are conserved quantities, meaning they can neither be consumed nor produced, the following equations can be written when steady-state conditions apply:

$$r_s + r_n + r_{x_i} + r_p + r_l + r_a + r_c = 0 \quad (33)$$

$$c_n r_n + c_{x_i} r_{x_i} + c_p r_p + c_a r_a + c_m r_m = 0 \quad (34)$$

$$b_s r_s + b_n r_n + b_o r_o + b_{x_i} r_{x_i} + b_p r_p + b_l r_l + b_a r_a + b_c r_c + b_w r_w = 0 \quad (35)$$

$$a_s r_s + a_n r_n + a_{x_i} r_{x_i} + a_p r_p + a_l r_l + a_a r_a + a_m r_m + a_w r_w = 0 \quad (36)$$

where  $r_o$ ,  $r_b$ ,  $r_a$ ,  $r_c$ ,  $r_w$  are the production rates of oxygen, lactate, lumped amino acid, carbon dioxide, and water, respectively ((C-)mol.m<sup>-3</sup>.s<sup>-1</sup>). Since  $r_w$ ,  $r_{x_i}$ ,  $r_p$  and  $r_m$  are known, the production rate of the lumped amino acid,  $r_a$ , may be calculated directly from the nitrogen balance [Eq. (36)].

The fifth equation is the equation from Glacken et al.<sup>16</sup> describing the production of ATP, based on glycolysis and the citric-acid cycle. For every oxygen atom consumed about three ATP molecules are formed in the oxidative phosphorylation. Furthermore, the formation of one lactate molecule from glucose results in the production of one ATP. Because lactate formed from glutamine does not result in the production of ATP, the amount of lactate coming from glucose has to be known in order to calculate the ATP production. The required ATP production rate,  $r_e$ , may thus be described by:

$$r_e = -b_o p_o r_o + p_l X_{lc} r_l \quad (37)$$

where  $p_o$  is the amount of ATP formed per oxygen atom consumed (=3 mol.mol<sup>-1</sup>),  $b_o$  the amount of oxygen atoms in one oxygen molecule (=2),  $p_l$  is the amount of ATP formed per C-mol of lactate produced from glucose (=1/3 mol.C-mol<sup>-1</sup>), and  $X_{lc}$  is the fraction of lactate coming from glucose.

In combination with the three remaining balance equations for carbon, hydrogen, and oxygen, four equations and four unknown conversion rates are left. By elimination the following equations are obtained:

$$r_l = -\frac{p_o}{\gamma_p p_o + p_l X_{lc}} (\gamma_s r_s + \gamma_n r_n + \gamma_{x_i} r_{x_i} + \gamma_p r_p + \gamma_a r_a - \frac{a_m b_w}{a_w} r_m - \frac{r_e}{p_o}) \quad (38)$$

$$r_o = -\frac{p_l X_{lc}}{\gamma_p p_o b_o + p_l X_{lc} b_o} (\gamma_s r_s + \gamma_n r_n + \gamma_{x_i} r_{x_i} + \gamma_p r_p + \gamma_a r_a - \frac{a_m b_w}{a_w} r_m + \frac{\gamma_l}{p_l X_{lc}} r_e) \quad (39)$$

$$r_c = -(r_s + r_n + r_{x_i} + r_p + r_l + r_a) \quad (40)$$

$$r_w = -\frac{1}{\alpha_w}(a_s r_s + a_n r_n + a_x r_x + a_p r_p + a_l r_l + a_a r_a + a_m r_m) \quad (41)$$

with  $\gamma_i$  defined as:

$$\gamma_i = b_i - b_c - \frac{a_i b_w}{\alpha_w} \quad i = s, n, x, p, l, a \quad (42)$$

The conversion part of the macroscopic balance is now completely solved.

### Transport

With respect to the transport of compounds in the reactor a distinction can be made between transport by the entering and exiting medium flow, and transport between the liquid and gas phase. The volumetric transport rate of compound  $i$  as a result of the medium flow,  $\Phi_i$  ((C-) mol.m<sup>-3</sup>.s<sup>-1</sup>), can be described by:

$$\Phi_i = \frac{\phi_v^i C_i^i - \phi_v^e C_i^e}{V} \quad (43)$$

where  $C_i^i$ ,  $C_i^e$  are the entering and exiting concentrations of compound  $i$  ((C-)mol.m<sup>-3</sup>), respectively,  $\phi_v^i$ ,  $\phi_v^e$  the entering and exiting medium flow rates (m<sup>3</sup>.s<sup>-1</sup>), respectively, and  $V$  is the culture volume (m<sup>3</sup>). In an ideally mixed reactor the exiting concentration  $C_i^e$  is equal to the concentration in the reactor  $C_i$ . The volumetric transport rate of compound  $i$  between the liquid and the gas phase,  $\psi_i$  ((C-)mol.m<sup>-3</sup>.s<sup>-1</sup>), can be described by:

$$\psi_i = k_i A (C_i^* - C_i) \quad (44)$$

where  $k_i$  is the specific transport coefficient (m.s<sup>-1</sup>),  $C_i^*$  is the equilibrium concentration of compound  $i$  in the medium ((C-)mol.m<sup>-3</sup>), and  $A$  is the specific gas-liquid interfacial area (m<sup>2</sup>.m<sup>-3</sup>).

### Steady-state solution

In a steady state the conversion rates must equal the transport rates according to Equation (19). The steady-state concentrations for glucose, lactate, total biomass, lumped amino acid and water may be calculated from the following equation:

$$\frac{dC_i}{dt} = D(C_i^i - C_i) + r_i = 0 \quad i = s, l, x, p, a, w \quad (45)$$

To obtain the steady-state concentration of glutamine an extra rate term has to be added to the balance equation representing the spontaneous decay of glutamine into pyrrolidone carboxylic acid and ammonia following first-order kinetics:

$$\frac{dC_n}{dt} = D(C_n^i - C_n) + r_n - k_{dn} C_n = 0 \quad (46)$$

with  $k_{dn}$  being the first-order rate constant ( $s^{-1}$ ). Since out of each C-mol of glutamine decayed 1/5 mol of ammonia is formed, this has also to be taken into account when calculating the steady-state ammonia concentration:

$$\frac{dC_m}{dt} = D(C_m^i - C_m) + r_m + \frac{1}{5} k_{dn} C_n = 0 \quad (47)$$

Furthermore, the product may also be degraded and thus the steady-state product concentration is calculated from:

$$\frac{dC_p}{dt} = D(C_p^i - C_p) + r_p - k_{dp} C_p = 0 \quad (48)$$

where  $k_{dp}$  is the first-order degradation constant ( $s^{-1}$ ). For the two gaseous compounds the transport to and from the gas phase has to be accounted for. The balance equations thus become:

$$\frac{dC_i}{dt} = D(C_i^i - C_i) + k_i A(C_i^* - C_i) + r_i = 0 \quad i = o, c \quad (49)$$

With the conversion rates and the concentrations of the different compounds in the incoming medium flow known, the steady-state concentrations of the compounds may now be calculated from Equation (45) to (49). On the basis of these concentrations a specific growth-rate constant may be calculated based upon Monod kinetics:

$$\mu_{Mo} = \mu_m \frac{C_s}{(K_{ss} + C_s)} \frac{C_n}{(K_{sn} + C_n)} \frac{1}{1 + \left(\frac{C_m}{K_{im}}\right)^2} \frac{1}{1 + \frac{C_l}{K_{il}}} \quad (50)$$

where  $\mu_{Mo}$  is the Monod-based specific growth-rate constant ( $s^{-1}$ ),  $\mu_m$  is the maximum specific growth-rate constant ( $s^{-1}$ ),  $C_s$ ,  $C_n$ ,  $C_b$ ,  $C_m$  are the concentrations of glucose, glutamine, lactate and ammonia (C-mol.m<sup>-3</sup>), respectively,  $K_{ss}$ ,  $K_{sn}$  are the Monod constants for glucose and glutamine (C-mol.m<sup>-3</sup>), respectively, and  $K_{ip}$ ,  $K_{im}$  are the inhibition constants for lactate and ammonia



((C)-mol.m<sup>-3</sup>), respectively. This equation is the combined result of the equations given by Glacken et al.<sup>17</sup> and Miller et al.<sup>28</sup> for the specific growth rate.

In case of a steady state the Monod-based growth-rate constant must be equal to the growth-rate constant,  $\mu$ , as calculated in the cell-cycle part. From this condition the last unknown term being the viable-cell concentration,  $C_{Xv}^{cell}$ , can be calculated. At a given dilution rate  $D$  the growth-rate constant,  $\mu$ , the death-rate constant,  $\mu_d$ , the average biomass contents per cell,  $CM_b$ , the transition rate from phase C to phase O,  $\lambda_{mC/O}$ , and the fraction of apoptotic cells,  $F_O$ , are derived [Eqs. (4)-(18)]. At an arbitrarily chosen viable-cell concentration,  $C_{Xv}^{cell}$ , the conversion rates and the steady-state concentrations may be calculated for all compounds [Eqs. (21)-(49)]. Since the Monod-based growth-rate constant,  $\mu_{Mo}$  [Eq. (50)], should equal the cell-cycle-based growth-rate constant,  $\mu$  [Eq. (4)], the viable-cell concentration must be increased or decreased until the conversion rates and steady-state concentrations make the Monod-based growth-rate constant equal to the cell-cycle-based growth-rate constant.

## RESULTS

In order to check the validity of the model, simulations were done for a continuous culture executed by Miller et al.<sup>28</sup>. Besides presenting data for a large number of variables and for a wide range of steady states, their data are also used by others for testing models<sup>10,23,44</sup>. Furthermore, they show that their data are comparable to steady-state data obtained by others.

### Continuous culture

In Figure 3 the viable-cell number, viability, and glucose concentration are shown as a function of time. Of every two original datum points only one is shown. The culture is maintained at each dilution rate for about 5 residence times. Only at the lowest dilution rate of 0.013 h<sup>-1</sup> this was three residence times.

As can be seen in Figure 3, it is questionable if a real steady state is actually reached for each dilution rate. At  $D=0.017$  h<sup>-1</sup> a change of pH disturbed the steady state, causing especially large fluctuations in the viability. At the lowest dilution rate of 0.013 h<sup>-1</sup> the viability and the glucose concentration are still decreasing as the culture is stopped and a steady state seems not to be reached. In general, however, the concentrations of the different compounds seem to approach their steady-state values.

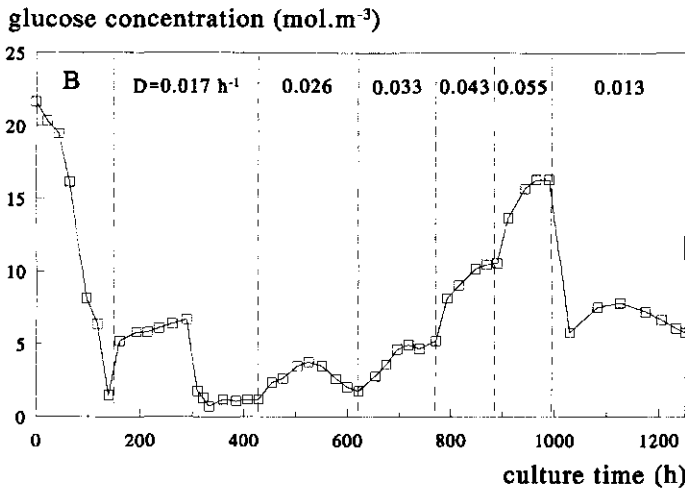
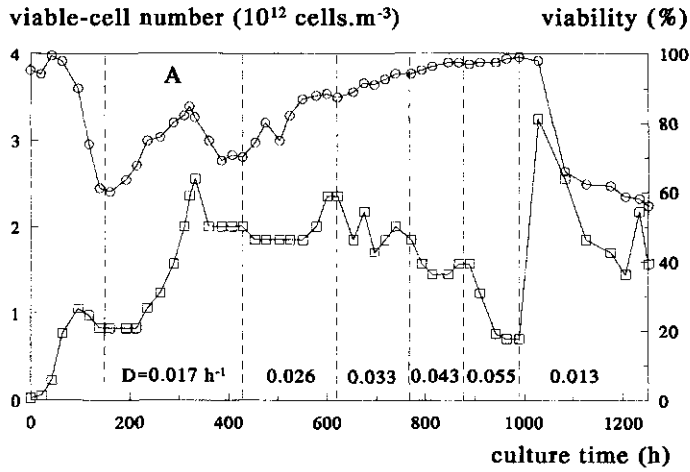


Figure 3. Data of Miller et al. as a function of culture time. (One out of every two points is shown.) A: ( $\square$ ) viable-cell number, ( $\circ$ ) viability. B: ( $\square$ ) glucose concentration.

**Table III.** Average literature values with references and the two parameter sets used for model calculations. The construction of set A and B is described in the text. In set A the parameter values which could be deduced from the data of Miller et al. are used except for the Monod constants. In set B also the Monod constants as calculated by Miller et al. are used. In case no specific values are given in the table, literature values were used.

Parameter	literature value	Set A.	Set B.	Units	Reference
$\lambda_{dO}, \lambda_{dO}$	$6.5 \cdot 10^{-7}$	$3.0 \cdot 10^{-7}$	$3.0 \cdot 10^{-7}$	$s^{-1}$	23, 31, 35
$t_O$	86400			s	33
$t_B$	44000	39600	39600	s	1
$t_{cr}$	59040	43200	43200	s	23
$t_m$	3600			s	1
$V_A$	$1.1 \cdot 10^{15}$			$m^3$	9, 12, 14, 15, 38, 39
$V_0$	$5.4 \cdot 10^{16}$			$m^3$	9, 12, 31, 38
$\rho_{cell}$	$1.95 \cdot 10^5$			$g \cdot m^{-3}$	12
$ash_X$	0.05				36
$Y_{sm}$	2.1	1.8	1.8	C-mol.C-mol <sup>-1</sup>	8, 11, 15, 16, 24, 28-31, 37, 47
$Y_{ss}$	0.47	0.47	0.47	C-mol.C-mol <sup>-1</sup>	8, 14, 15, 24, 28-31, 35, 37, 47
$Y_{se}$	0.78			C-mol.mol <sup>-1</sup>	30, 31
$m_n$	$2.64 \cdot 10^{-6}$			C-mol.C-mol <sup>-1</sup> .s <sup>-1</sup>	20
$m_s$	$2.67 \cdot 10^{-6}$	$15 \cdot 10^{-6}$	$15 \cdot 10^{-6}$	C-mol.C-mol <sup>-1</sup> .s <sup>-1</sup>	8, 28, 35
$m_e$	$1.06 \cdot 10^{-5}$			mol.C-mol <sup>-1</sup> .s <sup>-1</sup>	30
$Y_{nm}$	0.15	0.10	0.10	mol.C-mol <sup>-1</sup>	8, 13-15, 16, 19, 20, 28-31, 37, 47
$q_p$	$9.14 \cdot 10^{-7}$	$5 \cdot 10^{-7}$	$5 \cdot 10^{-7}$	C-mol.C-mol <sup>-1</sup> .s <sup>-1</sup>	16, 19, 29, 28, 35, 37, 46
$X_{lc}$	0.95				17, 31
$k_{db}$	$1.0 \cdot 10^{-6}$			$s^{-1}$	16, 24, 29, 31, 47
$k_{dp}$	0			$s^{-1}$	
$\mu_m$	$1.77 \cdot 10^{-5}$	$1.75 \cdot 10^{-5}$	$1.75 \cdot 10^{-5}$	$s^{-1}$	8, 13-15, 16, 20, 24, 28-31, 37, 47
$k_{sm}$	2.04	1.4	0.75	C-mol.m <sup>-3</sup>	8, 16, 28, 47
$k_{ss}$	0.41		0.90	C-mol.m <sup>-3</sup>	14, 15, 28
$k_{im}$	7.81		20	C-mol.m <sup>-3</sup>	8, 16, 28
$k_{ij}$	258		420	C-mol.m <sup>-3</sup>	8, 16, 28, 47

### Parameter values

The parameters necessary for the model are obtained from a number of publications<sup>3,8-17,19-25,28-33,35,37-39,44-47</sup>. If more than one value was found for a particular parameter, the values were averaged. However, values showing large deviations from the average value were

not taken into account. In this way a general parameter set was constructed containing average literature values, which are shown in Table III. For a number of parameters the values are given by Miller et al. themselves or may be easily deduced from their data using equations and assumptions from the model. Thus, these values are obtained by fitting separate model equations to the data and may therefore be regarded as optimal with respect to the model and the data set. Therefore, they are to be preferred above the average literature values for the model calculations. However, due to the limited amount of datum points, they may at the same time be quite unreliable.

The model parameters  $\mu_m$ ,  $\lambda_{dc}$ ,  $t_{cr}$ ,  $t_B$ , and  $Y_{mm}$  can be estimated quite easily. The maximum specific growth rate is given by Miller et al., who have measured it in continuous and batch cultures. From the maximum specific growth rate the duration of phase B can be calculated. Next the critical duration of phase A,  $t_{cr}$ , may be calculated from the critical specific growth rate, which is the specific growth rate where the viability starts decreasing. The death-rate constant for the cycling cells,  $\lambda_{dc}$ , is equal to the death-rate constant of the viable cells at high specific growth rates [Eq. (7)], which is calculated from the dilution rate and the corresponding measured steady-state concentrations of the viable and dead cells ( $\mu_d = DC_{Xd}^{cell}/C_{Xv}^{cell}$ ). The yield of ammonia on glutamine is obtained from their measured steady-state concentrations.

The parameters  $\lambda_{d0}$  and  $t_0$  cannot be determined independently from Equation (7). Thus,  $\lambda_{d0}$  is assumed to be equal to  $\lambda_{dc}$  (assumption 7) and for  $t_0$  a literature value is used<sup>33</sup>. In addition, the parameter values for  $V_A$ ,  $V_{Ov}$ ,  $t_m$ ,  $\rho_{cell}$ ,  $ash_X$ ,  $X_{lc}$ ,  $Y_{xe}$ ,  $m_v$ ,  $k_{dv}$ ,  $k_{dp}$ , and the composition of biomass, lumped amino acid and product cannot be identified, since no independent data are given with respect to these parameters. Therefore, average literature values are used in order to demonstrate the general applicability of the model.

The average biomass content of the cycling cells,  $CM_C$ , may now be calculated [Eq. (10)] and the yield and maintenance parameters in Equation (28) and (29) may next be obtained from a plot of the specific glucose and glutamine consumption rates versus the specific growth rate for specific growth rates higher than the critical specific growth rate. As long as the specific growth rate is higher than the critical specific growth rate, cells do not enter the apoptotic phase and no biomass decay occurs. Consequently, the observed biomass formation rate equals the true biomass formation rate and the specific consumption rates of glutamine and glucose ( $C\text{-mol}\cdot\text{cell}^{-1}\cdot\text{s}^{-1}$ ) become proportional to the specific growth rate according to Equation (28) and (29). Fitting a line through these datum points results in the yield and maintenance coefficients given in Table III. The obtained values are close to the average literature values (Table III). Only the maintenance coefficient for glucose is substantially larger than its average literature value.

The large value is considered the correct one for the studied cells and is used in the model calculations. The maintenance coefficient of glutamine is near zero and thus difficult to determine. For this reason, the average literature value is used in the model calculations.

Miller et al. found that the monoclonal-antibody production rate was negatively growth-rate associated at the lowest dilution rates, which cannot be described by Equation (32). For the moment it is assumed here that the antibody production rate is non-growth-rate associated ( $Y_{px}=0$ ) and for the productivity,  $q_p$ , an average of the minimum and maximum productivities found by Miller et al. is used.

Miller et al. have calculated values (Table III) for the 5 different parameters of the modified Monod equation [Eq. (50)] by fitting the equation for the 5 parameters to the experimental specific growth rate found at the different dilution rates. Consequently, considering the deviations of the points from the regression line and the fact that they use only 6 datum points to fit five parameters, the obtained values are not very reliable.

**Table IV. Culture volume and concentrations in the incoming medium flow.**

Parameter	Miller et al.	Units
Volume	$0.6 \cdot 10^{-3}$	$m^3$
D	$0 - 1.54 \cdot 10^{-5}$	$s^{-1}$
$C_n^i$ (gln)	24	$C\text{-mol}\cdot m^{-3}$
$C_s^i$ (glc)	132	$C\text{-mol}\cdot m^{-3}$
$C_o^i$ (O)	0.256	$mol\cdot m^{-3}$
$C_l^i$ (lac)	0	$C\text{-mol}\cdot m^{-3}$
$C_a^i$ (az)	14	$C\text{-mol}\cdot m^{-3}$
$C_p^i$ (MoAb)	0	$C\text{-mol}\cdot m^{-3}$
$C_m^i$ (amm)	0	$mol\cdot m^{-3}$
$C_c^i$ (CO <sub>2</sub> )	0	$mol\cdot m^{-3}$
$C_w^i$ (H <sub>2</sub> O)	55.6	$mol\cdot m^{-3}$

Two different data sets (Table III) were constructed now from the average literature data. In set A parameter values which could be reliably deduced from the data of Miller et al., being  $\mu_m$ ,  $\lambda_{dO}$ ,  $\lambda_{dO}$ ,  $t_{cr}$ ,  $t_B$ ,  $m_s$ ,  $Y_{x/s}$ ,  $Y_{xp}$ ,  $Y_{np}$ ,  $q_p$  are used instead of average literature values. Except for the maintenance coefficient of glucose, the values of the parameters as deduced from the data of Miller et al. are close to the average literature values. Using these values, model calculations resulted in wash out at the highest dilution rate. Thus, for the Monod constant of glutamine the average of the value of Miller et al. ( $0.15 \text{ mol}\cdot m^{-3}$ ) and the literature value ( $0.4 \text{ mol}\cdot m^{-3}$ ) is used.

In set B all the parameter values which could be deduced from the data of Miller et al. are used. Thus, the difference between set A and set B is formed by the parameters of the modified Monod equation [Eq. (50)],  $K_{sp}$ ,  $K_{sw}$ ,  $K_{\beta}$  and  $K_{im}$ , and thus the effect of changing these parameters on the model outcomes can be studied. The experimental data (symbols) and simulation results (lines) for both parameter sets are shown in Figures 4 to 8. The concentrations of the different compounds in the incoming medium flow, which are needed for the calculations, are given in Table IV.

### Simulation results

In general the trends are predicted very good for both parameter sets. However, the exact values show some deviations from the experimental data. In general deviations may be caused by both an incorrect model and incorrect values for the input parameters. Especially input parameters, which cannot be reliably determined from the data set itself are most likely to be wrong. Model predictions using parameter set A are somewhat better than those using set B, indicating that the parameters of the modified Monod equation as used in this set result in a better description of the results by our model than the values reported by Miller et al..

#### *Cell-cycle part*

In Figure 4 the specific growth rate and the viability are plotted as a function of the dilution rate. At any particular dilution rate the specific death rate, viability, specific growth rate, and the average cell volume are fixed totally by the cell-cycle parameters  $\lambda_{dC}$ ,  $\lambda_{dO}$ ,  $t_{cp}$ ,  $t_B$ , and  $t_O$ . Since these parameters are the same in both parameter sets, there is no difference in the viability and specific growth rate between the two simulation sets. The critical specific growth rate determines the point where cells start becoming apoptotic and where the viability starts decreasing. As can be seen in Figure 4, a value of  $0.030 \text{ h}^{-1}$  agrees well with the experimental data. Remarkably, this is about  $0.5\mu_m$ , which agrees with the finding that cells become apoptotic when the protein synthesis rate is reduced to 50% of the maximum value<sup>33</sup>. Above the critical value, the specific growth rate and viability are determined by the dilution rate  $D$  and the specific death rate of the cells in phase C,  $\lambda_{dC}$ . A higher value of  $\lambda_{dC}$  will result in a lower viability and a higher specific growth rate. Below the critical value, the specific growth rate and viability are determined mainly by the dilution rate  $D$  and the duration of phase O. A shorter duration of phase O results in a higher specific death rate and thus in a lower viability and a higher specific growth rate. As can be seen in Figure 4 the viability and specific growth rate are predicted very well by the model. Thus, a duration of 24 hours for the apoptotic phase agrees well with the data of Miller et al.

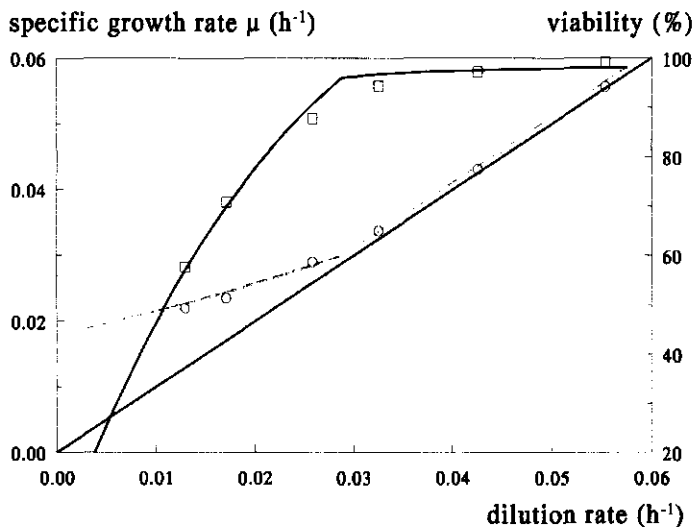


Figure 4. Simulation results (lines) and experimental data (symbols) as a function of dilution rate. ( $\square$ , —) viability, ( $\circ$ , ---) specific growth rate. The straight line represents  $\mu=D$ .

#### *Cell and metabolite concentrations*

At a certain specific growth rate the steady-state concentrations of glucose, glutamine, lactate and ammonia are determined mainly by the parameters of the modified Monod equation and the relative rates with which these compounds are consumed or produced. Next, the biomass concentration is dependent on the steady-state concentrations of the limiting compound and on the yield and maintenance parameters for this compound. If, for example, glutamine is the limiting substrate, the Monod-based growth-rate constant is mainly determined by the glutamine concentration, the maximum specific growth rate, and the Monod constant for this compound. A lower Monod constant for glutamine leads to a lower steady-state concentration of this substrate and, consequently, since more glutamine is converted to biomass, to a higher biomass concentration. In addition, also a higher yield of biomass on glutamine and a lower maintenance coefficient for glutamine will lead to an increase in biomass concentration. The concentrations of non-limiting substrates and of non-inhibiting products are determined by the relative rates with which they are produced and consumed as compared to the limiting substrates and inhibiting products.

Minimal predicted glucose concentrations of about  $5 \text{ mol.m}^{-3}$  are considerably higher than the Monod constant for glucose for both parameter sets ( $0.07$  and  $0.15 \text{ mol.m}^{-3}$ ). The maximum

predicted lactate concentration of about  $30 \text{ mol.m}^{-3}$  is below the inhibition constant of 86 and  $120 \text{ mol.m}^{-3}$ . The maximum predicted ammonia concentration of about  $2.2 \text{ mol.m}^{-3}$  is also well below the inhibition constant of 7.58 and  $20 \text{ mol.m}^{-3}$ . The minimal predicted glutamine concentration of about 0.1 to  $0.4 \text{ mol.m}^{-3}$  is, however, in the same range as the Monod constant being 0.28 and  $0.15 \text{ mol.m}^{-3}$ . Thus, in the model calculations glutamine is the main limiting substrate for both simulations. This means that the differences between simulation A and B are mainly due to the change in the Monod constant for glutamine, while the changes in the Monod constant for glucose and in the inhibition constants for lactate and ammonia contribute only little to these differences.

### *Cell concentrations*

The total biomass concentration expressed in  $\text{C-mol.m}^{-3}$  is dependent upon the yield of biomass on the limiting substrate, the maintenance requirements with respect to the limiting substrate, and the steady-state concentration of this limiting substrate. Thus, at a fixed steady-state concentration of the limiting substrate, a lower yield of biomass on this substrate will result in lower steady-state biomass concentrations. A higher maintenance coefficient will lead to more substrate being used for maintenance and thus less substrate is available for biomass formation and, consequently, the steady-state biomass concentration decreases. Since the specific death rate is independent of the yield and maintenance parameters, the ratio between viable and dead biomass stays the same. The total-, viable- and dead-cell numbers depend upon the total and viable biomass concentration and the amount of biomass per cell. Lower amounts of biomass per cell lead to higher cell concentrations.

Except for the continuous increase in the total-cell concentration with decreasing dilution rate at the three lowest dilution rates, the trends of the steady-state viable- and total-cell numbers are predicted correctly by the model for both parameter sets (Fig. 5). At the two highest dilution rates deviations of the biomass concentration from experimental data may be explained from the predicted glutamine concentration (Fig. 6). If the glutamine concentration is predicted too high this leads to less glutamine being converted to biomass and, consequently, to too low biomass concentrations (set A, highest dilution rate). If the glutamine concentration is predicted too low this leads to more glutamine being converted to biomass and, consequently, to too high biomass concentrations (set B, second highest dilution rate). Thus, if the glutamine concentration is predicted correctly so is the biomass concentration, indicating that the yield and maintenance coefficient for glutamine are correct. At the three lowest dilution rates the viable- and total-cell concentration are predicted too low for both parameter sets even if the glutamine concentration



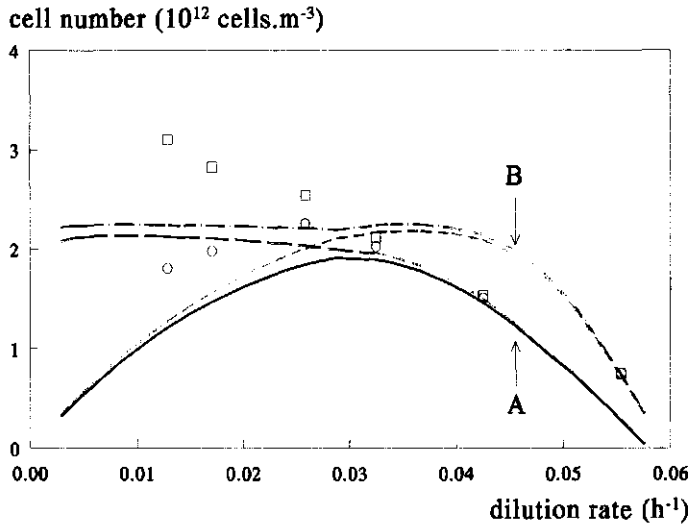


**Figure 5.** Simulation results (lines) and experimental data (symbols) as a function of dilution rate. (O), (Set A : —), (Set B : ---) viable cells; (□) (Set A : - - -), (Set B : - - -) total cells.

is predicted correctly. This may be caused by the biomass yield on glutamine becoming higher or the maintenance coefficient becoming smaller at low dilution rates. More likely, however, the amount of C-mols per cell becomes smaller at lower dilution rates. In other words, the volume of the cells after cell division, which is assumed to be constant by the model, decreases with the specific growth rate. Miller et al. also suggest that the specific cell mass decreases with decreasing dilution rates.

#### *Glutamine and ammonia*

In Figure 6 it can be seen that on average the glutamine concentration is best predicted by parameter set A. In addition, it can be seen that a lower Monod constant for glutamine (set B) results in lower glutamine concentrations and a steeper profile as expected. The ammonia concentrations are predicted too low for set A, which is probably caused by a too low yield of ammonia on glutamine. In case of set B the glutamine concentration is predicted too low. Consequently, more glutamine is consumed and more ammonia is formed, resulting in correct predictions for the ammonia concentration. The maximum occurring in the ammonia concentration is not predicted by the model for both parameter sets. As stated, at the lowest dilution rate a steady state is probably not reached and, thus, the actual steady-state ammonia concentration might have been higher than the measured ammonia concentration. This would

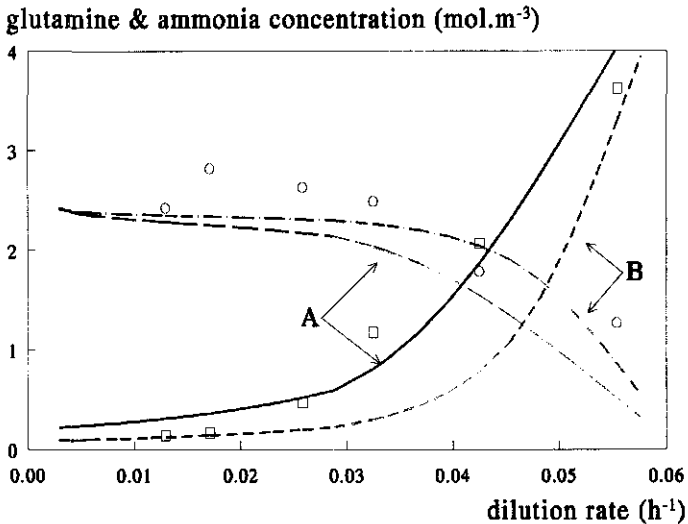
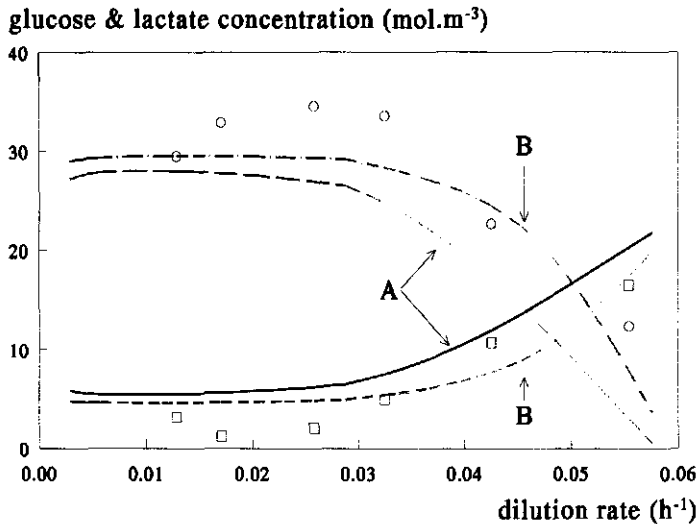


Figure 6. Simulation results (lines) and experimental data (symbols) as a function of dilution rate. ( $\square$ ), (Set A: —), (Set B : ---) glutamine concentration; (O) (Set A : ---), (Set B : - - -) ammonia concentration.

then result in a more or less constant ammonia concentration at lower dilution rates, which agrees with the predicted trend by the model. However, ammonia is a waste product of the nitrogen metabolism. Since nitrogen metabolism comprises many other compounds besides ammonia and glutamine, the assumption of a constant yield of ammonia on glutamine is probably too simple, leading to wrong model predictions. This is supported by the different values found by Miller et al.<sup>28</sup> at the different dilution rates for the ammonia yield ranging from 0.08-0.15 mol.C-mol<sup>-1</sup>.

#### Glucose and lactate

As stated, in the model calculations the culture is clearly not glucose limited and the Monod constant for glucose may be expected to have only little influence on the steady-state glucose concentration. Thus, the steady-state glucose concentration is dependent on the volumetric consumption rate of glucose, which in turn is determined by the yield and maintenance coefficient for glucose and by the steady-state concentration of biomass. This can be clearly seen in Figure 7, where a higher Monod constant for glucose (set B) is not accompanied by higher glucose concentrations, as would be expected in the case glucose had been limiting, but by lower glucose concentrations. Since the yield and maintenance coefficient do not change, this lower glucose concentration is a consequence of the higher biomass concentration in situation B, leading to a higher volumetric glucose consumption rate. For both parameter sets the glucose



**Figure 7.** Simulation results (lines) and experimental data (symbols) as a function of dilution rate. ( $\square$ ), (Set A : —), (Set B : - -) glucose concentration; ( $\circ$ ) (Set A : - - -), (Set B : - - -) lactate concentration.

concentrations are predicted a little too high and the lactate concentrations a little too low. This might be caused by wrong values for the yield and maintenance coefficient for glucose. A lower biomass yield on glucose and a higher maintenance coefficient will result in lower glucose concentrations and higher lactate concentrations. Additionally, the maintenance model for the consumption of glucose [Eq. (28)] may be incorrect, as is also suggested by Miller et al. themselves. Last, in the model calculations glucose is not rate limiting, whereas in the actual culture at low dilution rates the glucose concentrations become so low that it may be expected to be limiting. Thus, the actual culture might shift from being mainly glucose limited to being glutamine limited and vice-versa, which could be the explanation for the unpredicted minima and maxima seen in the experimental glucose and lactate concentrations. However, as mentioned, at a dilution rate of  $0.013 \text{ h}^{-1}$  it is questionable if a real steady state is reached and the glucose concentration is still decreasing as the culture is stopped. Thus, the actual steady-state concentration probably is lower and the observed minimum and maximum in the glucose and lactate concentration, respectively, would be at least less pronounced.

### Product

The product concentration is not described very good by the model especially at the two lowest dilution rates, where it is predicted too low (Fig. 8). This may be partly explained by the too low predictions of the viable-cell concentration at the two lowest dilution rates. In addition, Equation (32) does not describe the negative growth-rate-associated production as found by Miller et al.<sup>28</sup>. Of the other presented model results only the lactate concentrations may be influenced by the wrong predictions of the product concentration. However, in a short sensitivity study this effect appeared to be negligible small. At present, work is proceeding on constructing a model for negative growth-rate-associated product formation.

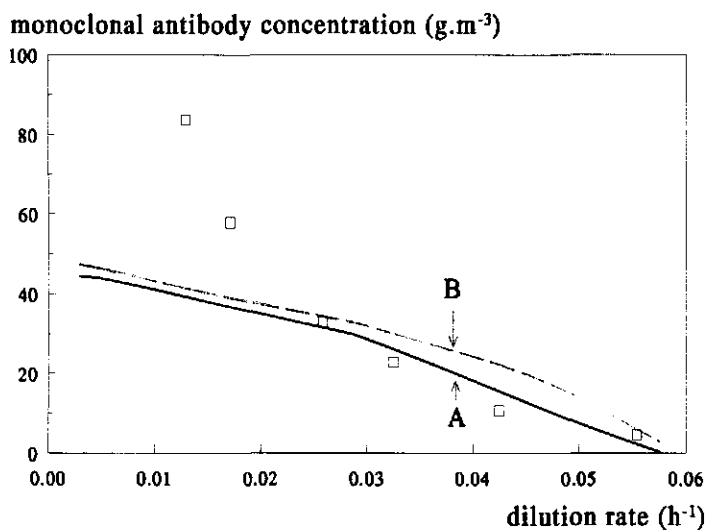


**Figure 8.** Simulation results (lines) and experimental data (symbols) as a function of dilution rate. (□), (Set A: —), (Set B: ---) product (IgG) concentration.

### CONCLUSIONS

The model presented in this work is a combination of a cell-cycle model and a metabolic model. It is able to predict qualitatively the behaviour of animal cells in continuous culture under steady-state conditions. Quantitative predictions, however, are less accurate for some of the measured variables. This is at least in part due to the use of average literature values for a number of parameters.

The specific growth rate below which cells start to show apoptosis is about half the maximum specific growth rate.

Based on the assumption that the volume of a newborn cell does not depend on the dilution rate, the total-cell number is predicted too low at low dilution rates. The constant yield of ammonia on glutamine is probably incorrect and may be object for improvement. The model may also be improved with respect to product formation.

## APPENDIX A

### Death-rate constant [Eq. (7)]

Cell death occurs during the progression through phases A, B and O and at the end of phase O, where cells have an age  $t_O$ . The cell death during the progression through phase O may be obtained by multiplying the first-order death-rate constant of phase-O cells,  $\lambda_{dO}$ , with the total amount of cells in phase O:

$$\text{Death rate during state O} = \lambda_{dO} F_O C_{x_v}^{cell} \quad (\text{A1})$$

The cell-death rate at the end of phase O is equal to the number of cells at age  $t_O$ , which may be obtained from the age distribution of phase-O cells [Table I, Eq. (T4)]. The number of cells at age zero,  $n_O(0)$ , may be expressed as a function of the total number of cells in phase O, by re-arranging Equation (T5) in Table I. Substitution into Equation (T4) and re-arranging then results in the next equation for the cell-death rate at the end of phase O:

$$\text{Death rate at age } t_O = \frac{D + \lambda_{dO}}{e^{(D + \lambda_{dO})t_O} - 1} F_O C_{x_v}^{cell} \quad (\text{A2})$$

The first-order death-rate constant may be easily obtained by adding the rate with which cells die in phase C,  $\lambda_{dC}(1-F_O)C_{x_v}^{cell}$ , to that with which cells die in phase O [Eqs. (A1), (A2)]:

$$\mu_d C_{x_v}^{cell} = \lambda_{dC}(1-F_O)C_{x_v}^{cell} + \left( \lambda_{dO} + \frac{D + \lambda_{dO}}{e^{(D + \lambda_{dO})t_O} - 1} \right) F_O C_{x_v}^{cell} \quad (\text{A3})$$

Dividing by  $C_{x_v}^{cell}$  results in Equation (7).

### Dead biomass formation rate [Eq. (25)]

The amount of biomass dying in phase C may be obtained by multiplying the amount of cells that die in this phase with the average amount of C-moles per phase C cell,  $CM_C$  [Eq. (10)]. Next, multiplying the right side of Equation A1 with the average amount of C-moles per phase-O

cell,  $CM_O$  [Eq. (15)], gives the amount of biomass dying during the progression through phase O. The amount of biomass dying at the end of phase O at age  $t_O$  can be calculated in a similar way by multiplying the right side of Equation A2 with the amount of C-moles per phase-O cell at age  $t_O$ ,  $CM_{Oe}$  [Eq. (16)]. Summating these terms then results in the dead-biomass formation rate:

$$r_{x_d} = \left[ (\lambda_{do} CM_O + \frac{D + \lambda_{do}}{e^{(D + \lambda_{do})t_O} - 1} CM_{Oe}) F_O + \lambda_{dc} CM_C (1 - F_O) \right] C_{x_v}^{cell} \quad (\text{A4})$$

This equation is equal to Equation (25).

## ACKNOWLEDGEMENTS

The authors thank J.J. Meijer and B. Romein of the Delft University of Technology for kindly providing the elemental composition of biomass<sup>26</sup>.

## SYMBOLS

$a$	Cell age	(s)
$a_i$	Hydrogen content per C-mol of compound $i$	(-)
$A$	Specific gas-liquid interface area	( $\text{m}^2 \cdot \text{m}^{-3}$ )
$ash_x$	Ash content of the biomass	(-)
$b_i$	Oxygen content per C-mol of compound $i$	(-)
$c_i$	Nitrogen content per C-mol of compound $i$	(-)
$C_i$	Steady-state concentration of compound $i$ in C-moles	(C-mol. $\text{m}^{-3}$ )
$C_i^*$	Equilibrium concentration compound $i$ in medium	(C-mol. $\text{m}^{-3}$ )
$C_i^{cell}$	Concentration of compound $i$ in cell numbers	(cells. $\text{m}^{-3}$ )
$C_i^e$	Concentration compound $i$ in the exiting medium flow	(C-mol. $\text{m}^{-3}$ )
$C_i^i$	Concentration compound $i$ in the incoming medium flow	(C-mol. $\text{m}^{-3}$ )
$CM_O$	Average amount of C-moles per apoptotic, phase-O cell	(C-mol.cell <sup>-1</sup> )
$CM_{Oe}$	Average amount of C-moles per apoptotic cell at the end of phase O	(C-mol.cell <sup>-1</sup> )
$CM_c$	Average amount of C-moles per cycling cell	(C-mol.cell <sup>-1</sup> )
$CM_v$	Average amount of C-moles per viable cell	(C-mol.cell <sup>-1</sup> )
$D$	Dilution rate	( $\text{s}^{-1}$ )
$F_O$	Fraction of apoptotic, phase-O cells	(-)
$k_{db}$	First-order degradation constant for glutamine	( $\text{s}^{-1}$ )
$k_{dp}$	First-order degradation constant for product	( $\text{s}^{-1}$ )
$k_i$	Specific transport coefficient	( $\text{m} \cdot \text{s}^{-1}$ )
$K_{m_g}$	Monod constant for glucose	(C-mol. $\text{m}^{-3}$ )
$K_{m_s}$	Monod constant for glutamine	(C-mol. $\text{m}^{-3}$ )
$K_{im}$	Inhibition constant for ammonia	(mol. $\text{m}^{-3}$ )

Chapter 7

$K_{il}$	Inhibition constant for lactate	(C-mol.m <sup>-3</sup> )
$k_{vo}$	First-order rate constant for the decrease of cell volume	(s <sup>-1</sup> )
$k_{zo}$	First-order rate constant for biomass decay	(s <sup>-1</sup> )
$M_{cell}$	Mass of one C-mol of biomass	(g.C-mol <sup>-1</sup> )
$m_i$	Maintenance coefficient compound i	(C-mol.C-mol <sup>-1</sup> .s <sup>-1</sup> )
$n_i(a,t)$	Age density function of cells in phase i	(cells.m <sup>-3</sup> .s <sup>-1</sup> )
$n_i(a)$	Steady-state age density function of cells in phase i	(cells.m <sup>-3</sup> .s <sup>-1</sup> )
$N_i$	Total concentration of cells in phase i	(cells.m <sup>-3</sup> )
$p_l$	Amount of ATP formed per C-mol lactate produced	(mol.C-mol <sup>-1</sup> )
$p_o$	Amount of ATP formed per 0.5 mol O <sub>2</sub> consumed	(mol.mol <sup>-1</sup> )
$q_p$	Specific productivity	(C-mol.C-mol <sup>-1</sup> .s <sup>-1</sup> )
$r_{Xv}^{cell}$	Production rate of viable cells.	(cells.m <sup>-3</sup> .s <sup>-1</sup> )
$r_{Xd}^{cell}$	Production rate of dead cells.	(cells.m <sup>-3</sup> .s <sup>-1</sup> )
$r_{Xt}^{cell}$	Production rate of total cells.	(cells.m <sup>-3</sup> .s <sup>-1</sup> )
$r_{Xv}$	Production rate of viable biomass	(C-mol.m <sup>-3</sup> .s <sup>-1</sup> )
$r_{Xd}$	Production rate of dead biomass	(C-mol.m <sup>-3</sup> .s <sup>-1</sup> )
$r_{Xt}$	Production rate of total biomass	(C-mol.m <sup>-3</sup> .s <sup>-1</sup> )
$r_{Xtrue}$	True biomass production rate in C-moles	(C-mol.m <sup>-3</sup> .s <sup>-1</sup> )
$r_i$	Production rate of compound i in C-moles	(C-mol.m <sup>-3</sup> .s <sup>-1</sup> )
$t$	Time	(s)
$t_A$	Duration of phase A	(s)
$t_B$	Duration of phase B	(s)
$t_C$	Duration of the cell cycle	(s)
$t_{cr}$	Maximum critical duration of phase A	(s)
$t_m$	Duration of the mitosis	(s)
$t_O$	Duration of the apoptotic O phase	(s)
$V$	Volume of the culture	(m <sup>3</sup> )
$V_A$	Cell volume of newborn cells immediately after division	(m <sup>3</sup> .cell <sup>-1</sup> )
$V_c$	Average cell volume of the cycling cells	(m <sup>3</sup> .cell <sup>-1</sup> )
$V_o$	Average cell volume of the apoptotic phase-O cells	(m <sup>3</sup> .cell <sup>-1</sup> )
$V_{oe}$	Average cell volume of cells at the end of the apoptotic phase	(m <sup>3</sup> .cell <sup>-1</sup> )
$V_v$	Average cell volume of the viable cells	(m <sup>3</sup> .cell <sup>-1</sup> )
$X_{lc}$	Fraction of lactate coming from glucose	(-)
$Y_{ij}$	Yield of compound i on j	(C-mol.C-mol <sup>-1</sup> )
$\Upsilon_i$	Calculation factor of compound i	(-)
$\lambda_{do}$	Death-rate constant of cells progressing through phase O	(s <sup>-1</sup> )
$\lambda_{dC}$	Death-rate constant of the cycling cells	(s <sup>-1</sup> )
$\lambda_{mij}$	Migration rate of cells from phase i to phase j	(s <sup>-1</sup> )
$\lambda_{mCO}$	Migration rate of cells from phase C to phase O	(s <sup>-1</sup> )
$\phi_v^e$	Exiting medium flow rate	(m <sup>3</sup> .s <sup>-1</sup> )

## Chapter 7

$\Phi_v^i$	Incoming medium flow rate	( $\text{m}^3 \cdot \text{s}^{-1}$ )
$\Phi_i$	Volumetric transport rate of compound i by medium flow	( $\text{C} \cdot \text{mol} \cdot \text{m}^{-3} \cdot \text{s}^{-1}$ )
$\Psi_i$	Volumetric transport rate of compound i between gas and liquid	( $\text{C} \cdot \text{mol} \cdot \text{m}^{-3} \cdot \text{s}^{-1}$ )
$\mu$	Cell-cycle-based specific growth rate	( $\text{s}^{-1}$ )
$\mu_{cr}$	Critical specific growth rate	( $\text{s}^{-1}$ )
$\mu_d$	First-order death-rate constant	( $\text{s}^{-1}$ )
$\mu_m$	Maximum specific growth rate	( $\text{s}^{-1}$ )
$\mu_{Mo}$	Monod-based specific growth rate	( $\text{s}^{-1}$ )
$\rho_{cell}$	Density of the biomass	( $\text{g} \cdot \text{m}^{-3}$ )

### Compound subscripts

a	Lumped amino acid
c	Carbon dioxide
l	Lactate
m	Ammonia
n	Glutamine
o	Oxygen
p	Product
s	Glucose
w	Water
$x_v$	Viable biomass
$x_d$	Dead biomass
$x_t$	Total biomass

### REFERENCES

1. Alberts, B., Bray, D., Lewis, J., Raff, M., Roberts, K., Watson, J.D. 1983. *Molecular biology of the cell*. Garland Publishing, New York.
2. Al-Rubeai, M., Chalder, S., Bird, R., Emery, A.N. 1991. Cell cycle, cell size and mitochondrial activity of hybridoma cells during batch cultivation. *Cytotechnol.* **7**: 179-186.
3. Al-Rubeai, M., Emery, A.N., Chalder, S. 1991. Flow cytometric study of mammalian cells. *J. Biotechnol.* **19**: 67-82.
4. Barford, J.P., Phillips, J.P., Harbour C. 1992. Simulation of animal cell metabolism. *Cytotechnol.* **10**: 63-74.
5. Batt, B.C., Kompala, D.S. 1989. A structured kinetic modelling framework for the dynamics of hybridoma growth and monoclonal antibody production in continuous suspension cultures. *Biotechnol. Bioeng.* **34**: 515-531.
6. Beefink, H.H., Heijden, R.T.J.M. van der, Heijnen, J.J. 1990. Maintenance requirements: energy supply from simultaneous respiration and substrate consumption. *FEMS Microbiol. Ecol.* **73**: 203-210.
7. Bibila, T., Flickinger, M.C., 1991. A structured model for monoclonal antibody synthesis in exponentially growing and stationary phase hybridoma cells. *Biotechnol. Bioeng.* **37**: 210-226.



8. Bree, M.A., Dhurjati, P., Geoghegan Jr., R.F., Robnett, B. 1988. Kinetic modelling of hybridoma cell growth and immunoglobulin production in a large-scale suspension culture. *Biotechnol. Bioeng.* **32**: 1067-1072.
9. de la Broise, D., Noiseux, M., Lemieux, R., Massie, B. 1991. Long-term perfusion culture of hybridoma: A "grow or die" cell cycle system. *Biotechnol. Bioeng.* **38**: 781-787.
10. Cazzador, L., Mariani, L. 1993. Growth and production modelling in hybridoma continuous cultures. *Biotechnol. Bioeng.* **42**: 1322-1330.
11. Duval, D., Demangel, C., Munier-Jolain, K., Miossec, S., Geahel, I. 1991. Factors controlling cell proliferation and antibody production in mouse hybridoma cells: I. Influence of the amino acid supply. *Biotechnol. Bioeng.* **38**: 561-570.
12. Frame, K.K., Hu, W.-S. 1990. Cell volume measurement as an estimation of mammalian cell biomass. *Biotechnol. Bioeng.* **36**: 191-197.
13. Frame, K.K., Hu, W.-S. 1991. Comparison of growth kinetics of producing and nonproducing hybridoma cells in batch culture. *Enzyme Microb. Technol.* **13**: 690-696.
14. Frame, K.K., Hu, W.-S. 1991. Kinetic study of hybridoma cell growth in continuous culture: I. A model for non-producing cells. *Biotechnol. Bioeng.* **38**: 1020-1028.
15. Frame, K.K., Hu, W.-S. 1991. Kinetic study of hybridoma cell growth in continuous culture: II. Behaviour of producers and comparison to nonproducers. *Biotechnol. Bioeng.* **38**: 1020-1028.
16. Glacken, M.W., Fleishaker, R.J., Sinskey, A.J. 1986. Reduction of waste product excretion via nutrient control: Possible strategies for maximizing product and cell yields on serum in cultures of mammalian cells. *Biotechnol. Bioeng.* **28**: 1376-1389.
17. Glacken, M.W., Adema, E., Sinskey, A.J. 1988. Mathematical descriptions of hybridoma culture kinetics: Initial metabolic rates. *Biotechnol. Bioeng.* **32**: 491-506.
18. Golstein, P., Ojcius, D.M., Young, J.D.-E. 1991. Cell death mechanisms and the immune system. *Immunol. Rev.* **121**: 29-65.
19. Graf, H., Schügerl, K. 1991. Some aspects of hybridoma cell cultivation. *Appl. Microbiol. Biotechnol.* **35**: 165-175.
20. Hiller, G.W., Aeschlimann, A.D., Clark, D.S., Blanch, H.W. 1991. A kinetic analysis of hybridoma growth and metabolism in continuous suspension culture on serum-free medium. *Biotechnol. Bioeng.* **38**: 733-741.
21. Jenkins, H.A., Butler, M., Dickson, A.J. 1992. Characterization of glutamine metabolism in two related murine hybridomas. *J. Biotechnol.* **23**: 167-182.
22. Kromenaker, S.J., Srienc F. 1991. Cell-cycle dependent protein accumulation by producer and nonproducer murine hybridoma cell lines: A population analysis. *Biotechnol. Bioeng.* **38**: 665-677.
23. Linardos, T.I., Kalogerakis, N., Behie, L.A. 1992. Cell cycle model for growth rate and death rate in continuous suspension hybridoma cultures. *Biotechnol. Bioeng.* **40**: 359-368.
24. Ljunggren, J., Häggström, L. 1992. Glutamine limited fed-batch culture reduces the overflow metabolism of amino acids in myeloma cells. *Cytotechnol.* **8**: 45-56.
25. Martens, D.E., de Gooijer, C.D., van der Velden-de Groot, C.A.M., Beuvery, E.C., Tramper, J. 1993. Effect of dilution rate on Growth, Productivity, cell cycle and size, and shear sensitivity of a hybridoma cell in a continuous culture. *Biotechnol. Bioeng.* **41**: 429-439.

26. Meijer, J.J., van Dijken, J.P. 1995. Effects of glucose supply on myeloma growth and metabolism in chemostat culture. *J. Cell.Physiol.* **162**: 191-198.
27. Mercille, S., Massie, B. 1994. Induction of apoptosis in nutrient-deprived cultures of hybridoma and myeloma cells. *Biotechnol. Bioeng.* **44**: 1140-1154.
28. Miller, W.M., Blanch, H.W., Wilke C.R. 1988. A kinetic analysis of hybridoma growth and metabolism in batch and continuous suspension culture: Effect of nutrient concentration, dilution rate, and pH. *Biotechnol. Bioeng.* **32**: 947-965.
29. Miller, W.M., Wilke, C.R., Blanch H.W. 1988. Transient responses of hybridoma metabolism to changes in the oxygen supply rate in continuous culture. *Bioproc. Eng.* **3**: 103-111.
30. Miller, W.M., Wilke, C.R., Blanch H.W. 1989. The transient responses of hybridoma cells to nutrient additions in continuous culture: II Glutamine pulse and step changes. *Biotechnol. Bioeng.* **33**: 487-499.
31. Ozturk, S.S., Palsson, B.O. 1991. Growth, metabolic, and antibody production kinetics of hybridoma cell culture: 1. Analysis of data from controlled batch reactors. *Biotechnol. Prog.* **7**: 471-480.
32. Pardee, A.B. 1989. G1 events and regulation of cell proliferation. *Science.* **246**: 603-608.
33. Perreault, P., Lemieux, R. 1993. Essential role of optimal protein synthesis in preventing the apoptotic death of cultured B cell hybridomas. *Cytotechnol.* **13**: 99-105.
34. Piacentini, M., Fesus, L., Farrace, G. M., Ghibelli, L., Piredda, L., Melino, G. 1991. The expression of "tissue" transglutaminase in two human cancer cell lines is related with the programmed cell death (apoptosis). *Eur. J. Cell Biol.* **54**: 246-254.
35. Ray, N.G., Karkare, S.B., Runstadler, Jr., P.W. 1989. Cultivation of hybridoma cells in continuous cultures: Kinetics of growth and product formation. *Biotechnol. Bioeng.* **33**: 724-730.
36. Roels, J.A. 1983. *Energetics and kinetics in biotechnology.* Elsevier Biomedical Press, Amsterdam.
37. Schmid, G., Wolke, C.R., Blanch, H.W. 1992. Continuous hybridoma suspension cultures with and without cell retention: kinetics of growth, metabolism and product formation. *J. Biotechnol.* **22**: 31-40.
38. Sen, S., Srienc, F., Hu, W.-S. 1989. Distinct volume distribution of viable and non-viable hybridoma cells: A flow cytometric study. *Cytotechnol.* **2**: 85-94.
39. Shields R., Brooks, R.F., Riddle, P.N., Capellaro, D.F., Delia, D. 1978. Cell size, cell cycle and transition probability in mouse fibroblasts. *Cell.* **15**: 469-474.
40. Singh, R.P., Al-Rubeai, M., Gregory, C.D., Emery, A.N. 1994. Cell death in bioreactors: A role for apoptosis. *Biotechnol. Bioeng.* **44**: 720-726.
41. Singh, R.P., Al-Rubeai, M., Goldman, M.H., Emery, A.N. 1994. Apoptosis - The program for cell death in agitated bioreactors. *ICHEME Advances in biochemical engineering.*
42. Smith, J.A., and Martin, L. 1973. Do cells cycle? *Proc. Nat. Acad. Sci. USA.* **70**: 1263-1267.
43. Stouthamer, A.H., Bettenhausen, C.W. 1973. Utilization of energy for growth and maintenance in continuous and batch cultures of microorganisms. *Biochim. Biophys. Acta* **301**: 53-70.
44. Suzuki, E., Ollis, D.F. 1989. Cell cycle model for antibody production kinetics. *Biotechnol. Bioeng.* **34**: 1398-1402.
45. Suzuki, E., Ollis, D.F. 1990. Enhanced antibody production at slowed growth rates: Experimental demonstration and a simple structured model. *Biotechnol. Prog.* **6**: 231-236.

## Chapter 7

46. Tremblay, M. de, Perrier, M., Chavarie, C., Archambault, J. 1993. Fed-batch culture of hybridoma cells: comparison of optimal control approach and closed loop strategies. *Bioproc. Eng.* **9**: 13-21.
47. Truskey, G.A., Nicolakis, D.P., DiMasi, D., Haberman, A., Swartz, R.W. 1990. Kinetic studies and unstructured models of lymphocyte metabolism in fed-batch culture. *Biotechnol. Bioeng.* **36**: 797-807.
48. Vomastek, T. Franeck F. 1993. Kinetics of development of spontaneous apoptosis in B cell hybridoma cultures. *Immunol. Lett.* **35**:19-24.
49. Von Foerster H. 1959. Some remarks on changing populations. Pp 382-407. In: F. Stohman, Jr (ed.), *The kinetics of cellular proliferation*. Grune and Stratton, New York.

## CHAPTER 8

# USE OF A COMBINED CELL-CYCLE AND METABOLIC MODEL FOR THE STUDY OF HYBRIDOMA CELLS IN STEADY-STATE CONTINUOUS CULTURE

### ABSTRACT

In an earlier paper a combined cell-cycle and metabolic model for hybridoma cells in steady-state continuous culture is presented. This model is used in the present paper to describe the behaviour of the hybridoma cell Mn12 in continuous culture at six different dilution rates. The studied variables are the specific growth and death rate, the mean forward scatter as measured by flow cytometry, the cell-cycle distribution, and the productivity.

The mean forward scatter, which is linear proportional to the size of the cells, decreases at decreasing dilution rates and correlates linearly with the increase in the calculated fraction of apoptotic cells.

The fraction of viable cells in the  $G_1$ , S, and  $G_2/M$  phase is calculated on the basis of the age-distribution function for the cycling cells as given by the model. The fraction of S-phase cells as well as the trend in the  $G_1$ -phase fraction are predicted well by the model, which assumes a constant duration of the  $G_{1B}$ , S,  $G_2$ , and M phase. The less good prediction of the  $G_1$  and  $G_2/M$  fractions may be due to cell-cycle-phase specificity of apoptosis, which is not accounted for in the model. In addition, a good prediction of all cell-cycle fractions is obtained if it is assumed that above the critical specific growth rate the length of the  $G_2/M$  phase increases with decreasing specific growth rates.

Equations derived for two different hypotheses regarding the production of monoclonal antibody are incorporated in the model and compared in their ability to describe the experimental data. The first hypothesis assumes passive release of antibody from dead cells. In case of the second hypothesis, a higher production rate of antibody by non-proliferating cells as compared to cycling cells is assumed. For both hypotheses the equations can describe the negative growth-rate-associated production kinetics well.

## INTRODUCTION

Mathematical models are a valuable tool in obtaining a better understanding of reality. With respect to animal-cell cultivation, the use of a mathematical model can lead to a better insight in the physiological behaviour of the cells, which eventually can be used for the optimisation of process conditions and for process control. In a previous manuscript<sup>18</sup> a combined cell-cycle and metabolic model is presented describing the growth of hybridoma cells in steady-state continuous cultures. The model can describe the steady-state data as presented by Miller et al.<sup>20</sup> well with respect to the specific growth rate, the specific death rate, and the concentrations of viable cells, dead cells, glutamine, ammonia, glucose, and lactate. However, the data presented by Miller et al.<sup>20</sup> represent the average behaviour of the cell population as a whole. Consequently, the segregated nature of the model could not be validated using their data. In addition, the negative growth-rate-associated production rate of monoclonal antibody, as is found for many hybridoma cell lines, could not be accurately described by the model.

In the first part of this work the cell-cycle section of the model is evaluated, which is based on a population-balance model as described by Cazzador and Mariani<sup>8</sup>. In Figure 1 a schematic representation of the possible phases a cell may be in is given. A short summary of the cell-cycle part of the model, as developed previously, is given in appendix A. In this paper the equations for the calculation of the average cell volume as given in appendix A are rewritten in terms of the forward scatter and fitted to experimental data. Furthermore, an equation for the calculation of the distribution of the viable cells over the  $G_1$ , S,  $G_2$ , and M phase of the cell cycle is additionally derived from the age-distribution functions as given in appendix A. The thus calculated cell-cycle fractions are compared to experimental values in order to evaluate the segregated nature of the model.

In the second part of this work equations concerning two often reported hypotheses for negative growth-rate-associated antibody production are derived. These equations are substituted for the original equation describing product formation as is also given in appendix A. With respect to the first hypothesis a constant productivity and antibody content of the viable cells is assumed in addition to immediate passive release of all intracellular antibody at cell death<sup>2,3,21</sup>. For the second hypothesis an increased productivity of antibody by apoptotic cells is assumed and the passive release of antibody at cell death is assumed to be negligible<sup>8,16,33</sup>.

The results of the model calculations are compared to steady-state data obtained from a set of six continuous cultures of the hybridoma cell line Mn12.

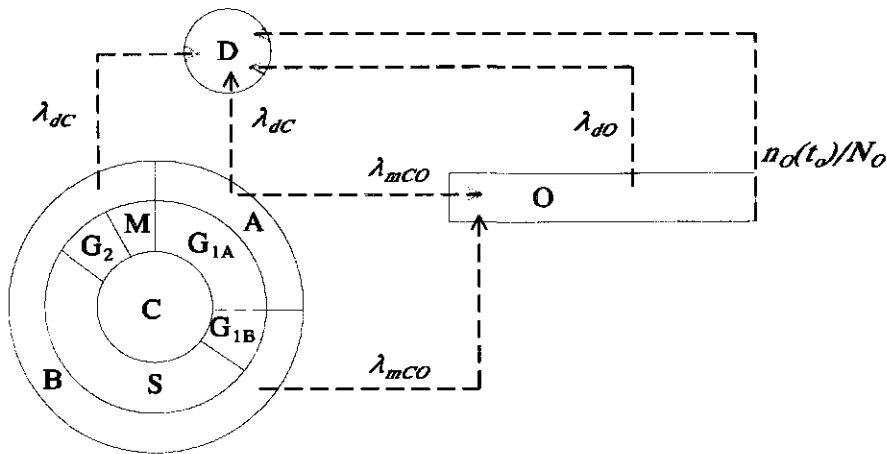


**Figure 1.** Schematic representation of the cell cycle. A, B : phase A and B. O : apoptotic phase. D : dead-cell state.  $G_{1A}$ ,  $G_{1B}$ , S,  $G_2$ , and M :  $G_{1A}$ ,  $G_{1B}$ , S,  $G_2$ , and M phase.  $\lambda_{dC}$ ,  $\lambda_{dO}$  : death-rate constants for cells in the cycling and apoptotic state, respectively.  $\lambda_{mCO}$  : rate constant for the transition from the cycling to the apoptotic phase.  $n_O(t_O)$  : number of cells at the end of the apoptotic phase.  $N_O$  : total number of apoptotic cells.

## MATERIAL AND METHODS

### Cell culture

The mouse-mouse hybridoma MN12 (RIVM Bilthoven, The Netherlands), producing IgG2a antibodies directed against the outer-membrane protein P1.16 of *Neisseria meningitidis*, was grown in a series of six continuous cultures in a stirred fermenter (at 60 rpm) with a working volume of 2 dm<sup>3</sup> as described elsewhere<sup>17</sup>. The used dilution rates are I: 0.011 h<sup>-1</sup>, II: 0.021 h<sup>-1</sup>, III: 0.023 h<sup>-1</sup>, IV: 0.030 h<sup>-1</sup>, V: 0.042 h<sup>-1</sup>, and VI: 0.058 h<sup>-1</sup>.

### Flow cytometry

Samples were analysed with a flow cytometer (FACScan; Becton Dickinson BV, Etten-Leur, The Netherlands). An HP310 computer (Hewlett-Packard corporation, Pittsburgh, PA) with a Consort 30 program (Becton Dickinson) was used for data processing.

The forward scatter (FCS) and side scatter (SSC) of the cells were measured with the flow cytometer without pretreatment of the samples.

The distribution of the cells over the  $G_1$ , S, and  $G_2/M$  phase was determined using the incorporation of 5-BromodesoxyUridine (BrdU) (Sigma, St.Louis, MO) in the DNA of S-phase cells in combination with propidium-iodide staining as described elsewhere<sup>17</sup>.

### Cell counts

Cells were counted using a Fuchs-Rosenthal haemocytometer, using the exclusion of trypan blue (1% w/v) as a measure for culture viability. The samples were diluted to such an extent that a minimal number of 200 cells were counted.

### Productivity

The monoclonal-antibody concentration was determined by a mouse-IgG-specific ELISA as described by Jiskoot et al.<sup>13</sup>.

## RESULTS AND DISCUSSION

### Parameter estimation

By substituting Equation (A2) in the equations for the specific death rate [Eq. (A4)], specific growth rate [Eq. (A5)], mean forward scatter [Eq. (1)], fraction of cells in the G<sub>1</sub>, S, and G<sub>2</sub>/M phase [Eq. (2)], and the productivity [Eqs. (8) and (9)], these variables may be written explicitly as a function of the dilution rate and the unknown model parameters. The model parameters are now obtained by fitting the substituted equations to the experimental data using non-linear least-square curve-fitting (TableCurve 2D windows V2.03, Jandel scientific, San Rafael, USA) as described further on.

In the model, as presented in appendix A, cells start entering apoptosis as the specific growth rate drops below a defined critical specific growth rate. However, recent studies of apoptosis show that cells become apoptotic during the whole period of a batch culture, even at the high specific growth rates occurring early in the exponential growth phase<sup>22,32</sup>. Also in this work, apoptosis is observed to occur at high specific growth rates above the critical specific growth rate. Therefore, it is more likely that the change from no cells entering apoptosis and a varying cycle time to a situation with a constant cycle time and cells entering apoptosis is gradual rather than sudden at a defined critical specific growth rate. In order to describe this gradual transition, an empirical function is derived in appendix B which calculates the duration of phase A as a function of the dilution rate making use of an extra curvature parameter  $C$ . For values of  $C$  equal to zero a sharp transition point is obtained at the critical dilution rate and the result of Equation (B1) is the same as that of Equation (A2.a) in appendix A, whereas an increasing value for  $C$  results in a more gradual transition. In Figure 2 the duration of phase A [Eq. (B1)] and the fraction of apoptotic cells [Eqs. (B1), (A2.b), and (A3)] are shown as a function of the dilution rate for  $C=0 \text{ h}^2$  and  $C=15.4 \text{ h}^2$ .

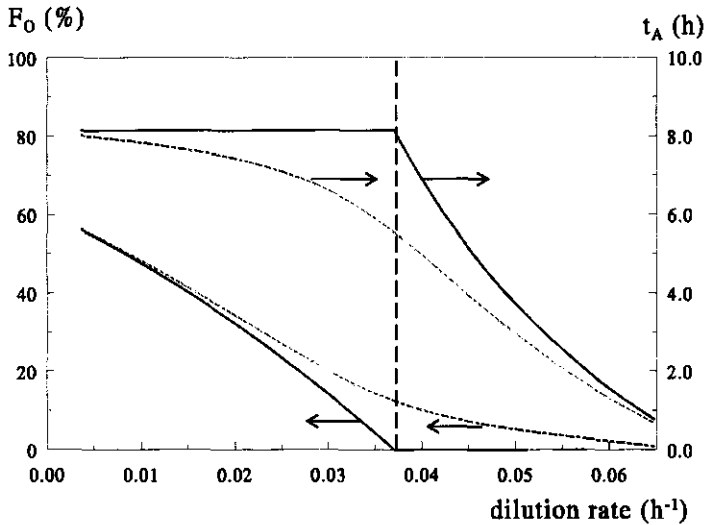


**Figure 2.** The fraction of apoptotic cells and the duration of phase A as calculated from Equations (A1), (B1), (A2.b), and (A3) as a function of dilution rate. The solid lines (—) represent the sharp-transition case ( $C=0 \text{ h}^2$ ) and the dashed lines (- -) represent the gradual-transition case ( $C=15.4 \text{ h}^2$ ). The vertical dashed line marks the critical dilution rate.

The addition of the curvature parameter results in a better correlation between the model and the datum points. However, based on the F test the model with the gradual transition is in general not better than the model with the sharp transition, due to the introduction of an extra parameter and due to the limited number of datum points. Thus, the gradual transition, which is more plausible on the basis of observations done in literature and in this work (Fig. 6), is used solely to demonstrate the effect of a gradual transition on the model outcomes and it is not used to estimate model parameters.

### Specific growth and death rate

In Figure 3 the specific growth- and death-rate constant are shown as a function of the dilution rate. By substitution of Equation (A1), (A2), and (A3) in Equation (A4), the specific death-rate constant,  $\mu_d \text{ (s}^{-1}\text{)}$ , can be explicitly written as a function of the dilution rate, the maximum specific growth rate,  $\mu_m \text{ (s}^{-1}\text{)}$ , the critical specific growth rate,  $\mu_{cr} \text{ (s}^{-1}\text{)}$ , the death-rate constant of the cycling cells,  $\lambda_{dc} \text{ (s}^{-1}\text{)}$ , the death-rate constant during progression of cells through apoptosis,  $\lambda_{d0} \text{ (s}^{-1}\text{)}$ , and the duration of apoptosis,  $t_o \text{ (s)}$ . The maximum specific growth rate of the hybridoma cell line Mn12 is estimated from the specific growth rates observed during



start-up of the continuous culture at the highest dilution rate, resulting in a value of  $0.072 \pm 0.004 \text{ h}^{-1}$ . This gives a duration of phase B, as calculated from Equation (A1), of  $9.6 \pm 0.5 \text{ h}$ . In general, the membrane of apoptotic cells will become permeable to trypan blue, which means they are marked as dead, after a certain time,  $t_0$ . Furthermore, in the model it is assumed that the rate constant for necrosis of apoptotic cells,  $\lambda_{dO}$ , is the same as that for cycling cells,  $\lambda_{dC}$ . The parameters  $\lambda_{dC}$  ( $=\lambda_{dO}$ ),  $\mu_{cr}$ , and  $t_0$  are now obtained by fitting Equations (A1), (A2), (A3), and (A4) to the experimental data for the death-rate constant as shown in Figure 3.

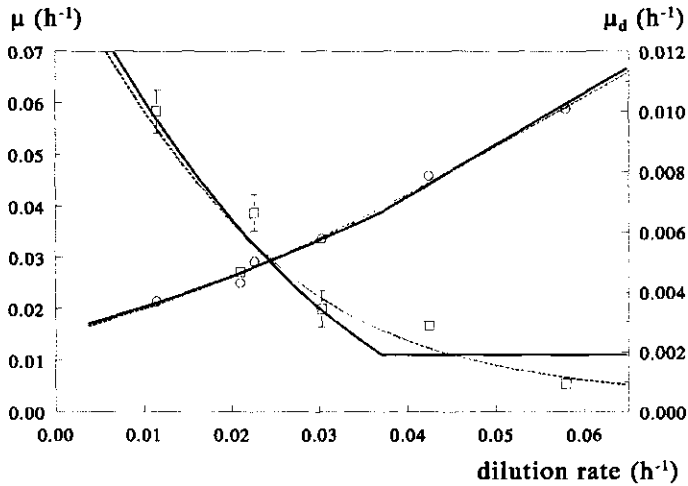


**Figure 3.** Measured (symbols) and fitted (lines) specific growth-rate constant,  $\mu$  ( $\circ$ ) and specific death-rate constant,  $\mu_d$  ( $\square$ ) as a function of the dilution rate. The solid lines (—) represent the sharp-transition case ( $C=0 \text{ h}^2$ ) while the dashed lines (- -) represent the gradual-transition case ( $C=38.6 \text{ h}^2$ ). The bars represent the 95% confidence intervals of the datum points.

The experimental death-rate constant is calculated from the measured steady-state dead- and viable-cell concentrations and the dilution rate. Simultaneously, the critical specific growth rate is also estimated from the measured forward-scatter data, as discussed below. As can be seen in Figure 3 the specific death rate and the specific growth rate [Eq. (A5)] can be fitted well by the model for the sharp-transition case. For comparison also the fit for the gradual-transition case is shown. The parameter values resulting from the simultaneous fitting of the specific death rate (Fig. 3) and the mean forward scatter (Fig. 4) are given in Table I.

**Table I.** Average literature values and experimental estimates of cell-cycle-related parameters [Eqs. (1), (2), (A1)-(A10)] with their 95% confidence limits and literature reference.

	Average literature	MN12	Units	reference
$t_B$	12±1.2	9.6±0.5	h	18
$t_{cr}$	14	8.1±3.0	h	16,18
$\lambda_{dC}, \lambda_{dO}$	2.3±1.5 10 <sup>-3</sup>	1.8±1.8 10 <sup>-3</sup>	h <sup>-1</sup>	18
$t_O$	4-10	43±21	h	6,10,25,35
$t_{G1B}$	2	0±0.2	h	26
$t_S$	7	7.8±0.1	h	1
$t_{G2}+t_M$	3	1.8±0.1	h	1

The critical specific growth rate as estimated by the fitting procedure is  $0.039 \pm 0.01 \text{ h}^{-1}$ , corresponding to a critical duration of phase A ( $= [\ln(2)/\mu_{cr}] - t_B$ ) of  $8.1 \pm 5$  hours. Remarkably, the critical specific growth rate is again about  $0.5 \mu_m$ , as was the case for the data of Miller et al.<sup>18</sup>.

The duration of apoptosis as obtained from the fit is  $43 \pm 21$  h. This is considerable longer than the time span between the first detectable event of apoptosis and the moment the cell membrane of apoptotic cells becomes permeable to viability dyes like trypan blue, which is generally estimated to be between 4 and 10 hours<sup>10,22,32</sup>. The fraction of apoptotic cells is calculated from the growth and death rate and the duration of the cell cycle. Therefore, this fraction contains all cells which are not stained by trypan blue and are non-proliferative, or in other words, cells that are viable and that on the basis of their physiological condition will not divide under the pertinent steady-state conditions. In the steady-state continuous cultures, as run here, these non-proliferative cells are destined to die through apoptosis and for this reason will be referred to as early apoptotic. However, it is not known whether the moment on which the cells become non-proliferative coincides with the first detectable apoptotic event or that it takes some time before apoptotic features become detectable. Thus, the duration of apoptosis as given in the model by  $t_O$  is the sum of the period between the moment a cell becomes committed to apoptosis under the pertinent steady-state conditions and the moment apoptosis can be detected and the period between detection of the first apoptotic events and the moment the apoptotic cell becomes stainable by trypan blue. Response times for apoptosis upon different apoptotic stimuli that have been reported may range from minutes (specific allergized T lymphocytes) to hours (irradiation and specific drugs) or even the order of a day (atrophy)<sup>35</sup>. Upon glutamine deprivation Mercille and Massie<sup>19</sup> could detect apoptosis after 12 hours with 50% apoptosis

reached after 32 hours, which is considerably longer than the response time of 2-3h for drugs that inhibit protein synthesis<sup>6,10,28,32</sup>. The slower kinetics of apoptosis upon nutrient deprivation was attributed to the slower decrease of protein synthesis due to the existence of intracellular nutrient pools<sup>19</sup>. It was proposed that in hybridoma cells a critical state must be reached in order to initiate apoptosis<sup>19</sup>. This is consistent with the findings of Perreault and Lemieux<sup>27</sup>, who suggest that apoptosis is rapidly triggered in B-cell hybridomas when protein synthesis is reduced to less than 50%. In addition, it is also consistent with the fact that the critical specific growth rate, as found for our own data and the data of Miller et al., is about  $0.5\mu_m$ <sup>18</sup>. In the continuous cultures run at the lowest dilution rates there is always some glutamine present and growth conditions are therefore less unfavourable as compared to the batch experiments of Mercille and Massie<sup>19</sup>, where cells were totally deprived of glutamine and glucose. This may result in even longer response times. In conclusion, cells in continuous cultures run at low dilution rates may remain in a non-proliferating, early-apoptotic, phase for some time before they actually show apoptotic features. In combination with the time required for apoptotic cells to become stainable by trypan blue the rather large value of 43 hours for  $t_o$  can be explained.

### Cell volume

In Figure 4 representative contour plots and histograms are shown for the side scatter versus the forward scatter obtained at the different dilution rates. At the highest dilution rate (Fig. 4.VI) one population of cycling cells (C) is present. As the dilution rate decreases the peak of the side scatter broadens and shifts towards higher values while the forward-scatter peak shifts towards smaller values. At the two lowest dilution rates this results in the emergence of a separate population of cells with a higher side scatter and a lower forward scatter, which is characteristic for apoptotic cells<sup>10</sup> (O). Although it is not known if the cells in this population all exclude trypan blue and should therefore be marked as viable, they are included in the measurement of the mean forward scatter.

The population of cells in the lower left corner consists of necrotic cells and late apoptotic cells and is excluded from the forward-scatter measurements. In the model it is assumed that the volume of the new-born cells is constant due to the size control exerted in the  $G_1$  phase<sup>26</sup>. As a consequence, the average cell volume of the cycling cells in the model [Eq. (A8)] varies less than 1% over the whole range of dilution rates. Thus, according to the model, the decrease in average cell volume of the viable cells as observed for dilution rates below the critical dilution rate is entirely due to the appearance of the apoptotic cells with a smaller average cell volume.

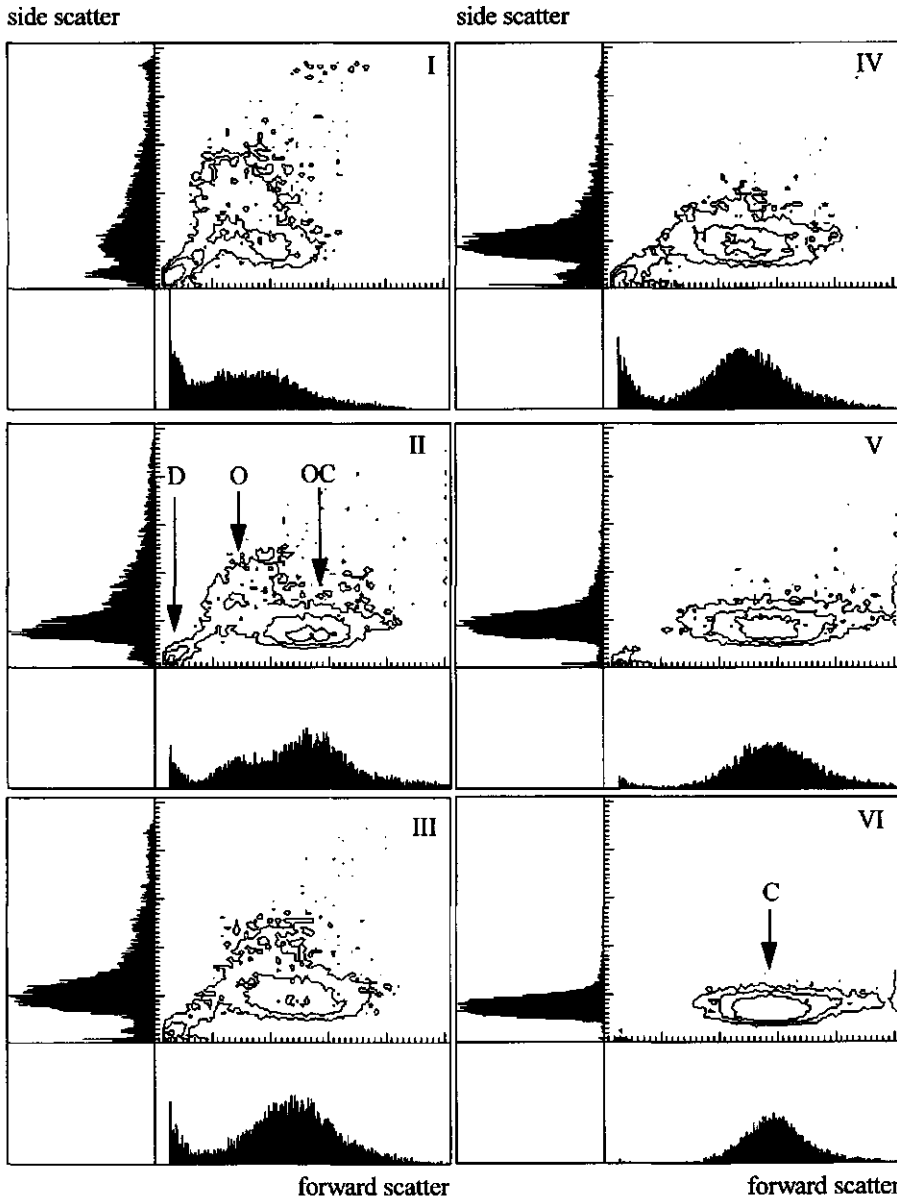


**Figure 4.** Contour plots of the side scatter versus the forward scatter as measured by flow cytometry from different steady-states. I :  $D=0.011 \text{ h}^{-1}$ . II :  $D=0.021 \text{ h}^{-1}$ . III  $D=0.023 \text{ h}^{-1}$ . IV  $D=0.030 \text{ h}^{-1}$ . V :  $D=0.042 \text{ h}^{-1}$ . VI  $D=0.058 \text{ h}^{-1}$ . C : cycling cell population. O : apoptotic cell population. OC : mixed population of cycling and apoptotic cells. D : necrotic and late-apoptotic cell population.

In Figure 4 it can be seen that the decrease in the mean forward scatter of the viable cells at decreasing dilution rates as shown in Figure 5 can be explained, at least in part, by the appearance of a population of smaller, probably apoptotic cells as assumed in the model. Whether the average volume of the cycling cells is more or less constant is difficult to conclude from Figure 4 due to the poor separation of the apoptotic and cycling cell population.

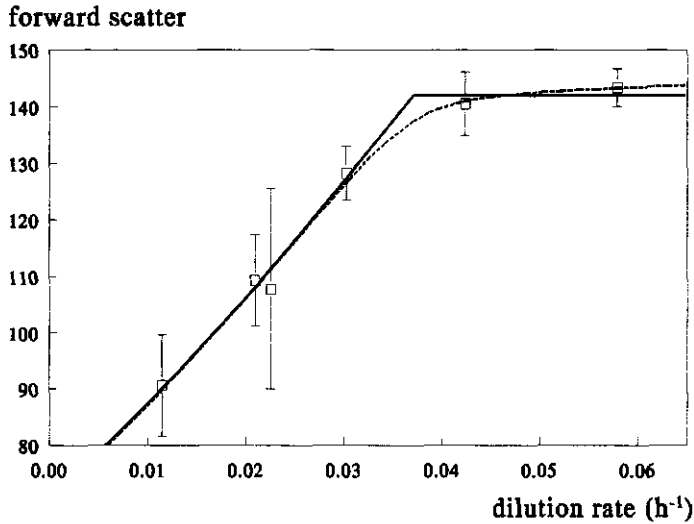


**Figure 5.** Measured (symbols) and fitted (lines) mean forward scatter of the viable cells as a function of dilution rate. The solid lines (—) represent the sharp-transition case ( $C=0 \text{ h}^2$ ) and the dashed lines (- -) represent the gradual-transition case ( $C=3.9 \text{ h}^2$ ).

The forward scatter is assumed to be linear proportional to the volume of the cells<sup>23,30</sup> or:  $\text{cell volume} = \alpha + \beta * \text{forward scatter}$ , where  $\alpha$  ( $\text{m}^3$ ) and  $\beta$  ( $\text{m}^3 \cdot \text{Unit FSc}^{-1}$ ) are unknown scaling parameters. By straightforward substitution of this linear relation in Equation (A8), (A9), and (A10), these equations may be rewritten in terms of the forward scatter. Equation (A10) then becomes:

$$FSc_v = FSc_c - (\omega + FSc_c) \left( 1 - \frac{(D + \lambda_{d0})(1 - e^{-(k_w + D + \lambda_{d0})t_0})}{(k_{vo} + D + \lambda_{d0})(1 - e^{-(D + \lambda_{d0})t_0})} \right) F_0 \quad (1)$$

where  $FSc_v$  and  $FSc_c$  are the mean forward scatter values of the viable and cycling cells, respectively, and  $\omega$  (Unit FSc) is an additional scaling parameter being equal to  $\alpha/\beta$ . Next, by substituting Equations (A1), (A2), and (A3) in Equation (1), the mean forward scatter of the viable cells may be written explicitly as a function of  $FSc_c$ ,  $\omega$ ,  $\mu_{cr}$ ,  $t_0$ ,  $\lambda_{d0}$  and  $k_{vo}$ , which is the

first-order rate-constant for the decrease of the cell volume during apoptosis ( $s^{-1}$ ). Since the average cell volume of the cycling cells varies less than 1%, the value of the forward scatter of the cycling cells is assumed constant at a value of 142, which is the average of the forward-scatter values measured at the two highest dilution rates. The parameters  $t_0$ ,  $k_{v,0}$  and  $\omega$  showed a high correlation and could not be estimated from the forward-scatter data, which is logical if it is realized that they all three influence the way and extent the forward scatter decreases at dilution rates below the critical dilution rate. However, the values of these parameters hardly affect the value of the critical specific growth rate, which can thus be quite accurately estimated from the measured forward-scatter data shown in Figure 5. Therefore, Equations (A1), (A2), (A3), and (1) are fitted to the measured forward-scatter data, with  $FSc_C$  and  $t_0$  fixed at, respectively 142 and the previously found value of 43 h and with  $k_{v,0}$ ,  $\omega$  and  $\mu_{cr}$  as variable parameters. This results in a good fit as shown in Figure 5 and an estimated critical specific growth rate of  $0.039 \pm 0.01 \text{ h}^{-1}$ . In addition, also the fit obtained for the gradual-transition case is shown in Figure 5.

### Cell-cycle distributions

$G_1$ -, S- and  $G_2/M$ -phase cells can be distinguished on the basis of propidium-iodide staining. In addition, S-phase cells can be discriminated from  $G_1$ - and  $G_2/M$ - phase cells by the active incorporation of BrdU. In Figure 6 typical dot plots of the cell-cycle distribution as measured by flow cytometry are shown for cells obtained from the steady-state cultures run at the different dilution rates. Horizontally the amount of red fluorescence, which is proportional to the amount of propidium iodide intercalated in the DNA, is plotted and vertically the green fluorescence, which is proportional to the amount of incorporated BrdU, can be found. Besides the  $G_1$ , S, and  $G_2/M$  population, a distinct population (O) with a low red fluorescence can be discerned, which is characteristic for apoptotic cells<sup>6,10</sup>. It is not known if these cells excluded trypan blue before the DNA-staining treatment.

The low red fluorescence is most likely caused by the loss of short DNA fragments from the cell during and after fixation<sup>6,10</sup>, but may also be caused by the decreased ability of propidium iodide to completely access the DNA in apoptotic cells. All S-phase cells having an intermediate DNA content actively incorporate BrdU, which is in agreement with results of Al-Rubeai et al.<sup>4</sup>. This indicates either that S-phase cells do not become apoptotic or that the cessation of DNA synthesis in the S-phase cells is rapidly followed by chromatin fragmentation and the formation of apoptotic bodies, rendering these cells part of the O population. If cessation of DNA synthesis

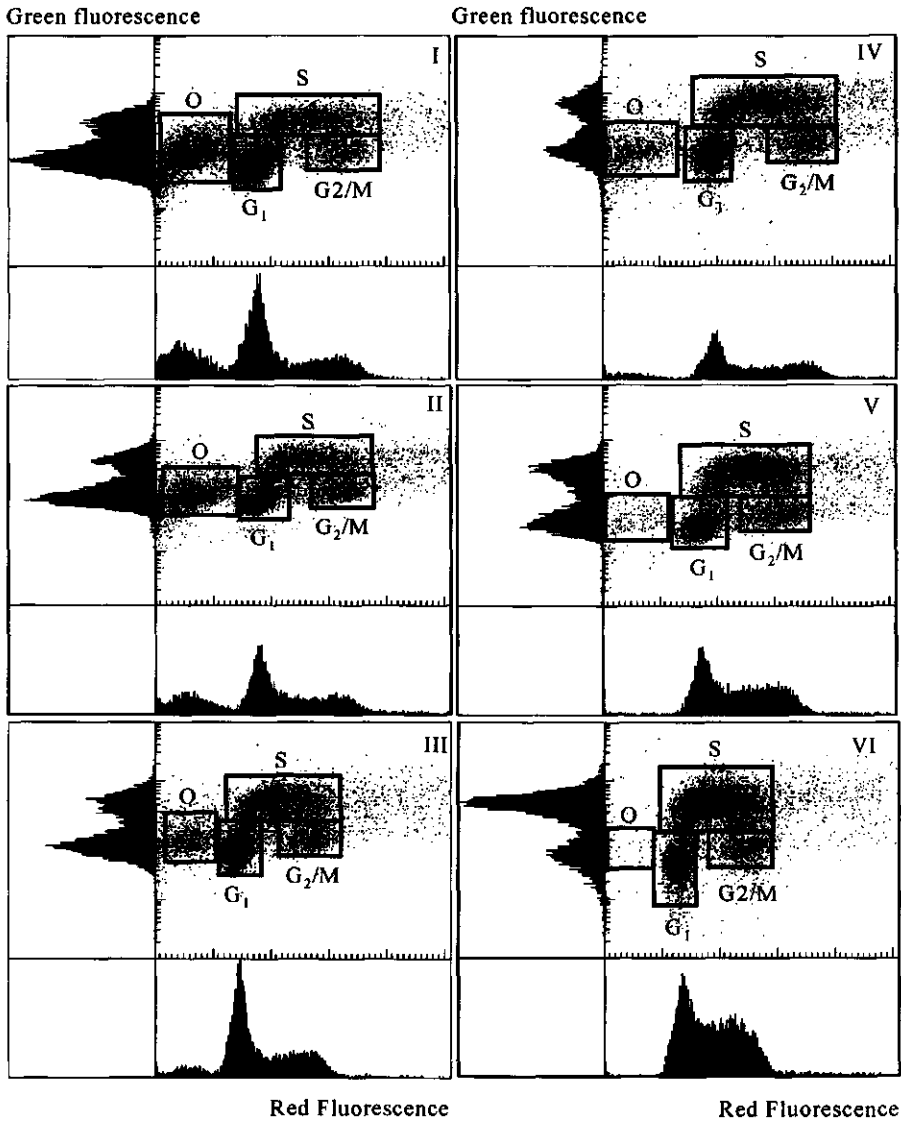


**Figure 6.** Typical dot plots for the determination of the cell-cycle distribution. Cells were obtained from the steady states of cultures run at I :  $D=0.011 \text{ h}^{-1}$ . II :  $D=0.021 \text{ h}^{-1}$ . III  $D=0.023 \text{ h}^{-1}$ . IV  $D=0.030 \text{ h}^{-1}$ . V :  $D=0.042 \text{ h}^{-1}$ . VI :  $D=0.058 \text{ h}^{-1}$ . The rectangles encompass the apoptotic cells (O), G<sub>1</sub>-phase cells (G<sub>1</sub>), S-phase cells (S) and G<sub>2</sub>- and M-phase cells (G<sub>2</sub>/M), respectively.

would not be rapidly followed by chromatin fragmentation one would expect a population of cells with an intermediate DNA content and a low green fluorescence to be present in Figure 6.I-6.IV, which is not the case. Last, as can be seen in Figure 6.V and 6.VI, a small amount of apoptotic cells is present at specific growth rates above the critical specific growth rate, supporting the assumption of a gradual increase of the rate of apoptosis going from the highest dilution rate towards the lowest dilution rate, instead of a sudden start of apoptosis below a critical specific growth rate.

The amount of cycling cells with an age between  $t_1$  and  $t_2$  may be obtained by integrating the age-distribution function [Eq. (A6)] from age  $t_1$  to age  $t_2$ . Doing the integration from age 0 to age  $t_c$  gives the total amount of cycling cells. Thus, the fraction of cells between age  $t_1$  and age  $t_2$  may be obtained according to:

$$F_{t_1-t_2} = \frac{\int_{t_1}^{t_2} n_c(0) 2^{-\frac{a}{t_c}} da}{\int_0^{t_c} n_c(0) 2^{-\frac{a}{t_c}} da} = 2^{\frac{1-t_1}{t_c} - 2^{\frac{1-t_2}{t_c}}} \quad (2)$$

With  $t_1$  and  $t_2$  being the age of the cells when entering and exiting, respectively, the  $G_1$ , S,  $G_2$  or M phase (s).

As discussed in the previous section, the moment a cell is destined to die through apoptosis may not coincide with the first detectable events of apoptosis. Thus, the measured cell-cycle distribution of the viable cells will be a combination of the distribution of the cycling cells and of the early-apoptotic cells that not yet show the reduction in propidium-iodide fluorescence. In order to allow for a comparison of the calculated distribution of cycling cells with the measured distribution of the viable cells, it is assumed that the cell-cycle distribution of these early-apoptotic cells equals that of the cycling cells. For this to be true, first the previously made assumption that cells at every stage of the cell cycle exit the cycle at an equal rate must be true. If this is the case, the DNA distribution of the early-apoptotic cells at age 0 is equal to that of the cycling cells. Second, it must be assumed that the cell-cycle distribution of the early-apoptotic cells does not change with the age of these cells or, in other words, every set of early-apoptotic cells of a certain age is assumed to have the same cell-cycle distribution.

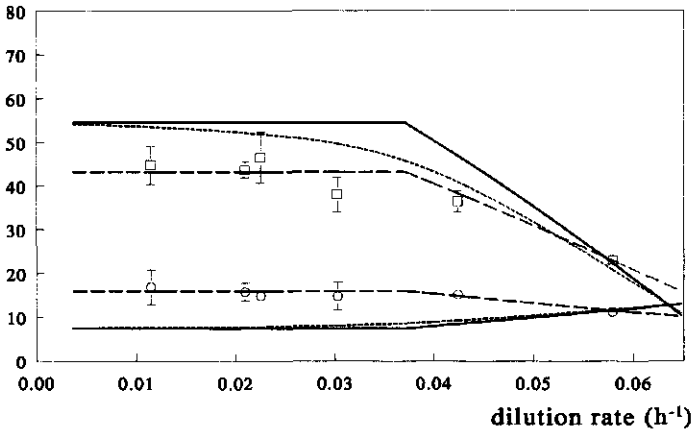
The durations of the  $G_{1B}$ , S, and  $G_2/M$  phase are calculated from the fractions measured at the highest dilution rate. At this dilution rate the amount of apoptosis is negligible (Fig. 6.VI) and, consequently, the cell-cycle distribution of the cycling cells is the same as that of the viable cells. Since the specific growth rate is known, the duration of  $G_{1A}$  ( $=t_d$ ) may be calculated from



$[\ln(2)/\mu]-t_B$ . The durations of the  $G_{1B}$ , S, and  $G_2/M$  phase are assumed to be constant and their sum must equal the duration of phase B, which was calculated earlier from the maximum specific growth rate. Thus, at a given duration of the S, and  $G_2/M$  phase the duration of the  $G_{1B}$  phase is fixed. The duration of the  $G_1$  phase is equal to the sum of the duration of  $G_{1A}$  and  $G_{1B}$ . The durations of the S and  $G_2/M$  phase were changed until an optimal fit of the computed fractions to the experimental fractions was found at the highest dilution rate. The thus obtained durations of the  $G_{1B}$ , S, and  $G_2/M$  phase are presented in Table I and agree well with literature values. Using these durations and the previously found critical specific growth rate of  $0.039 \text{ h}^{-1}$  the cell-cycle fractions are calculated as a function of the dilution rate using Equations (A1), (B1), (A2), and (2). The computed fractions are shown in Figure 7 for the sharp and gradual ( $C=15.4 \text{ h}^2$ ) transition together with the experimental values. In general the gradual-transition case results in a better correlation with the experimental data. The S-phase fraction is predicted well by the model. In fact, independent fitting of Equations (A1), (A2), and (2) to the S-phase fractions with the critical specific growth rate as a single parameter resulted in a good fit with an estimated critical specific growth rate of  $0.039 \pm 0.004 \text{ h}^{-1}$ . The trend in the  $G_1$ -phase fraction is predicted correctly. However, the values are predicted too high. The  $G_2/M$  fractions are predicted too low, while also the slight increase at the decreasing dilution rates is not predicted by the model. The differences between the model predictions and experimental values for the  $G_1$  and  $G_2/M$  fraction may have several causes.

First, the assumption of a constant duration of the S and  $G_2/M$  phase may be incorrect. In the model as presented in appendix A only the length of the  $G_{1A}$  phase increases for decreasing specific growth rates above the critical specific growth rate. If it is assumed, as proposed by Kromenaker and Srienc<sup>14</sup>, that above the critical specific growth rate the duration of all cell-cycle phases, including the duration of the S and  $G_2/M$  phase, may increase linearly with the cycle time as calculated by Equation (A2.a), Equation (4) can be fitted well to the experimental data for all cell-cycle fractions as shown in Figure 7. In this way it was found that the length of the S-phase was constant at 7.7 h, which is comparable to the previously found value of 7.8 h (Table I). Furthermore, at decreasing specific growth rates above the critical specific growth rate the duration of the  $G_2/M$  phase was found to increase from 1.2 h to 3.8 h, while the duration of the  $G_1$  phase increased twice as fast from 0 h to 5.5 h.

fraction viable cells (%)



fraction viable cells (%)

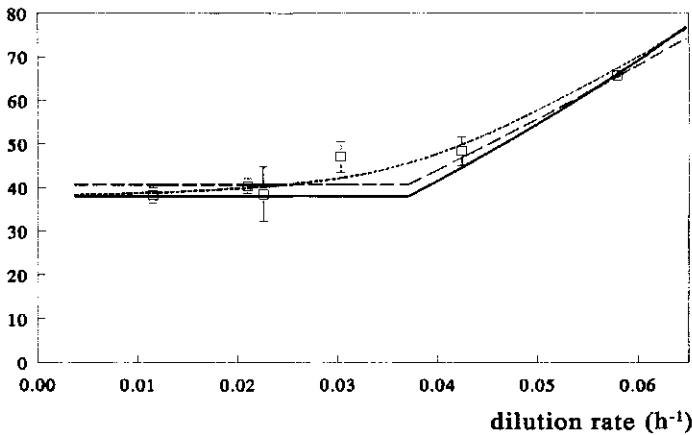


**Figure 7.** Calculated (lines) and measured (symbols) cell-cycle fractions as a function of the dilution rate. The bars represent the 95% confidence intervals of the datum points. A:  $G_1$  ( $\square$ ),  $G_2/M$  ( $\circ$ ); B: S ( $\square$ ). The solid lines represent the sharp-transition case ( $C=0 h^2$ ), while the small dashed lines ( $---$ ) represent the gradual-transition case ( $C=15.4 h^2$ ). The large dashed lines ( $---$ ) represent the sharp-transition case where the length of the  $G_1$  and  $G_2/M$  phase increases linearly with cycle time from 0 to 5.5 hours and 1.8 to 3.8 hours, respectively (see text).

Second, the earlier made assumption that the cell-cycle distribution of the early apoptotic cells not yet showing a reduction in propidium iodide fluorescence is equal to the distribution of the cycling cells may not be correct. The rate of apoptosis in different phases of the cell cycle appears to be dependent on the cell type and line and the applied stimulus. Apoptosis has been found to occur solely in  $G_0^{10}$ ,  $S^{10}$  or  $G_1$  and  $S^{32}$ , in all phases<sup>10</sup> or in all phases with preference for  $G_1^{22}$  or  $S$  and  $G_2^5$ . Thus, the above deviation may be explained by cells entering apoptosis preferentially from the  $G_2/M$  phase or by a more rapid DNA fragmentation in apoptotic cells originating from the  $G_1$  phase.

Last, CHO cells may become multinucleate<sup>22</sup> and if this also occurs in hybridoma cells it cannot be excluded that part of the  $G_2$ -phase cells are in fact multi-nucleate  $G_1$ -phase cells.

With the assumption, that, for specific growth rates above the critical specific growth rate, not only the length of the  $G_{1A}$  phase but also that of the  $G_2/M$  phase increases at decreasing specific growth rates, the model can be fitted well to the data. However, to validate this assumption more information is needed with respect to the rate with which cells become apoptotic in the individual cell-cycle phases and with respect to the rates with which individual cells pass through the different phases of the cell cycle.

### **Specific monoclonal-antibody production rate.**

The equation for the production rate of monoclonal antibody in the previous reported model contains a term for positive-growth-rate-associated production and for non-growth-rate-associated production [Eq. (A11)]. A number of authors including Miller et al.<sup>20</sup>, as well as the data presented here, show an increased specific antibody production rate at lower specific growth rates. This is either a consequence of negative-growth-rate-associated production kinetics or caused by the passive release of antibody from dead cells. Kromenaker and Srien<sup>14</sup> studied the synthesis, accumulation, and secretion pattern of monoclonal antibody during the cell cycle at different specific growth rates. The net rate of antibody synthesis was found to be independent of the specific growth rate. The increase in productivity at reduced specific growth rates was due to an increase of the secretion rate in the  $G_1$  and  $S$  phase. Bibila and Flickinger<sup>7</sup> describe the synthesis of monoclonal antibody based on intracellular balances of mRNAs coding for heavy and light chains, intracellular balances for heavy and light chains themselves, and the kinetics of their assembly. Suzuki and Ollis<sup>34</sup> model monoclonal-antibody production by combining the estimated number of mRNAs coding for antibody with a cell-cycle theory, that assumes that no arrest of cells occurs. All these models predict higher antibody production rates at lower specific growth rates. In another approach Suzuki and Ollis<sup>33</sup> as well as Linardos et al.<sup>16</sup> and Cazzador

and Mariani<sup>8</sup> assume the presence of arrested cells, which have a higher productivity as compared to cycling cells. Thus, an increase in the number of arrested cells at lower specific growth rates causes an increase in the antibody production rate. Apart from negatively growth-rate-associated production kinetics, a number of authors<sup>2,3,21,29</sup> suggest that the increased production may also be caused by the passive release of antibody from dead cells.

Antibody may be excreted actively by cycling and apoptotic cells or it may be released passively by dead cells. The active release by cycling cells,  $r_{pC}^{act}$  ( $\text{g.m}^{-3}.\text{s}^{-1}$ ), and apoptotic cells,  $r_{pO}^{act}$  ( $\text{g.m}^{-3}.\text{s}^{-1}$ ), may be described by:

$$r_{pC}^{act} = \int_0^{t_C} q_{pC}(a)n_C(0)e^{-(D+\lambda_{dC}+\lambda_{mCO})a} da \quad (3)$$

$$r_{pO}^{act} = \int_0^{t_O} q_{pO}(a)n_O(0)e^{-(D+\lambda_{dO})a} da \quad (4)$$

where  $q_{pC}(a)$ , and  $q_{pO}(a)$  are the productivities ( $\text{g.cell}^{-1}.\text{s}^{-1}$ ) for the cycling and apoptotic phase, respectively, which are a function of the age  $a$  (s), and  $n_C(0)$  and  $n_O(0)$  are the number of cells of age zero ( $\text{cells.m}^{-3}.\text{s}^{-1}$ ) for the cycling and apoptotic phase, respectively. For the passive release it is assumed that the cells release all their intracellular antibody immediately upon cell death. If this is not the case, the age distribution of the dead cells and the release kinetics of antibody from dead cells have to be taken into account. In the case of immediate release, the passive release by cycling cells of age  $a$  is given by the rate with which the cells of that age die [ $=\lambda_{dC}n_C(a)$ ] multiplied with their antibody content,  $CP_C(a)$  ( $\text{g.cell}^{-1}$ ). Integrating these rates from age zero to age  $t_C$  gives the passive release rate of the cycling cells,  $r_{pC}^{pas}$  ( $\text{g.m}^{-3}.\text{s}^{-1}$ ):

$$r_{pC}^{pas} = \int_0^{t_C} \lambda_{dC}n_C(0)e^{-(D+\lambda_{dC}+\lambda_{mCO})a} CP_C(a) da \quad (5)$$

The passive release of antibody by apoptotic cells of age  $a$  is likewise given by the rate with which the cells of that age die [ $=\lambda_{dO}n_O(a)$ ] multiplied by their antibody content,  $CP_O(a)$  ( $\text{g.cell}^{-1}$ ). Integrating these rates from age zero to age  $t_O$  gives the passive release rate during the process of apoptosis. In addition, apoptotic cells die at the end of the apoptotic phase at age  $t_O$  with a rate  $n_O(t_O)$  and an antibody content  $CP_O(t_O)$ , which results in an additional release rate of  $n_O(t_O)CP_O(t_O)$ . Thus, the passive release rate of antibody by apoptotic cells,  $r_{pO}^{pas}$  ( $\text{g.m}^{-3}.\text{s}^{-1}$ ), becomes equal to:

$$r_{pO}^{pas} = \int_0^{t_O} \lambda_{dO}CP_O(a)n_O(0)e^{-(D+\lambda_{dO})a} da + CP_O(t_O)n_O(0)e^{-(D+\lambda_{dO})t_O} \quad (6)$$

The intracellular antibody contents  $CP_C(a)$  and  $CP_O(a)$  as well as the release rates  $q_{pC}(a)$  and  $q_{pO}(a)$  as a function of age are not known. Furthermore, not much is known about the fate of antibodies during apoptosis. Consequently, certain assumptions have to be made with regard to these parameters. In this work the use of Equations (3), (4), (5), and (6) is illustrated with respect to two hypotheses often encountered in literature to explain the increase of productivity at decreasing growth rates: An equation assuming passive release of antibody by dead cells is compared with an equation based on a higher production rate of antibody by the non-cycling, apoptotic cells as compared to cycling cells.

#### *Passive release of monoclonal antibody by dead cells*

For this case, it is assumed that the increase of productivity at low growth rates is caused by the passive release of intracellular antibody from dead cells. For the moment, it is assumed that all antibody is released immediately upon cell death. Furthermore, the specific secretion rates of the cycling cells,  $q_{pC}(a)$ , and apoptotic cells,  $q_{pO}(a)$  are assumed to be the same and independent of the age of the cell. Since we did not determine the intracellular antibody contents  $CP_C(a)$  and  $CP_O(a)$  they are replaced by the average antibody content of the cycling and apoptotic cells,  $CP_C$  and  $CP_O$  ( $\text{g}\cdot\text{cell}^{-1}$ ), respectively. The total production rate of antibody,  $r_p$  ( $\text{g}\cdot\text{m}^{-3}\cdot\text{s}^{-1}$ ), can then be shown to be given by:

$$r_p = q_{pV} C_{X_v}^{cell} + [\lambda_{dc} CP_C (1 - F_O) + (\lambda_{do} + \frac{D + \lambda_{do}}{e^{(D + \lambda_{do})t_o} - 1}) CP_O F_O] C_{X_v}^{cell} \quad (7)$$

where  $q_{pV}$  is the average specific productivity of the viable cells ( $\text{g}\cdot\text{cell}^{-1}\cdot\text{s}^{-1}$ ). Assuming the average antibody content of the cycling cells is equal to that of the apoptotic cells and dividing Equation (7) by the viable-cell concentration results in the following equation for the overall specific productivity,  $q_p$  ( $\text{g}\cdot\text{cell}^{-1}\cdot\text{s}^{-1}$ ):

$$q_p = q_{pV} + \mu_d CP_V \quad (8)$$

where  $\mu_d$  is the first-order death-rate constant ( $\text{s}^{-1}$ ) and  $CP_V$  is the average amount of intracellular antibody of the viable cells ( $\text{g}\cdot\text{cell}^{-1}$ ).

Substituting  $\mu_d$  in Equation (8) using Equations (A1), (A2), (A3), and (A4) and applying the previous found values for  $\mu_{cr}$ ,  $\lambda_{dc}$ , and  $t_o$ , Equation (8) is fitted to the experimental data with  $q_{pV}$  and  $CP_V$  as the only parameters. This results in a good fit of the experimental data as can be seen in Figure 8A. The parameter values are given in Table II. For comparison, also the fit for the gradual-transition case is shown in Figure 8A.

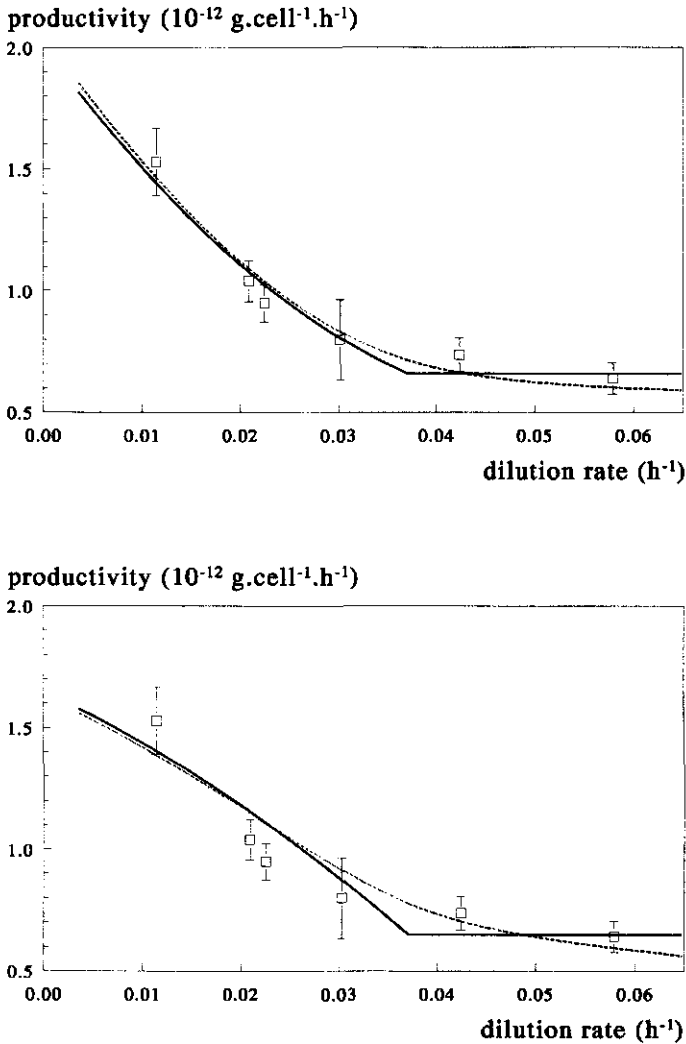


**Figure 8.** Measured specific production rate of monoclonal antibody ( $\square$ ) and calculated values as a function of dilution rate with passive release from dead cells (A) and increased productivity of apoptotic cells (B). The bars represent the 95% confidence intervals of the datum points. The solid lines ( $\text{—}$ ) represent the sharp-transition case ( $C=0 \text{ h}^2$ ), while the dashed lines ( $\text{- -}$ ) represent the gradual-transition case ( $C=15.4 \text{ h}^2$ ).

The thus obtained intracellular antibody content,  $CP_i = 1 \pm 0.25 \cdot 10^{-10} \text{ g.cell}^{-1}$  (Table II) is of the same order as values found in literature<sup>2,14,15,21</sup>.

**Table II.** Average literature values and experimental estimates of production parameters [Eqs (8) and (9)] with their 95% confidence limits and literature reference.

	Average literature	MN12	Units	reference
$q_{pv}$	$2.7 \pm 0.2 \cdot 10^{-16}$	$1.3 \pm 0.4 \cdot 10^{-16}$	$\text{g.cell}^{-1} \cdot \text{s}^{-1}$	18
$CP_v$	$0.5 \cdot 10^{-10}$	$1 \pm 0.25 \cdot 10^{-10}$	$\text{g.cell}^{-1}$	2,14,15,21
$q_{pc}$	$8.2 \cdot 10^{-17}$	$1.9 \pm 0.6 \cdot 10^{-16}$	$\text{g.cell}^{-1} \cdot \text{s}^{-1}$	8,16,33
$q_{pO}$	$5 \cdot 10^{-16}$	$6.4 \pm 2.2 \cdot 10^{-16}$	$\text{g.cell}^{-1} \cdot \text{s}^{-1}$	8,16,33

#### *Increased production rate apoptotic cells*

In this case no passive release of antibody occurs. This can be made plausible if it is realized that the specific death rate of the cycling cells,  $\lambda_{dC}$ , and of the apoptotic cells,  $\lambda_{dO}$ , may be neglected as compared to the specific death rate at the end of the apoptotic state,  $n_O(t_O)$ . If it is additionally assumed that apoptotic cells have released all their intracellular antibody before they reach the age  $t_O$  meaning  $CP_O(t_O)$  in Equation (6) equals zero, the amount of antibody released passively at cell death is negligible ( $r_{pO}^{pas} = r_{pC}^{pas} = 0$ ). Furthermore,  $q_{pO}(a)$  is assumed to be larger than  $q_{pC}(a)$  and both are assumed to be independent of the age. The specific production rate,  $q_p$ , is then equal to the specific production rate of the viable cells and is given by:

$$q_p = q_{pv} = q_{pc}(1 - F_O) + q_{pO}F_O \quad (9)$$

where  $q_{pc}$  and  $q_{pO}$  are the average productivities of the cycling and apoptotic cells, respectively ( $\text{g.cell}^{-1} \cdot \text{s}^{-1}$ ). Again, after substituting Equations (A1), (A2), and (A3) in Equation (9) and using the previously found values for  $\mu_C$ ,  $\lambda_{dC}$ , and  $t_O$  (Table I), Equation (9) is fitted to the experimental data. The resulting fit is shown in Figure 8B, while the parameters are listed in Table II. Again, for comparison also the fit for the gradual-transition case is shown in Figure 8B. Other authors<sup>8,16,33</sup> used a comparable model to describe the monoclonal-antibody productivity. Using the data of Miller et al.<sup>20</sup> they found a value of  $8.2 \cdot 10^{-17} \text{ g.cell}^{-1} \cdot \text{s}^{-1}$  for the productivity of the cycling cells, which is a little lower than the value found here. For the productivity of the arrested cells they found a value of  $5.0 \cdot 10^{-16} \text{ g.cell}^{-1} \cdot \text{s}^{-1}$ , which is comparable to the value found here for apoptotic, state-O cells. Although the passive-release model results in a better fit of the

experimental data, it is not significantly better than the model assuming a higher productivity by the apoptotic cells on the basis of the F test using a 95% confidence limit.

In conclusion, the increase in productivity at decreasing dilution rates can be described by assuming passive-release of intracellular antibody from dead cells as well as by assuming an increased productivity of apoptotic cells.

## CONCLUSIONS

The model can be fitted well to the data with respect to the specific death rate and the specific growth rate. This results in a critical specific growth rate above which cells become apoptotic of  $1.1 \cdot 10^{-5} \text{ s}^{-1}$ , which is about half the maximum specific growth rate.

The decrease in mean forward scatter of the viable cells at decreasing dilution rates can at least in part be explained by the appearance of an apoptotic cell population and is linear proportional to the increase in the calculated fraction of apoptotic cells.

The fraction of S-phase cells as well as the trend in the  $G_1$ -phase fraction are predicted well by the model, which assumes a constant duration of the  $G_{1B}$ , S, and  $G_2/M$  phase. However, the  $G_1$ -phase fraction is predicted somewhat too high and the  $G_2/M$  fractions are predicted somewhat too low by the model. This may be due to cell-cycle-phase specificity of apoptosis, which is not accounted for in the present model. In addition, a good fit is obtained for all cell-cycle fractions if it is assumed that the length of the  $G_2/M$  phase is not constant but increases linearly with the cycle time for specific growth rates above the critical specific growth rate.

The increase in productivity at lower dilution rates may be explained by the passive release of intracellular monoclonal antibody from dead cells as well as by a higher specific production rate of antibody by apoptotic cells as compared to cycling cells.

## APPENDIX A

In this appendix a short summary of the cell-cycle part of the previously developed model as well as the equation for the calculation of the monoclonal-antibody production rate are given. A complete description of the model can be found in a previous paper<sup>18</sup>. As shown in Figure 1, the cell cycle may be divided in two different ways. Besides a division into an indeterminate phase A and a determinate phase B, which together form the cycling phase C, the cell cycle can also be divided into a  $G_1$ , S,  $G_2$ , and M phase. Comparing the two divisions, phase A falls entirely within the  $G_1$  phase ( $G_{1A}$ ) and phase B consists out of a small part of  $G_1$  ( $G_{1B}$ ) and the S,  $G_2$  and M phase. The duration of the determinate part (B),  $t_B$  (s), is constant and can be calculated from the maximum specific growth rate,  $\mu_m$  ( $\text{s}^{-1}$ ), according to:



$$t_B = \frac{\ln(2)}{\mu_m} \quad (\text{A1})$$

Besides in a cycling phase, cells may be in an apoptotic phase (O). For specific growth rates below a certain critical specific growth rate,  $\mu_{cr}$  ( $s^{-1}$ ), the duration of phase A,  $t_A$  (s), stays constant and cells start entering the apoptotic state. Cells enter apoptosis from every position in the cell cycle with an equal rate constant. For specific growth rates above the critical specific growth rate the duration of phase A, and thus of the  $G_{1A}$  phase, varies with the specific growth rate and no cells enter the apoptotic phase. The rate with which cells enter the apoptotic phase,  $\lambda_{mCO}$  ( $s^{-1}$ ), and the duration of the cell cycle,  $t_C$  (s), may now be calculated according to:

$$\begin{aligned} a) \quad t_C = t_A + t_B = \frac{\ln(2)}{\lambda_{dC} + D}, \quad \lambda_{mCO} = 0 \quad \mu \geq \mu_{cr} \\ b) \quad \lambda_{mCO} = \frac{\ln(2)}{t_{cr} + t_B} - \lambda_{dC} - D, \quad t_A = t_{cr} \quad \mu < \mu_{cr} \end{aligned} \quad (\text{A2})$$

where  $\lambda_{dC}$  is the specific death-rate constant for the cycling cells ( $s^{-1}$ ) and  $D$  is the dilution rate ( $s^{-1}$ ). The apoptotic phase has a fixed duration,  $t_O$  (s), after which the cells die, which in this case means they take up trypan blue. Furthermore, cells die at a constant and relatively slow rate during the progression through the cell cycle and the apoptotic phase as represented by the death-rate constants  $\lambda_{dC}$  ( $s^{-1}$ ) and  $\lambda_{dO}$  ( $s^{-1}$ ), respectively. With the duration and cell-loss rate known for each phase, the fraction of apoptotic cells,  $F_O$ , the specific death-rate constant,  $\mu_d$  ( $s^{-1}$ ), the specific growth-rate constant,  $\mu$  ( $s^{-1}$ ), and the age-distribution function of the cycling cells,  $n_C(a)$ , (cells.m<sup>-3</sup>.s<sup>-1</sup>) and apoptotic cells,  $n_O(a)$  (cells.m<sup>-3</sup>.s<sup>-1</sup>), may be calculated according to:

$$F_O = \frac{\lambda_{mCO}}{\lambda_{mCO} + \frac{D + \lambda_{dO}}{1 - e^{-(D + \lambda_{dO})t_O}}} \quad (\text{A3})$$

$$\mu_d = (1 - F_O)\lambda_{dC} + \left(\lambda_{dO} + \frac{D + \lambda_{dO}}{e^{(D + \lambda_{dO})t_O} - 1}\right)F_O \quad (\text{A4})$$

$$\mu = D + \mu_d \quad (\text{A5})$$

$$n_c(a) = n_c(0) e^{-\frac{\ln(2)a}{t_c}} = n_c(0) 2^{-\frac{a}{t_c}} \quad 0 \leq a \leq t_c \quad \text{B.C.: } n_c(0) = 2n_c(t_c) \quad (\text{A6})$$

$$n_o(a) = n_o(0) e^{-(D+\lambda_o)a} \quad 0 \leq a \leq t_o \quad \text{B.C.: } n_o(0) = \lambda_{mco} N_c \quad (\text{A7})$$

Where  $a$  is the cell age (s) and  $N_c$  is the concentration of cycling cells (cells.m<sup>-3</sup>).

The average volume of a cycling cell is assumed to increase exponentially to twice its value at birth during a period ranging from the moment of birth to the moment of entrance into mitosis. The average volume of the new-born cells,  $V_A$  (m<sup>3</sup>), is assumed to be constant, which reflects the size control exerted in the G<sub>1</sub>-phase<sup>1,26</sup>. In combination with the known age distribution, the average cell volume of the cycling cells,  $V_C$  (m<sup>3</sup>) can now be calculated by:

$$V_C = 2V_A \frac{t_c}{t_m} (e^{\frac{t_m \ln(2)}{t_c}} - 1) \quad (\text{A8})$$

where  $t_m$  is the duration of the M phase (s). During apoptosis the average volume of the apoptotic cells is assumed to decrease exponentially to the volume of the dead cells with a rate constant  $k_{vo}$  (s<sup>-1</sup>). With the known age-distribution function of the apoptotic cells the average cell volume of these cells may be calculated according to:

$$V_o = \frac{V_C(D + \lambda_{do})(1 - e^{-(k_{vo} + D + \lambda_{do})t_o})}{(k_{vo} + D + \lambda_{do})(1 - e^{-(D + \lambda_{do})t_o})} \quad (\text{A9})$$

Next, the average cell volume of the viable cells,  $V_V$  (m<sup>3</sup>), is calculated from the fraction of apoptotic cells by:

$$V_V = (1 - F_o)V_C + F_o V_o \quad (\text{A10})$$

The equation describing the monoclonal-antibody production rate,  $r_p$  (g.m<sup>-3</sup>.s<sup>-1</sup>), as used in the previously developed model<sup>18</sup> is given by:

$$r_p = Y_{px} r_{x_i} + q_{pv}^{C-mole} C M_V C_{x_v}^{cell} - k_{dp} C_p \quad (\text{A11})$$

Where  $Y_{px}$  is the yield of monoclonal antibody on biomass (g.C.mol<sup>-1</sup>),  $r_{x_i}$  is the biomass formation rate (C.mol.m<sup>-3</sup>.s<sup>-1</sup>),  $q_{pv}^{C-mol}$  is the productivity of the viable biomass (g.C.mol<sup>-1</sup>.s<sup>-1</sup>),  $C M_V$  is the average biomass content of the viable cells (C.mol.cell<sup>-1</sup>),  $C_{x_v}^{cell}$  is the viable-cell concentration (Cells.m<sup>-3</sup>),  $k_{dp}$  is the first-order degradation constant of the product (s<sup>-1</sup>) and  $C_p$  is the product concentration (g.m<sup>-3</sup>).

## APPENDIX B

In the previously developed model, as presented in appendix A, no apoptosis occurs and the length of the cell cycle varies with the specific growth rate above a defined critical specific growth rate. As the specific growth rate drops below the critical value a sharp transition occurs, at which cells start entering apoptosis and the duration of the cell cycle becomes constant. However, it is more likely that this change from no cells entering apoptosis and a varying cycle time to a situation with a constant cycle time and cells entering apoptosis is gradual rather than sudden at a defined critical specific growth rate. In case of the sharp transition, the duration of phase A,  $t_A$  (s), is equal to a maximum critical duration,  $t_{cr}$  (s), below the critical specific growth rate, whereas above the critical specific growth rate it is given by  $\ln(2)/(D+\lambda_{dc})-t_B$ . A gradual-transition function for the calculation of  $t_A$  should now asymptotically approach the duration of phase A as calculated for the sharp-transition case at low and high dilution rates. In addition, the duration of phase A should always be smaller than for the sharp-transition case. These demands are present in the next function:

$$t_A = t_{cr} - \sqrt{[0.5\ln(2)\left(\frac{1}{D+\lambda_{dc}} - \frac{1}{D_{cr}+\lambda_{dc}}\right)]^2 + \left(1 - \frac{D}{D_m}\right)C + 0.5\ln(2)\left(\frac{1}{D+\lambda_{dc}} - \frac{1}{D_{cr}+\lambda_{dc}}\right)} \quad (\text{B1})$$

where  $D$ ,  $D_{cr}$  and  $D_m$  are the dilution rate, the critical dilution rate ( $=\mu_{cr}-\lambda_{dc}$ ) and the maximum dilution rate ( $=\mu_m-\lambda_{dc}$ ) ( $s^{-1}$ ), respectively,  $\mu_{cr}$  and  $\mu_m$  are the critical and the maximum specific growth rate ( $s^{-1}$ ), respectively,  $\lambda_{dc}$  is the specific death-rate constant of the cycling cells ( $s^{-1}$ ), and  $C$  is a curvature parameter ( $s^2$ ). Equation (B1) replaces Equation (A2.a), while the rate constant for the transition from the cycling phase to the apoptotic phase,  $\lambda_{mCO}$  ( $s^{-1}$ ), is still calculated from Equation (A2.b).

## ACKNOWLEDGEMENTS

The authors thank Taco Wijtzes for mathematical support in deriving Equation (B1).

## SYMBOLS

$a$	Cell age	(s)
$CM_V$	Average biomass content viable cells.	(g.cell $^{-1}$ )
$CP_C$	Intracellular antibody content of phase-C cells	(g.cell $^{-1}$ )
$C_p$	Product concentration.	(g.m $^{-3}$ )
$CP_O$	Intracellular antibody content of apoptotic cells	(g.cell $^{-1}$ )
$CP_V$	Intracellular antibody content of viable cells	(g.cell $^{-1}$ )
$C_{v}^{cell}$	Viable-cell concentration.	(cells.m $^{-3}$ )

Chapter 8

$D$	Dilution rate	(s <sup>-1</sup> )
$F_i$	Fraction of cells in the G <sub>1</sub> , S, and G <sub>2</sub> /M phase	(-)
$F_O$	Fraction of apoptotic cells	(-)
$FSc_C$	Mean forward scatter cycling cells.	(-)
$FSc_V$	Mean forward scatter viable cells.	(-)
$k_{dp}$	First-order degradation constant for product	(s <sup>-1</sup> )
$k_{vo}$	First-order rate constant for the volume decrease of apoptotic cells	(s <sup>-1</sup> )
$n_i(a)$	Steady-state age density function of cells in state i	(cells.m <sup>-3</sup> .s <sup>-1</sup> )
$N_C$	Total number of cycling cells.	(cells.m <sup>-3</sup> )
$r_p$	Volumetric monoclonal-antibody production rate.	(g.m <sup>-3</sup> .s <sup>-1</sup> )
$r_{\lambda}$	Biomass formation rate.	(C-mol.m <sup>-3</sup> .s <sup>-1</sup> )
$q_{pV}^{C-mole}$	Specific productivity viable biomass	(g.C-mol <sup>-1</sup> .s <sup>-1</sup> )
$q_{pV}$	Specific productivity viable cells	(g.cell <sup>-1</sup> .s <sup>-1</sup> )
$q_{pO}$	Specific productivity apoptotic cells.	(g.cell <sup>-1</sup> .s <sup>-1</sup> )
$q_{pC}$	Specific productivity cycling cells.	(g.cell <sup>-1</sup> .s <sup>-1</sup> )
$t_A$	Duration of phase A	(s)
$t_B$	Duration of phase B	(s)
$t_C$	Duration of the cell cycle	(s)
$t_{cr}$	Maximum critical duration of phase A	(s)
$t_m$	Duration of the mitosis	(s)
$t_O$	Duration of apoptosis	(s)
$V_A$	Cell volume of newborn cells immediately after division	(m <sup>3</sup> .cell <sup>-1</sup> )
$V_C$	Average cell volume of the cycling cells	(m <sup>3</sup> .cell <sup>-1</sup> )
$V_O$	Average cell volume of the apoptotic cells	(m <sup>3</sup> .cell <sup>-1</sup> )
$V_V$	Average cell volume of the viable cells	(m <sup>3</sup> .cell <sup>-1</sup> )
$Y_{px}$	Yield of monoclonal antibody on biomass.	(g.C-mol <sup>-1</sup> )
$\lambda_{dO}$	Death-rate constant of cells progressing through apoptosis	(s <sup>-1</sup> )
$\lambda_{dC}$	Death-rate constant of the cycling cells	(s <sup>-1</sup> )
$\lambda_{mCO}$	Transition rate of cells from state C to the apoptotic state	(s <sup>-1</sup> )
$\alpha$	Intercept for the cell volume forward scatter relation	(m <sup>3</sup> )
$\beta$	Slope for the cell volume to forward scatter relation	(m <sup>3</sup> .Unit FSc <sup>-1</sup> )
$\mu$	Specific growth rate	(s <sup>-1</sup> )
$\mu_{cr}$	Critical specific growth rate	(s <sup>-1</sup> )
$\mu_d$	Overall death-rate constant	(s <sup>-1</sup> )
$\mu_m$	Maximum specific growth rate	(s <sup>-1</sup> )
$\omega$	$\alpha/\beta$	(Unit FSc)

## REFERENCES

1. Alberts, B., Bray, D., Lewis, J., Raff, M., Roberts, K., Watson, J.D. 1983. *Molecular Biology of the Cell*. Garland, New York.
2. Al-Rubeai, M., Emery, A.N. 1990. Mechanisms and kinetics of monoclonal antibody synthesis and secretion in synchronous and asynchronous hybridoma cell cultures. *J. Biotechnol.* **16**: 67-86.
3. Al-Rubeai, M., Mills, D., Emery, A.N. 1990. Electron microscopy of hybridoma cells with special regard to monoclonal antibody production. *Cytotechnol.* **4**: 13-28.
4. Al-Rubeai, M., Emery, A.N., Chalder, S. 1991. Flow cytometric study of cultured mammalian cells. *J. Biotechnol.* **19**: 67-82.
5. Al-Rubeai, M., Singh, R.P., Goldman, M.H., Emery, A.N. 1995. Death mechanisms of animal cells in conditions of intensive agitation. *Biotechnol. Bioeng.* **45**: 463-472.
6. Afanasyev, V.N., Korol, B.A., Matylevich, N.P., Pechatnikov, V.A., Umansky, S.R. 1993. The use of flow cytometry for the investigation of cell death. *Cytometry.* **14**: 603-609.
7. Bibila, T., Flickinger, M.C. 1991. A structured model for monoclonal antibody synthesis in exponentially growing and stationary phase hybridoma cells. *Biotechnol. Bioeng.* **37**: 210-226.
8. Cazzador, L., Mariani, L. 1993. Growth and production modelling in hybridoma continuous cultures. *Biotechnol. Bioeng.* **42**: 1322-1330.
9. Coco-Martin, J.M., Martens, D.E., van der Velden-de Groot, T.A.M., Beuvery, E.C. 1993. Cultivation of hybridoma cell line MN12 in a homogeneous continuous culture system: Effect of culture age. *Cytotechnol.* **13**: 213-220.
10. Darzynkiewicz, Z., Bruno, S., Del Bino, G., Gorczyca, W., Hotz, M. A., Lassota, P., Traganos, F. 1992. Features of apoptotic cells measured by flow cytometry. *Cytometry* **13**: 795-808.
11. Frame, K.K., Hu, W.-S. 1990. Cell volume measurement as an estimation of mammalian cell biomass. *Biotechnol. Bioeng.* **36**: 191-197.
12. Goldstein, P., Ojcius, D.M., Young, J.D.-E. 1991. Cell death mechanisms and the immune system. *Immunol. Rev.* **121**: 29-65.
13. Jiskoot, W., Hertrooij, J.C.C. Van, Klein Gebbinck, J.W.T.M., Van der Velden-de Groot, T., Crommelin, D.J.A., Beuvery, E.C. 1989. Two-step purification of a murine monoclonal antibody intended for therapeutic application in man Optimisation of purification conditions and scaling up. *J. Immunol. Methods.* **124**: 143-156.
14. Kromenaker, S.J., Srienc, F. 1994. Effect of lactic acid on the kinetics of growth and antibody production in a murine hybridoma: secretion patterns during the cell cycle. *J. Biotechnol.* **34**: 13-34.
15. Leno, M., Merten, O.-W., Hache, J. 1992. Kinetic analysis of hybridoma growth and monoclonal antibody production in semicontinuous culture. *Biotechnol. Bioeng.* **39**: 596-606.
16. Linardos, T.I., Kalogerakis, N., Behie, L.A. 1992. Cell cycle model for growth rate and death rate in continuous suspension hybridoma cultures. *Biotechnol. Bioeng.* **40**: 359-368.
17. Martens, D.E., de Gooijer, C.D., van der Velden-de Groot, C.A.M., Beuvery, E.C., Tramper, J. 1993. Effect of dilution rate on growth, productivity, cell cycle and size, and shear sensitivity of a hybridoma cell in a continuous culture. *Biotechnol. Bioeng.* **41**: 429-439.

18. Martens, D.E., Sipkema, E.M., de Gooijer, C.D., Beuvery, E.C., Tramper, J. 1995. A combined cell-cycle and metabolic model for the growth of hybridoma cells. *Biotechnol. Bioeng.* **48**: 49-65.
19. Mercille, S., Massie, B. 1994. Induction of apoptosis in nutrient-deprived cultures of hybridoma and myeloma cells. *Biotechnol. Bioeng.* **44**: 1140-1154.
20. Miller, W.M., Blanch, H.W., Wilke C.R. 1988. A kinetic analysis of hybridoma growth and metabolism in batch and continuous suspension culture: Effect of nutrient concentration, dilution rate, and pH. *Biotechnol. Bioeng.* **32**: 947-965.
21. Mohan, S.B., Lyddiatt, A. 1991. Passive release of monoclonal antibodies from hybridoma cells. *Cytotechnol.* **5**: 201-209.
22. Moore, A., Donahue, C.J., Hooley, J., Stocks, D.L., Bauer K.D., Mather, J. 1995. Apoptosis in CHO cell batch cultures: examination by flow cytometry. *Cytotechnol.* **17**: 1-11.
23. Mullaney, P.F., Van Dilla, M.A., Coulter, J.R., Dean, P.N. 1969. Cell sizing: A light scattering photometer for rapid volume determination. *Review Scientific Instr.* **40**: 1029-1032.
24. Ohtsubo, M., Roberst, J.M. 1993. Cyclin-dependent regulation of G<sub>1</sub> in mammalian fibroblasts. *Science* **259**: 1908-1912.
25. Ormerod, M.G., Sun, X.-M., Snowden, R.T., Davies, R., Fearnhead, H., Cohen, G.M. 1993. Increased membrane permeability of apoptotic thymocyte: A flow cytometric study. *Cytometry* **14**: 595-602.
26. Pardee, A.B. 1989. G<sub>1</sub> events and regulation of cell proliferation. *Science.* **246**: 603-608.
27. Perreault, P., Lemieux, R. 1993. Essential role of optimal protein synthesis in preventing the apoptotic death of cultured B cell hybridomas. *Cytotechnol.* **13**: 99-105.
28. Piacentini, M., Fesus, L., Farrace, M.G., Ghibelli, L., Piredda, L., Mellino, G. 1991. The expression of "tissue" transglutaminase in two human cancer cell lines is related with programmed cell death (apoptosis). *Eur. J. Cell Biol.* **54**: 246-254.
29. Reddy, S., Bauer, K.D., Miller, W.M. 1992. Determination of antibody content in live versus dead hybridoma cells: Analysis of antibody production in osmotically stressed cultures. *Biotechnol. Bioeng.* **40**: 947-964.
30. Sen, S., Srienc, F., Hu, W.-S. 1989. Distinct volume distribution of viable and non-viable hybridoma cells: A flow cytometric study. *Cytotechnol.* **2**: 85-94.
31. Smith, J.A., Martin, L. 1973. Do cells cycle? *Proc. Nat. Acad. Sci. USA.* **70**: 1263-1267.
32. Solis-Recendez, M.G., Perani, A., D'Habit, B., Stacey, G.N., Maugras, M. 1995. Hybridoma cell cultures continuously undergo apoptosis and reveal a novel 100 bp DNA fragment. *J. Biotechnol.* **38**: 117-127.
33. Suzuki, E., Ollis, D.F. 1989. Cell cycle model for antibody production kinetics. *Biotechnol. Bioeng.* **34**: 1398-1402.
34. Suzuki, E., Ollis, D.F. 1990. Enhanced antibody production at slowed growth rates: Experimental demonstration and a simple structured model. *Biotechnol. Prog.* **6** 231-236.
35. Wyllie, A.H., Kerr, J.F.R., Currie, A.R. 1980. Cell death: The significance of apoptosis. *Int. Rev. Cytol.* **68**: 251-305.

## CHAPTER 9

## GENERAL DISCUSSION

## INTRODUCTION

The occurrence of cell death is a main problem in animal-cell cultivation. It interferes with the attainment of high viable-cell densities and it shortens the culture span, which both will result in lower volumetric product yields (kg product/m<sup>3</sup> reactor volume/year). Furthermore, the release of cell debris and intracellular compounds from dead cells may cause problems in process control and down-stream processing and it may affect the quality of the product. Cell death may be caused by hydrodynamic forces, which can be generated, for instance, by sparging. Sparging is often necessary at larger scales to supply the culture with sufficient oxygen. In addition, cell death may be the consequence of adverse medium conditions like substrate limitation or the accumulation of toxic products. Cell death caused by sparging is studied in Chapters 3, 4, 5, and 6 with the hypothetical-killing-volume theory<sup>51-54</sup> as a central theme. Cell death as a consequence of adverse medium conditions is amongst other aspects of animal-cell cultivation the subject of Chapters 7 and 8.

## HYPOTHETICAL-KILLING-VOLUME THEORY

In order to describe the death of shear-sensitive cells due to sparging Tramper et al.<sup>51-54</sup> developed the hypothetical-killing-volume theory, which is described in Chapters 3, 4, and 5. The hypothetical killing volume is a hypothetical volume associated with an air bubble during its life time in which all cells are killed. The first-order death-rate constant,  $k_d$  (s<sup>-1</sup>), in bubble-column and air-lift reactors can then be derived to be the product of this hypothetical killing volume and the number of bubbles formed per unit time and unit reactor volume and is given by:

$$k_d = \frac{24FV_k}{\pi^2 d_b^3 D_r^2 H} = \frac{FV_k'}{V} \quad (1)$$

where  $F$  is the gas-flow rate ( $\text{m}^3 \cdot \text{s}^{-1}$ ),  $D$ , is the reactor diameter (m),  $H$  is the reactor height (m),  $d_b$  is the bubble diameter (m),  $V_k$  is the hypothetical killing volume ( $\text{m}^3$ ), and  $V$  is the reactor volume ( $=4\pi D_r^2 H, \text{m}^3$ ). Tramper et al.<sup>53</sup> showed that the first-order death-rate constant is independent of the bubble diameter for bubble diameters between 2-6 mm, which has led to the introduction of the specific hypothetical killing volume,  $V_k'$  (-), which is equal to the hypothetical killing volume divided by the bubble volume ( $\pi d_b^3/6, \text{m}^3$ ). The above theory has at the moment been verified by a number of researchers for a variety of cell types and process conditions, which are summarized in Table I together with other studies concerning cell death caused by bubbles.

**Table I.** Studies concerning the death of animal and insect cells through the presence of bubbles.

Author	Year	Topic	Ref.
Al-Rubeai et al.	1995	Effect of sparging on cell-cycle distribution and the occurrence of apoptosis.	3
Bavarian et al.	1991	Adsorption of insect cells to bubbles in bubble columns.	4
Chalmers and Bavarian	1991	Adsorption of insect cells onto the bubble films at the medium surface; process of bubble rupture; physical interpretation of the hypothetical killing volume as the medium making up the bubble film and a thin shell surrounding the bubble cavity.	7
Chalmers	1994	Review: Cell-bubble interactions; hydrodynamics of bubble rupture; correlation of these aspects with cell death;	8
Chattopadhyay et al.	1995	Protective effect of additives (Pluronic, Methocels, dextran, polyvinyl alcohol, polyethylene glycol) on death of insect cells due to sparging; effect on cell-bubble attachment and the relation with surface tension.	9,10
Cherry and Hulle	1992	Death of insect cells in rupturing bubble films present in foams and in a wire loop; physical interpretation of the hypothetical killing volume as the thin medium layer surrounding the bubble.	11
Garcia Briones and Chalmers	1994	Theoretical calculation of hydrodynamic stress in collapsing bubbles	13
Gardner et al.	1990	Effect of sparging on productivity and death of hybridoma cells in a sparged stirred-tank reactor; effect of addition of Pluronic.	14
Handa et al.	1985 1989	Effect of bubble size, column height and the bubble frequency on the death of myeloma, hybridoma and BHK cells in bubble columns; protection by Pluronic through formation of stable foams.	15, 16
Hülscher and Onken	1988 1990	Influence of protein concentration on productivity and growth of hybridoma cells in an air-lift loop reactor.	17, 18
Jöbses et al.	1991	Hypothetical-killing-volume theory; effect of reactor height, diameter, gas flow, number of nozzles and Pluronic on cell death in bubble columns.	20
Jordan et al.	1994	Adsorption of surfactants (Pluronic, serum and medium supernatant) onto bubbles; effect of the level of saturation of the bubble on its interactions with hybridoma and CHO cells; physical interpretation of the hypothetical killing volume as the volume within which cells make contact with a bubble uncovered with surfactants.	21
Kunas and Papoutsakis	1990	Death of hybridoma cells in stirred-tank reactors with and without bubble entrainment.	24



Author	Year	Topic	Ref.
Lu et al.	1992	Breakage of nylon microcapsules in a stirred-tank reactor with bubble entrainment and in a bubble column; effects of Tween and Pluronic addition.	25
Martens et al.	1992 1993	Hypothetical-killing-volume theory; effect of reactor height and diameter, gas flow rate, serum and dilution rate on death of hybridoma cells in air-lift loop reactors.	27, 28
Martens et al.	1996	Hypothetical-killing-volume theory; effect of gas flow rate on cell death of Vero cells on Cytodex-3 microcarriers in bubble columns; protection of Vero cells by immobilisation inside macroporous carriers.	29
Michaels et al.	1991 1995	Effect of shear-protective agents (serum, albumin, polyethyleneglycol, Pluronic, polyvinylalcohol, polyvinylpyrrolidone, Methocel) on cell death, cell-bubble attachment and interfacial properties of media for hybridoma and CHO cells in suspension.	31-34
Murhammer and Goochee	1988 1990	Growth of insect cells with and without Pluronic in sparged stirred-tank reactor and in air-lift reactors with different sparger designs.	36, 37
Oh et al.	1989 1992	Death and physiological aspects of hybridoma cells in sparged stirred-tank reactors; effect of Pluronic addition.	38, 39
Papoutsakis	1991	Reviews on shear protective additives and fluid-mechanical damage of animal and insect cells in bioreactors.	41, 42
van der Pol et al.	1990 1992 1993	Hypothetical-killing-volume theory; effect of reactor height and diameter, gas flow rate, serum and silicon antifoam on death of hybridoma cells in bubble-column reactors.	45-47
Tan et al.	1994	Effect of serum and Pluronic on interaction of hybridoma cells with bubbles.	50
Tramper et al.	1986 1987 1988	Hypothetical-killing-volume theory; effect of reactor height and diameter, gas flow rate, bubble size and methyl cellulose on death of insect cells in bubble-column reactors.	51-54
Trinh et al.	1994	Number of cells killed per bubble rupture; number of cells in the bubble film and killed after rupture; number of cells and viability in the upward jet; physical interpretation of the hypothetical killing volume as the medium in the bubble film and the thin layer surrounding the bubble cavity.	55
Wang et al.	1994	Modelling framework for cell death caused by bubbles; inactivation zone associated with a bubble where a fraction of cells is killed.	56
Wu et al.	1995	Protective effect of polymer additives (Pluronic, polyethyleneglycol, Tween) on insect cells in rapidly falling liquid films.	57
Wu and Goosen	1995	Hypothetical-killing-volume theory; effect of bubble diameter and gas flow on the death of insect cells in bubble columns; physical interpretation of the killing volume as the liquid layer surrounding the bubble before rupture.	58
Zhang et al.	1995	Protective effect of albumin on death of erythrocytes in an air-lift reactor.	60

In this thesis the hypothetical-killing-volume theory is validated for two different hybridoma cell lines being Db2 (Chapter 3) in bubble columns and Mn12 (Chapters 4 and 5) in air-lift loop reactors at varying gas-flow rates, reactor heights and reactor diameters. In Chapter 6 the death rate of Vero cells grown on Cytodex-3 microcarriers is shown to be proportional to the gas-flow rate in

a small air-lift reactor. In addition, immobilisation of the Vero cells inside macroporous Asahi microcarriers is shown to result in a reduction of the hypothetical killing volume, which means that the macroporous carriers protect the cells against the hydrodynamic forces. The hypothetical-killing-volume theory in itself gives no explanation with respect to the mechanisms of cell death due to sparging nor does it state anything about the nature and location of the volume. With respect to the mechanism of cell damage caused by air bubbles the reactor can be divided in three regions where the cells may be killed.

### Events in the sparger region

Only a few studies are devoted to the effect of the sparger on the cell death rate. Murhammer and Goochee<sup>37</sup> compared two air-lift reactors with an identical geometry and comparable flow rates and bubble sizes, but with a different sparger design. Whereas Pluronic offered full protection in the air-lift reactor with a thin membrane distributor, it provided essentially no protection in the air-lift reactor with a stainless-steel distributor. They hypothesize that there exists a killing zone near the sparger and that the death of cells at the sparger is related to the gas entrance rate, which in turn is related to the pressure drop over the orifice. In Chapter 3 of this thesis the number of nozzles is varied between one and four at a constant gas flow rate. The variation in bubble size was minimal. No effect of gas entrance velocity on the first-order death-rate constant is observed for which there are two explanations. First, no cell death may occur at the sparger. Second, cell death at the sparger does occur and is related to an unknown mechanism that is independent of the gas entrance velocity and the number of nozzles. Such a mechanism is given by Jordan et al.<sup>21</sup>, who postulate a theory for the action of protective additives like Pluronic and serum. The theory is schematically shown in Figure 1. If bubbles are formed at the sparger site they are initially not covered with surfactants. During formation and rising of a bubble, surfactants become adsorbed at the bubble interface. Until a critical saturation is reached cell-bubble interactions lead to immediate cell death (Figs. 1a and 1b). As more surfactant molecules adsorb to the bubble it becomes partially saturated and cells can adsorb to the bubbles without being damaged (Fig. 1c). Adsorbed cells may move on the surface of the bubble. If the bubble gets totally saturated no more cells can attach to the bubble and cells that have adsorbed to the bubble rise with the bubble to the surface (Fig. 1d), where they may eventually be killed if the bubble breaks up (Fig. 1e). Notably, at a 1% serum concentration bubbles were already fully saturated at 2.5 cm above the riser. Because the heights of the bubble-column and air-lift reactors used by us and in other studies are considerably higher than 2.5 cm, this would mean that in these experiments cell death at the sparger due to bubble-cell interactions cannot be discerned

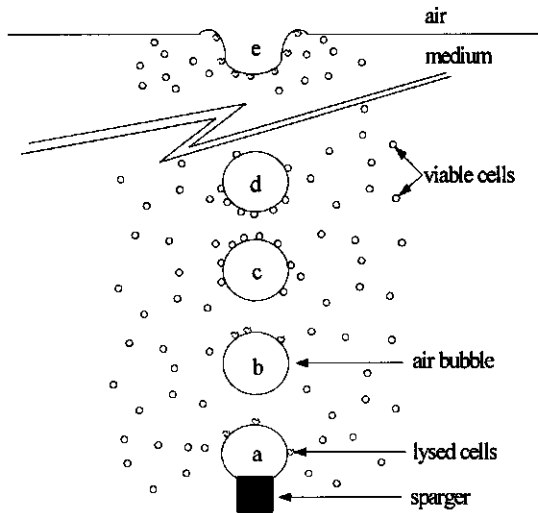


**Figure 1.** Schematic figure after Jordan et al.<sup>21</sup> of the model for interactions of cells and bubbles as postulated by Jordan et al.

from cell death at the surface. Jordan et al.<sup>21</sup> define the hypothetical killing volume as a real volume within which cells have a high probability of making contact with an uncovered bubble. Adsorption of cells to bubbles has also been shown by Bavarian and Chalmers<sup>4</sup>. The physical protection offered by surfactants, resulting in a reduction of the hypothetical killing volume, is now explained by a rapid covering of the bubble surface with surfactant molecules, which prevents the attachment of cells. Thus, this theory may explain the fast-acting protection mechanism of serum observed in Chapter 4 and the protection offered by Pluronic as described in Chapter 3. Nevertheless, Pluronic also provided protection in an agitated cylinder without gas entrainment and thus in the absence of bursting bubbles (Chapter 3). However, a large vortex was formed and in the absence of Pluronic cell death may have occurred at the surface of this vortex. Addition of Pluronic may have prevented cells from being near this surface.

### Bubble rising

As is shown in Chapters 3 and 4 and by a number of other authors (Table I), the first-order death-rate constant is proportional with the reciprocal height indicating that the rising of bubbles is not detrimental for shear-sensitive cells. However, as discussed in Chapter 6, this may be different

for cells immobilized on microcarriers due to the larger size of the carriers and the lack of flexibility of the immobilized cells.

### Bubble disengagement

The dynamics of bubble break-up have been extensively studied<sup>13,26</sup> and the different stages are schematically shown in Figure 2. In short, when a bubble reaches the surface it will partially rise out of the liquid and a thin film is formed separating the air inside the bubble from the air above the surface (Fig. 2a). Depending on the medium conditions this film may either rapidly drain and rupture or it may stabilize causing the bubble to stay on the surface for a longer time. If the film breaks, a rapidly retracting toroidal ring is formed (Fig. 2b). As this ring reaches the edge of the

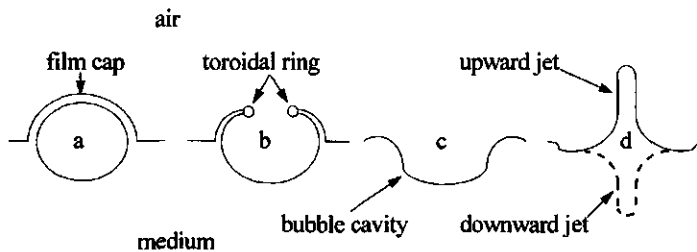


Figure 2. Schematic presentation of the different stages of bubble rupture.

bubble cavity, liquid flows rapidly down into the cavity (Fig. 2c) until it reaches the bottom of the cavity, where two jets are formed: an upward jet that emerges from the gas-liquid interface and a downward jet into the liquid beneath the cavity (Fig. 2d). Garcia-Briones and Chalmers<sup>13</sup> show that the energy-dissipation rates occurring at bubble break-up are sufficient to kill cells in well-defined flow devices. However, they also remark that the time scales of bubble break-up and cell death in flow devices are quite different. Trinh et al.<sup>55</sup> show that in their experiments the cell concentration in the upward jet is twice as high as the bulk concentration and that about 74% of the cells in this upward jet are dead. The liquid in the upward jet originates from the bubble film and a thin layer surrounding the bubble cavity<sup>26</sup>. Consequently, the cells in the upward jet probably also stem from these regions. In addition, they observed that at a cell concentration of  $10^6$  cells.cm<sup>-3</sup> about 1050 cells were killed per bubble rupture of which about 292 cells were present on the bubble film. Trinh et al.<sup>55</sup> suggest that the liquid layer which surrounds the bubble cavity before break up forms the hypothetical killing volume. They state that the higher cell concentration in the upward jet can be explained if the concentration of cells adsorbed to the bubble is twice that of the bulk concentration.

Cherry and Hulle<sup>11</sup> suggest that cell death is caused by the extreme energetic conditions in the expanding rim. They observed that about 20% of the cells present in the bubble film are immediately killed by this expanding rim. In addition, they observed that cells are partially excluded from the bubble film resulting in a cell density that is about 0.6 times that of the bulk concentration. Based on these numbers they were able to accurately predict the death rate in a sparging experiment. As may be calculated from their data about 204 cells were killed per rupturing bubble at a cell density of  $10^6$  cells.cm<sup>-3</sup>, which is lower than the value of 1050 found by Trinh et al.. However, it is of the same order as the number of cells Trinh et al. observed on the bubble film. The discrepancies may be explained from the different experimental conditions. In the case of Cherry and Hulle there was a foam layer and bubble cavities may not have been present due to the fact that only bubbles present in the foam ruptured. Consequently, only cells in the film will have been killed. Like Jordan et al. also Trinh et al. suggest that the protective effect of Pluronic may be explained by preventing the adsorption of cells onto air bubbles. Finally, Wu and Goosen<sup>57</sup> suggest that the hypothetical killing volume is formed by the liquid in the film cap and a thin layer of liquid surrounding the bubble cavity. For bubble diameters between 2.5 and 5  $10^{-3}$  m they calculate that about 18% of the cell death is accounted for by the film cap, which corresponds to the value found by Trinh et al.. Furthermore, they show that the hypothetical killing volume is proportional to the surface area of the bubble.

### The killing volume

As mentioned, different authors give different physical interpretations of the hypothetical killing volume (Table I). The hypothetical killing volume is defined as a hypothetical volume associated with an air bubble during its life time in which all cells are killed. Thus, the hypothetical killing volume is related to the number of cells killed per bubble introduced into the reactor,  $N_{killed}$  (cells.bubble<sup>-1</sup>), by:

$$V_K = \frac{N_{killed}}{C_{X_v}^{bulk}} \quad (2)$$

where  $C_{X_v}^{bulk}$  (cells.m<sup>-3</sup>) is the viable-cell concentration in the bulk. In general, the number of cells killed per bubble introduced in the reactor and thus the magnitude of the hypothetical killing volume will be determined by a number of factors depending on the mechanism causing cell death. For example, the magnitude of the shear forces associated with the killing event in relation to the fragility of the cells will probably be of importance. Higher hydrodynamic forces and more fragile

cells will cause more cells to be killed per bubble introduced in the reactor, which will result in a higher value for the hypothetical killing volume. In addition, the enrichment of cells in the detrimental zone, where shear forces are high enough to damage the cells, is likely to influence the value of the hypothetical killing volume. If the local cell concentration in the detrimental zone is higher than the bulk concentration, as is shown experimentally by Trinh et al.<sup>55</sup>, more cells will be killed, leading to an increase of the hypothetical killing volume. Enrichment may be caused by the adsorption of cells to air bubbles. Adsorption of cells to bubbles depends on the presence of protective additives like Pluronic and serum and likely also on cell properties like membrane composition, presence of microvilli, and cell size and shape. The local cell concentration may also be lower than the bulk concentration as shown to be the case for the bubble film by Cherry and Hulle<sup>11</sup>.

In Chapter 4 it is shown that the protection offered by serum has a fast-acting (minutes) and a slow-acting component (days). The fast-acting effect may be caused by the prevention of cell adsorption to air bubbles, which leads to a decrease in the cell concentration in the detrimental zone and thus to a decrease in the hypothetical killing volume. The slow-acting effect may be due to a change in the physiology of the cells. This may directly reduce the fragility of the cell or it may affect the adsorption of cells to air bubbles due to a change of membrane properties, which both lead to a decrease in the number of cells killed per bubble introduced in the reactor and thus to a decrease in the hypothetical killing volume. In Chapter 5 it is shown that the hypothetical killing volume decreases with the dilution rate in continuous culture. However, the decrease in dilution rate is accompanied by a change in many other variables, like a decrease in specific growth rate and mean forward scatter, a change in the distribution of cells over the different phases of the cell cycle, an increase in the specific death rate in the continuous cultures themselves, and an increase in the fraction of apoptotic cells. Since many variables change at the same time, it is difficult to relate the change in hypothetical killing volume to one of these variables.

### **APOPTOSIS**

In situations of substrate depletion and the accumulation of toxic products the main mode of cell death is shown to be apoptosis for a number of different cell lines<sup>30</sup>. As shown in Chapter 8 also the hybridoma cell line, Mn12, studied in this work dies at least in part through apoptosis in continuous culture. Kinetic studies of apoptosis are limited and mainly focus on the different stages of the process and not on the rate of initiation. In Chapter 7 a combined cell-cycle and metabolic model is developed to describe the behaviour of hybridoma cells in steady-state continuous culture.

In the model apoptosis is assumed to start occurring if the specific growth rate drops below a critical value. The rate with which cells die through apoptosis is next assumed to be proportional to the difference between the intrinsic specific growth rate and this critical specific growth rate. The critical specific growth rate has a value equal to about half the maximum specific growth rate. Assuming the specific growth rate is related to the total protein synthesis rate in the cells, this value corresponds with the results of Perreault and Lemieux<sup>43</sup>, who found that apoptosis is rapidly triggered if the protein-synthesis rate is reduced by less than 50% of the maximum rate.

### **Killing volume**

An important aspect of apoptotic cells is that they maintain the integrity of their plasma membrane and exclude vital dyes like trypan blue for some hours<sup>12,59</sup>. However, the plasma membrane does undergo several changes, like for instance a reduction in lectin binding sites, reduced expression of certain surface antigens, changes in membrane lipids and a reduction of membrane blebbing and microvilli<sup>40,59</sup>. The shear experiments in the small air-lift and bubble-column reactors as described in this thesis were all performed within three hours and the death-rate constant is calculated from the decrease in the viable-cell concentration as determined by trypan-blue exclusion. Consequently, part of the cells being marked as viable may have been apoptotic, which implies that the death-rate constant is underestimated. In addition, apoptotic cells as compared with proliferating cells may have a different sensitivity to disruption by air bubbles either due to a changed attachment to air bubbles or due to a different shear sensitivity. A change in cell-bubble attachment may be the consequence of altered membrane properties and the decrease in size of the apoptotic cells. A different shear sensitivity may be due to the smaller size of the apoptotic cells or the altered physiology of the apoptotic cells. It has been reported that during apoptosis high levels of transglutaminase activity can be detected, resulting in the cross linkage of cytoplasmic proteins, which turns the cell into a highly rigid and stable structure<sup>44</sup>. In Figure 3 the first-order death-rate constant as measured in a small air-lift-loop reactor under standard conditions (Chapter 5) is plotted as a function of the calculated (Chapter 8) fraction of apoptotic cells in steady-state continuous cultures run at different dilution rates. An increase in the number of apoptotic cells is actually observed at decreasing dilution rates on the basis of a reduction in stainability of the DNA of these cells by propidium iodide (Chapter 8). However, the fraction of apoptotic cells measured in this way is probably not the same as the fraction of apoptotic cells that still can exclude trypan blue and are thus marked as viable, which is the fraction that is of relevance for the determination of the first-order death-rate constant. This is the reason why the calculated fraction is used in Figure 3. As can

be seen the death-rate constant decreases linearly with an increase in the calculated fraction of apoptotic cells. This implies that the observed decrease of the hypothetical killing volume at decreasing dilution rates is caused by the appearance of apoptotic cells, which would be less sensitive to disruption by air bubbles than proliferating cells. However, many other parameters change as the dilution rate decreases, which all may affect the magnitude of the specific hypothetical killing volume. For instance, also the dead-cell concentration increases at decreasing dilution rate and adsorption of dead cells to air bubbles may interfere with adsorption of viable cells thus decreasing the specific killing volume. On the other hand, this would mean that the killing of cells in the small bubble-column and air-lift reactors would also decrease if more dead cells are present, which is not seen.

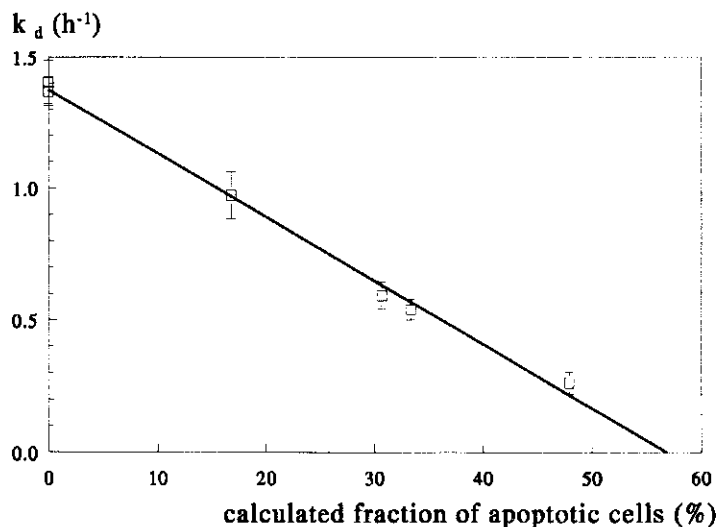


**Figure 3.** First-order death-rate constant ( $\square$ ) as determined in a small air-lift-loop reactor at constant conditions as a function of the calculated fraction of apoptotic cells in steady-state continuous cultures run at different dilution rates. Error bars represent the 95% confidence intervals.

### Cell cycle

In a cell culture the specific growth rate is regulated by the fraction of arrested cells and the length of the cell cycle. Thus, a decrease in specific growth rate is accompanied by an increase in non-proliferating cells or an increase in cycle time or both. The increase in cycle time is in general



due to an increase in the length of the  $G_1$  phase, while the lengths of the other phases remain constant<sup>1</sup>. However, Kromenaker and Srienc<sup>22</sup> observed that as they decreased the specific growth rate of hybridoma cells through the addition of lactate, the length of all cell-cycle phases increased. In Chapter 5 two different situations are discerned with respect to the cell cycle. In the first case there are no non-proliferating cells present and, consequently, the cycle time increases as the specific growth rate decreases. In this case, it was found that the length of all cell-cycle phases increased linearly with the cycle time, with the length of the  $G_1$  phase increasing twice as fast as that of the other phases. In the second situation the cycle time is assumed constant and the fraction of non-proliferating cells increases at decreasing specific growth rates, which, consequently, leads to a constant duration of all cell-cycle phases. Both situations are not very realistic. With respect to the first situation it is known that apoptosis occurs (Chapter 8) and thus that part of the viable cells are in fact non-proliferative. Furthermore, the variation in duration of especially the S phase, ranging from 8 to 13.5 hours deviates quite much from literature values ranging from 6 to 8 hours<sup>1</sup>. With respect to the second situation, a constant duration of the  $G_1$  phase over a large range of specific growth rates is quite unlikely<sup>1</sup>. In the model developed in Chapter 7 two different situations are combined. Thus, the duration of the cell cycle is assumed to be constant below the critical specific growth rate. Above the critical specific growth the duration of the cell cycle decreases due to a decrease in the length of the  $G_{1A}$  phase, while the duration of the other phases remains constant. On the basis of the age-distribution function for the cycling cells as given in Chapter 7 the fractions of cells in the different phases of the cell-cycle are calculated in Chapter 8. Thus, the fraction of S-phase cells could be well described as a function of the dilution rate. However, the fraction of  $G_1$ -phase cells was predicted too high and the fraction of  $G_2/M$ -phase cells was predicted too low by the model. This may be due to the rate of apoptosis being different for different cell-cycle phases as has been observed in literature<sup>12</sup>. In addition, a good prediction of all cell-cycle fractions is obtained if it is assumed that above the critical specific growth rate the length of the  $G_2/M$  phase is not constant but increases from 1.2 to 3.8 hours with decreasing specific growth rates. These values are rather small as compared to literature values, which range from 3 to 6 hours for  $G_2$  and 1 to 1.5 hour for the M phase<sup>1</sup>.

### **Production and consumption rates**

As stated, apoptosis is induced by substrate depletion and the presence of toxic products. Furthermore, the concentration of substrates and toxic products may influence the specific productivity of the cells. In the model as developed in Chapter 7 a maintenance-energy model for

the consumption of the main substrates glutamine and glucose is introduced that combines the approaches of Herbert and Pirt<sup>49</sup> by assuming that apoptotic cells have a low metabolic activity and consume no glucose and glutamine.

In Chapter 8 equations are derived for two different hypotheses regarding the production of monoclonal antibody. The first hypothesis assumes passive release of antibody from dead cells. For the second hypothesis a higher production rate by non-proliferating apoptotic cells is assumed as compared to cycling cells. Both hypothesis could describe the increase in productivity at decreasing dilution rates well. Bibilla and Flickinger<sup>6</sup> show that for their cells newly synthesized antibody may remain inside the cell for a period of 0.5 to 3 hours. In addition, Al-Rubeai et al.<sup>2</sup> show that large vesicles containing antibody may be present inside the cell. This intracellular antibody may be released upon cell death<sup>35</sup> or it may be excreted during apoptosis. More information is needed on, for instance, the intracellular antibody content of cycling and apoptotic cells and the fate of antibody in apoptotic cells.

## **IMPLICATIONS FOR PROCESS AND REACTOR DESIGN**

In animal-cell cultivation the overall product yield ( $\text{kg}\cdot\text{Year}^{-1}$ ) is closely related to the attainment of high viable-cell densities for prolonged periods of time, which may be prevented by the occurrence of substantial cell death. Consequently, reactor, process, and medium design are partly aimed at reducing the amount of cell death.

### **Reactor design**

As shown in this thesis the hypothetical-killing-volume theory is valid for hybridoma cells in air-lift reactors with respect to the major design parameters being the gas flow rate and the reactor height and diameter. Consequently, the procedure for optimal design is not different from the one used for bubble columns<sup>48</sup>. Because the death rate of cells due to sparging is proportional to the number of bubbles formed, an optimal design is reached by transferring a maximal amount of oxygen for each bubble introduced in the reactor. The amount of oxygen transferred per bubble may be increased by increasing the residence time of the bubble in the reactor, increasing the specific surface area of the bubble, and increasing the oxygen concentration inside the bubble. An increase in residence time can be obtained by increasing the reactor height or decreasing the bubble rise velocity. The specific surface area may be increased by decreasing the bubble diameter. Since the bubble rise velocity and the bubble diameter are difficult parameters to control, the reactor height and the oxygen concentration inside the bubbles are the best design parameters.

In general the oxygen transfer in bubble columns is better than that of air-lift reactors of the same dimensions<sup>48</sup>, which would favour the bubble-column reactor for the cultivation of animal cells. In addition, oxygen depletion may occur in the downcomer section of the air-lift reactor, which may induce apoptosis. On the other hand the difference in liquid flow between the air-lift reactor and bubble column may have an effect on the size of the hypothetical killing volume and the rate of apoptosis, which remains to be investigated.

### **Medium and process design**

The amount of cell death due to sparging may be reduced by adding shear-protective agents like Pluronic. However, it must be taken into account that these agents must be removed from the product during downstream processing, which may be difficult and costly. According to the results of Chapter 5, maintaining the cells at a low specific growth rate will also reduce the amount of cell death due to sparging. However, this reduction in shear-related cell death may be related to the appearance of apoptotic cells at decreasing specific growth rates, which would mean that it will always be accompanied by an increase in apoptotic cell death. Thus, it seems better to keep the cells at a specific growth rate just above the critical specific growth rate.

As shown in this work and by other authors also the productivity of hybridoma cells often increases at decreasing specific growth rates. This also would favour culturing the hybridoma cells at low specific growth rates, which as stated before would be accompanied by an increase in apoptotic cell death. At present the cause for the increased productivity at low specific growth rates is not exactly known.

A careful control of the medium conditions is desired to obtain optimal product yields. This may be achieved in fed-batch, continuous and perfusion systems.

### **Genetic manipulation**

The genetic manipulation of cells is used to introduce or amplify genes for specific products in animal cells in order to reach higher production levels. In addition, genetic manipulation may be used for the alleviation of metabolic bottlenecks<sup>5</sup>. An example of this is the introduction of genes that inhibit apoptosis like the *bcl-2* gene. The *bcl-2* gene product is known to suppress apoptosis induced by a variety of factors like serum deprivation and heat shock. Itoh et al.<sup>19</sup> showed that the high-level expression of the human *bcl-2* gene in murine hybridomas resulted in higher viable-cell concentrations during the late exponential and stationary growth phase in batch cultures. However, the period of cell growth was about the same for transfected and non-transfected cells. In addition,

a two-fold increase in the specific productivity of the cells in the exponential and stationary growth phase is observed for which no possible explanation is given. This increase in productivity may, however, be related to keeping the cells in a non-proliferating viable state. The increased viable culture period and the two-fold increase in productivity led to a four-fold increase in the total batch productivity. Eventually, with a delay of about two hours, also the transfected cells died through apoptosis.

Kumar<sup>23</sup> shows that the expression of antisense Nedd2 mRNA in the cell line FDC-P1 leads to inhibition of apoptosis upon the removal of cytokines. Nedd2 belongs to a family of mammalian cysteine proteases which share similarity with a cell-death protein found in *Caenorhabditis elegans*.

## CONCLUSIONS

A careful reactor design may lead to a reduction in mainly necrotic cell death through a reduction of the amount of shear in the reactor and to the prevention of apoptosis by preventing the development of adverse medium conditions in specific zones of the reactor. With respect to reducing the amount of shear, the hypothetical-killing-volume theory is a useful tool for the design of air-lift and bubble-column reactors. Especially the reactor height and the oxygen tension in the air bubbles are useful parameters for the optimal design of these reactors. Furthermore, the addition of shear-protective agents can reduce the shear-related death. However, these substances must be removed from the final product and may interfere with the down-stream processing. Last, immobilisation inside porous microcarriers can reduce the amount of shear-related cell death presumably by shielding the cells from the detrimental hydrodynamic forces. However, due to mass-transfer limitations cells inside such a carrier may experience adverse medium conditions which would induce apoptosis.

For hybridoma cells low specific growth rates often result in higher productivities. In addition, low specific growth rates may reduce the shear sensitivity of the cells. However, at specific growth rates below a critical specific growth rate cells become apoptotic leading to an increase in the specific death rate. Apoptosis may be prevented by a careful process design, which should also include an optimal yield of product on medium. In addition, inhibition of apoptosis may be obtained by genetic manipulation of the cells, which makes it possible to maintain culture viability at low substrate concentrations and in this way may lead to higher product yields on medium. However, more information is needed with respect to the causes for the increase in productivity at low specific growth rates.

## REFERENCES

1. Alberts, B., Bray, D., Lewis, J., Raff, M., Roberts, K., Watson, J.D. 1983. *Molecular biology of the cell*. Garland, New York.
2. Al-Rubeai, M., Mills, D., Emery, A.N. 1990. Electron microscopy of hybridoma cells with special regard to monoclonal antibody production. *Cytotechnol.* **4**: 13-28.
3. Al-Rubeai, M., Singh, R.P., Emery, A.N., Zhang, Z. 1995. Cell cycle and cell size dependence of susceptibility to hydrodynamic forces. *Biotechnol. Bioeng.* **46**: 88-92.
4. Bavarian, F., Fan, L.S., Chalmers, J.J. 1991. Microscopic visualization of insect cell-bubble interactions. I: Rising bubbles, air-medium interface, and the foam layer. *Biotechnol. Prog.* **7**: 140-150.
5. Bell, S.L., Bebbington, C., Scott, F., Wardell, J.N., Spier, R.E., Bushell, M.E., and Sanders, P.G. 1995. Genetic engineering of hybridoma glutamine metabolism. *Enzyme Microbiol. Technol.* **17**: 98-106.
6. Bibila, T.A., Flickinger, M.C. 1991. A model of intraorganelle monoclonal antibody transport and secretion in mouse hybridoma cells. *Biotechnol. Bioeng.* **38**: 767-780.
7. Chalmers, J.J., Bavarian, F. 1991. Microscopic visualization of insect cell-bubble interactions. II: The bubble film and bubble rupture. *Biotechnol. Prog.* **70**: 151-158.
8. Chalmers, J.J. 1994. Cells and bubbles in sparged bioreactors. *Cytotechnol.* **15**: 311-320.
9. Chattopadhyay, D., Rathman, J.F., Chalmers, J.J. 1995. The protective effect of specific medium additives with respect to bubble rupture. *Biotechnol. Bioeng.* **45**: 473-480.
10. Chattopadhyay, D., Rathman, J.F., Chalmers, J.J. 1995. Thermodynamic approach to explain cell adhesion to air-medium interfaces. *Biotechnol. Bioeng.* **48**: 649-658.
11. Cherry, R.S., Hulle, C.T. 1992. Cell death in the thin films of bursting bubbles. *Biotechnol. Prog.* **8**: 11-18.
12. Darzynkiewicz, Z., Bruno, S., Del Bino, G., Gorczyca, W., Hotz, M.A., Lassota, P., Traganos, F. 1992. Features of apoptotic cells measured by flow cytometry. *Cytometry* **13**:795-808.
13. Garcia-Briones, M.A., Chalmers, J.J. 1994. Flow parameters associated with hydrodynamic cell injury. *Biochnol. Bioeng.* **44**: 1089-1098.
14. Gardner, A.R., Gainer, J.L., Kirwan, D.J. 1990. Effects of stirring and sparging on cultured hybridoma cells. *Biotechnol. Bioeng.* **35**: 940-947.
15. Handa, A., Emery, A.N., Spier, R.E. 1985. On the evaluation of gas-liquid interfacial effects on hybridoma viability in bubble column bioreactors. *Dev. Biol. Stand.* **66**: 241-253.
16. Handa-Corrigan, A., Emery, A.N., Spier, R.E. 1989. Effect of gas-liquid interfaces on the growth of suspended mammalian cells: mechanisms of cell damage by bubbles. *Enzyme Microb. Technol.* **11**: 230-235.
17. Hülsher, M., Onken, U. 1988. Influence of bovine serum albumin in the growth of hybridoma cells in airlift loop reactors using serum-free medium. *Biotechnol. Lett.* **10**: 689-694.
18. Hülsher, M., Pauli, J., Onken, U. 1990. Influence of protein concentration on mechanical cell damage and fluid dynamics in airlift reactors for mammalian cell culture. *Food Biotechnol.* **4**: 157-166.
19. Itoh, Y., Ueda, H., Suzuki, E. 1995. Overexpression of bcl-2, apoptosis suppressing gene: prolonged viable culture period and enhanced antibody production. *Biotechnol. Bioeng.* **48**: 118-122.
20. Jöbses, I., Martens, D., Tramper, J. 1991. Lethal events during gas sparging in animal cell culture. *Biotechnol. Bioeng.* **37**: 484-490.

21. Jordan, M., Sucker, H., Einsele, F., Eppenberger, H.M. 1994. Interactions between animal cells and gas bubbles: The influence of serum and Pluronic F68 on the physical properties of the bubble surface. *Biotechnol. Bioeng.* **43**: 446-454.
22. Kromenaker, S.J., Srienc, F. 1994. Effect of lactic acid on the kinetics of growth and antibody production in a murine hybridoma: secretion patterns during the cell cycle. *J. Biotechnol.* **34**: 13-34.
23. Kumar, S. 1995. Inhibition of apoptosis by the expression of antisense Nedd2. *FEBS Lett.* **368**: 69-72.
24. Kunas, K.T., Papoutsakis, E.T. 1990. Damage mechanisms of suspended animal cells in agitated bioreactors with and without bubble entrainment. *Biotechnol. Bioeng.* **36**: 476-483.
25. Lu, G.Z., Thompson, B.G., Gray, M.R. 1992. Physical modelling of animal cell damage by hydrodynamic forces in suspension cultures. *Biotechnol. Bioeng.* **40**: 1277-1281.
26. MacIntyre, F. 1972. Flow patterns in breaking bubbles. *J. Geophysical Research* **77**: 5211-5228.
27. Martens, D.E., Gooijer, C.D. de, Beuvery, E.C., Tramper, J. 1992. Effect of serum concentration on hybridoma viable cell density and production of monoclonal antibodies in CSTRs and on shear sensitivity in air-lift loop reactors. *Biotechnol. Bioeng.* **39**: 891-897.
28. Martens, D.E., Gooijer, C.D. de, Velden-deGroot, C.A.M. van der, Beuvery, E.C., Tramper, J. 1993. Effect of dilution rate on growth, productivity, cell cycle and size, and shear sensitivity of a hybridoma cell in a continuous culture. *Biotechnol. Bioeng.* **41**: 429-439.
29. Martens, D.E., Nollen, E.A.A., Hardeveld, M., van der Velden-de Groot, C.A.M., de Gooijer, C.D., Beuvery, E.C., Tramper, J. 1996. Death rate in a small air-lift loop reactor of Vero cells grown on solid microcarriers and in macroporous microcarriers. Accepted for publication in *Cytotechnol.*
30. Mercille, S., Massis, B. 1994. Induction of apoptosis in nutrient-deprived cultures of hybridoma and myeloma cells. *Biotechnol. Bioeng.* **44**: 1140-1154.
31. Michaels, H.D., Petersen, J.F., McIntire, L.V., Papoutsakis, E.T. 1991. Protection mechanisms of freely suspended animal cells (CRL 8018) from fluid-mechanical injury. Viscometric and bioreactor studies using serum, Pluronic F68 and polyethylene glycol. *Biotechnol. Bioeng.* **38**: 169-180.
32. Michaels, J.D., Papoutsakis, E.T. 1991. Polyvinyl alcohol and polyethylene glycol as protectants against fluid-mechanical injury of freely -suspended animal cells (CRL 8018). *J. Biotechnol.* **19**: 241-258.
33. Michaels, J.D., Nowak, J.E., Mallik, A.K., Koczo, K., Wasan, D.T., Papoutsakis, E.T. 1995. Analysis of cell-to-bubble attachment in sparged bioreactors in the presence of cell-protecting agents. *Biotechnol. Bioeng.* **47**: 407-419.
34. Michaels, J.D., Nowak, J.E., Mallik, A.K., Koczo, K., Wasan, D.T., Papoutsakis, E.T. 1995. Interfacial properties of cell culture media with cell-protecting additives. *Biotechnol. Bioeng.* **47**: 420-430.
35. Mohan, S.B., Lydiatt, A. 1991. Passive release of monoclonal antibodies from hybridoma cells. *Cytotechnol.* **5**: 201-209.
36. Murhammer, D.W., Goochee, C.F. 1988. Scale-up of insect cell cultures: Protective effects of Pluronic F-68. *Bio/Technol.* **6**: 1411-1418.
37. Murhammer, D.W., Goochee, C.F. 1990. Sparged animal cell bioreactors: Mechanisms of cell damage and Pluronic F-68 protection. *Biotechnol. Prog.* **6**: 391-397.

38. Oh, S.K.W., Nienow, A.W., Al-Rubeai, M., Emery, A.N. 1989. The effects of agitation intensity with and without continuous sparging on the growth and antibody production of hybridoma cells. *J. Biotechnol.* **12**: 55-62.
39. Oh, S.K.W., Nienow, A.W., Al-Rubeai, M., Emery, A.N. 1992. Further studies of the culture of mouse hybridomas in an agitated bioreactor with and without continuous sparging. *J. Biotechnol.* **22**: 245-270.
40. Ormerod, M.G., Sun, X.-M., Snowden, R.T., Davies, R., Fearnhead, H., Cohen, G.M. 1993. Increased membrane permeability of apoptotic thymocytes: A flow cytometric study. *Cytometry* **14**: 595-602.
41. Papoutsakis, E.T. 1991. Media additives for protecting animal cells against agitation and aeration damage in bioreactors. *TibTech.* **9**: 316-324.
42. Papoutsakis, E.T. 1991. Fluid-mechanical damage of animal cells in bioreactors. *TibTech.* **9**: 427-437.
43. Perreault, J., Lemieux, R. 1993. Essential role of optimal protein synthesis in preventing the apoptotic death of cultured B cell hybridomas. *Cytotechnol.* **13**: 99-105.
44. Piacentini, M., Fesus, L., Farrace, M.G., Ghibelli, L., Piredda, L., Melino, G. 1991. The expression of "tissue" transglutaminase in two human cancer cell lines is related with the programmed cell death (apoptosis). *Eur. J. Cell Biol.* **54**: 246-254.
45. Pol, L. van der, Zijlstra, G., Thalen, M., Tramper, J. 1990. Effect of serum concentration on production of monoclonal antibodies and on shear sensitivity of a hybridoma. *Bioproc. Eng.* **5**: 241-245.
46. Pol, L. van der, Bakker, W.A.M., Tramper, J. 1992. Effects of low serum concentrations (0%-2.5%) on growth, production, and shear sensitivity of hybridoma cells. *Biotechnol. Bioeng.* **40**: 179-182.
47. Pol, L. van der, Bonarius, D., Wouw, G. van de, Tramper, J. 1993. Effect of silicone antifoam on shear sensitivity of hybridoma cells in sparged cultures. *Biotechnol. Prog.* **9**: 504-509.
48. Riet, K. van't, Tramper, J. 1991. *Basic bioreactor design.* Marcel Dekker Inc, New York.
49. Roels, J. A. 1983. *Energetics and kinetics in biotechnology.* Elsevier Biomedical Press, Amsterdam.
50. Tan, W.S., Dai, G.C., Chen, Y.L. 1994. Quantitative investigations of cell-bubble interactions using a foam fractionation technique. *Cytotechnol.* **15**: 321-328.
51. Tramper, J., Williams, J.B., Joustra, D. 1986. Shear sensitivity of insect cells in suspension. *Enzyme Microbiol. Technol.* **8**: 33-36.
52. Tramper, J., Vlak, J.M. 1987. Bioreactor design for growth of shear-sensitive mammalian and insect cells. In: Webb C., Ativuna F., (Eds.): *Plant and animal cell cultures: Process possibilities*, 125-136. Chichester: Ellis Horwood. 125-136.
53. Tramper, J., Smit, D., Straatman, J., Vlak, J.M. 1988. Bubble column design for growth of fragile insect cells. *Bioproc. Eng.* **3**: 37-41.
54. Tramper, J., Vlak, J.M. 1988. Some engineering and economic aspects of continuous cultivation of insect cells for the production of baculo viruses. *Biochem. Eng. (Annals of the New York academy of sciences)* **469**: 279-288.
55. Trinh, K., Garcia-Briones, M., Chalmers, J.J. 1994. Quantification of damage to suspended insect cells as a result of bubble rupture. *Biotechnol. Bioeng.* **43**: 37-45.
56. Wang, N.S., Yang, J.-D., Calabrese, R.V., Chang, K.-C. 1994. Unified modelling framework of cell death due to bubbles in agitated and sparged bioreactors. *J. Biotechnol.* **33**: 107-122.
57. Wu, J., Goosen, F.A. 1995. Evaluation of the killing volume of gas bubbles in sparged animal cell culture bioreactors. *Enzyme Microbiol. Technol.* **17**: 241-247.

## Chapter 9

58. Wu, J., Daugulis, A.J., Faulkner, P., Goosen, M.F.A. 1995. Protective effect of polymer additives on animal cells exposed to rapidly falling films. *Biotechnol. Prog.* **11**: 127-132.
59. Wyllie, A.H., Kerr, J.F.R., Currie, A.R. 1980. Cell death: The significance of apoptosis. *Int. Rev. Cytol.* **68**: 251-306.
60. Zhang, Z., Chisti, Y., Moo-Young, M. 1995. Effects of the hydrodynamic environment and shear protectants on survival of erythrocytes in suspension. *J. Biotechnol.* **43**: 33-40.



## SUMMARY

Animal-cell cultivation is becoming increasingly important especially for the area of human-health products. The products range from vaccines to therapeutic proteins and the cells themselves. The therapeutic application of proteins puts high demands upon their quality with respect to purity and structure. For example, a correct folding and glycosylation is of importance for the activity, the *in vivo* clearance rate and the possible immunogenicity of the protein, and can often only be obtained by production in animal cells. An important class of proteins produced by animal cells is formed by monoclonal antibodies. Monoclonal antibodies are produced by hybridoma cells and have the capacity to bind very specifically to a particular molecular structure (epitope), a quality that makes them suitable for application in *in vivo* and *in vitro* diagnostics, in separation technology and for the *in vivo* targeting of drugs.

The occurrence of substantial cell death and the presence of cell debris is a major problem in animal-cell cultivation. It interferes with the attainment of high volumetric productivities and with a proper functioning of the process. In addition, it may affect the quality of the product and cause problems in down-stream processing. Cell death may follow two different pathways, being apoptosis and necrosis, which have very distinct physiological and morphological features. Necrosis is a passive process generally caused by sudden high levels of environmental stress, whereas apoptosis is an active, genetically controlled process induced by mild stress conditions or specific signals from the environment.

After the introduction in Chapter 1, the application of a general framework for the construction of segregated models is discussed in Chapter 2 with respect to the behaviour of animal-cell populations. For the construction of segregated models, the physiological state of an animal cell must be specified, which is discussed in this chapter with special attention for the experimental verification of the models. Finally, a number of age-structured, segregated models, which are of importance for animal-cell cultivation are reviewed in this chapter.

The required amounts of animal-cell products are expected to be in the order of kilograms or even tonnes on a yearly basis. In order to produce these amounts, scale-up is necessary, which is most easily done in conventional reactor systems like the stirred-tank, bubble-column, and air-lift reactor. A main problem in the scale-up of these reactors is the supply

of sufficient oxygen to the culture, which often requires sparging. Hydrodynamic forces associated with sparging cause cell death. In Chapters 3, 4, and 5 the specific death rate of hybridoma cells in bubble-column and air-lift reactors is studied with the hypothetical-killing-volume theory as a central theme. The hypothetical killing volume is a hypothetical volume associated with an air bubble during its lifetime in the reactor in which all cells are killed. The first-order death-rate constant in bubble-column and air-lift reactors can then be derived to be the product of this hypothetical killing volume and the number of bubbles introduced into the reactor per unit time and per unit reactor volume. The specific death rate of the hybridoma cells in the bubble-column and air-lift reactors is shown to be proportional to the gas flow rate and the reciprocal reactor height. Furthermore, in bubble columns the specific death rate is shown to be proportional to the square of the reciprocal reactor diameter. These results are in accordance with the hypothetical-killing-volume theory. The main cause of cell death is found to be bubble break-up at the surface, although detrimental effects at the sparger cannot be excluded. In Chapter 6 the specific death rate of Vero cells immobilized on microcarriers is shown to be proportional to the gas flow rate. Since the height of the reactor is not varied, it cannot be excluded that in this case also the rising of the bubbles or the associated liquid flow cause cell damage.

A common method to reduce the detrimental effects of air bubbles is the use of protective additives. In this thesis it is shown that the addition of two such protectants, Pluronic F68 (Chapter 3) and serum (Chapter 4), respectively, reduces the amount of cell death as a consequence of sparging. Furthermore, as demonstrated in Chapter 4, the protective effect of serum has a fast-acting, physical, and a slow-acting, physiological component. In Chapter 5 the effect of the specific growth rate on the specific death rate of cells due to sparging is studied in air-lift loop reactors. Cells with varying specific growth rates are obtained from steady-state continuous cultures run at different dilution rates. Remarkably, the specific death rate of the cells due to sparging decreased as their specific growth rate decreased. Furthermore, in Chapter 6 it is shown that the specific death rate of Vero cells is reduced by immobilisation of the cells inside porous carriers.

Below a critical dilution rate in continuous culture as well as towards the end of batch cultures, the specific death rate of hybridoma cells increases rapidly. In this case, the cells mainly die through apoptosis as a consequence of substrate depletion and the accumulation of toxic products. In Chapter 7 an age-structured model is developed to describe the rate of apoptosis as a function of the dilution rate in continuous culture. In this model a critical specific growth rate is introduced below which the cells start becoming apoptotic. In addition to the specific death- and growth rate, the average cell volume of the viable cells and the specific consumption and

production rates for glucose, glutamine, lactate and ammonia are calculated. The model can reasonably well describe a set of literature data, with respect to the specific growth- and death rate and the concentrations of viable cells, dead cells, glucose, glutamine, lactate, and ammonia. In Chapter 8 the model is extended with equations concerning two hypotheses for the production of monoclonal antibody being:

- (1) Passive release of antibody from dead cells.
- (2) Increased productivity by the apoptotic cells.

Both hypotheses can describe the increase in productivity at decreasing dilution rates as observed in Chapter 5. Furthermore, the distribution of cells over the different phases of the cell cycle is calculated and the equations for the average cell volume are rewritten in terms of forward scatter as measured by flow cytometry. Model predictions concerning these variables are compared to results obtained in Chapter 5. The  $G_1$ - and  $G_2/M$ -phase fractions are not predicted correctly, which may be caused by a cell-cycle-phase specificity of apoptosis. In addition, a good prediction of all cell-cycle fractions can be obtained if it is assumed that the duration of the  $G_2/M$  phase is not constant, but increases as the specific growth rate decreases from the maximum to its critical value. Furthermore, the calculated fraction of apoptotic cells is shown to be proportional to the forward scatter.

Cell death associated with sparging may be minimised by:

- (1) Maximizing the amount of oxygen transferred per bubble introduced in the reactor.
- (2) The addition of a shear-protective agent like Pluronic F68 or serum.
- (3) The immobilisation of cells inside porous microcarriers.

Point one is most easily done by increasing the reactor height and the oxygen tension in the air bubbles. With respect to the second point, it should be mentioned that the additive must be removed from the final product and can cause problems in down-stream processing. This may lead to an increase in the product cost. Finally, in the case of immobilisation of cells inside carriers, transport limitations may occur, which may in turn induce apoptosis. Cell death through apoptosis as caused by low levels of shear, substrate limitation and the presence of toxic products may be reduced through a careful process design and genetic manipulation of the cells.

## SAMENVATTING

De kweek van dierlijke cellen is van groot belang voor de productie van farmaceutische eiwitten. De producten variëren van vaccins tot therapeutische eiwitten en de dierlijke cellen zelf. De therapeutische toepassing van deze eiwitten stelt hoge eisen aan de kwaliteit van het product met betrekking tot de zuiverheid en de eiwitstructuur. Zo zijn de correcte vouwing en glycosilering van het eiwit van belang voor de activiteit, de *in vivo* verwijderingssnelheid en de immunogeniciteit van het eiwit. Een correcte vouwing en glycosilering kan veelal alleen verkregen worden met behulp van dierlijke cellen. Monoklonale antilichamen vormen een belangrijke groep van, door dierlijke cellen geproduceerde, eiwitten. Een monokonaal antilichaam wordt uitgescheiden door hybridomacellen en heeft de eigenschap zeer specifiek te binden aan bepaalde moleculaire structuren (epitopen). Deze eigenschap maakt antilichamen geschikt voor toepassing in de *in vivo*- en *in vitro*-diagnostiek, in de scheidingstechnologie en voor het afleveren van medicijnen op specifieke plaatsen in het lichaam.

Het optreden van celdood en de aanwezigheid van celresten vormen een belangrijk probleem bij de kweek van dierlijke cellen. Het optreden van celdood verhindert het bereiken van een hoge volumetrische productiviteit en de aanwezigheid van celresten bemoeilijkt een goede procesvoering. Verder kan de aanwezigheid van celresten de kwaliteit van het product negatief beïnvloeden en problemen veroorzaken bij de opwerking van het product. Celdood kan verlopen volgens apoptose en necrose, twee verschillende processen met zeer uiteenlopende morfologische en fysiologische kenmerken. Necrose is een passief proces, dat in het algemeen veroorzaakt wordt door het plotseling optreden van zeer schadelijke omstandigheden in de omgeving van de cel. Apoptose, daarentegen, is een actief, genetisch-gereguleerd proces dat geïnduceerd wordt door licht-schadelijke condities of de aanwezigheid van specifieke signalen in de omgeving van de cel.

Na de inleiding in hoofdstuk 1 behandelt hoofdstuk 2 aspecten die van belang zijn voor het beschrijven van dierlijke-celpopulaties met een gesegregeerd model. De specificatie van de fysiologische toestand van een dierlijke cel wordt besproken met betrekking tot de experimentele validatie van het model. Tot slot beschrijft dit hoofdstuk een aantal, op basis van leeftijd gesegregeerde, modellen, die van belang zijn in de dierlijke-celkweektechniek.

De verwachte jaarlijkse vraag naar dierlijke-celkweekproducten ligt in de orde van kilogrammen of zelfs veelvoud daarvan. Voor de productie van deze hoeveelheden is opschaling noodzakelijk. Deze opschaling is het meest eenvoudig te realiseren met conventionele reactoren als de geroerde-tank-, bellenkolom- en airliftreactor. Een belangrijk probleem bij de opschaling van deze reactoren is de overdracht van voldoende zuurstof naar het kweekmedium. Voor het overdragen van voldoende zuurstof is het vaak noodzakelijk lucht door het kweekmedium te borrelen. De hydrodynamische krachten die hiermee gepaard gaan, veroorzaken celsterfte. In hoofdstukken 3, 4 en 5 wordt de specifieke afsterfsnelheid van hybridomacellen in bellenkolom- en airliftreactoren beschreven aan de hand van het 'hypothetical killing volume' model. Het hypothetisch 'killing' volume is een hypothetisch volume, geassocieerd met een luchtbel gedurende haar verblijf in de reactor, waarin alle cellen worden gedood. Vervolgens kan worden afgeleid dat de eerste-orde afsterfsnelheidsconstante in bellenkolom- en airliftreactoren gegeven wordt door het product van dit hypothetisch 'killing' volume en het aantal luchtbellen dat per tijdseenheid en eenheid reactorvolume in de reactor geïntroduceerd wordt. De specifieke afsterfsnelheid van de cellen in deze reactoren is evenredig met de doorvoersnelheid van de lucht en omgekeerd evenredig met de hoogte van de reactor. Daarnaast is in de bellenkolom-reactor de specifieke afsterfsnelheid omgekeerd evenredig met de reactordiameter in het kwadraat. Deze resultaten zijn in overeenstemming met het hypothetisch 'killing' volume model. De voornaamste oorzaak voor celdood is het breken van de luchtbellen aan het oppervlak. Desalniettemin kan het optreden van schadelijke effecten bij de luchtinlaat niet worden uitgesloten. In hoofdstuk 6 wordt aangetoond dat in een airliftreactor de specifieke afsterfsnelheid van Vero-cellen geïmmobiliseerd op dragerdeeltjes evenredig is met de gasdoorvoersnelheid. Aangezien de hoogte van de airliftreactor niet gevarieerd is, kan het niet uitgesloten worden dat ook het stijgen van luchtbellen, en de hierdoor veroorzaakte vloeistofstroming, schadelijk zijn voor de cellen.

De toevoeging van beschermende stoffen is een veel gebruikte methode om de schadelijke effecten van luchtbellen te verminderen. Dit proefschrift toont aan dat de toevoeging van twee van dergelijke beschermende stoffen, respectievelijk Pluronic F68 (hoofdstuk 3) en serum (hoofdstuk 4), celdood tengevolge van het inblazen van lucht in de reactor vermindert. In hoofdstuk 4 blijkt dat de beschermende werking van serum bestaat uit een snelwerkende, fysische component en een langzaamwerkende, fysiologische component. Hoofdstuk 5 beschrijft vervolgens het effect van de specifieke groeisnelheid op de specifieke afsterfsnelheid van cellen in een airliftreactor. Cellen met verschillende specifieke groeisnelheden zijn verkregen uit continuculturen in stationaire toestand bij verschillende verdunningssnelheden. Een opvallend

resultaat is dat de specifieke afsterfsnelheid van de cellen afneemt met een afnemende specifieke groeisnelheid. Hoofdstuk 6 laat tot slot zien dat de specifieke afsterfsnelheid van Vero-cellen in een airlifreactor afneemt door immobilisatie van de cellen in poreuze dragerdeeltjes.

De specifieke afsterfsnelheid van hybridomacellen neemt snel toe als de verdunningssnelheid in continuculturen onder een kritieke waarde komt. Ook tegen het eind van een batchkweek neemt de specifieke afsterfsnelheid van hybridomacellen snel toe. De cellen sterven in deze situaties voornamelijk af via apoptose ten gevolge van substraatdepletie en de accumulatie van toxische producten in het medium. Hoofdstuk 7 behandelt de ontwikkeling van een gestructureerd model voor het beschrijven van de groei en afsterving van hybridoma cellen in een continucultuur. Het model is gebaseerd op de leeftijd van de cel en berekent de snelheid waarmee cellen apoptotisch worden als een functie van de verdunningssnelheid. In dit model wordt een kritieke groeisnelheid geïntroduceerd. Beneden deze kritieke groeisnelheid treedt apoptose op. Behalve de specifieke afsterfsnelheid en de specifieke groeisnelheid, berekent het model ook het gemiddelde volume van de levende cellen en de consumptie- en productiesnelheden van glucose, glutamine, lactaat en ammoniak. De specifieke groei- en afsterfsnelheid en de concentraties van levende cellen, dode cellen, glucose, glutamine, lactaat en ammoniak, als berekent door het model, komen goed overeen met een dataset verkregen uit de literatuur. Het model wordt in hoofdstuk 8 uitgebreid met vergelijkingen die voortkomen uit twee hypothesen voor de productie van monoklonale antilichamen, te weten:

- (1) het passief vrijkomen van antilichaam uit dode cellen;
- (2) een hogere productiesnelheid door apoptotische cellen in vergelijking tot cellen die de celcyclus doorlopen.

Beide hypothesen resulteren in een goede beschrijving van de toename in productiesnelheid bij afnemende groeisnelheid, als waargenomen in hoofdstuk 5. In hoofdstuk 8 wordt verder de verdeling van de cellen over de verschillende fasen van de celcyclus berekend. Tevens worden de vergelijkingen voor het berekenen van het gemiddelde volume van de levende cellen herschreven in termen van 'forward scatter'. De modelvoorspellingen voor deze variabelen zijn vergeleken met de experimentele data als beschreven in hoofdstuk 5. Het model voorspelt de fractie cellen in de  $G_1$  en  $G_2/M$  fase niet goed. Dit wordt mogelijk veroorzaakt doordat het optreden van apoptose afhankelijk is van de positie in de celcyclus. Daarnaast voorspelt het model alle cel-cyclusfracties goed, als wordt aangenomen dat de lengte van de  $G_2/M$  fase niet constant is, maar toeneemt als de specifieke groeisnelheid afneemt van de maximale tot de kritieke waarde. Tot slot blijkt in hoofdstuk 8 dat de berekende toename in de fractie apoptotische cellen lineair proportioneel is met de afname in 'forward scatter'.

## Samenvatting

De mate van celdood, veroorzaakt door het borrelen van lucht door de reactor, kan worden geminimaliseerd door:

- (1) de hoeveelheid zuurstof die per luchtbel naar het medium wordt overgedragen te maximaliseren;
- (2) een stof toe te voegen die bescherming biedt tegen celdood veroorzaakt door luchtbellen;
- (3) cellen te immobiliseren in poreuze dragerdeeltjes.

Het eerste kan het meest eenvoudig bereikt worden door de hoogte van de reactor te vergroten of door de zuurstofspanning in de luchtbellen te verhogen. Bij punt twee is het belangrijk op te merken dat de toegevoegde component ook weer verwijderd moet worden uit het uiteindelijke product. De component kan dientengevolge problemen veroorzaken bij de opwerking, hetgeen mogelijk leidt tot een verhoging van de productiekosten. Bij immobilisatie van cellen in poreuze dragerdeeltjes kan transportlimitatie optreden. Dit leidt lokaal tot een tekort aan substraat danwel ophoping van toxische producten, hetgeen mogelijk apoptose induceert. Celdood door apoptose is te verminderen door een goed ontwerp van het proces en het door genetische manipulatie van cellen.

## BIBLIOGRAPHY

Randolph, T.W., Marison, I.W., Martens, D.E., von Stockar, U. 1990. Calorimetric control of fed-batch fermentations. *Biotechnol. Bioeng.*, **36**: 678-684.

Martens, D.E., Coco-Martin, J., van der Velden-de Groot, C.A.M., Beuvery, E.C., de Gooijer, C.D., Tramper, J. 1990. To an optimal design of an air-lift loop reactor for the cultivation of hybridomas. In: *From clone to clinic: Developments in biotherapy, Proceedings of the conference on between clone and clinic, Amsterdam, The Netherlands, 1990*, (Crommelin, D.J.A., Schellekens, H. Eds.).

Jöbses, I., Martens, D., Tramper, J. 1991. Lethal events during gas sparging in animal cell culture. *Biotechnol. Bioeng.*, **37**: 484-490.

Martens, D.E., de Gooijer, C.D., Beuvery, E.C., Tramper, J. Effect of the growth rate on hybridoma viability, size and production and on the shear sensitivity in air-lift loop reactors. In: *Abstracts of the 4th Nethl. Biotechnology Congress, Amsterdam, The Netherlands, February 1992*, (Netherlands Biotechnological Society Ed.).

Coco-Martin, J.M., Martens, D.E., Dorresteyn, R.C., van der Velden-de Groot, C.A.M., Beuvery, E.C. Long term culture of hybridoma cell line MN12 in homogeneous continuous culture systems. In: *Abstracts of the 4th Nethl. Biotechnology Congress, Amsterdam, The Netherlands, February 1992*, (Netherlands Biotechnological Society Ed.).

Martens, D.E., de Gooijer, C.D., Beuvery, E.C., Tramper, J. 1992. Effect of serum concentration on hybridoma viable cell density and production of monoclonal antibodies in CSTRs and on shear sensitivity in air-lift loop reactors. *Biotechnol. Bioeng.*, **39**: 891-897.



## Bibliography

Martens, D.E., van der Velden-de Groot, C.A.M., Beuvery, E.C., de Gooijer, C.D., Tramper, J. The influence of serum, growth rate, reactor height, and gas flow on the cell death in air-lift loop reactors. Paper presented at the AIChE Annual Meeting, Miami, Florida, USA, November 1992, 156a.

Martens, D.E., de Gooijer, C.D., van Velden-de Groot, C.A.M., Beuvery, E.C., Tramper, J. 1993. Effect of dilution rate on growth, productivity, cell cycle and size, and shear sensitivity of a hybridoma cell in a continuous culture. *Biotechnol. Bioeng.*, **41**: 429-439.

Coco-Martin, J.M., Martens, D.E., van der Velden-de Groot, C.A.M., Beuvery, E.C. 1993. Cultivation of hybridoma cell line Mn12 in a homogeneous continuous culture system. *Cytotechnol.*, **13**: 213-220.

Martens, D.E., Sipkema, E.M., de Gooijer, C.D., Beuvery, E.C., Tramper, J. 1995. A combined cell-cycle and metabolic model for the growth of hybridoma cells in steady-state continuous culture. *Biotechnol. Bioeng.*, **48**: 49-65.

Martens, D.E., Béal, C., Zwietering, M.H., van't Riet, K. Modelling of microbial interactions. In: *Proceedings of the IMACS/IFAC first international symposium on Mathematical Modelling and Simulation in Agriculture and Bio-Industries.*, Brussels, Belgium, May 1995.

Martens, D.E., de Gooijer C.D. Combined cell-cycle and metabolic model for the growth of hybridoma cells in steady-state continuous culture. Presentation for the animal and plant cell technology working party of the EFB, Zürich, Switzerland, June 1995.

Martens, D.E., Nollen, E.A.A., Hardeveld, M., van der Velden-de Groot, de Gooijer, C.D., Beuvery, E.C., Tramper, J. 1996. Death rate in a small air-lift loop reactor of Vero cells grown on solid microcarriers and in macroporous microcarriers. Accepted for publication in *Cytotechnol.*

Martens, D.E., de Gooijer, C.D., Beuvery, E.C., Tramper, J. Use of a combined cell-cycle and metabolic model for the study of hybridoma cells in steady-state continuous culture. Submitted for publication.

## Bibliography

Martens, D.E., de Gooijer, C.D., Beuvery, E.C., Tramper, J. Segregated models in animal-cell cultivation. Submitted for publication.

Martens, D.E., Béal, C., Zwietering, M.H., van't Riet, K. Modelling of microbial interactions in preservation and spoilage of foods. Poster presented at the second international conference on predictive microbiology, Hobart, Australia , Februari 1996, P03.2.

## CURRICULUM VITAE

Derk Egbert Martens werd op 1 oktober 1963 geboren te Westervelde, gemeente Norg. Hij behaalde het diploma VWO-B in 1982 aan het Dr. Nassau-College te Assen.

De in 1982 gestarte studie Moleculaire Wetenschappen aan de Landbouwwuniversiteit Wageningen werd met de buluitreiking op 23 januari 1989 afgesloten. Afstudeervakken waren Celbiologie, Moleculaire Biologie en Proceskunde. Het laatst genoemde vak werd gedaan bij TNO te Zeist. De stage voor Proceskunde werd doorlopen bij het Institute de Génie Chimique van de École Polytechnique Fédérale de Lausanne te Lausanne.

In de periode 1989-1993 werkte Dirk als Assistent in Opleiding bij de sectie Proceskunde. Het werk werd uitgevoerd bij het Laboratorium voor Procesontwikkeling van het Rijksinstituut voor Volksgezondheid en Milieuhygiëne te Bilthoven en heeft geleid tot dit proefschrift.

In juni 1994 startte hij een tweejarige Post-doc betrekking bij Proceskunde. Het ging dit keer om de rol van microbiële interacties bij het bederf van levensmiddelen. Een nieuw dienstverband bij de sectie Proceskunde is per oktober 1996 van start gegaan. Als toegevoegd onderzoeker zal Dirk opnieuw belast zijn met onderzoek aan dierlijke cellen.